Fusogenic liposomes: the innovative delivery of compounds into human platelets to reduce animal use in platelet research.

A thesis submitted for the degree of Doctor of Philosophy

School of Biological Sciences

Carly Kempster

January 2023

Declaration:

I confirm that this is my own work and the use of all material from other sources has been properly and fully acknowledged.

Signed: Carly Kempster

Date: 25/01/2023

Abstract

Background

Platelets lack a nucleus meaning that conventional methods, used to investigate nucleated cells, cannot be applied. As a result, the platelet field has become heavily reliant on genetically modified mouse models to investigate platelet function. Fusogenic liposomes have been used to facilitate the delivery of water-soluble cargo directly into cells. This project investigates, for the first time, if fusogenic liposomes can fuse directly with platelets and if they can be used as a delivery method to release cargo directly into the cytoplasm of platelets.

Aims

To develop a convolutional neural network (CNN) to automate and standardise platelet spreading analyses throughout this project. To determine if fusogenic liposomes can be used in combination with platelets without impacting on normal platelet function. To identify if cargo, encapsulated in fusogenic liposomes, can be delivered directly into platelets following fusion.

Methods

A CNN was trained using 120 Differential Interference Contrast microscopy images where model performance was evaluated against an independent test set and five manual annotators. Any impact on normal platelet behaviour, due to fusion by fusogenic liposomes with the platelet membrane, was assessed by measuring P-selectin exposure, phosphatidylserine translocation, platelet spreading, and platelet aggregation.

Results

A CNN abrogates time consuming and biased manual analyses for both human and mouse platelets. Platelets were efficiently labelled with fluorescently labelled fusogenic liposomes without causing significant impact to normal platelet function, or significant increase to platelet activation. Fusogenic liposomes were able to deliver cargo, such as fluorescently labelled Lifeact peptides and whole antibody cargo directly into platelets.

Conclusions

A CNN delivers a tool that can be used to standardise platelet spreading assays in the wider platelet field, eliminating differences to scientific conclusions. Fluorescently labelled fusogenic liposomes offer an alternative method to fluorescently label platelets for *in vitro* and *in vivo* applications, while, with additional optimisation to cargo encapsulation and

delivery efficiency, the delivery of cargo directly into live human platelets offers the potential to investigate intracellular processes *in vitro*. This opens up the opportunity to interrogate mechanisms which may govern platelet activation, unveil novel drug targets, and reduce the need to use platelets from genetically modified animal models.

Acknowledgements

First and foremost, a HUGE thank you to Alice – I feel extremely lucky to have you as my supervisor! Thank you for your continued support and guidance throughout the past three years. Thank you for listening to my ideas, allowing me to grow as a researcher, and showing me that I should have more confidence in myself. You're the Queen of the microscope (helping me out more times than I can even remember!), you always ask the best questions in lab meetings, and you're so helpful and available always. You're someone who I aspire to be, and it goes without saying that I hope to stay in touch.

A big thank you also to Jon! Thanks for being my second supervisor and for encouraging me to apply for this PhD - I have had the best time! Thank you for continually being all-round approachable, a fountain of knowledge, and so supportive. Here's to seeing you at the next conference!

A huge thank you to everyone in the Reading platelet lab, both past and present, for always putting a smile on my face even in the bleakest of lab days - we've all been there when things don't quite work out!

I couldn't write these acknowledgements without a shout out to some of my lab besties! To Safa, lab pals from the start with the ability to understand each other by facial expressions alone! It was meant to be! Here's to the future, and a long friendship ahead! See you soon! To Ilaria, thanks for being a great lab pal both inside and outside of work. To Daniel, thanks for being 'so Daniel' and bringing a smile to my face always – the recent Greggs story is still a firm favourite!

A big thank you to Kirk, Alex, Gemma, Sophie, Eva, and Marcin for not only a great time in the lab, but the pub too! Thank you to Neline and Tanya, for your help and support, and for being such lovely desk neighbours!

Wishing good luck to those also submitting in 2023! Abdul, Daniel, Safa, Taysseer, Yasmin, Salihah, and Fahd, wishing you all the very best!

A big shout out to my parents – you may not understand what on earth I research, but I appreciated the phone conversations and company when walking home – it meant more than you'll know.

Cheers to my best Wolfpack and Cambs gals, for checking in on me and being there always!

Lastly, but by no means least, to Joe. I couldn't have got through the last few years without you always having my back, always championing me when the going got tough, and always making me extra pack up when I headed back to Reading! I am very grateful.

Publications

Fully automated platelet differential interference contrast image analysis via deep learning. **Carly Kempster**, George Butler, Elina Kuznecova, Kirk A. Taylor, Neline Kriek, Gemma Little, Marcin A. Sowa, Tanya Sage, Louise J. Johnson, Jonathan M. Gibbins & Alice Y. Pollitt. *Scientific Reports* (2022); 12, 4614. https://doi.org/10.1038/s41598-022-08613-2

Presentations

Oral Presentation	'Fusogenic liposomes label human platelets without impacting normal platelet function.'
	3rd Platelet Society Meeting (Hull, 2022).
Poster Presentation	'Fusogenic liposomes label human platelets without impacting normal platelet function.'
	3rd Platelet Society Meeting (Hull, 2022) and International Society on Thrombosis and Haemostasis (ISTH, London, 2022).
Poster Presentation	'Fully automated platelet Differential Interference Contrast image analysis via deep learning.'
	3rd Platelet Society Meeting (Hull, 2022) and International Society on Thrombosis and Haemostasis (ISTH, London, 2022).

Contents

i. List of Figures

ii. Abbreviations

ACD	Acid-citrate-dextrose
ANOVA	Analysis of variance
AU	Arbitrary units of fluorescence
CHO	Chinese Hamster Ovary cells
CLEC-2	C-type lectin-like type II
CNN	Convolutional neural network
CP488	488nm fluorescent tag for labelling peptides
CPP	Cell penetrating peptide
CRP-XL	Cross-linked collagen-related peptide
CVD	Cardiovascular disease
dETOH	Dry ethanol
DIC	Differential Interference Contrast
DiR	1,1'-Dioctadecyl-3,3,3',3'-Tetramethylindotricarbocyanine Iodide
DMEM	Dulbecco's modified Eagle medium
DOPE	1,2-di-(9Z-octadecenoyl)-sn-glycero-3-phosphoethanolamine
DOTAP	1,2-dioleoyl-3-trimethylammonium-propane
EDTA	Ethylenediaminetetraacetic acid
ETOH	Ethanol
Fab	Fragment antigen-binding regions (Fab fragments)
FBS	Fetal bovine serum
FITC	Fluorescein isothiocyanate
FLs	Washed platelets fused with in-house fusogenic liposomes
FS	0.2% formyl saline
FSC	Forward scattered light
GFP	Green fluorescent protein

GP	Glycoprotein
GPIIb/IIIa	Glycoprotein IIb IIIa complex (integrin αIIbβ3)
GPRP	Gly-Pro-Arg-Pro, fibrin polymerisation inhibitor
GPVI	Glycoprotein 6
HBS	HEPES buffered saline
HBSc	HEPES buffered saline supplemented with 2mM calcium
HEPES	N-2-Hydroxyethylpiperazine-N-2-Ethane Sulfonic Acid
kDa	Kilodalton
LTA	Light transmission aggregometry
M	Molar
mAP	Mean average precision
MFI	Median fluorescent intensity
mg	Milligram
MK	Megakaryocyte
mL	Millilitre
mM	Millimolar
MWCO	Molecular weight cut off
Myr	Myristoylated carriers
NaCl	Sodium chloride
nm	Nanometre
nM	Nanomolar
PARs	Protease-activated receptors
PBS	Phosphate buffered saline
PE	Phycoerythrin
PE-Cy5	Tandem conjugate combining Phycoerythrin and a Cyanine dye
PGI_2	Prostacyclin

pHLIP	pH low insertion peptide
PLCγ2	Phospholipase Cγ2
PROTAC	PROteolysis TArgeting Chimera
PRP	Platelet rich plasma
PRP.FLs	Platelet rich plasma fused with Fuse-It-Color
PRT	PRT-060318 (Syk inhibitor) [2-((1R,2S)-2-aminocyclohexylamino)-4-(m-tolylamino)pyrimidine-5-carboxamide]
PS	Phosphatidylserine
RSTB	Reducing Sample Treatment buffer (1X)
SD	Standard deviation
SDS	Sodium Dodecyl Sulphate
SDS-PAGE	Sodium dodecyl-sulphate polyacrylamide gel electrophoresis
SEM	Standard error of the mean
Src	Proto-oncogene tyrosine-protein kinase Src
SSC	Side scattered light
Syk	Spleen tyrosine kinase
TBST	Tris buffered saline with Tween 20
TRAP-6	Thrombin receptor-activating peptide-6
TRIM21	Tripartite motif containing-21
v/v	Volume per volume
vWF	von Willebrand factor
WPs	Washed platelets
w/v	Weight per volume
w/w	Weight per weight
w/w/w	Weight per weight per weight

µg	Microgram
µL	Microliter
µm	Micrometre
µM	Micromolar

ns	Non significant (> 0.05)
*	≤ 0.05 significant
**	≤ 0.01 significant
***	≤ 0.001 significant
****	≤ 0.0001 significant

1. Introduction

1.1 Introduction to platelets, haemostasis, and thrombosis

Platelets are small anucleate cells, typically 2-4 µm in diameter, that are derived from megakaryocyte (MK) precursor cells in the bone marrow [1,2]. In healthy individuals, they are the second most abundant blood cell [3], with a normal platelet count ranging between 150 – 450 x10^3 platelets/µL of blood [4]. Platelets play a pivotal role during haemostasis and thrombosis at sites of vascular injury. Haemostasis is the process of controlling and preventing bleeding from an injury to restore continued blood flow within the vascular system [5]. A haemostatic plug, or a thrombus in the event of pathological causes, is the final step of haemostasis where blood coagulates to plug an injury site [5]. Platelets are increasingly being recognised as multifunctional cells, with roles in other physiological processes such as wound repair, lymphatic development, tumour metastasis and immune responses [6-10]. When compared to other cells within the blood, the lifespan of human platelets is short; typically surviving in the circulation for approximately 7-10 days [9]. Meaning that approximately 10% of an individual's platelet count is replenished each day to maintain normal platelet counts [11].

Due to their small size, platelets are pushed to the periphery of blood vessels during circulation [12,13]. This proximity to the endothelium facilitates a rapid platelet response in the event of injury. Platelets are activated by receptor mediated cascades upon contact with the damaged endothelium [14]. In the first instance, the plasma protein von Willebrand factor (vWF) binds to exposed collagen and interacts with the platelet cell surface receptor glycoprotein (GP) Ibα [15]. These interactions slow down circulating platelets and permit tethering, allowing for other platelet surface receptors such as GPVI and $\alpha_2\beta_1$ to bind to exposed collagen [15,16]. Intracellular signalling cascades as a result of receptor engagement induces rapid changes to platelet morphology due to cytoskeletal rearrangements and integrin activation of heterodimeric GPIIb/IIIa (αIIbβ3); conducive to an increase in platelet surface area, and initiation of platelet-platelet interactions, respectively, leading to thrombus formation to prevent excessive bleeding at the injury site [16-18].

Conversely, however, platelet activation and subsequent pathological thrombus formation within the vascular system, such as at sites of atherosclerotic plaque formation, are causative factors in the development and risk prevalence of cardiovascular diseases (CVD) [17]. Cardiovascular diseases, such as myocardial infarction and stroke, are a leading cause of death globally, taking an estimated 17.9 million lives each year [19]. CVD is a main contributor to an ever-increasing health burden within our ageing and growing population [20]. While recent increases in the prevalence of cardiovascular disease in developing countries is due to demographic and lifestyle changes such as ageing and adopting a western diet [21]. It is

therefore essential to understand the mechanisms which govern platelet activation to discover new therapeutics and preventative treatments.

1.2 Platelet granule release and P-selectin exposure

Platelets contain three types of secretory granules – lysosomes, dense granules, and α-granules – and their contents are specific to each type of granule [22]. Platelets contain 1-3 lysosomes per platelet, and each lysosome ranges from 175 – 250 nm in size [23,24]. Lysosomes contain enzymes, such as acid hydrolases, and have been hypothesised to support extracellular functions such as receptor cleavage and vasculature remodelling [25]. Dense granules are the smallest platelet granule with an approximate size of 150 nm [25]. Dense granule content includes concentrated levels of ADP [653 mM] and calcium [2.2 M] for example which, upon release, support the amplification of platelet activation [25,26]. However, it is the α-granule which is the most abundant secretory granule within the platelet [27]. Typically, α-granules range from 200-500 nm in size, and each platelet contains around 50-80 α-granules, accounting for approximately 10% of their volume [28,29]. The formation of α-granules begins at the platelet precursor cell, the megakaryocyte (MK).

In the mature platelet, and upon activation by agonist stimulation or injury, α-granules translocate and fuse to the plasma membrane causing both an exocytosis release of granule contents from the platelet, and a 2 - 4 fold increase of the surface area of the platelet (Figure 1.1) [27]. The content of α-granules consists of soluble proteins which are secreted during platelet activation, where proteomic studies have revealed that hundreds of proteins could be released during α-granule release, with many of these proteins such as vWF and coagulation factors already present in plasma [27]. Despite the challenges presented when trying to determine the physiological function of each individual α-granular derived protein, evidence suggests that α-granule content are involved in haemostasis, coagulation, adhesion, inflammation, and atherosclerosis [27,30].

As well as the release of proteins, α-granules also contain membrane bound proteins that reside on the inner α-granule membrane. Most of these membrane bound proteins are already expressed on the surface of resting platelets including integrins such as αIIbβ3 (also known as glycoprotein IIb/IIIa) and glycoproteins such as glycoprotein (GP) VI. However, proteins such as P-selectin are not expressed on the surface of resting platelets and can be used as a marker of platelet activation and α-granule release [27]. Commercially available antibodies can be purchased to measure the extent of P-selectin exposure on the platelet

surface following platelet activation. P-selectin exposure is therefore regularly used as a measure of platelet activation when investigating platelet function.

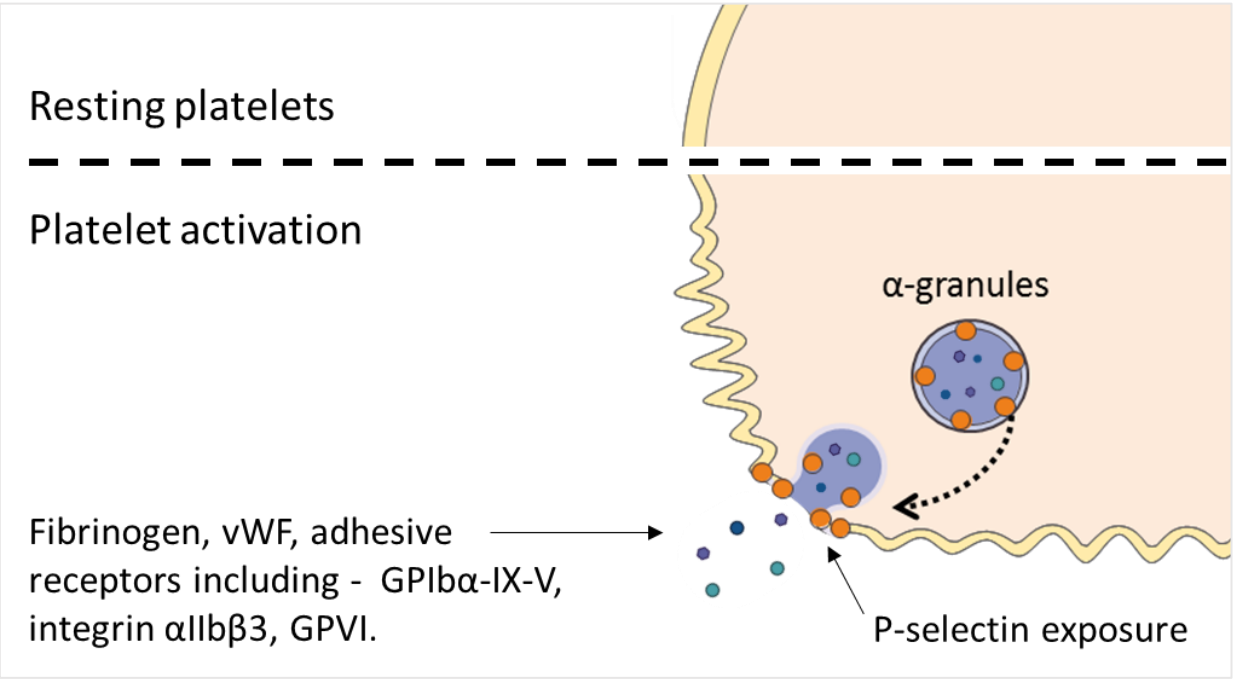

Figure 1.1 Alpha (α-) granule release

Schematic detailing alpha (α-) granule release from platelets upon agonist or injury mediated activation. At rest, platelets retain a discoid shape. During platelet activation, α-granules translocate and fuse to the plasma membrane resulting in an exocytosis release of granule contents from the platelet. P-selectin, a transmembrane protein (orange circles) found on the luminal side of α-granules is exposed at the cell surface of activated platelets and can be identified using commercially available antibodies.

1.3 Platelet adhesion, signalling and aggregation.

Platelets can adhere to sites of vascular damage during injury, for example during cuts and scrapes or during atherosclerotic plaque rupture, where endothelial matrix proteins become exposed [31]. The exposure of sub-endothelial collagen mediates the initial adhesion of circulating platelets to the exposed collagen surface via von Willebrand factor (vWF) which binds to the platelet GPIbα receptor, a subunit of the GP-Ib-IX-V complex on the platelet membrane (Figure 1.2A) [32,33].

As well as GPIb-IX-V, other platelet surface receptors able to bind to exposed collagen include GPVI and $\alpha_2\beta_1$, with GPVI having been identified as the major signalling receptor for

collagen (Figure 1.2B) [34,35]. Cross-linked collagen-related peptide (CRP-XL), a triple helical collagen-mimetic peptide can be used to induce platelet activation via dimeric GPVI, independently of $\alpha_2\beta_1$ [34].

Like collagen, activation of GPVI by CRP-XL induces strong tyrosine phosphorylation due to GPVI associating with transmembrane protein Fc receptor γ-chains (FcRγ) containing immunoreceptor tyrosine-based activation motifs (ITAMs) [34,35]. This, in turn, leads to Src Family Kinase (SFK)–dependent phosphorylation of the conserved ITAM tyrosines, the binding of Spleen Tyrosine Kinase (Syk), which triggers activation and binding of phospholipase Cγ2 (PLCγ2) to the phosphorylated scaffolding protein, linker for activation of T-cells (LAT) [34,35]. These signalling cascades result in platelet degranulation, intracellular Ca^{2+} release and inside-out activation of platelet integrins, including the GPIIb/IIIa (αIIbβ3) complex, which leads to platelet aggregation [33,35].

On activated platelets, the calcium-dependent association of GPIIb and GPIIIa can bind several adhesive proteins including vWF and fibrinogen, amongst others (Figure 1.2C). Whilst vWF allows for the adherence of platelets over the sub endothelium, fibrinogen allows for platelet aggregation [33,36]. Platelet aggregation is the ability of platelets to adhere to each other. During aggregation, the integrin undergoes conformational change from an inactive form to an active form due to “inside out” signalling triggered by an agonist [37]. This conformational change causes an increase in the affinity of the receptor to bind fibrinogen which acts as a bridging molecule to facilitate interactions with nearby platelets (Figure 1.2C) [37,38]. Furthermore, α-granule release due to agonist-induced platelet activation also results in an increased number of membrane-bound GPIIb/IIIa (αIIbβ3) on the platelet surface [39]. An overall increase in integrin levels and platelet-platelet interactions allows platelets to rapidly generate a thrombus and plug the site of injury to arrest bleeding.

The ability of platelets to stick together can be monitored using a platelet aggregometer in a platelet aggregation assay. Platelet aggregation is regularly assessed *in vitro* as a measure of platelet function and to understand the interactions and mechanisms involved during platelet aggregation. A range of different agonists, inhibitors and anti-platelet drugs can be used to compare aggregation responses in platelets.

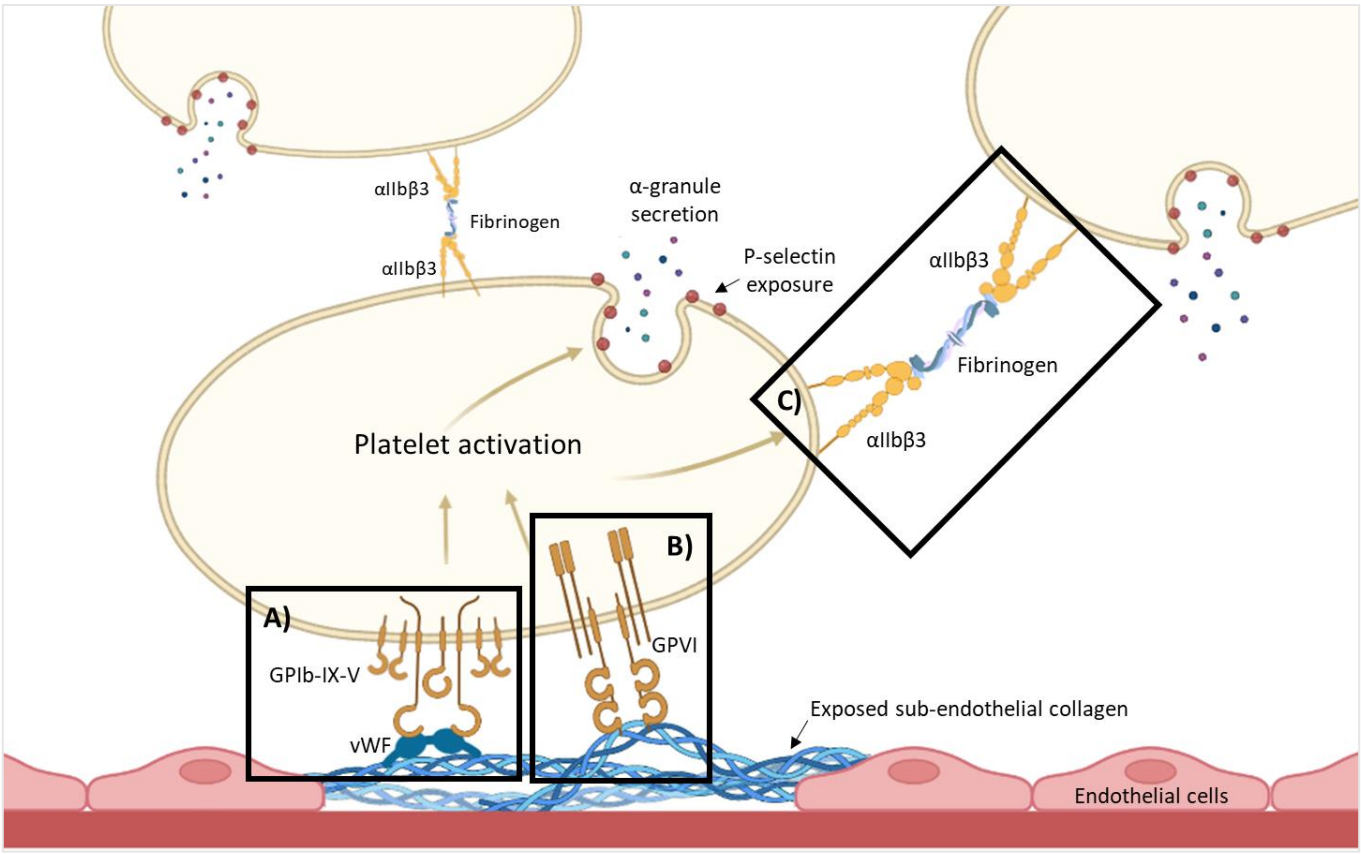

Figure 1.2 Platelet adherence and aggregation

Schematic detailing the interactions between platelet glycoprotein (GP)-Ib-IX-V and von Willebrand Factor (vWF) which initiates the adhesion of platelets to exposed collagen on the damaged blood vessel wall (A), interactions between platelet glycoprotein (GP)VI and exposed collagen which initiates platelet signalling cascades (B), and the platelet-platelet interactions between platelet glycoprotein (GP)IIb/IIIa (integrin αIIbβ3) which utilise fibrinogen as a bridging molecule, initiating platelet aggregation (C). Schematic adapted from "Platelet Activation" template by Biorender.com (2022); retrieved from http://app.biorender.com/biorender_templates.

1.4 Platelet phosphatidylserine translocation

As well as platelet aggregation at sites of injury to reduce blood loss, platelets can also contribute to localised coagulation when prothrombin is converted into thrombin due to the exposure of the phospholipid phosphatidylserine (PS) on the outer platelet membrane [40-42].

In healthy cells, PS resides on the inner cytoplasmic membrane (Figure 1.3*i*). When PS is translocated extracellularly, it is a marker for early apoptosis, or programmed cell death. This is a regulated process and is an essential aspect of maintaining cell populations and tissues by initiating phagocytosis of unwanted cells *in vivo* [43,44]. Despite apoptosis being a normal

process, PS exposure is rapidly induced on the surface of a subpopulation of platelets in the event of platelet activation [41].

PS is typically translocated extracellularly as a result of a combination of agonists such as collagen and thrombin, which initiate the GPVI and protease activated receptor (PAR) pathways of activation respectively, causing a sustained increase to cytosolic calcium (Ca^{2+}) [41]. This brings about a subpopulation of PS-exposing platelets (Figure 1.3*ii*), where translocated PS exposure facilitates the intrinsic coagulation cascade by enabling tenase (factor (F)VIIIa, FIXa, and FX) and prothrombinase (FVa, FXa and prothrombin) complexes to assemble (coagulation cascade not shown) [41]. The conversion of prothrombin to thrombin results in a rapid increase in thrombin generation and, in turn catalyses the conversion of soluble fibrinogen to insoluble fibrin, which contributes to the stabilisation of thrombi in order to prevent bleeding [42].

Annexins are calcium-dependant binding proteins, and the binding of Annexin V can be used to measure apoptotic platelets [44,45]. Fluorescently conjugated Annexin V (or Annexin A5) is commonly used in flow cytometry to detect apoptotic, or procoagulant, platelets since it binds to translocated PS on the outer platelet membrane.

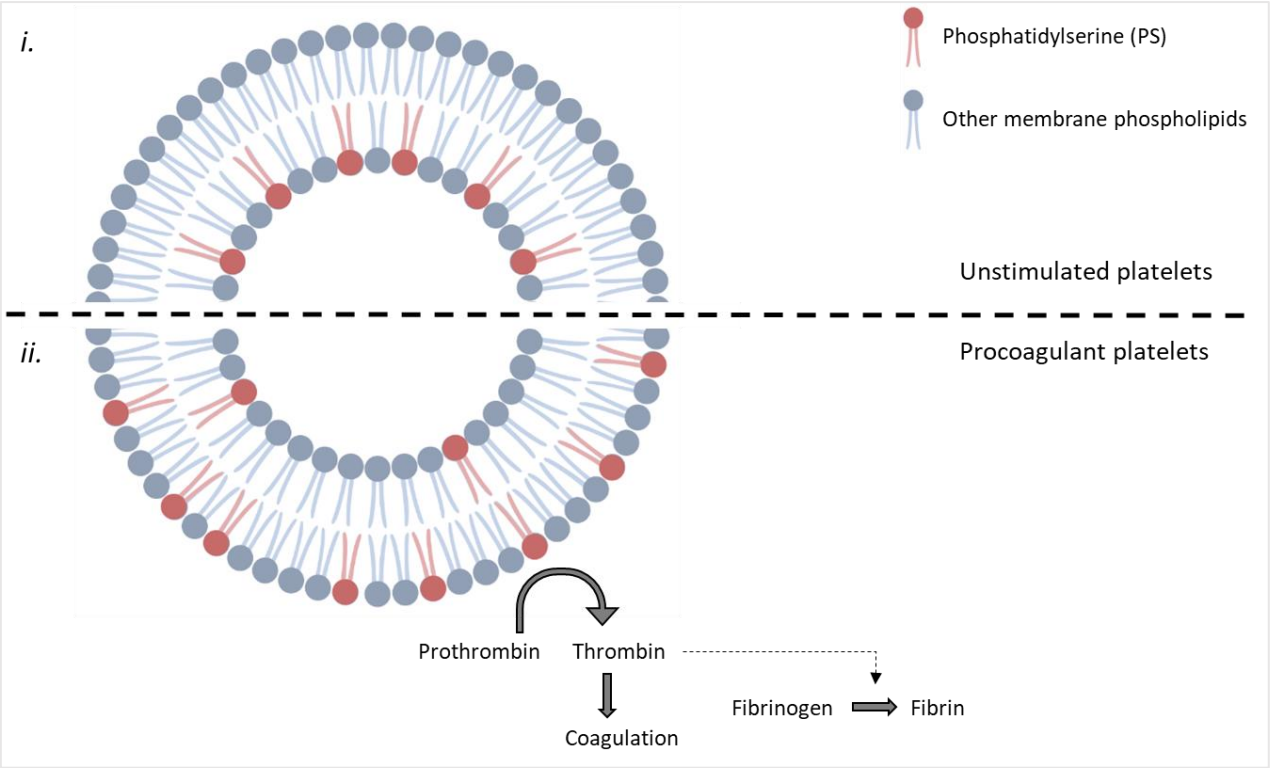

Figure 1.3 Apoptotic platelets

A schematic detailing a phospholipid bilayer representative of a platelet cell membrane where phosphatidylserine (PS) (red) resides on the inner cell membrane during unstimulated and rested cells. Translocation of phosphatidylserine (PS) to the outer platelet membrane during agonist and injury induced platelet activation induces procoagulant platelets. Procoagulant platelets initiate thrombin generation, contributing to coagulation and fibrin formation. Schematic created with biorender.com.

1.5 Platelet morphology

Platelets undergo rapid cytoskeletal rearrangements of actin filaments during injury or agonist-induced activation. Actin is the most abundant protein in platelets [46], and is frequently investigated using platelet spreading assays [47-49]. The rapid rearrangements of actin drastically increases the spread surface area of platelets where filamentous actin (F-actin) facilitates platelet spreading with filopodia extensions and lamellipodia protrusions [50]. Differential Interference Contrast (DIC) microscopy is an example of an imaging technique used to capture unlabelled adhered platelets (Figure 1.4*i*), and platelets undergoing filopodia extensions (Figure 1.4*ii*) and lamellipodia protrusions (Figure 1.4*iii*).

In spread and spreading platelets, actin rearrangements can be readily visualised using fluorescent microscopy techniques by fixing, permeabilising and labelling the actin cytoskeleton with fluorescently labelled Phalloidin or Lifeact [51]. Fluorescent labelling allows

the visualisation of structures such as actin nodules which arise during early spreading (Figure 1.4*iv*) [52,53]; actin filled filopodia extensions which have been implicated with searching and locating neighbouring platelets (Figure 1.4*v*) [54]; and actin stress fibres typical of fully spread platelets demonstrating lamellipodia protrusions which have been implicated in thrombus stability and wound covering (Figure 1.4*vi*) [53,54].

Impaired platelet spreading can be indicative of platelet-related disorders [55,56], and hence there remains not only a demand for real-time monitoring of actin structures in the event of platelet disorders, but also to investigate the off-target effect of drugs and inhibitors required for the treatment of other diseases which may directly impact on platelets.

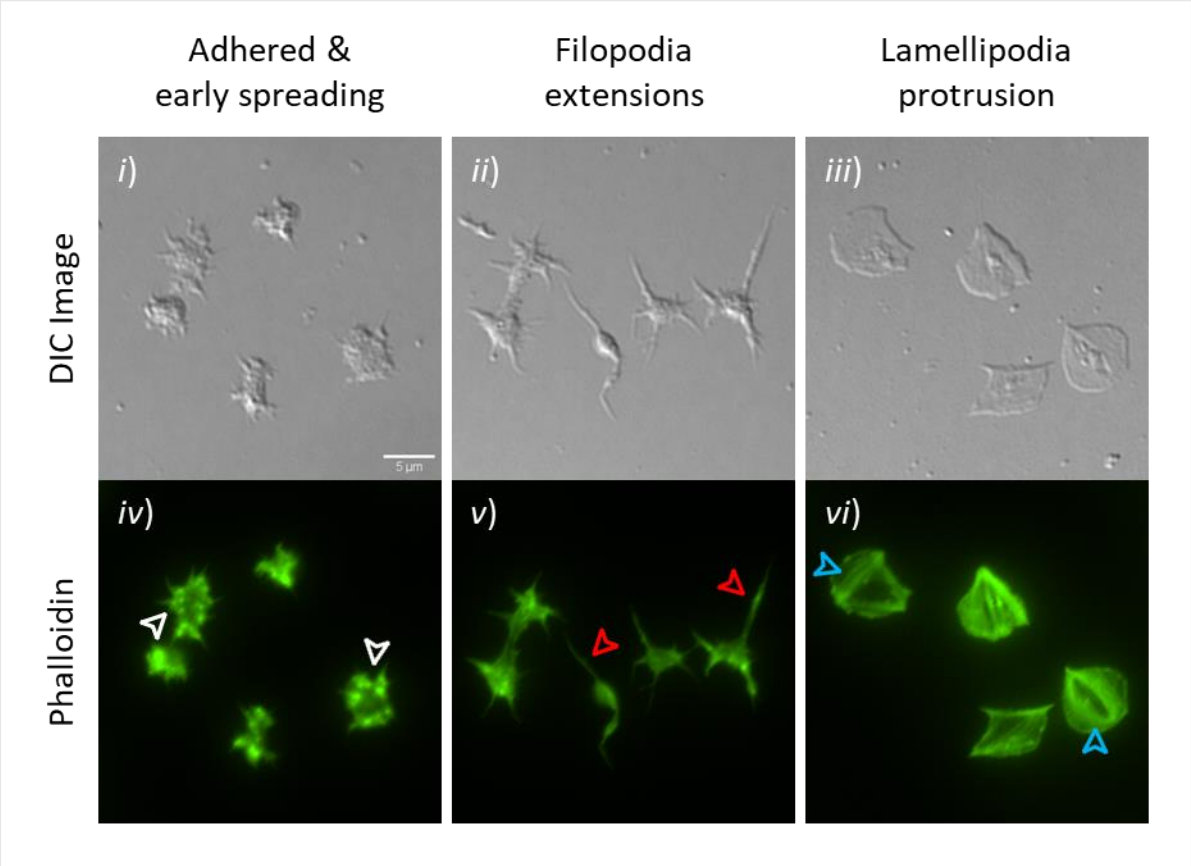

Figure 1.4 Platelet Spreading

Representative DIC images of fixed and permeabilised platelets provide an example of platelet spreading over a fibrinogen substrate. Platelets first adhere to a substrate and undergo early spreading (*i*), extend filopodia extensions (*ii*) and lamellipodia protrusions (*iii*). Corresponding phalloidin staining provides an example of the actin structures during spreading and spread platelets. During adherence and early spreading of platelets actin nodules can be detected (*iv*) (white arrows). Actin filament elongation is typical of filopodia extensions (*v*) (red arrows), and actin stress filaments are typical of lamellipodia protrusions (*vi*) (blue arrows). Scale bar represents 5 µm.

1.6 Importance of platelet research

Platelets are the main contributor to arterial thrombosis which is a leading cause of heart attack and stroke [57,58]. Platelets are also involved in venous thrombosis which is a leading cause of deep vein thrombosis (DVT) and pulmonary embolism (PE) [59]. Arterial and venous thrombi are structurally different. Arterial thrombi are rich in platelets and will form during injury, yet venous thrombi are typically rich in red cells and form despite absence of endothelial injury [60]. Since the pathophysiology of arterial thrombi and venous thrombi are different, they are subsequently treated differently. For those who are fortunate to survive a heart attack or a stroke, individuals are treated with drugs which supress platelet function (e.g., aspirin or clopidogrel) [61]. For those suffering with DVT or PE, individuals are treated with drugs which target the coagulation cascade [61].

Currently, heart and circulatory diseases cause a quarter of all deaths in the UK, equating to more than 460 deaths per day [62]. Over the past few decades, death rates due to CVD have declined. For example, 7 out of 10 heart attacks in 1960 were fatal, however now, 7 out of 10 individuals who suffer a heart attack survive [62]. This is partly attributed to advances in pharmacological drugs which are used to treat those living with CVD or have survived a cardiovascular event. However, there are the undesirable side effects of nuisance bleeding impacting approximately 37.5% of patients receiving anti-platelet therapies [63-65]. While therapeutics can effectively manage CVD in a large number of patients, there remains a subset of approximately 35% of patients who will succumb to another heart attack or stroke [66]. Either a large bleed, or indeed a second thrombotic event, will be fatal for some patients.

Furthermore, patients who present with co-morbidities, such as CVD and diabetes, respond inadequately to anti-platelet drugs. This is due to platelets of diabetic patients being hyperreactive such that platelet adhesion, aggregation, and activation are elevated [67,68]. High levels of procoagulant factors such as fibrinogen and vWF further exacerbate the condition [69,70].

It is also estimated that inherited platelet disorders, a heterogenous group of rare diseases which can cause severe bleeding, affect between 1 in 10^4 and 1 in 10^6 individuals worldwide; although the true prevalence currently remains unknown [71,72]. Inherited platelet disorders include inherited thrombocytopenia's where patients present with a low number of circulating platelets which can also be large, small or normal in size [72]. Inherited platelet function disorders, meanwhile, are characterised by dysfunctional platelets resulting from, for example, loss of membrane receptors (e.g., Glanzmann Thrombasthenia; defect of the integrin αIIbβ3, and Bernard-Soulier Syndrome; absence or nonfunction of GPIbα) or absence of platelet granules (e.g., Grey Platelet Syndrome; reduction or absence of α-

granules) [72,73]. Platelet disorders can also be 'acquired' later in life, for example Idiopathic Thrombocytopenic Purpura (ITP) where the immune system depletes circulating platelets, or due to medications which interfere with haemostatic efficacy [71].

Although advanced sequencing technologies are becoming more commonly applied in the clinical setting to detect inherited platelet disorders, it is moderate to life-threatening bleeding phenotypes which are more commonly diagnosed since they often require medical intervention, yet, many patients with a negligible bleeding phenotype often go undiagnosed for many years [72,74].

Understanding the molecular mechanisms which govern platelet function, therefore, is fundamental when understanding platelet response during both health and disease. Whilst elucidating undiscovered molecular mechanisms will allow identification of novel drug targets to better treat patients with cardiovascular related diseases, co-morbidities, and inherited and acquired platelet disorders.

1.7 Platelets and research limitations

Since platelets lack a cell nucleus, they have previously been stereotyped as a cell which lacks biosynthetic potential. This is because the transcription of DNA to RNA largely takes place in the nucleus of nucleated cells, leading platelet researchers to conclude that the platelet proteome consists of proteins obtained directly from the MK. Yet, recent reports suggest that gene expression in the platelet may be regulated by translational mechanisms as opposed to transcriptional mechanisms [75]. The translation of MK-derived messenger (m)RNA into a functional protein does not require nuclei driven mechanisms [75], providing platelets with a potential route for synthesising proteins.

Transfection approaches have included the electroporation and lipofectamine transfection of platelets with small interfering (si)RNA targeted to the glycolytic enzyme glyceraldehyde 3-phosphate dehydrogenase (GAPDH). The siRNA interferes with protein expression by causing the mRNA to be broken prior to translation. Several studies have demonstrated a reduction in GAPDH messenger RNA (mRNA) when compared to a scrambled siRNA over 24 hours [76,77]. However, although there was a reduction in GAPDH mRNA, too few platelets remained following cell sorting to determine GAPDH protein levels in these platelets, and platelet activation as a result of transfection was not investigated [76]. Moreover, while nucleic acids can be delivered into platelets and modify platelet gene expression, protein knockdown by this approach will not work if the proteins are stable, is only temporary, or is incomplete [78].

It has also been demonstrated that platelets can synthesise proteins such as actin, thrombospondin, fibrinogen, vWF, and glycoproteins (namely GPIb and integrin β3) [75,79,80]. For example, the surface expression of GPIIb/IIIa (αIIbβ3) measured by flow cytometry increased by 13% on day 7 and by 42% on day 10 of platelet concentrates stored at 22ºC. While western blot analyses found similar scientific conclusions where GPIIIa was increased by two-fold by day 7 of storage, and four-fold by day 10 of storage, not only indicating that biosynthesis of glycoproteins occurs in platelets, but also suggesting that GPIIIa protein synthesis could be functionally important for the duration of the platelet lifespan in the circulation [80]. Despite these recent reports, standard molecular biology methods used to physically study biological processes in nucleated cells remain difficult to apply to platelets.

Furthermore, due to the nature of platelets, and their role in haemostasis and thrombosis, platelets activate rapidly upon removal from the circulation due to the loss of inhibitory effects of nitrogen oxide (NO) and prostacyclin (PGI_2) [81]. This activation can make platelets challenging cells to work with. Careful platelet preparation is required to avoid artefactual platelet activation prior to treatment or functional analyses. For example, washed platelet methods allows the removal of the plasma environment which contains thrombin; an enzyme involved in the conversion of fibrinogen to stable fibrin during coagulation. The removal of such coagulation factors and other plasma components contributes to rested platelets. The addition of PGI_2, heparin, and apyrase can also help to reduce platelet activation during preparation [82]. PGI_2 acts on the prostaglandin I2 (IP) receptor on platelets which increases intracellular cyclic adenosine monophosphate (cAMP), a secondary messenger which inhibits platelet aggregation [83,84]. Heparins enhance the activity of the proteinase inhibitor antithrombin (AT), which causes a direct inhibition of thrombin amongst other coagulation factors [85]. While apyrase catalyses the hydrolysis of extracellular adenosine triphosphate (ATP) and adenosine diphosphate (ADP), preventing platelet activation since these extracellular molecules would normally interact with the purinergic receptors $P2Y_1$ and $P2Y_{12}$ on the cell surface of platelets, mobilising intracellular calcium stores and whose combined actions would lead to platelet aggregation [86,87].

Another limitation regarding platelet research is that platelets cannot be maintained in culture. A ready supply of platelets in research is often provided using daily blood donors. There have been, however, advances regarding *in vitro* platelet production derived from induced pluripotent stem cells (iPSCs) directed to the MK lineage [88-90]. These cells are derived from somatic cells which can be reprogrammed back into an embryonic-like pluripotent state, enabling the production of different cell types for therapeutic purposes [91].

However, *in vitro* production of MKs capable of generating large amounts of platelets, for both transfusion and platelet research, is still under optimisation [89,92]. In recent years, the yield of MK derived platelets *in vitro* has remained low with approximately <10 platelets/MK [93]. In contrast, it is estimated that one *in vivo* MK can produce up to 1000 – 2000 platelets [93], while approximately 300 x 10^9 platelets are currently administered as a single transfusion dose [93,94]. Despite these low yields, *in vitro* MK derived platelets demonstrated similar surface expression of platelet receptors including the GPIIb/IIIa, GPIb, GPIX, GPIIa and GPVI when compared to fresh blood derived platelets [89]. Furthermore, MK derived platelets were able to adhere and spread over fibrinogen, aggregate in response to agonists, and degranulate such that P-selectin could be identified on the surface of MK derived platelets during thrombus formation [89].

More recently, MK derived platelets produced using bioreactor systems have demonstrated a two-fold increase in platelet production per MK by mimicking the bone marrow environment [92]. A bioreactor supports proplatelet formation by firstly increasing the surface area for each MK to generate proplatelet extensions in the three-dimensional environment, and secondly, by creating shear stress which induces platelet release from proplatelet extensions [93,95,96].

These platelets have demonstrated normal platelet function *in vitro* when assessed by thrombus formation, and also *in vivo,* where clinical benefit was described during the transfusion of *in vitro*-derived platelets into thrombocytopenic mice [92]. Despite these recent advances, current limitations are associated with platelet yield, and the equipment and cytokine requirements to achieve this remains costly and involves specialised expertise.

Alternatively, gene editing methodologies have been employed to edit human iPSCs (hiPSCs), such as by clustered, regularly interspaced, short palindromic repeats (CRISPR) and CRISPR-associated protein (CRISPR/Cas9) [97]. However, if gene editing by this method impacts on MK differentiation and maturation then this approach cannot be utilised to directly understand platelet function. As a result, the combination of limitations mentioned above have resulted in a greater use of animal models, particularly mouse models, in platelet research.

1.8 Mouse models and platelet research

An International Society of Thrombosis and Haemostasis (ISTH) survey identified at least 78 research groups in at least 11 different countries which used mouse models for platelet research [98]. For example, genetically modified mice, where genes of interest have been disrupted in the mouse genome, allows platelets which are deficient in specific proteins to be

researched. It is possible for target genes to be disrupted at the conventional level where a gene is knocked out in all tissues in the animal, while a conditional knock-out is tissue specific and permits where and when a target gene is disrupted by rendering genes of interest in specific cell types and tissues as inactive due to 'floxing' [99]. This is the introduction of specific sequences which flank either side of a genomic region of interest with two lox sites (flox) and can initiate a deletion, inversion or translocation of the floxed locus when crossing a floxed mouse with a *Cre* mouse containing a Cre recombinase transgene [99,100]. A similar breeding method can be employed to generate inducible mouse models which, conversely, permits the activation of genes of interest in specific cells and tissues [101,102]. In addition to manipulating the mouse genome, arterial thrombosis mouse models are also regularly used in platelet research, where vascular damage is induced by ferric chloride, laser, mechanical or by photochemical injury [98,103]. Such models are widely used to study *in vivo* thrombosis formation permitting real-time platelet-platelet and platelet-vessel interactions [98,103].

The use of genetically modified mice and different injury models permits the research of complex mechanisms contributing to thrombus formation that cannot be performed in humans. Furthermore, mouse platelets have many similarities to human platelets. Similarities include the storage of proteins such as vWF, P-selectin, and surface receptor GPIIb/IIIa (αIIbβ3), which, similar to human, are compartmentalised within the α-granules [104]. Platelet formation observed in murine models also mimics processes normally found in humans; namely proplatelet formation and MK maturation reaching the same modal ploidy level in both human and mouse (16N) [104,105]. Moreover, mouse platelets have mirrored the phenotype of known human platelet disorders during the manipulation, or knockout, of common platelet receptors [105]. A genetic deletion of the mouse gene encoding GPIbα, which is known to cause Bernard-Soulier syndrome in humans, recapitulated the giant platelet and low circulating platelet count associated with the human syndrome [105].

Despite the similarities, there are several differences where mouse platelets differ from human platelets. As expected, mouse platelets are smaller at 1-2 µm in diameter, when compared to human platelets. Mouse platelets also have a shorter circulating life span of approximately 4 days, and an increased circulating platelet count of 1000 –1500 $x10^3$ platelets/µL when compared to human subjects [104,105]. Mouse platelets also differ in the expression of some cell surface receptors. Most notably the expression of different thrombin receptors (protease activated receptors, PARs); mouse platelets express PAR3 and PAR4, while human platelets express PAR1 and PAR4 [106]. Furthermore, sequence differences between mouse and human platelet receptors, such as GPVI, mean that humanised mouse models are required to assess anti-GPVI compounds [107]. Mouse platelets also lack

expression of the low affinity immune receptor FcγRIIa. FcγRIIa is involved in regulating and executing antibody mediated responses, suggesting a role for human platelets during inflammation and immunity, but not mouse platelets [108,109]. As a result of these differences, findings generated using mouse models do not always translate well to humans.

As well as biological differences, there are stark differences regarding inter-lab standardisation and transferability which directly impacts on reproducibility of results. For example, Seok et al (2013) describe poorly correlated immune responses between human and mouse [110]. Yet, Takao et al (2015) reanalysed the same data and presented a complete disagreement in results [111]. There were several differences to the analysis methods applied which directly impacted on scientific conclusions obtained [111]. As well as standardisation, inter-species and habitat differences can directly impact on translatability of results too. A mouse model should therefore be appropriate for the biological question being asked, while husbandry conditions may impact on mouse phenotypes [112]. For example, mice housed in groups or individually may be impacted by stress as a result of aggression or isolation respectively [113], while temperature has been shown to impact cardiovascular parameters [114]. Furthermore, commonly used anaesthetics such as ketamine are known to directly impact on platelet function [115-117].

Although mouse models have vastly contributed and advanced understanding regarding platelet function and MK maturation in the field, there remain functional consequences due to biological and inter-laboratory differences which may bring about implications for new drug development. For instance, the systemic reviews by O'Collins et al (2006) [118] reported 1,026 candidate stroke treatments trialled in mouse models, amounting to 8,500 experiments in 3,500 publications (1957 - 2003), yet none were successful as human pharmacological stroke treatments [119]. Furthermore, only 21% of cardiovascular treatments found to be effective in animal models were successfully replicated in clinical trials [120]. These statistics highlight that an alternative experimental system to animal models may be advantageous to the field since many aspects of platelet research consequently remain poorly understood.

1.9 Project aim

Since standard molecular biology methods used to study nucleated cells cannot be applied directly to platelets, platelet research has resulted in a greater use of mouse models. However, differences between human and mouse platelets mean that findings generated do not always translate well to human. Consequences of these differences include impacting on

drug development targeting platelets and mean that many aspects of platelet biology remain to be fully elucidated.

This project, therefore, aims to use fusogenic liposomes as a delivery vehicle to deliver cargo directly into the cytoplasm of isolated human platelets *in vitro* to investigate biological processes which may govern platelet function. Fusogenic liposomes comprise a unique fusogenic nature meaning they can spontaneously fuse with the membrane of a cell [121]. Furthermore, they are biocompatible with the phospholipid bilayer of a cell membrane and become an extension of the cell membrane upon fusion [121].

If successful, this novel platform will allow human platelets to be researched *in vitro* and mechanisms observed in real-time, directly reducing the need for mouse models in cardiovascular research.

1.10 Alternative delivery methods to date

To date, there have been a variety of delivery carriers which have attempted to deliver cargo directly into mammalian cells, including platelets. These delivery carriers have a range of uptake mechanisms and are summarised below.

1.10.1 Cell Penetrating peptides

Cell penetrating peptides (CPPs) have been used to deliver cargo by internalisation into the cell cytoplasm (Figure 1.5A) [122]. CPPs were first discovered when it was recognised that the transactivation TAT-protein encoded by the human immunodeficiency virus (HIV) could penetrate cells and activate specific genes [123]. They are short peptides which have the capacity to cross cell membranes with minimal toxicity [124]. CPP mediated cargo delivery is achieved by either covalent binding of the cargo using disulphide or amine bonds, or by physical complexation via electrostatic or hydrophobic interactions achieved by bulk-mixing [125]. Yet the physiochemical properties of these peptides, and their cargo, can impact on the binding ability of the peptide-cargo complex, and can greatly hamper the efficiency of cellular uptake [122]. Published data suggests that the majority of CPP uptake is via the energy-dependant mechanism of endocytosis, but despite localisation within a cell's cytoplasm, CPPs can encounter lysosome degradation due to prolonged containment within endosomes (Figure 1.5A) [122,124].

CPPs have been used to study platelet receptor function. For example, David et al (2006) used a CPP approach to evaluate the role of the GPIbα intracellular domain in platelets [126].

The GPIbα cell surface receptor is part of the GPIb-V-IX complex responsible for binding vWF at sites of endothelial injury [127]. Significantly decreased agglutination and adhesion in response to vWF was observed when using a CPP targeted to the intracellular domain ranging from amino acids 557 to 569, while a scrambled peptide decreased adhesion with lower efficacy [126]. However, it is not known if the peptide impacted on distribution or clustering of the receptor, which would not affect the binding capacity of the ligand, and could therefore be responsible for the decreased signalling on the immobilised matrix [126].

Additionally, Dimitriou et al (2009) demonstrated platelet inhibition to the integrin αIIbβ3 when utilising a TAT-derived CPP conjugated to two sequences of interest on the β3 cytoplasmic tail [128]. The two separate regions of interest were specifically targeted since they are responsible for inside-out and outside-in signalling. On activated platelets, the calcium-dependent association of αIIb and β3 binds several adhesive proteins including vWF on the exposed endothelium, and fibrinogen, which acts as a bridging molecule with neighbouring platelets [129]. They were able to identify inhibition to integrin association and subsequent activation of αIIbβ3, which therefore inhibited fibrinogen binding and platelet aggregation.

Furthermore, although both David et al (2006) and Dimitriou et al (2009) identified that CPPs could penetrate the cell membrane of platelets, adherence of platelets to a vWF substrate was assessed. David et al (2006) identified a reduction in adhesion having targeted the intracellular domain of GPIbα, while Dimitriou et al (2009) captured platelets over vWF-coated slides to assess CPP internalisation. However, despite vWF being a mediator of platelet adhesion, under static conditions, adherence to vWF is not known to demonstrate high levels of adherence or platelet spreading [130-132]. Conversely, Cardo et al (2015) did describe a negative impact to platelet viability when using a TAT-derived CPP to deliver fluorescently tagged Lifeact into platelets, specifically, 50% of platelets did not spread as expected over a fibrinogen substrate when compared to other delivery techniques [51].

Neither example using CPPs to deliver cargo directly into platelets completely ruled out endocytic uptake. This may explain the need for high concentrations of CPP conjugates to identify a biological effect. In addition, recent literature reviews of CPPs state that the process is poorly understood, delivery is likely a result of endocytic uptake, CPPs can negatively impact the potency of conjugated cargo, and non-specifically impact normal cellular function [122,124,125].

1.10.2 pH low insertion peptide

Another method which delivers compounds intracellularly without permeabilisation is the pH low insertion peptide (pHLIP) (Figure 1.5B) [133]. Research has demonstrated the successful intracellular delivery of cargo directly into HeLa cells and cancer cells using the pHLIP peptide [134,135]. In acidic conditions (pH ≤6.5) pHLIPs form stable, monomeric transmembrane alpha-helixes as a result of the protonation of two aspartate residues, leading to the C-terminal entering directly into the cytoplasm of cells [133]. This pH-selective delivery offers a promising treatment approach to diseases demonstrating low-pH of the extra-cellular environment such as tumours, tissue impacted by stroke, and atherosclerotic lesions, where current treatments may have off-target effects [134].

Furthermore, Davies et al (2012) demonstrated successful peptide delivery of luminescent gold nanoparticles into platelets using this pHLIP delivery peptide [136]. This technique specifically uses gold (Au) nanoparticles to scaffold europium luminescent (EuL) probes, as well as the delivery peptide (pHLIP), to create a multiprobed pHLIP·EuL·Au complex. This complex has been shown to rapidly deliver the luminescent nanoparticles into human platelets *in vitro* upon lowering of physiological pH to ≤6.5 [136]. Data demonstrated that following delivery of the pHLIP·EuL·Au complex platelet function remained unchanged with platelets able to spread onto a fibrinogen coated surface. In contrast to CPPs, where delivery can be impaired by endocytosis, the pHLIP delivery method can deliver peptides directly to the cytoplasm of cells. More recently, there has been further advances in the release of cargo from the pHLIP carrier peptide by disulphide bond cleavage due to the reducing environment of the cell's cytoplasm [49]. Therefore, conjugated fluorescently labelled Lifeact, a small 17-residue cell impermeable peptide, has been delivered into human platelets using pHLIP to observe real-time F-actin dynamics. However, for reasons unknown, live cell imaging of actin dynamics in human platelets were not comparable to transgenic mouse models expressing a fluorescent fusion of Lifeact [49].

There remains continued research in developing new microscopy methods to visualise F-actin in human platelets *in vitro*, especially since imaging of actin dynamics have mostly been achieved by injection of fluorescently labelled actin which is not suitable for platelets [48]. However, a recently presented cell permeable fluorogenic silicon-rhodamine (SiR) probe has been conjugated to the ligand desbromo-desmethyl-jasplakinolide (SiR-actin), which binds with high affinity to filamentous actin (F-actin) in living cells, including platelets [137,138]. These SiR probes are particularly suited to cells, such as platelets, which are difficult to transfect [50]. Nevertheless, many intracellular targets of interest will not have cell permeable cargos, and

despite the successful delivery of gold nanoparticles, the low pH required for pHLIP insertion could be a limitation by impacting on or impairing platelet function [139].

1.10.3 Myristoylated (myr) carriers

A myristate is a saturated carboxylic acid containing 14 carbons in its chain. Myristate has been implemented in the regulation of protein-protein interactions, the trafficking of proteins, and plasma membrane association [140]. Lipid modifications such as the attachment of a myristoyl group increases protein–protein interactions and can lead to subcellular localisation of those myristoylated proteins [140]. Myristoylation was, therefore, investigated as a means to deliver peptides directly into living cells where a myristoylated fluorescent peptide was delivered directly into a B lymphocyte cell line [141]. This technique was subsequently applied to platelets during the delivery of fluorescently labelled Lifeact (Figure 1.5C) [51].

Cardo et al (2015) conjugated fluorescently tagged Lifeact to a myr carrier by disulfide-bond-based linkers (Myr-S-S-Life). Lifeact cleavage was possible upon contact with the reducing environment of the cytoplasmic environment and delivered intracellularly [51]. Platelets were incubated with Myr-S-S-Life prior to spreading and fixation and compared to an uncleavable derivative [51]. Normal spreading was observed, and F-actin structures such as filopodia and lamellipodia were identified as a result of Lifeact delivery by Myr-S-S-Life [51]. No actin labelling was detected when observing the non-cleavable derivative. However, despite the labelling of actin structures in fixed platelets, the delivery of Lifeact by the Myr carrier into live platelets was not satisfactory [51].

Palmitoylation, a similar concept to myristoylation, where a palmitate group was attached to peptides derived from the intracellular G-protein-coupled receptor (GPCR) of protease-activated receptor-1 (PAR1) was also investigated with potential to deliver anti-platelet drugs [142]. Covic et al (2002) describe effective inhibition to PAR1-dependent platelet aggregation by extracellular agonists when selectively blocking an intracellular domain using palmitoylated peptides [142].

Although both examples identify interactions of cargo with intracellular targets, there was no extensive investigation on the possible impact of these approaches on platelet function, and the cleaving of Lifeact cargo was only detected in fixed platelets. Furthermore, the time of delivery and the detailed mechanism of myr membrane-translocalisation currently remains poorly defined.

1.10.4 Liposomes

Liposomes, also known as phospholipid vesicles, are another example of a delivery carrier which has been used to deliver cargo into mammalian cells (Figure 1.5D). Liposomes consist of amphiphilic molecules; that is, molecules containing a hydrophilic head (polar) and a hydrophobic tail (non-polar) [143]. The physiochemical properties of these amphiphilic molecules means that they self-assemble into vesicles when dispersed into aqueous solutions [143]. Noncovalent interactions such as Van der Waals forces hold the hydrophobic tails together, while hydrogen bonding binds the hydrophilic heads with water, ensuring the lipid vesicles are held together [144]. Their composition makes them an attractive biological tool since they are naturally inert and have low inherent toxicity [145]. Due to the biocompatibility and biodegradability of liposomes, they were the first drug delivery system which was approved clinically, and includes the delivery of antitumour drugs Doxil® and Myocet® [146]. Liposomes have worked well as drug delivery carriers since they protect the encapsulated drug from biological processes such as enzyme degradation or metabolism [146]. They can also be targeted to specific tissues or cells by ligand mediated targeting [146]. Ligand-targeted liposomes can be adapted to contain monoclonal antibodies or receptor ligands which can interact with specific antigens or receptors located on the surface of target cells [146,147]. The benefit of ligand-targeted delivery also minimises drug toxicity to healthy tissue yet has the potential to deliver the desired cytotoxic effects to diseased areas [143,146].

Huang et al (2019) incorporated a peptide sequence of fibrinogen into liposomal carriers to selectively deliver tissue plasminogen activators (tPA) directly to a thrombus [148]. Currently, tPA is the most widely used intravenous strategy for clot lysis in patients presenting with thrombotic stroke, however, side-effects include bleeding [149]. These therapeutics work by catalysing the conversion of plasminogen to plasmin; a major enzyme associated with fibrin clot breakdown [149]. The incorporated fibrinogen sequence into fluorescently labelled liposomes was therefore able to bind the αIIbβ3 integrin on the surface of activated platelets directly at the thrombus site where fluorescent labelling was observed [148]. When the αIIbβ3 integrin was blocked by eptifibatide, there was little detection of fluorescent labelling by the fibrinogen tagged liposomes [148]. It was therefore thought that the direct association of the fibrinogen tagged liposomes interacting with the αIIbβ3 integrin increased delivery of tPA directly at the thrombus site [148]. Huang et al (2019) describe tPA delivery as a result of liposome membrane destabilisation due to direct interactions of the fibrinogen sequence coating with activated platelets. However, the mechanism of tPA release at the thrombus site remains to be elucidated, and to what extent activated platelets control the release of tPA is also not fully understood.

The main uptake method of standard liposomes for intracellular drug delivery is similar to that of CPPs, where the majority of uptake is thought to be by endocytosis (Figure 1.5D) [150]. Adsorption is also thought to be just as likely to occur, whilst membrane fusion and bilayer component exchange are actually considered much rarer uptake methods [145]. Liposomes, therefore, are likely to encounter endocytosis degradation mechanisms just like CPPs, meaning that cargo could be degraded before it reaches the cytoplasm. Furthermore, the uptake of liposomes by a ligand targeted approach, despite improved drug delivery to diseased cells, is also considered a majority endocytic uptake method.

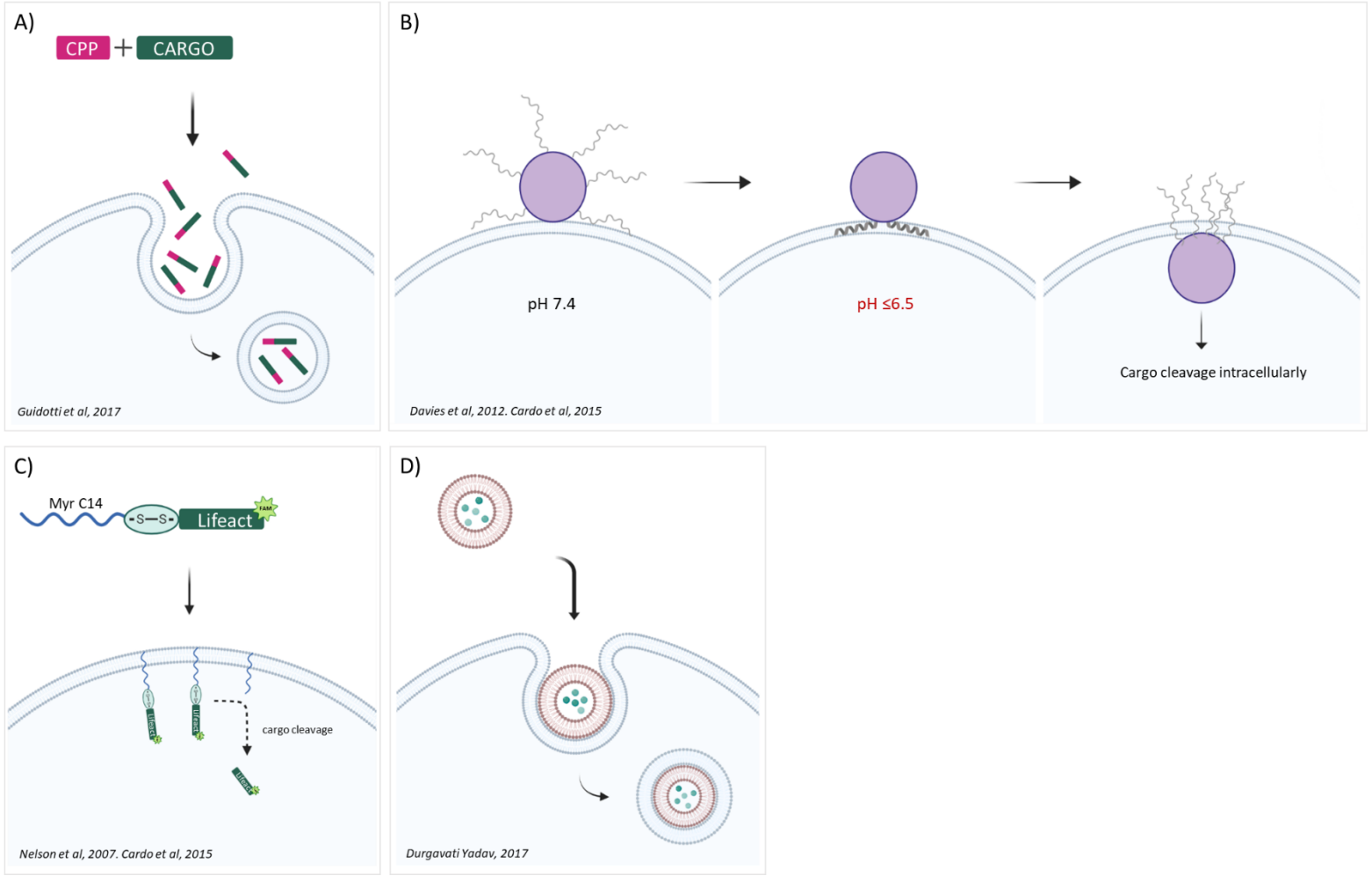

Figure 1.5 Cargo delivery methods

Graphics illustrate the concept of cargo delivery by cell penetrating peptides (CPPs) where uptake of a CPP-cargo complex is typically by endocytosis (A). The pH low insertion peptide (pHLIP) delivers cargo intracellularly during acidic conditions as a result of monomeric transmembrane alpha-helixes which transports cargo intracellularly (B). The myristoylated (myr) carrier can bind cargo by disulphide bonds, where protein–protein interactions are thought to be increased due to the myristoyl group supporting trafficking through the cell membrane,

resulting in cargo delivery by disulphide bond cleavage due to the reducing environment of the cell cytoplasm (C). Phospholipid liposomes consist of a lipid bilayer similar to that of a cell membrane, where cargo can be loaded and can reside in the liposome lumen or the phospholipid bilayer, yet uptake is typically thought to be by endocytosis (D). Schematics created with biorender.com.

1.10.5 Fusogenic liposomes

Given the biological potential that previously discussed delivery methods have demonstrated, this project will focus on the delivery of cargo directly into platelets using fusogenic liposomes. Fusogenic liposomes consist of amphiphilic phospholipids similar to standard liposomes, meaning that they are biocompatible with the phospholipid bilayer of cell membranes. They have previously facilitated the delivery of water-soluble cargo directly into cells [121]. A dried lipid film comprising amphiphilic phospholipids can be reconstituted using water soluble cargo (Figure 1.6A*i*). The cargo becomes encapsulated within the lumen of fusogenic liposomes as they spontaneously form into vesicles due to the hydrophobic and hydrophilic interactions of the lipids (Figure 1.6A*ii*). In contrast to standard liposomes, fusogenic liposomes comprise a unique fusogenic nature allowing spontaneous fusion directly with the membrane of a cell (Figure 1.6A*iii*), resulting in an extension of the cell membrane, and subsequent release of cargo directly into the cell's cytoplasm (Figure 1.6A*iv*) [121].

Csiszár et al (2010) describe that for a successful cellular fusion to occur, the fusogenic liposomes must contain neutral lipids, cationic lipids and lipids modified by an aromatic group [151]. Although the full mechanism of cellular fusion remains to be fully elucidated, it is thought that the synergistic interactions of lipids containing the above characteristics result in a successful fusogenic mixture [151]. In particular, the cationic lipids provide an overall positive charge to the vesicles which, due to attractive forces, brings the fusogenic liposomes into close proximity with the overall negative charge of a cell (Figure 1.6B*i*) [151,152]. While lipids containing an aromatic group, a planar cyclic structure, containing a heteroatom with high electronegativity, such as oxygen or nitrogen, converts vesicles to a universal fusogenic method of cellular uptake [151]. This is thought to be as a result of positively charged lipid and aromatic lipid interactions causing local dipoles and cell membrane instabilities [151]. It is thought that these instabilities first result in a hemifusion between the membrane of a fusogenic liposome and a cell membrane (Figure 1.6B*ii*) [153]. Phospholipid bilayer reorganisation results in full membrane fusion (Figure 1.6B*iii*).

Published literature has demonstrated successful delivery of cargo into several different cell lines using fusogenic liposomes as a delivery vehicle [121,154,155]. Kube et al (2017) attempted to deliver a range of differently sized (2.3 kDa, 27 kDa and 240 kDa), and differently charged (zeta potential range -30mV to +15mV) peptides and proteins into mammalian cells using fusogenic liposomes [121]. The zeta potential of the fusogenic liposome carriers remained a constant at +75 ± 5 mV, and intracellular delivery of proteins was confirmed using fluorescence microscopy and flow cytometry [121].

Kube et al (2017) reports that fusogenic liposomes can deliver proteins efficiently into mammalian cells with no limitation regarding molecular size. However, the repulsive charges of a positively charged cargo and the positively charged fusogenic liposomes prevented vesicle formation; identifying that cargo charge can hinder vesicle formation [121]. Yet, attracting electrostatic charges of a negatively charged cargo and the positively charged fusogenic liposomes resulted in efficient formation of cargo containing fusogenic liposomes [121]. Subsequently, upon efficient fusion of fusogenic liposomes to a cell membrane, non-specific and specific fluorescently labelled proteins or peptides were directly transferred into mammalian Chinese hamster ovary (CHO) cells. Furthermore, Kube et al (2017) reports successful delivery of the fluorescently labelled Lifeact-FITC peptide directly into rat cardiac myofibroblasts where fluorescently labelled actin filaments were identified by microscopy post fusion [121]. Fusogenic liposomes, therefore, have shown promising potential to be superior to other previously identified intracellular delivery methods by avoiding endosomal uptake or cargo degradation and the need for a pH dependent mechanism of delivery. Their natural composition means cell toxicity is minimised, while previous studies have demonstrated nearly 100% labelling efficiency and rapid fusion times of 10-15 minutes [121].

Here, it is proposed for the first time, to apply this method of cargo delivery to human platelets, where fusogenic liposomes can be utilised to deliver cargo directly into the cytoplasm of human platelets enabling intracellular mechanisms and dynamics to be investigated in real time. The benefits of delivering cargo directly into human platelets in real time are that immediate feedback on intracellular molecular mechanisms is achieved, as opposed to complications as a result of compensatory mechanisms where different pathways or proteins in a cell can compensate for each other as a result of functional overlap [156]; a caveat of using transgenic mouse models. Also, possible translational issues arising as a result of findings from genetically modified mouse models with known differences would be removed. This approach also represents a 3Rs (Replacement, Reduction and Refinement) reduction approach which may result in a decrease in the number of mouse models required in platelet research.

Successful cargo delivery will enable opportunities to investigate intracellular signalling pathways and proteins of interest. In particular, the delivery of labelled fragment antigen-binding (Fab) regions (Fab fragments) against proteins of interest would enable single molecule tracking (SMT), which is a method for imaging and tracking single molecules conjugated to a fluorescent probe [157]. SMT has become a valuable research tool in cell biology as it allows single molecule behaviours to be studied. This technique provides real-time quantitative data specifically on molecule kinetics and locations, such as where they bind, when they disengage, and where they cluster within the cell [157,158]. A current challenge

of the SMT technique surrounds the delivery of labelled molecules past the intact cell membrane of the human platelet [159]. Therefore, loading fluorescently labelled Fab fragments inside the lumen of fusogenic liposomes, where fusion would result in cargo release into the platelet cytoplasm, would directly overcome this current limitation.

In addition, there is also the potential to investigate the depletion of specific proteins by antibody-mediated protein depletion. This technique specifically takes advantage of an E3 ubiquitin ligase, **TRI**partite **M**otif-containing **21** (TRIM21). Cytosolic TRIM21 can recognise and rapidly bind to incoming antibody-bound pathogens with high affinity via the antibody Fc domain [160,161]. The TRIM21 antibody-bound-pathogen complex then recruits the ubiquitin-proteasome system by catalysing ubiquitin, targeting the complex to the proteasome for rapid proteolytic degradation [160,162]. Therefore, Clift et al (2017) repurposed the TRIM21 mechanism, which is widely expressed in varied cell types, to establish a method to degrade endogenous proteins named Trim-Away [162].

Trim-Away is a novel technique successfully used in mammalian cells to acutely degrade intracellular proteins at the protein level instead of prior genetic or transcriptional modifications [162]. This offers the potential for proteins of interest to be studied in a wide range of cells, including those where DNA and RNA techniques are limited [162], such as platelets.

Trim-Away has successfully targeted 9 different subcellular proteins including membrane-anchored, chromatin bound and nuclear bound, without degradation to non-targeted proteins or proteins in close spatial proximity [162]. Furthermore, the Trim-Away technique has since been used to successfully degrade proteins in zebrafish embryos [163], mouse embryos [164], and xenopus embryos [165], to allow protein function during embryogenesis to be studied. In contrast to other previously used methods such as gene silencing, the acute nature of Trim-Away drastically reduces the impact of cellular compensatory mechanisms which can incur phenotypic changes [162]. Compensatory mechanisms which can alter protein phenotypes are a common phenomenon, presenting a caveat when employing genetically modified animal models [166]. Trim-Away, therefore, allows specific protein function to be observed acutely and in real time [162].

The cellular machinery, TRIM21, required to support the use of Trim-Away is present in platelets with an estimated copy number of 2,200 copies per platelet [46]. Furthermore, platelets have been shown to express the machinery for ubiquitination of proteins including a functional proteasome [167-169]. There are also the added benefits of rapid protein degradation times, and a range of commercially available antibodies. Making this a promising method which could be implemented in platelet research upon the delivery of whole antibodies by

fusogenic liposomes (Figure 1.7). Although the expression level of TRIM21 in the platelet may be a limiting factor for abundantly expressed proteins of interest, this may also be overcome by co-administration of recombinant TRIM21 [170], using fusogenic liposomes as a delivery vehicle.

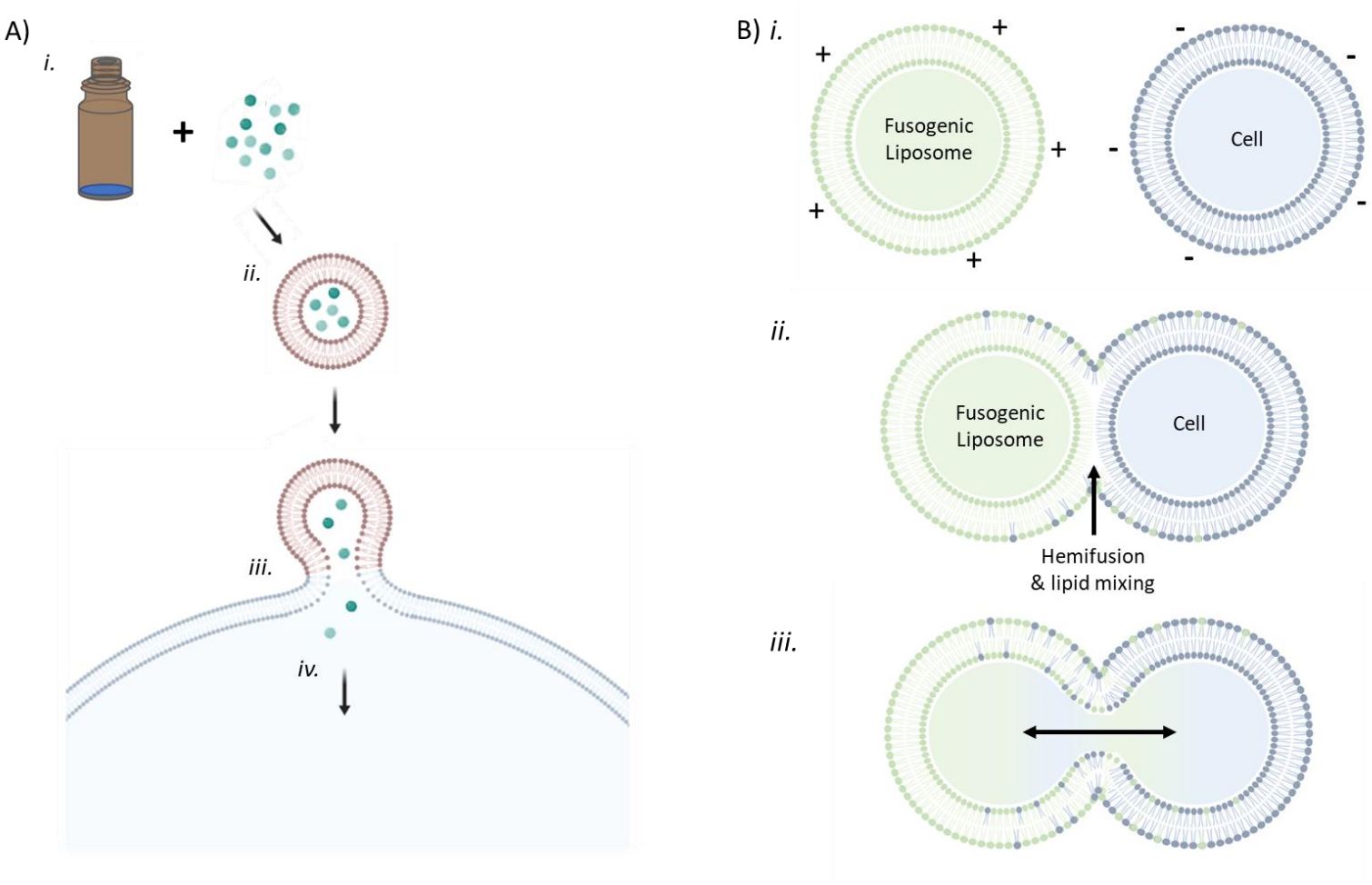

Figure 1.6 Fusogenic Liposome Fusion

Schematic illustrates the concept of resuspending a dried lipid film in water soluble cargo (A*i*) to encapsulate cargo in the lumen of fusogenic liposomes (A*ii*) prior to fusion (A*iii*) and the subsequent delivery of cargo intracellularly (A*iv*). Positively charged fusogenic liposomes are attracted to the overall negative charge of a cell (B*i*.). Local dipoles cause instabilities in the phospholipid bilayer of both membranes allowing

hemifusion (B*ii*.). Phospholipid reorganisation leads to full fusion, where phospholipids from each membrane can diffuse laterally and lumen contents between the fusogenic liposome and the cell can mix (B*iii*.). Schematic not to scale (B). Schematics created with biorender.com.

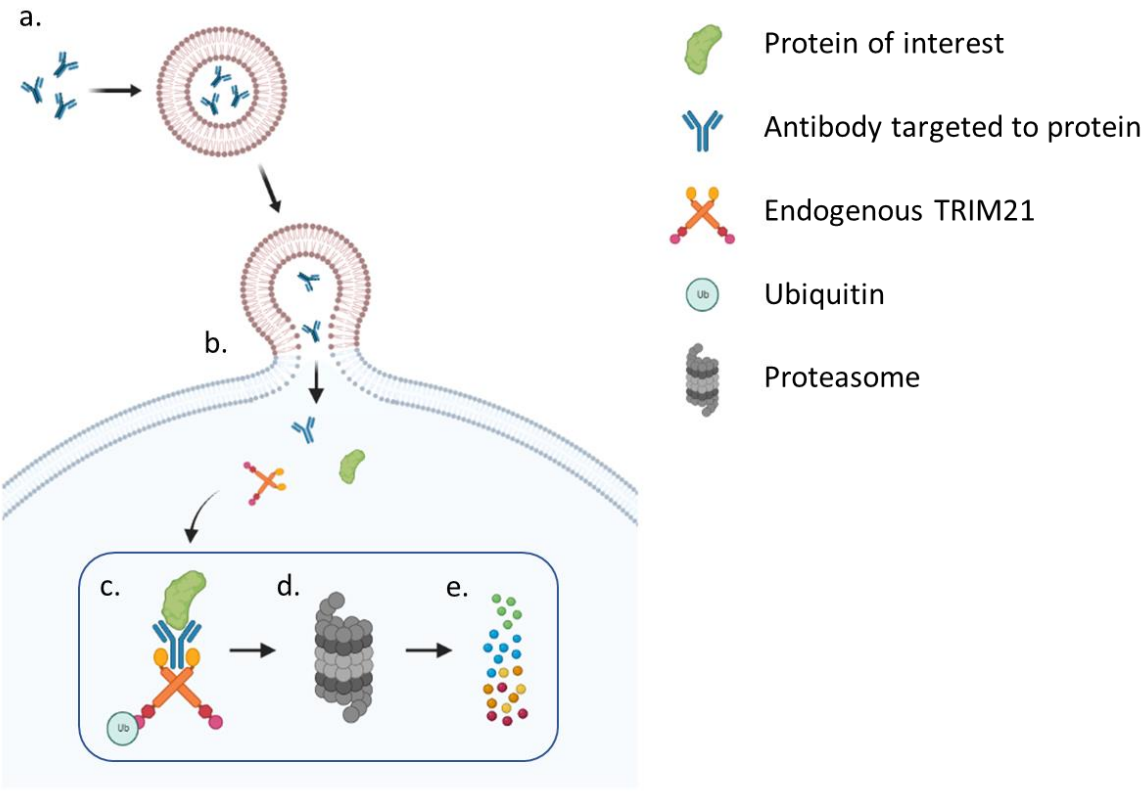

Figure 1.7 Trim-Away and platelets

Schematic illustrates the concept of antibody delivery by their encapsulation as cargo inside fusogenic liposomes (a). Fusion with the cell membrane of platelets allows antibody delivery into the cytoplasm which can bind to the protein of interest (b). Cytosolic, or recombinant, TRIM21 can bind with high affinity to the antibody Fc domain where, upon antibody engagement, TRIM21 is ubiquitinated (Ub) (c). The ubiquitination of TRIM21 targets the TRIM21-antibody-protein complex to the proteasome (d) for rapid proteolytic degradation (e). This may result in the knock down of a protein of interest directly in the platelet. Schematic created with biorender.com, and adapted from Clift et al (2017) [162].

1.11 Aims and hypotheses

In the first instance, a commercial source of fusogenic liposomes will be used to label platelets (Fuse-It-Green, Benaig, Germany). This will be used as a proof of principle to investigate compatibility of fusogenic liposomes with human platelets to determine if fusogenic liposomes can be fused with platelets without impacting normal platelet function. A commercial source of fusogenic liposomes is favourable as shared methods and commercial resources would be available to other platelet research laboratories.

The aims of this thesis include:

- Design and implement a convolutional neural network (CNN) to automate platelet spreading analyses. Assessment of platelet morphology is used to assess platelet interactions with substrates and will be used to determine the impact fusogenic liposomes have on platelet spreading.
- Develop and optimise a method of labelling platelets using fluorescently labelled fusogenic liposomes and assess any impacts fusion has on normal platelet function.
- Develop and optimise a method to deliver a range of peptide and protein cargo directly into the cytoplasm of platelets using fusogenic liposomes.

This thesis hypothesises that:

- A CNN can automate platelet spreading analyses.
- Platelets can be labelled with fluorescently labelled fusogenic liposomes without impacting normal platelet function.
- Fusogenic liposomes can deliver cargo such as small peptides and proteins directly into the cytoplasm of platelets.

2. Materials and methods

2.1 Materials

2.1.1 Agonists, inhibitors, and protein substrates

Name	Type (agonist / inhibitor / protein substrate)	Working conc^{n} / dilution	Manufacturer
Synthetic cross-linked collagen-related peptide (CRP-XL) $[GCO[GPO]_{10}GCOG\text{-}amide]_3$	Agonist Protein substrate	3 µg/mL 10 µg/mL	CambCol Laboratories, Cambridge, UK
Type 1 collagen	Agonist	3 µg/mL	Nycomed, Munich, Germany
Thrombin receptor-activating peptide-6 (TRAP-6)	Agonist	15 µM	Sigma-Aldrich, Gillingham, UK
Thrombin	Agonist:	Annexin V assay: 0.05 U/mL Aggregation: 0.05 U/mL Spreading: 0.1 U/mL	Roche via Sigma-Aldrich, Gillingham, UK
Dasatinib	Inhibitor (Src)	10 µM	Sigma-Aldrich, Gillingham, UK
Ibrutinib	Inhibitor (BTK)	1 µM	Sigma-Aldrich, Gillingham, UK
PRT-060318 (PRT)	Inhibitor (Syk)	5 µM	Sigma-Aldrich, Gillingham, UK
Human Fibrinogen	Protein substrate	100 µg/mL	Sigma-Aldrich, Gillingham, UK
von Willebrand factor (vWF)	Protein substrate	10 µg/mL	Sigma-Aldrich, Gillingham, UK

2.1.2 Antibodies, isotype controls and fluorescently labelled imaging peptides and proteins

Antibody	Type	Host	Species Reactivity	Clone	Application	Conc^{n} / dilution	Manufacturer
Phycoerythrin and cyanine 5 (PE-Cy5) conjugated Mouse Anti-human CD62P	Monoclonal antibody	Mouse	Human	AK-4	Flow cytometry	0.2 µg/mL	BD Pharmingen, BD Biosciences, Wokingham, UK.
Phycoerythrin and cyanine 5 (PE-Cy5) conjugated Mouse Anti-human IgG1 $_{K}$ Isotype control	Monoclonal antibody	Mouse	Human	MOPC-21	Flow cytometry	0.2 µg/mL	BD Pharmingen, BD Biosciences, Wokingham, UK.
Phycoerythrin (PE) conjugated Mouse Anti-Human CD62P	Monoclonal antibody	Mouse	Human	AC1.2	Flow cytometry	0.2 µg/mL	BD Pharmingen, BD Biosciences, Wokingham, UK.
Phycoerythrin (PE) conjugated Mouse Anti-human IgG1 $_{K}$ Isotype control	Monoclonal antibody	Mouse	Human	MOPC-21	Flow cytometry	0.2 µg/mL	BD Pharmingen, BD Biosciences, Wokingham, UK.
Cyanine 5.5 (Cy 5.5) conjugated Annexin V	Phospholipid-binding protein	-	-	-	Flow cytometry	2.2 µg/mL	BD Pharmingen, BD Biosciences, Wokingham, UK.
Fluorescein isothiocyanate (FITC) Annexin V	Phospholipid-binding protein	-	-	-	Flow cytometry	2.2 µg/mL	BD Pharmingen, BD Biosciences, Wokingham, UK.

488 fluorescently tagged Lifeact (Lifeact-488) (custom peptide sequence: cp488-MGVADLIKKFESISKEE)	Peptide	-	-	-	Immunofluorescence	10 µM 50 µM 100 µM	Sigma-Aldrich, Gillingham, UK.
Alexa Fluor® 488 conjugated phalloidin	Peptide	-	-	-	Immunofluorescence	200 U/mL	
Alexa Fluor® 488 Goat anti-Mouse IgG (H+L) Highly Cross-Adsorbed Secondary Antibody	Polyclonal antibody	Goat	Mouse	-	Flow cytometry Immunofluorescence Western blotting	0.1 mg/mL 0.25 mg/mL 0.4 mg/mL	Invitrogen via ThermoFisher Scientific, UK.
β-Tubulin Loading Control Antibody	Monoclonal antibody	Mouse	Human	BT7R	Western blotting	1:2000	Invitrogen via ThermoFisher Scientific, UK.
Alexa Fluor® 568 Donkey anti-Goat IgG (H+L) Cross-Adsorbed Secondary Antibody	Polyclonal antibody	Donkey	Goat	-	Flow cytometry	1:2000	Invitrogen via ThermoFisher Scientific, UK.
Alexa Fluor® 647 goat anti-mouse IgG (H+L) Cross-Adsorbed Secondary Antibody	Polyclonal antibody	Goat	Mouse	-	Western blotting	1:4000	Invitrogen via ThermoFisher Scientific, UK.

2.1.3 Other reagents

Gly-Pro-Arg-Pro amide (GPRP) [1.1 mg/mL equal to 2.5 mM] - Sigma-Aldrich, Gillingham, UK

Ethylenediaminetetraacetic acid disodium salt solution (EDTA) [0.01 M] – Invitrogen, UK

2.2 Methods

2.2.1 Platelet Preparation

2.2.1.1 Blood draw and consent

All protocols were approved by the University of Reading Research Ethics Committee and informed consent was obtained from all blood donors prior to donation. Briefly, blood was drawn from healthy, drug free donors, from the antecubital fossa vein into sodium citrated (3.2%) vacutainers using a 21-gauge (G) butterfly needle following tourniquet removal. The first 3mL of blood was taken into an EDTA vacutainer and discarded to avoid any tissue factor contamination [171].

2.2.1.2 Platelet rich plasma preparation

Citrated whole blood was centrifuged at 150 x *g* for 20 minutes. Platelet rich plasma (PRP) was harvested into a 15 mL falcon tube, taking care to leave 0.5 mL above the red cell and buffy coat layers to avoid contamination. PRP was maintained at 30 ^{o}C in a water bath and used in all experimental set ups within 30 minutes of centrifugation end.

2.2.1.3 Human washed platelet preparation

Acid-citrate-dextrose 10% v/v (ACD: 85 mM sodium citric acid, 111 mM glucose and 78 mM citric acid) was added to citrated whole blood prior to centrifugation at 200 x *g* for 20 minutes, and the platelet rich plasma (PRP) harvested. Platelet sedimentation at 1000 x *g*, for 10 minutes in the presence of 45 ng/mL prostacyclin (PGI_2) preceded the removal of the plasma supernatant. The platelets were resuspended in modified Tyrode's-HEPES buffer (Tyrode's: 134 mM NaCl, 2.9 mM KCl, 0.34 mM $Na_2HPO_4.12H_20$, 12 mM $NaHCO_3$, 20 mM HEPES, 1 mM $MgCl_2$ and 5 mM Glucose, pH 7.3), ACD (10% v/v) and 45 ng/mL PGI_2 and centrifuged at 1000 x *g*, for a further 10 minutes. Finally, the platelet pellet was resuspended to 4 x 10^8 platelets/mL in Tyrode's buffer and rested at 30 ^{o}C for 30 minutes. Platelets were diluted further to 1 x 10^7 platelets/mL prior to platelet spreading assays.

2.2.1.4 Mouse washed platelet preparation

All procedures were undertaken in accordance with a UK Home Office license. Blood was drawn by cardiac puncture into 50 µL 3.2% sodium citrate. Whole blood was diluted using

modified Tyrode's-HEPES buffer and centrifuged at 200 x *g* for 8 minutes. PRP was aspirated and centrifuged at 200 x *g* for 2 minutes in the presence of 0.1 µg/mL PGI_2. The supernatant was carefully aspirated avoiding the red cell pellet. Finally, platelets were pelleted at 1000 x *g* for 5 minutes before resuspension in Tyrode's buffer at 2 x 10^8 platelets/mL and rested at 30 ^oC for 30 minutes. Platelets were diluted further to 1 x 10^7 platelets/mL prior to platelet spreading assays.

2.2.2 Platelet spreading assay

2.2.2.1 Substrates

Glass coverslips were coated with either 100 µg/mL human fibrinogen which was not depleted of von Willebrand factor (vWF) or plasminogen (Sigma), 10 µg/mL cross-linked collagen-related peptide (CRP-XL), or 10 µg/mL vWF overnight at 4 °C. Unbound substrates were removed and coverslips washed x3 using phosphate buffered saline (PBS: 10 mM Na_2HPO_4, 1.8 mM KH_2PO_4, 2.7 mM KCl and 137 mM NaCl, pH 7.4).

2.2.2.2 Blocking and platelet spreading

Coverslips were blocked with 5 mg/mL heat denatured, fatty acid free, bovine serum albumin (BSA) dissolved in PBS for 45 minutes to avoid unspecific platelet attachment. Coverslips were washed x3 with PBS before spreading washed platelets at 1 × 10^7 platelets/mL and incubating at 37 °C in a humidified atmosphere, 5% CO_2 for 45 minutes. The time from venepuncture to human platelet spreading remained constant at 1.5 hours for all experiments. The time from cardiac puncture to mouse platelet spreading remained constant at 1 hour for all experiments.

2.2.2.3 Fixation of spread platelets

Platelets were fixed using 10% formalin solution (Sigma) for 10 minutes, washed x3 with PBS, and coverslips mounted onto glass slides using hydromount mounting media (Scientific Laboratory Supplies, SLS) ready for imaging.

2.2.2.4 Permeabilisation of spread platelets

For phalloidin labelling of the actin cytoskeleton, platelets were permeabilised using 0.1% (v/v) Triton X-100 for 5 minutes after fixation, washed x3 with PBS before labelling with 200 U/mL Alexa Fluor-488 conjugated phalloidin for 30 minutes. Coverslips were subsequently washed x3 with PBS before mounting onto glass slides using hydromount mounting media ready for imaging.

2.2.2.5 Inhibitor and agonist-induced platelet spreading

Platelets treated with inhibitors (Dasatinib [10 µM], Ibrutinib [1 µM] and PRT-060318 [5 µM]) and thrombin [0.1 U/mL] were incubated at 30 ^{o}C for 10 minutes prior to spreading over coated and blocked coverslips.

2.2.3 DIC imaging

Platelets were imaged by Köhler illuminated Nomarski differential interference contrast (DIC) optics using a Nikon eclipse Ti2 inverted microscope, equipped with a Nikon DS-Qi2 camera, and visualised using a 100x oil immersion objective lens. NIS Elements software was used for image capture. Fiji Image J analysis software was used to analyse images.

2.2.4 Automated DIC platelet image analysis

2.2.4.1 Image conversion

The original 16-bit DIC images acquired using a Nikon eclipse Ti2 inverted microscope with dimensions 2424 x 2424 and were rescaled and converted to 8-bit images with dimensions 970 x 970 to reduce the file size. This was performed using a custom macro installed into ImageJ analysis software [172].

2.2.4.2 Manual analysis of platelet spreading

The perimeter of all platelets in each image were manually annotated using a pen tablet (Wacom Intuos). All manual annotators were provided with the same protocol, given a virtual demonstration, and requested to practise on a subset of images prior to commencing annotations. In line with manual analysis, all manual annotators were instructed to avoid annotating touching platelets to avoid both boundary ambiguity and instances where platelet-platelet interactions could influence platelet spreading.

2.2.4.3 CNN training

A convolutional neural network (CNN) was trained based on a modified version of the Usiigaci pipeline which is an automated cell tracking software [173]. Training involved a supervised approach where labelled images were used as a guide to assist learning. Firstly, 120 training images were manually curated using ImageJ [172], where the perimeter of each individual platelet was annotated. The LOCI plug-in for ImageJ was then used to label the individual platelets within each of the DIC images according to manual annotations. Finally, the hyperparameters and learning rate structure were kept constant when training three neural network models as described in Butler et al (2020) [174].

2.2.4.4 Automated segmentation and quality control

Automated segmentations represent the average of three independently trained models which were all trained using the same training material. After segmentation, a filter where objects comprising an area of <250 pixels, or any pixels within a 10-pixel range of the image edge, were eliminated from the analysis. A manual quality control step was maintained, allowing users to further remove any platelets that were either touching, mislabelled, or incorrectly segmented in each image. All quantifications in each image were outputted into a .csv file. All code and corresponding data are available at: https://github.com/george-butler/Automated_DIC_platelet_analysis.

2.2.4.5 DIC and fluorescent image analysis comparison

Phalloidin labelled platelets were imaged using a Nikon eclipse Ti2 inverted microscope using a green fluorescent protein (GFP) filter (Excitation wavelength 450-490 nm). NIS Elements software was used for both image capture and fluorescent analysis (NIS-Elements AR Analysis, version 5.21.02). Briefly, each image was converted into a binary image where a threshold was applied to each individual image. Touching platelets were excluded by setting a size criterion, and fluorescent staining irregularities were corrected by selecting the fill criteria.

2.2.5 Confocal imaging

Platelets were imaged by confocal scanning contrast microscopy using a Nikon A1R confocal inverted microscope, equipped with a Nikon A1 camera, and visualised using a 100x oil immersion objective lens. NIS Elements software was used for image capture. Fiji Image J analysis software was used to analyse images.

Chinese Hamster Ovary (CHO) cells were imaged by confocal scanning contrast microscopy using a Nikon A1R confocal inverted microscope, equipped with a Nikon A1 camera, and visualised using a 60x oil immersion objective lens. NIS Elements software was used for image capture. Fiji Image J analysis software was used to analyse images.

2.2.6 Fusogenic liposomes

2.2.6.1 Fuse-It-Color preparation

Aliquots of fluorescently labelled fusogenic liposomes (Benaig, GmbH) were sonicated in a benchtop ultrasonic bath (70 W, 40 khz) which was chilled with wet ice maintaining temperatures < 21^{o}C for 15 minutes prior to 1:100 dilution [30 µM] with Tyrode's buffer. A

final 5-minute sonication ensured homogenous dispersion. Fusogenic liposomes were finally diluted to 10 µM prior to adding to platelets.

2.2.6.2 Labelling of platelets with Fuse-It-Color

Prostacyclin (PGI_2, [0.5 ng/mL]) was added 1% (v/v) to platelet rich plasma (PRP) and incubated at room temperature for 3 minutes. Fusogenic liposomes were added 1:1, dropwise, to PGI_2 treated PRP and incubated for 3 minutes at room temperature. Fusion was reduced by diluting 1:1 with Tyrode's buffer. Fused platelets were rested at 30°C for 30 minutes prior to platelet function assays to allow for rapid hydrolysis of PGI_2.

Prior to PGI_2 optimisation, fusogenic liposomes were added 1:1, dropwise, to platelet rich plasma (PRP).

2.2.6.3 Fuse-It-P preparation (appendix data)

Dried lipid films were reconstituted in 25 µL 20 mM HEPES buffer or 25 µL water soluble cargo diluted in 20 mM HEPES buffer. Lipid films were pipette mixed using a gel-loading tip to ensure full lipid resuspension. Lipid resuspensions were vortex mixed for 1 - 2 minutes prior to 10 minutes sonication in a benchtop ultrasonic bath (70 W, 40 khz) which was chilled with wet ice maintaining temperatures < 21°C. Fusogenic liposomes were finally diluted with PBS to 9.2 µM and pipette mixed prior to fusion with platelets.

2.2.6.4 Labelling of platelets with Fuse-It-P (appendix data)

Prostacyclin (PGI_2, [10 ng/mL]) was added 1% (v/v) to washed platelets (WPs) resuspended at 400 x 10^6 platelets/mL and incubated at room temperature for 3 minutes. Fusogenic liposomes [9.2 µM] were added 1:1, dropwise, to PGI_2 treated WPs and incubated for 3 minutes at room temperature. Fusion was reduced by diluting 1:1 with Tyrode's buffer. Fused platelets were rested at 30°C for 30 minutes prior to functional assays to allow for rapid hydrolysis of PGI_2.

2.2.6.5 In-house fusogenic liposome formulation

Equimolar stock solutions of 1,2-di-(9Z-octadecenoyl)-sn-glycero-3-phosphoethanolamine (DOPE) and 1,2-dioleoyl-3-trimethylammonium-propane (chloride salt) (DOTAP) lipids were prepared in chloroform [10 mg/mL]. The lyophilised fluorescent 1,1'-Dioctadecyl-3,3,3',3'-Tetramethylindotricarbocyanine Iodide (DiR) lipid analogue was also prepared in chloroform [10 mg/mL]. Fusogenic liposomes were prepared by mixing the three lipid components in a weight ratio of 1/1/0.1 (w/w/w). 0.5 mg lipid stock was aliquoted into small glass vials containing glass inserts. Chloroform was evaporated under vacuum for 20-30 minutes prior to nitrogen flushing of each vial to ensure full evaporation of chloroform and reduce lipid

oxidisation during storage. Glass vials were stored at -20 until lipid reconstitution and dispersion.

2.2.6.6 In-house fusogenic liposomes

Individual lipid films were dispersed in 20 mM N-2-Hydroxyethylpiperazine-N-2-Ethane Sulfonic Acid (HEPES) buffer (Sigma, 1M stock) (pH 7.4) to a total lipid concentration of 2.5 mg/mL. For cargo delivery, lipid films were dispersed in proteins or peptides which had been diluted in 20mM HEPES buffer to a total lipid concentration of 2.5 mg/mL. Liposome formation was performed by either extrusion or sonication.

For the extrusion method, dispersed lipids were left to hydrate at room temperature for 30 minutes prior to vortexing for 1-2 minutes to promote formation of multilamellar fusogenic liposomes. An extruder (Avanti® Polar Lipids) fitted with a 0.1 µm polycarbonate membrane, was used to extrude the multilamellar fusogenic liposome mixture for a minimum of 15 times to produce uniformly sized unilamelar fusogenic liposomes. Extruded fusogenic liposomes were stored in glass vials at 4^{o}C, and further diluted in 20mM HEPES buffer before adding to washed platelets. Fusogenic liposomes were used on the day of extrusion only. Unencapsulated protein or peptides were not separated from proteins or peptides encapsulated inside fusogenic liposomes.

For the sonication method, once lipids were hydrated for 30 minutes and vortexed for 1-2 minutes, the fusogenic liposome solution was sonicated for 10 minutes using a bench top ultrasonic bath (70 W, 40 khz). The ultrasonic bath was chilled using wet ice to ensure the bath temperature remained < 21oC.

2.2.6.7 Labelling of platelets with in-house fusogenic liposomes

Prostacyclin (PGI_2, [10 ng/mL]) was added 1% (v/v) to washed platelets (WPs, [400 x 10^6 /mL]) and incubated at room temperature for 3 minutes. Fusogenic liposomes [10 µg/mL] were added 1:1, dropwise to PGI_2 treated WPs and incubated for 3 minutes at room temperature. Fusion was minimised by diluting 1:1 with Tyrode's buffer. Fused platelets were rested at 30^{o}C for 30 minutes prior to platelet function assays.

2.2.7 Cell culture

2.2.7.1 Maintaining CHO cells in culture

Chinese hamster ovary (CHO) cells were maintained in culture using Dulbecco's Modified Eagle Medium (DMEM) (supplemented with 10 % (v/v) Foetal Bovine Serum (FBS), 2 mM L-Glutamine, 100 U/mL Penicillin, and 0.1 mg/mL Streptomycin), and maintained at 37^{o}C and

5 % CO_2. Cells were sub-cultured at approximately 80 % confluence using tryspin-EDTA solution (Sigma). At which point 2 – 5 x10^4 CHO cells were seeded onto glass bottomed µ-dishes (ibidi GmbH) and allowed to adhere for 24-48 hours prior to further experimentation in phenol free DMEM, supplemented as above.

2.2.7.2 Addition of Fuse-It-P

Fuse-It-P preparation [24 µM] was added dropwise to washed (x3 PBS) CHO cells seeded on glass bottomed µ-dishes and incubated at 37^{o}C for 15 minutes. Each µ-dish was tilted every 5 minutes to support fusion. Fusogenic liposomes were subsequently discarded and replaced with Dulbecco's phosphate buffered saline and imaged using confocal microscopy.

2.2.8 Flow cytometry

2.2.8.1 Assessing CD62P expression

Briefly, 43.4 µL HEPES buffered saline (HBS: 10 mM HEPES, 150 mM NaCl, 1 mM MgSO4, 5 mM KCl, 0.22 µm filter sterilised), 1.6 µL phycoerythrin coupled to a cyanine dye (PECy5) or phycoerythrin (PE) labelled CD62P antibody or relevant isotype control, and 5 µL PRP or washed platelets were added to a 96 well flat bottomed plate and incubated in the dark for 20 minutes before being fixed with 0.2% (v/v) formyl saline (FS: 0.2% formaldehyde in 0.9% NaCl, 0.22 µm filter sterilised) for 10 minutes in the dark and acquired on an Accuri C6 flow cytometer (BD Bioscicences) within 4 hours.

Platelets were identified by forward scattered (FSC), and side scattered (SSC) light properties, a measure of size and granularity respectively. Data was analysed as a percentage of platelet activation greater than a 2% gate on the isotype control, while median fluorescent intensity (MFI) of the platelet population is representative of arbitrary units of fluorescence (AU).

Compensation values generated using single colour controls were applied where appropriate during multi-colour flow cytometry assays to correct spectral spill over. When using fluorescently labelled antibodies, anti-mouse BD CompBeads (BD Biosciences) were used to identify distinct positive and negative (background fluorescence) stained populations. When using fluorescent dyes, single colour cell populations were used to identify distinct positive and negative stained populations. The median statistics of both single colour and unlabelled controls were then entered into the 'BD Accuri™ C6 Plus Compensation Calculator' to generate a spill over matrix which was applied to all samples.

2.2.8.2 Agonist-induced platelet activation

In addition to assessing CD62P expression, agonist-induced platelet activation consisted of 5 µL of agonist (e.g., CRP-XL, TRAP-6 etc) diluted in HBS which was added to a 96 well flat-bottomed plate with 38.4 µL HBS, 1.6 µL antibody or isotype control, and 5 µL PRP or washed platelets. Final concentrations of all agonists used were a 1/10 dilution of the working concentration. Prior to acquisition by flow cytometry, platelets were fixed for 10 minutes by adding 200 µL 0.2% (v/v) formyl saline solution. Further dilution in formyl saline was necessary if there were a high number of platelets per second at acquisition.

Platelets were identified by FSC and SSC properties. Data was analysed as a percentage of platelet activation greater than a 2% gate on the isotype control, while MFI of the platelet population is representative of arbitrary units of fluorescence (AU). Compensation values generated using single colour controls, as described previously, and were applied where appropriate during multi-colour flow cytometry assays to correct spectral spill over.

2.2.8.3 Annexin V Assay

Briefly, 36 µL HBS supplemented with 2 mM calcium (HBSc) [175], 4µL fluorescein isothiocyanate (FITC) or cyanine 5.5 (Cy5.5) labelled Annexin V antibody, 5 µL Gly-Pro-Arg-Pro amide (GPRP) [2.5 mM], and 5 µL PRP or washed platelets were added to a flat bottomed 96 well plate. A negative control included 1 µL EDTA [0.01 M]. A positive control included the addition of 5 µL of each agonist (e.g. CRP-XL, and TRAP-6 or thrombin) diluted in HBSc. The volume of each well remained constant at 50 µL. The 96 well plate was incubated in the dark for 10 minutes before diluting in 200 µL HBSc and acquiring immediately by flow cytometry. Further dilution in HBSc was necessary if there were a high number of events per second at acquisition.

Platelets were identified by FSC and SSC properties. Data was analysed as a percentage of platelet activation greater than 2% gate on the EDTA negative control. Due to the bimodal population, MFI was not analysed. Compensation values generated using single colour controls, as described previously, and were applied where appropriate during multi-colour flow cytometry assays to correct spectral spill over.

2.2.9 Dynamic light scattering (Zetasizer)

Size and zeta potential analysis was performed by dynamic light scattering (DLS) using a Zetasizer Nano-ZS (Malvern Instruments Ltd, Malvern, UK). Scattered laser light was collected at a constant angle of 173°. Prior to measurements fusogenic liposome stock solutions were diluted to 10 µg/mL with 20mM HEPES buffer. All measurements were

performed at 25 °C where each sample was measured three times with 1-minute intervals. Data was collected from a minimum of three independently prepared fusogenic liposome samples and raw data was exported using the instrument software (DTS from Malvern Instruments). Reported data is representative of the mean peak position and standard deviation.

2.2.10 Quantification of Lifeact-488 delivery

Fusogenic liposomes were prepared as described previously (Section 2.2.6.6) using three concentrations of Lifeact conjugated to a 488-fluorescent label (Lifeact-488) [10 µM, 50 µM or 100 µM] and were added to washed platelets (1 x 10^7 /mL) which were spread over a fibrinogen substrate [100 µg/mL]. Lifeact-488 delivery was quantified by counting the absolute number of spread platelets and assigning each platelet into a category dependant on fluorescent labelling using the 'cell-counter' plug-in for ImageJ. Four categories consisted of platelets which represented no fusogenic liposome labelling and no Lifeact-488 delivery (-FL, -LA), platelets which represented fusogenic labelling and no Lifeact-488 delivery (+FL, -LA), platelets which represented fusogenic labelling and Lifeact-488 delivery (+FL, +LA), and platelets which represented no fusogenic labelling and Lifeact-488 delivery (-FL, +LA).

2.2.11 Antibody dialysis

Slide-A-Lyzer MINI Dialysis Devices with a 10,000 molecular weight cut off (10K MWCO) were used to remove low molecular weight contaminants (0.016% Methylisothiazolone and 0.016% Bromonitrodioxane) and buffer exchange 100 µL Alexa Fluor® 488 Goat anti-Mouse IgG secondary antibody. Buffer exchange was maintained in the dark at 4 ^{o}C for 24 hours in 500 mL 1x PBS which was replaced approximately every 8 hours.

2.2.12 Western blot & SDS-Page

2.2.12.1 Western blot platelet preparation

Platelets (160 x 10^6) were pelleted by centrifugation at 1000 x *g* to completely remove the supernatant and any unencapsulated cargo when platelets were pre-treated with cargo-containing fusogenic liposomes. Platelet pellets were lysed with 1X Reducing Sample Treatment buffer (RSTB: 2 % (w/v) Sodium Dodecyl Sulphate (SDS), 10 % (v/v) glycerol, 0.05 M Tris-HCl (pH 6.8), 5 % (v/v) b-mercaptoethanol, 0.0002 % (w/v) Brilliant Blue R). Samples were heated at 95°C for 5 minutes prior to freezing at -20 until SDS-PAGE.

2.2.12.2 SDS-PAGE to detect delivery of Alexa Fluor 488 conjugated antibodies into platelets.

Proteins were separated by 12% Sodium dodecyl-sulphate polyacrylamide gel electrophoresis (SDS-PAGE) gel submerged in 1X Tris-Glycine-SDS buffer (25mM Tris, 192mM glycine, 0.1% (w/v) SDS, pH 8.3) using a vertical electrophoresis cell (Bio-Rad). Electrophoresis was run at a constant voltage of 120 V.

Following protein separation, gels were removed from the plates and submerged into Towbin transfer buffer (25 mM Tris, 192 mM glycine, 20% (v/v) methanol, pH 8.3). A pre-cut polyvinylidene difluoride (PVDF) membrane was soaked in methanol followed by Towbin transfer buffer. Two pieces of extra thick filter paper were soaked in Towbin transfer buffer. Semi-dry western blotting was performed using a Trans-blot Turbo blotter (Bio-Rad). Proteins were transferred from the gel to the PVDF membrane for 40 minutes at 15 V.

PVDF membranes were scanned using a Typhoon Trio fluorescence imager (Amersham Biosciences, Buckinghamshire, UK) and the presence of Alexa Fluor 488 antibody analysed. PVDF membranes were then blocked using a 5% (w/v) solution of bovine serum albumin (BSA) dissolved in TBST (Tris buffered saline with Tween 20; 20mM Tris, 140mM NaCl, 0.1% (v/v) Tween, pH 7.6) for 1 hour at room temperature under constant rolling.

To determine equal protein lysate loading, PVDF membranes were incubated with a mouse antibody against tubulin [0.5 µg/mL] diluted in a 2.5% (w/v) solution of BSA dissolved in TBST for one hour under constant rolling. Membranes were washed 3x for 10 minutes each with TBST prior to labelling using a goat anti-mouse secondary antibody conjugated to an Alexa Fluor 647 fluorescent label. The antibody was diluted 1:4000 using a 2.5% (w/v) solution of BSA dissolved in TBST and incubated for one hour under constant rolling in the dark at 4^{o}C. Membranes were washed 3x for 10 minutes each with TBST prior to scanning as before, and the presence of Alexa Fluor 647 antibody analysed.

2.2.13 Statistics

All graphs and statistical tests were performed using Prism software version 8 for Windows (GraphPad Software, San Diego, California USA, www.graphpad.com). Data is presented as mean ± the standard deviation and further analysed using one-way analysis of variance (ANOVA) with Bonferroni post-test or a paired two-tailed t-test, unless stated otherwise.

Chapter 3: Fully automated platelet Differential Interference Contrast image analysis via deep learning

This chapter is based on the published paper:

Kempster, C., Butler, G., Kuznecova, E. et al. Fully automated platelet differential interference contrast image analysis via deep learning. Sci Rep 12, 4614 (2022). https://doi.org/10.1038/s41598-022-08613-2 [176].

The images which support the findings of this publication are openly available via The University of Reading Research Data Archive [177].

Contributions:

C.K. and G.B. designed experiments, performed and analysed data, and wrote the manuscript. E.K. performed and analysed data. K.A.T., N.K., G.L. and M.S. analysed data. T.S. acquired data. A.Y.P. designed the study, analysed data and edited the manuscript. All authors read and edited the manuscript.

3.1 Introduction

During injury, platelets rapidly adhere and spread over exposed subendothelial matrix substrates, such as collagen and vWF, of the damaged blood vessel wall to arrest bleeding and facilitate wound healing [31,178]. Platelets adhere to exposed collagen by the GPVI receptor and integrin α2β1, while the GPIb/IX/V receptor complex and GPIIb/IIIa (integrin αIIbβ3) bind vWF [179]. The ability of platelets to spread are a result of intracellular signalling and consequently, rapid rearrangements of filamentous actin (F-actin) [180,181]. These rearrangements drastically increase the spread surface area of platelets by facilitating filopodia extensions and lamellipodia protrusions [50,181]. The mechanisms which govern platelet activation and their interaction with a range of substrates are regularly assessed and investigated using platelet spreading assays. These assays allow biological processes such as platelet adhesion and changes in platelet morphology to be investigated [182,183].

3.1.1 Imaging platelet morphology

To image mammalian cells, contrast imaging methods are employed to permit detailed visualisation of unlabelled cells. Contrast imaging methods include Differential Interference Contrast (DIC) techniques, where specific objectives or prisms alter the light path to enhance contrast respectively. DIC microscopy is commonly used to quantify the behaviour of individual platelets within spreading assays; owing to its ability to enhance the contrast between the platelet and background. These DIC images can further be analysed to quantify individual platelet features such as spread area, perimeter, and circularity.

However, although DIC imaging enables the use of label free cells, it also creates a shadow artefact within the image [184]. This prevents the use of automated segmentation techniques commonly applied to epi-fluorescent images e.g., thresholding and edge detection. As a result, a process of manual segmentation is often used that is extremely time consuming since human input is required throughout and, depending on experimental setups and biological replicates, can result in hundreds of images requiring manual segmentation. Furthermore, manual segmentation also introduces a high degree of user subjectivity and variability into the analytical workflow that may consequently impact on the biological insight that is gained [185]. This chapter will moreover focus on the development of a convolutional neural network (CNN) in order to automate segmentation. The automation of DIC imaging will be of particular importance when quantifying any impact of fusogenic liposomes on platelet adherence and morphology.

3.1.2 Convolutional neural networks (CNN)

The introduction of deep learning approaches, such as CNNs, offer an opportunity to overcome the limitations associated with DIC imaging and leverages the power of high-throughput single cell analysis [186,187]. An automated approach such as a CNN would dramatically reduce analysis time and remove manual analysis associated subjectivity and biases.

Automated segmentation has two stages: feature computation and feature selection [188]. Feature computation captures the information that is encoded in an image and translates it into a numerical value, such as the colour and intensity of a pixel or the length of an object [189]. Feature selection then builds a model from the extracted features that can be used to segment cells in future unseen images. The parameters for each feature in the model are estimated dependent on their discriminatory power, the higher the power the larger the weighting [190]. Yet, whilst a number of different automated segmentation approaches exist [191-193], they typically all rely upon the same computed features that are defined a priori, for example the maximum area of a cell or the intensity of a pixel. In contrast, CNNs can achieve much higher levels of segmentation accuracy by using a data driven approach that deconstructs an image into multiple levels of abstraction [194]. Abstraction refers to the characterisation of essential, but often unintuitive, features within an image that reduce the informational load and complexity. The abstractions combine low level features such as edges and curves with higher order features such as shapes to detect complex objects within an image, for example the morphology of a platelet [195]. As a result, the application of CNNs to automate DIC imaging offers an exciting opportunity to overcome a major bottleneck in the experimental workflow.

3.1.3 Training Material

To produce a robust CNN, large quantities of training images are required as part of the training process to enable the CNN to learn accurate cell features. The number of training images required can both be costly and time consuming to curate, and exactly how much data is needed for adequate training remains poorly defined. Overall, it is well recognised that an increased amount of labelled training data improves performance as described in Cho et al (2015) [196]. Yet, medical image analysis, where there is often a lack of publicly available images, have demonstrated satisfactory performance despite small training datasets [197]. This is likely due to image homogeneity, and although performance may be satisfactory, extreme examples such as rare diseases may be missed due to inadequate training examples [197].

Therefore, to fully leverage the power of a CNN, the trained model needs to be generalisable [198]. That is, the same trained model needs to be applicable across multiple different experimental conditions. In a biological setting for example, where data are typically collected in a sequential manner, a high degree of generalisability is essential to ensure that the model does not need to be retrained between each experiment.

Figure 3.1 provides an overview of the CNN training process. A total of 120 images were acquired from several platelet spreading experiments where platelets were spread over a fibrinogen substrate. Fibrinogen was chosen as a substrate which demonstrated platelet morphology ranging from filopodia extensions to fully spread [199]. All images were manually annotated using a pen pad to curate a training set of images which were used to train the CNN. These manually annotated images, together with subsequent labelled images generated using the LOCI plug in for ImageJ, were used in a supervised approach to assist learning. Additional training material or model adaptions could be implemented in the event of sub-satisfactory platelet segmentation. An independent test set of 12 images assessed the performance of the trained CNN. This chapter firstly presents data regarding the performance of the CNN when trained using a set of 120 images, followed by direct comparisons with manual annotators, as well as investigating extremes to platelet morphology when inhibiting and activating pathways known to impact platelet morphology.

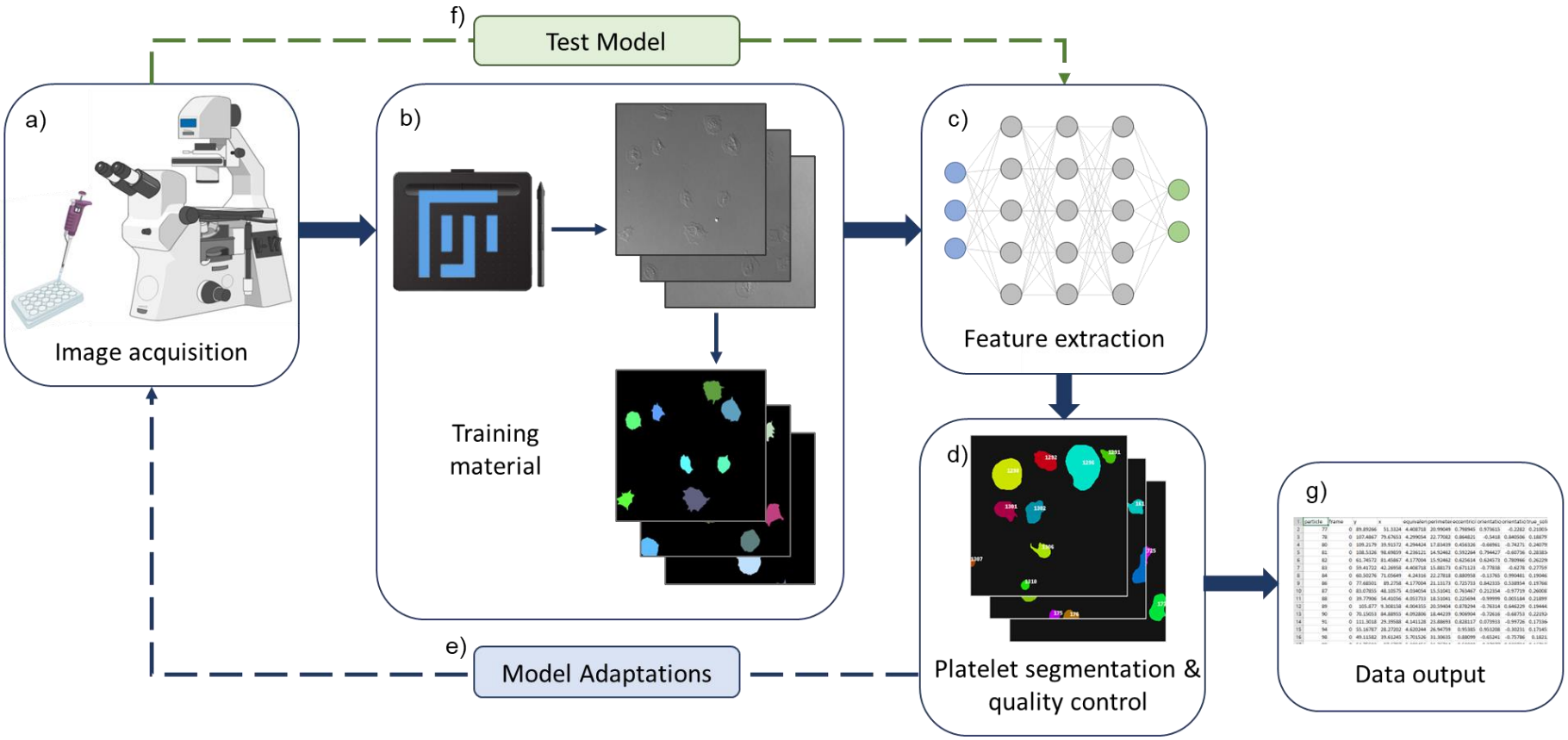

Figure 3.1 CNN training workflow

Schematic detailing an overview of the CNN training process. Platelets were imaged by Köhler illuminated Nomarski Differential Interference Contrast (DIC) optics (a). Rescaled images were manually annotated and LOCI plug-in for ImageJ was used to segment the individual platelets within each image (b). Manually segmented and labelled images provided a supervised approach where the CNN could learn platelet features (c). Automated platelet segmentation and quality control can be assessed (d). Model adaptions such as an increase in training material may improve CNN performance (e). Upon satisfactory performance, the model is tested using an independent image set (f). Finally, once CNN performs well on independent images, data can be outputted in a .csv format (g). Workflow created with BioRender.com.

3.2 Results

3.2.1 A practical increase in training data size will yield a significant increase in network performance.

Firstly, the mean average precision (mAP) was used to evaluate the effect of increased training data on the network performance. The mAP compares the predicted platelet boundary, as outputted by the CNN, against the true platelet boundary as identified by the manual annotations (Figure 3.2A*i-ii*). Assessing the overlap of these boundaries, over the union of both boundaries returns mAP (Figure 3.2A*ii*). The training data size was then increased from 10 to 120 images with a 10-image increase at each interval. The mAP at each interval was then calculated as the average across 3 independently trained models using an ensemble approach (Figure 3.2B). An ensemble approach combines the predictions from each model, reducing prediction variance and overall increasing model performance when compared to a single model [200-203]. As expected, increasing the amount of training data monotonically increases the network performance. That is, the accuracy of the predicted platelet boundary as identified by the trained CNN, increased as the number of training images increases (Figure 3.2B).

A mAP output of ≥0.5 is predictive of a sufficiently good model performance [204,205], and with the experimental setup presented here, a strong performance (0.55 ± 0.01 mAP) was achieved with a training set of 120 images (Figure 3.2B). Although this data does not indicate a saturation point for maximal performance, the size of this training set was realistic and manageable to curate. Furthermore, higher order polynomial models of the 2nd order (Figure 3.3A), the 3rd order (Figure 3.3B) and the 4th order (Figure 3.3C) did not describe the data any better when compared to a simple linear regression model. A corrected Akaike information criterion value (AICc) identifies a smaller value for the linear regression model, which is representative of a better model fit (Figure 3.3D). Suggesting that the saturation point was not imminent, and that considerably more training data would be needed to reach a maximal segmentation performance. As a result, the 3 models trained with 120 training images were used in an ensemble approach for all future segmentation.

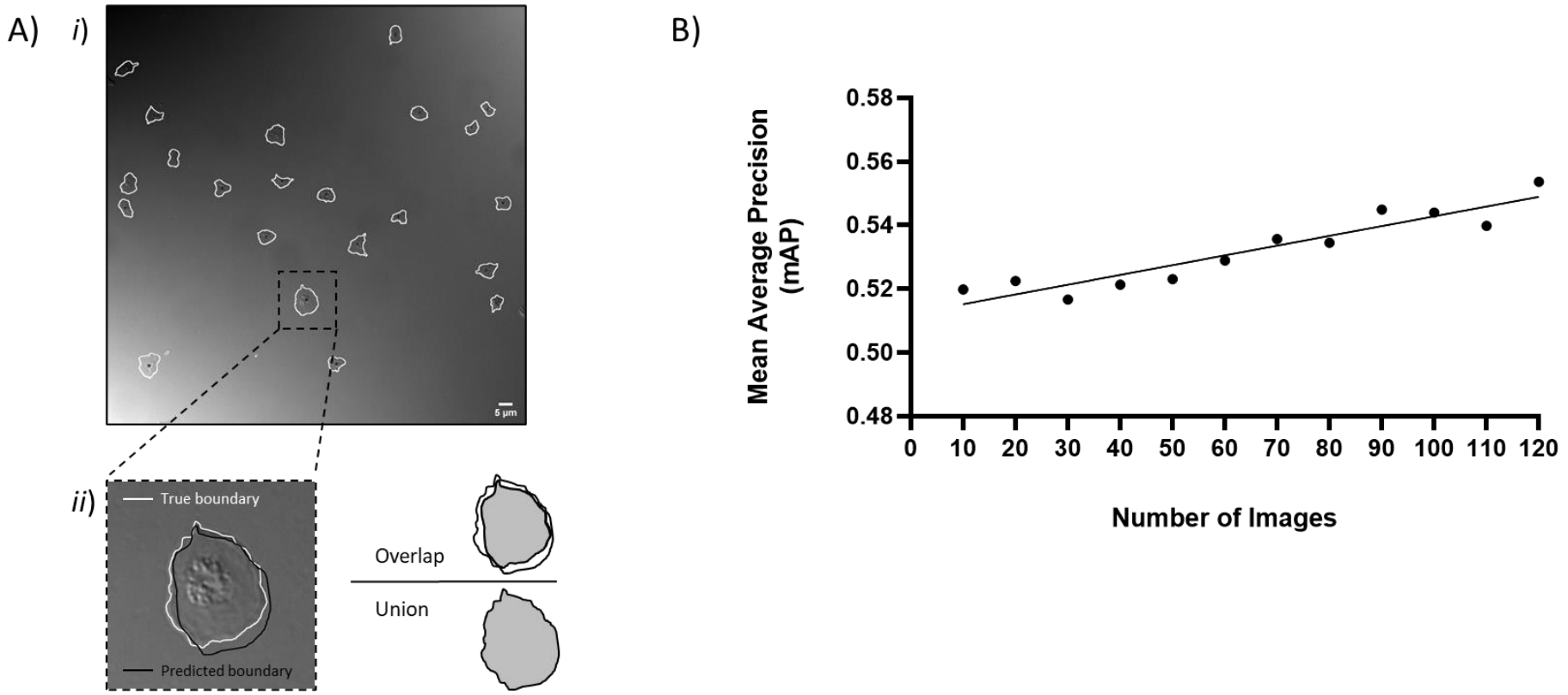

Figure 3.2 Increasing the number of images in the training set increases the performance of the CNN.

Training consisted of a supervised approach to assist the training of the CNN. Representative DIC image indicates the true platelet boundary (white) as identified by manual annotations (A*i*). A schematic illustrates the comparison of manual annotations (white) to the predicted boundary (black) of the CNN (A*ii*). Comparing these boundaries evaluated the extent of overlap and returned mean average precision (mAP) where increasing increments of 10 images assessed the network performance up to 120 images (B). A linear regression model shows mAP increased with an increasing training set. Data represents the mean of three independently trained models. Scale bar represents 5 µm.

A)

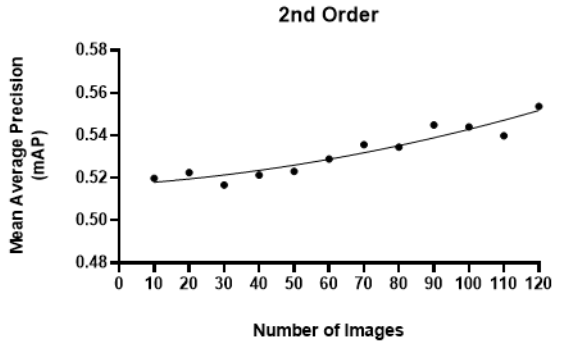

B)

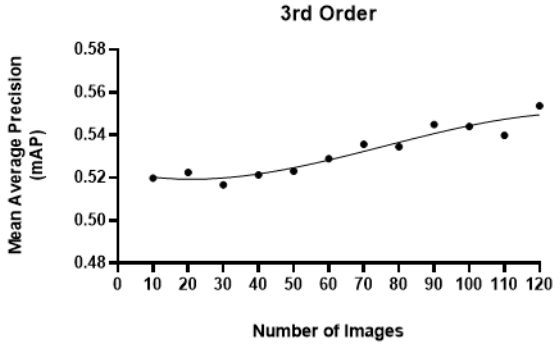

C)

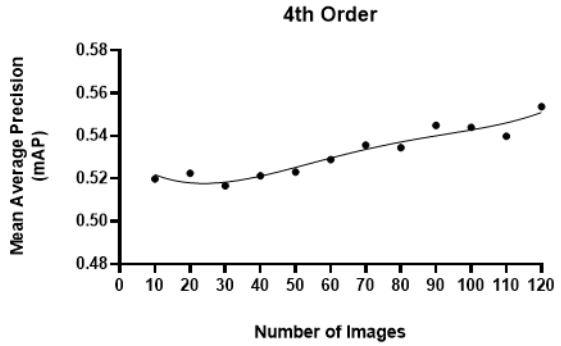

D)

Model	AICc	Delta AICc
Linear Regression Model	-314.9	-
Polynomial 2nd Order	-313.0	-1.84
Polynomial 3rd Order	-310.9	-3.95
Polynomial 4th Order	-308.5	-6.42

Figure 3.3 Polynomial models are not significantly different to a linear regression model.

Polynomial regression models of the 2nd order (A), 3rd order (B), and 4th order (C) are not significantly different to the linear regression model (Figure 3.2B). Indicating the relationship between independent and dependent variables is no further defined; exemplifying no reason to reject the linear regression model. A corrected Akaike information criterion value (AICc) identifies a smaller value for the linear regression model, which is representative of a better model fit (D). The delta AICc highlights the increasing difference in model fit when the polynomial models are compared to the linear regression model. Data representative as the mean of three independently trained models.

3.2.2 Trained CNN removes variation in manual annotations.

To test the performance of the CNN when compared to multiple manual annotators the outputs of six independent platelet annotators were assessed (Figure 3.4); where 'T' represents a network trainer, and 1-5 represent additional manual annotators. All annotators, including the trainer, were presented with the same 12 images which were different to training data, and instructed to manually annotate the perimeter of individual platelets in each image. The mAP of the CNN was directly compared to the mAP of the trainer and each manual annotator. The higher the mAP score, the more accurate the CNN or annotator was when detecting platelets in each image.

Unsurprisingly, the mAP of the trainer was generally higher than that of other manual annotators – that is to say, the CNN's output was similar to that of the person whose annotations were used to train the CNN (Figure 3.4). Despite the mAP of the trainer being significantly different to annotators 2-5, the mAP of these annotators (0.49 ± 0.13 – 0.63 ± 0.09 mAP) were similar and consistent with the mAP of the CNN (0.57 ± 0.08 mAP). There was also no significant difference in mAP between the trainer and annotator 1, indicating that the mAP was similar between these individuals. Overall, the high degree of variation between the manual annotators supports the need for an automated CNN to ensure data outputs are non-biased and reproducible across experiments.

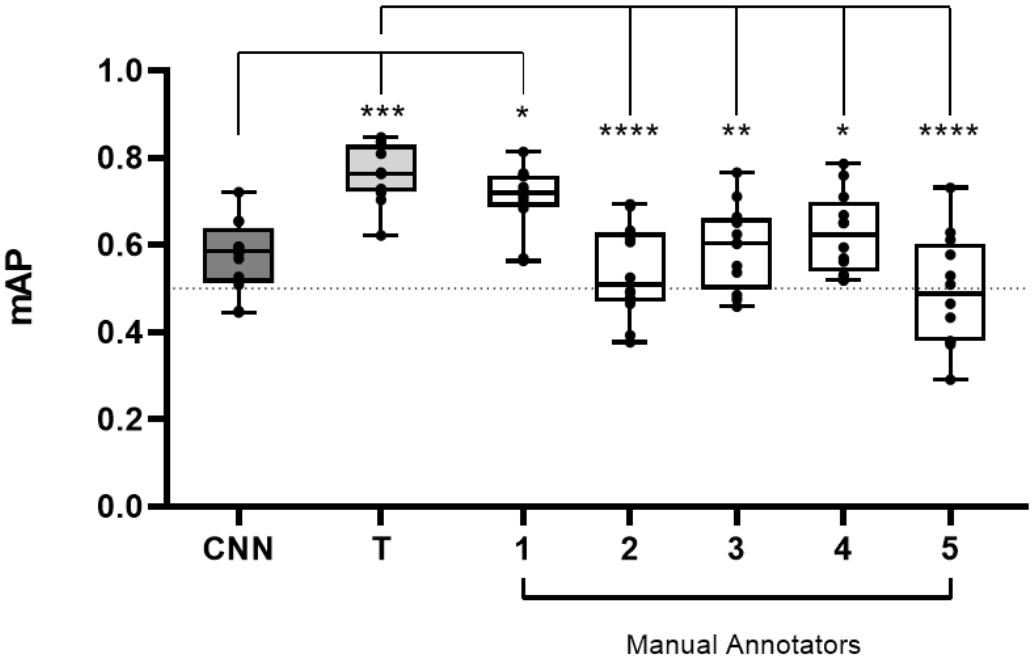

Figure 3.4 The CNN removes large variation between manual annotators.

Six independent annotators, including manual annotators (1 – 5) and a network trainer (T), manually outlined the perimeter of platelets in 12 images. The mAP of the CNN was compared to all manual annotators. The mAP of the trainer was compared to manual annotators 1-5. Dotted line represents mAP of 0.5 which indicates a satisfactory model performance. The mean ± SD of the 12 images was plotted and analysed using one-way ANOVA with Bonferroni post-test. *p ≤ .05, **p ≤ .01, ***p ≤ .001, ****p ≤ .0001.

3.2.3 Trained CNN removes variation in commonly assessed parameters of platelet morphology.

Spread area, perimeter, circularity and the number of adhered platelets are commonly assessed parameters of platelet spreading assays. These parameters were further investigated by comparing manual annotations to the CNN segmentation for the same 12 images mentioned previously (Section 3.2.2). When these parameters were compared between the trainer, annotators and the CNN, the spread area of platelets was found to be consistent (Figure 3.5A). The CNN successfully detects the spread area of platelets to be 32.4 ± 4.5 μm^2. This corresponds with the spread area for platelets interacting with fibrinogen reported in the literature [138]. When the outputs from the manual annotators were compared, annotator 5 estimates a significantly increased spread area (36.7 ± 4.4 μm^2) when compared to the spread area estimated by annotator 2 (29.5 ± 5.6 μm^2) (Figure 3.5A). Indicating that there is variability in manual analyses between different manual annotators.

When the perimeter was analysed, the CNN appears to lose detail from the platelet perimeter (Figure 3.5B). Representative images detail the DIC image, the corresponding manual segmentation using Image J, and the corresponding CNN segmentation. The CNN segmentation appears smoother when visually compared to manual segmentation (Figure 3.5B). This is reflected by the reduced perimeter when compared to the trainer and annotators 1, 3 and 5 (Figure 3.5C). The platelet perimeter determined by the CNN is 23.9 ± 1.0 µm, and when compared to the manual annotators, there is a significant increase in perimeter measurements identified by the trainer and manual annotators 1, 3 and 5 (25.8 ± 1.2 µm – 27.3 ± 1.3 µm). This suggests that the CNN has difficulty in detecting the intricate details of the platelet perimeter which the human eye can observationally identify. This variability in platelet perimeter in turn affects the data outputs for circularity (Figure 3.5D). Circularity is a normalised ratio between the area and perimeter [206]. Circularity can represent changes in platelet morphology with filopodia containing platelets having a lower circularity score when compared to fully spread platelets which have a high circularity score. The circularity for each platelet was calculated with a measurement between 0 – 1, where 0 is not circular and 1 is a perfect circle. An increase in circularity value was observed for the CNN (0.7 ± 0.1) when compared to the trainer and manual annotators 1 and 3 (0.56 ± 0.1 – 0.59 ± 0.1). This highlights that, since some finer detail in platelet perimeter is missed by the CNN, circularity score is directly impacted.

Despite the differences observed for perimeter and circularity, no differences in cell adhesion were observed between the CNN and the manual annotators (Figure 3.5E). Suggesting that the CNN can identify a similar number of adhered platelets as a manual annotator.

In summary, the CNN can accurately quantify spread platelet area and can identify a similar number of adhered platelets as manual annotators. However, differences are observed for perimeter and circularity where the CNN cannot depict the finer detail, indicating that automated outputs should be carefully interpreted and validated.

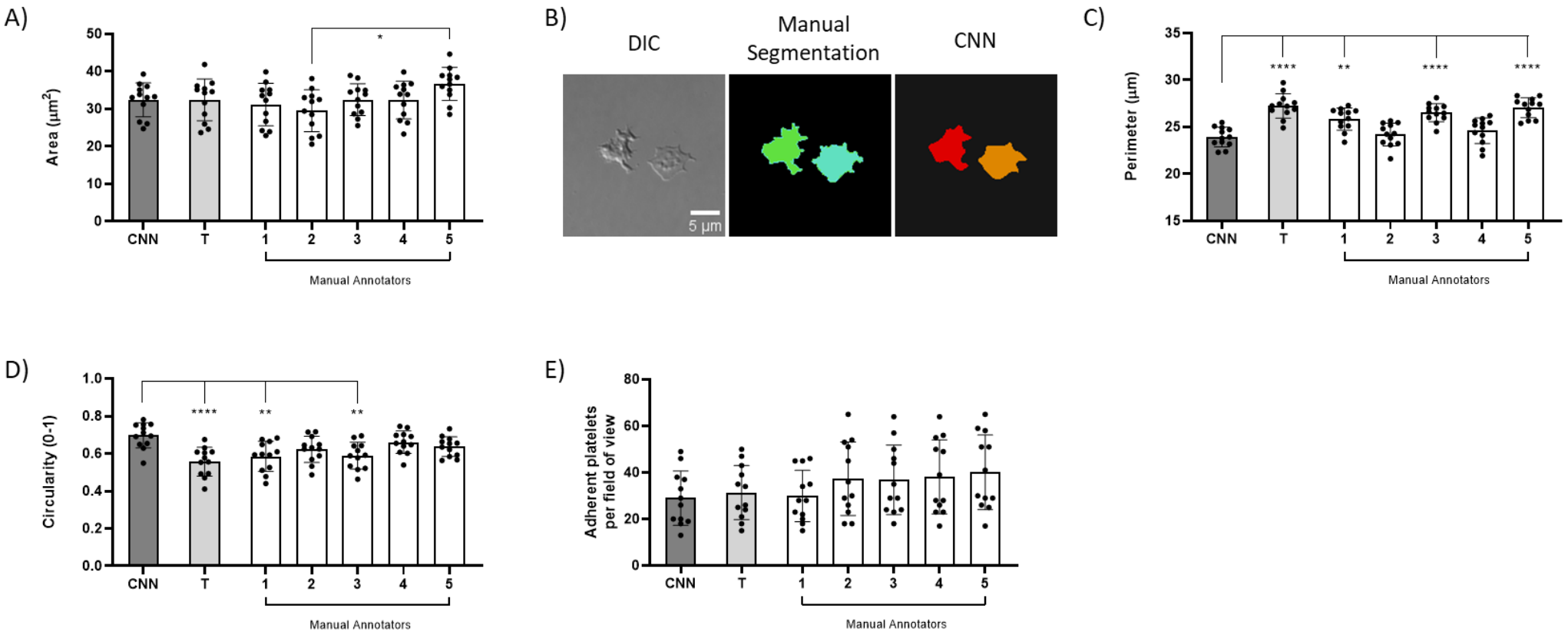

Figure 3.5 The CNN identifies differences in some metrics of morphology between annotators using the same data set.

Commonly evaluated platelet metrics were exported to further compare the CNN to manual analyses for platelet surface area (A), representative images detail manual segmentation and automated CNN segmentation (B), platelet perimeter (C), platelet circularity (D) and platelet adhesion (E) in 12 images independent of the training set. The automated output of the CNN was compared to a trainer (T) and manual annotators (1 - 5). The mean ± SD of the 12 images was plotted and analysed using one-way ANOVA with Bonferroni post-test. *p ≤ .05, **p ≤ .01, ***p ≤ .001, ****p ≤ .0001.

3.2.4 Trained CNN detects extremes in platelet morphology.

Platelet morphologies are often investigated in spreading experiments since they can be suggestive of platelet abnormalities or disorders and provide insight into anti-platelet drugs. It was therefore investigated if the CNN could detect extremes in platelet cell shape.

To do this, washed platelets were spread over three different substrates consisting of the synthetic cross-linked collagen-related peptide (CRP-XL), and glycoproteins fibrinogen or vWF (Figure 3.6). Washed platelets were also treated with a selection of inhibitors known to impair platelet spreading; Dasatinib [207,208], Ibrutinib [209] or PRT-060318 [210] which inhibit Src family kinases, Btk and Syk, respectively. In contrast, Thrombin, a potent platelet agonist which induces platelet activation independently of the adhesion receptors that control platelet spreading, was used to induce fully spread platelets by activating protease-activated receptors (PARs) [210-212]. Representative DIC images indicate the extremes in platelet morphology in the presence or absence of inhibitor or agonist when compared to a vehicle control (washed platelets). While corresponding segmented images detail the morphology as identified by the CNN (Figure 3.6).

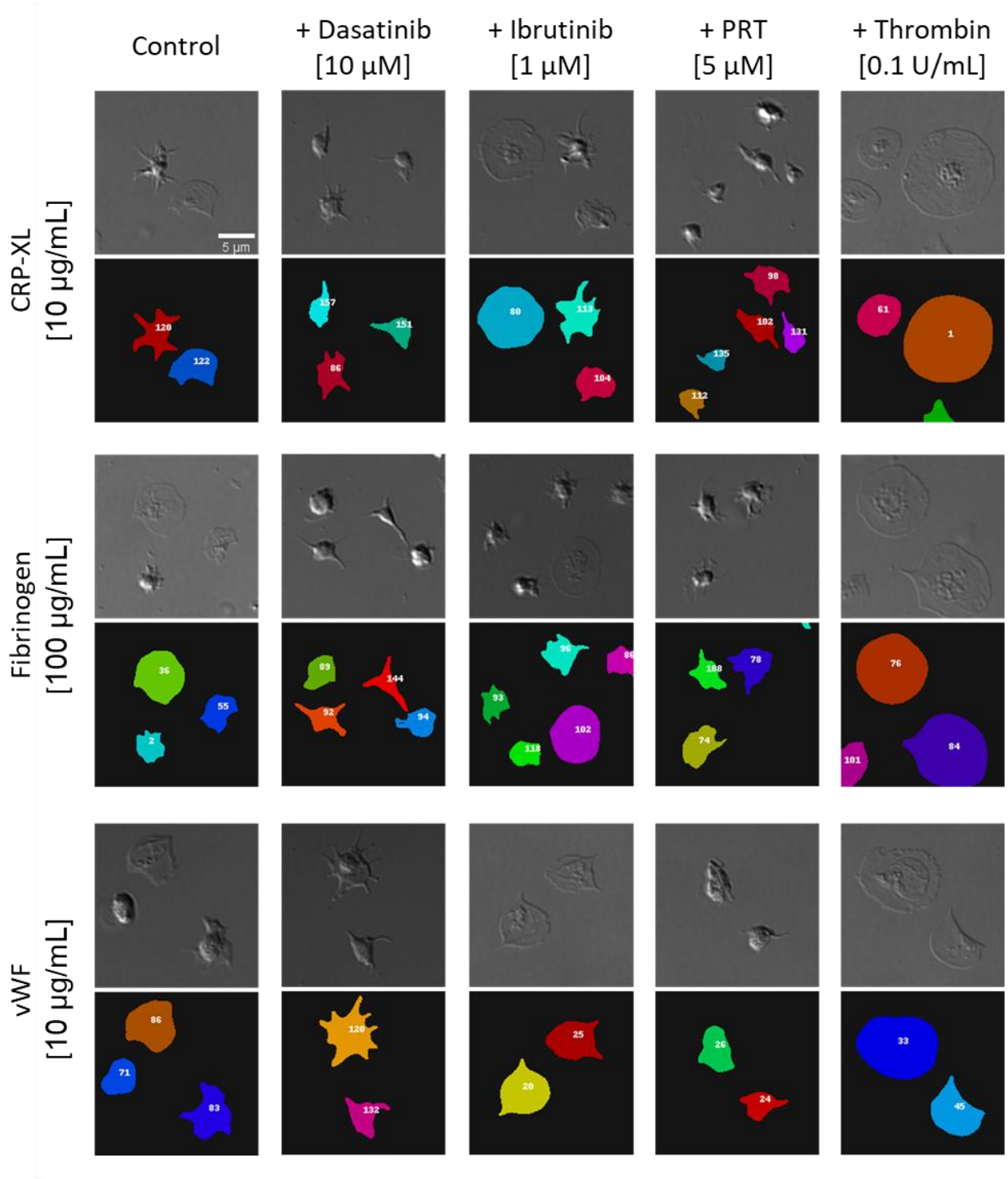

Figure 3.6 CNN can successfully identify inhibitor and agonist-induced changes in platelet morphology.

Washed platelets (1 x 10^7 /mL) were spread over three different substrates (CRP-XL [10 µg/mL], fibrinogen [100 µg/mL] or vWF [10 µg/mL]) in the presence of either Dasatinib [10 µM], Ibrutinib [1 µM], PRT-060318 [5 µM] or Thrombin [0.1 U/mL], or in the absence of inhibitor or agonist (control) to assess if the CNN could detect extremes in cell morphology. Representative cropped DIC images show the extremes in platelet cell shape, whilst corresponding segmented images demonstrate the cell morphology identified by the CNN. Scale bar represents 5 µm.

3.2.5 Trained CNN quantifies extremes in platelet morphology.

The data outputs from the CNN were further quantified to identify if extreme differences could be identified when using inhibitors and agonist known to impact on platelet morphology. The CNN identified that Dasatinib (13.66 ± 0.34 μm^2) and PRT-060318 (13.16 ± 1.48 μm^2) resulted in a significant decrease in platelet spread area when compared to control platelets spread on CRP-XL (38.52 ± 2.34 μm^2) (Figure 3.7A). Dasatinib is an inhibitor of Src family kinases (SFKs) known to impair collagen-induced signalling [213-215], whilst PRT-060318 is a Syk inhibitor previously shown to reduce platelet spreading over CRP-XL [216] and collagen [210,216,217]. Ibrutinib had no inhibitory effect on platelet spreading on CRP-XL (Figure 3.7A), which is supported by studies which suggest that the kinase activity of Btk does not play a major role downstream of GPVI [209,218]. No further increase in spread area was found in the presence of Thrombin, suggesting that control platelets were fully spread.

When platelets were spread on fibrinogen the CNN identified that thrombin (43.31 ± 3.60 μm^2) resulted in a significant increase in platelet spread area when compared to control platelets (23.97 ± 3.94 μm^2) (Figure 3.7B). This is a result of thrombin initiated integrin inside-out signalling, leading to enhanced activation and binding of GPIIb/IIIa (αIIbβ3) to fibrinogen and increased platelet spreading [219]. Dasatinib, Ibrutinib and PRT-060318 had no inhibitory effect on the platelet spread area over fibrinogen. PRT-060318 was found to have a significant inhibitory effect on the platelet spread area over a vWF substrate (18.38 ± 1.85 μm^2) when compared to control platelets (35.55 ± 6.38 μm^2) (Figure 3.7C). The role of Syk down stream of GPIb is controversial but Syk deficient platelets display inhibited platelet spreading on vWF [220]. Dasatinib, Ibrutinib and thrombin had no significant effect on platelet spreading over vWF (Figure 3.7C).

When observing perimeter measurements (Figure 3.7D-F), the CNN identified that Dasatinib (18.19 ± 0.25 μm) and PRT-060318 (18.18 ± 3.18 μm) resulted in a significant decrease in platelet perimeter when compared to control platelets on CRP-XL (Figure 3.7D). Further supporting the inhibition of Src and Syk signalling pathways which are known to impair platelet spreading on collagen [215,216]. There was no difference in perimeter measurements between platelets treated with Ibrutinib or thrombin.

The CNN identified that platelets treated with Dasatinib (24.99 ± 2.82 μm) have a significantly increased perimeter when compared to control platelets (20.68 ± 1.73 μm) on fibrinogen (Figure 3.7E). Consistent with the literature, Dasatinib results in small spikey platelets [221], described here by a decreased spread area and an increased perimeter. Additionally, when compared to control platelets, there are significant increases in the

perimeter when treated with thrombin (26.52 ± 1.07 μm), which is consistent with an increased spread area due to activated GPIIb/IIIa (αIIbβ3) (Figure 3.7E). No inhibitory effects on the perimeter were observed in the presence of Ibrutinib or PRT-060318 on fibrinogen, while the CNN identifies no difference in platelet perimeter when spread on vWF (Figure 3.7F).

Circularity scores were also outputted by the CNN, which identified that Dasatinib (0.57 ± 0.02) and PRT-060318 (0.56 ± 0.09) were significantly decreased and less circular than control platelets (0.72 ± 0.08) on CRP-XL (Figure 3.7G), consistent with reports that these inhibitors result in small and non-circular platelets as a result of abolished lamellipodia formation [222,223]. As with spread area and perimeter, there were no inhibitory effects in the presence of Ibrutinib and thrombin, suggesting that platelet spreading was not impacted by either. The CNN also identifies that circularity for both Dasatinib (0.45 ± 0.07) and PRT-060318 (0.55 ± 0.03) are significantly decreased when compared to control platelets (0.67 ± 0.01) on fibrinogen (Figure 3.7H). There was no inhibitory effect by Ibrutinib or reactivity to thrombin on fibrinogen, suggesting that Ibrutinib had no effect on platelet circularity, and that platelets were fully spread in the presence of thrombin. Similar to spread area and perimeter, no significant differences were observed between control, inhibited platelets and activated platelets on vWF (Figure 3.7I).

These data demonstrate that the trained CNN successfully detects extremes in platelet morphologies spread over different substrates when pre-treated with inhibitors or agonist known to impair platelet spreading. This data also provides evidence that the training material used to train the CNN is generalised. Allowing the CNN to identify and quantify platelets in a variety of independent images with extreme platelet morphologies.

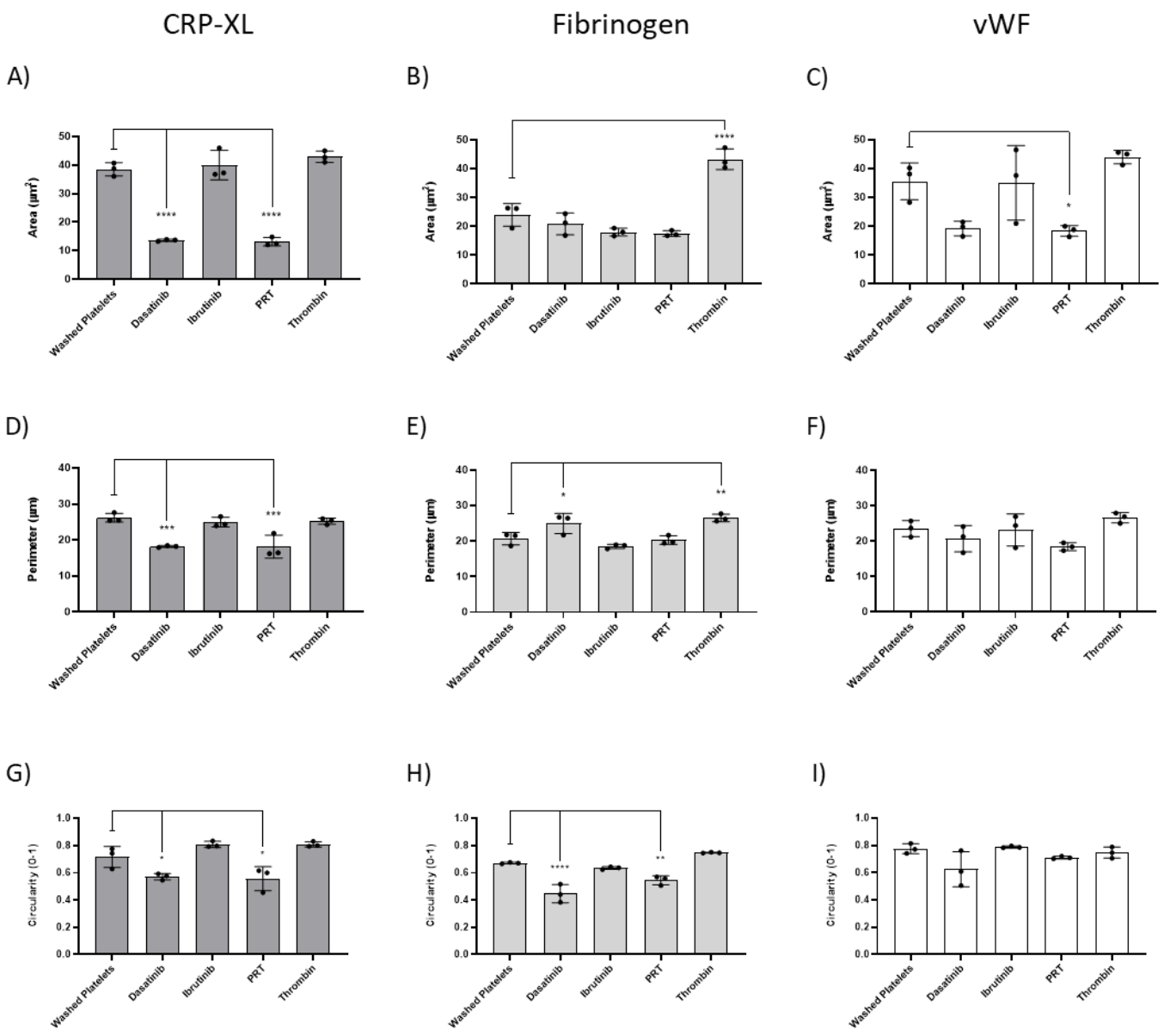

Figure 3.7 CNN can quantify inhibitor and agonist-induced changes in platelet morphology.

Platelet spread area (A, B, C), platelet perimeter (D, E, F) and platelet circularity (G, H, I) were quantified over the three different substrates (CRP-XL (A, D, G), Fibrinogen (B, E, H) and vWF (C, F, I)). The mean ± SD of three experimental replicates (n=3), whereby each experimental replicate was the mean of five fields of view, were plotted and analysed using one-way ANOVA with Bonferroni post-test. *p ≤ .05, **p ≤ .01, ***p ≤ .001, ****p ≤ .0001.

3.2.6 CNN eliminates bias identified between manual annotations when evaluating inhibitor and agonist-induced changes in platelet morphology.

To investigate if manual annotations ensued different scientific conclusions, the five manual annotators from previous analyses were requested to manually annotate a subset of images when platelets were spread over fibrinogen in the presence or absence of inhibitor or agonist. All manual annotators were blinded to the image selection. Fibrinogen was chosen as a substrate which showed subtle phenotypic changes in platelet morphology in the presence of inhibitors, with the aim to expose genuine similarities or differences between the five manual annotators. There were significant differences observed when investigating variation between individual manual annotators (Figure 3.8), indicating different interpretations of platelet morphology.

There were no significant differences when observing inter-individual differences between all the manual annotators and the CNN for washed platelets (Figure 3.8A). Indicating that the CNN could identify washed platelets spread over fibrinogen similarly to all manual annotators recruited for this study. When considering Dasatinib treated platelets however, manual annotator 5 estimated the spread area of platelets as significantly larger (22.5 ± 1.3 μm^2) than manual annotator 2 (18.3 ± 1.2 μm^2) (Figure 3.8B). There were no further differences between the CNN and manual annotators 1, 3 and 4.

Further inter-individual differences were identified when observing the spread area of platelets pre-treated with Ibrutinib (Figure 3.8C). Manual annotator 5 interpreted the spread area of platelets treated with Ibrutinib significantly differently (21.6 ± 1.1 μm^2) when compared to the CNN (18.9 ± 0.3 μm^2), and manual annotators 1 (19.1 ± 0.8 μm^2), 2 (17.5 ± 0.4 μm^2) and 4 (18.0 ± 0.9 μm^2). There were further significant inter-individual differences between manual annotators 2 (17.5 ± 0.4 μm^2) and 3 (19.8 ± 0.6 μm^2). Likewise, significant differences were observed when platelets were pre-treated with PRT (Figure 3.8D); namely manual annotator 5 estimated the spread area of PRT treated platelets as significantly larger (19.7 ± 0.4 μm^2) when compared to the CNN (17.2 ± 0.7 μm^2), and manual annotators 2 (16.1 ± 1.0 μm^2) and 4 (16.1 ± 0.4 μm^2). The data presented for Dasatinib, Ibrutinib and PRT suggests that the spread area of platelets pre-treated with inhibitors known to impact platelet morphology may be harder to interpret, and that a CNN would remove this subjectivity and bias.

Similar to washed platelets, there were no significant differences between the CNN and all manual annotators when observing the spread area of platelets pre-treated with thrombin (Figure 3.8E). In part, this may be explained by the fact that all platelets will be fully spread

and presenting lamellipodia. This may be easier to manually annotate when compared to filopodia extensions induced by inhibition to pathways known to impact platelet morphology.

Overall, the data presented in Figure 3.7 and Figure 3.8 is evidence that image analysis by the CNN, which is comparable to several manual annotators in this study, removes bias associated with time consuming manual analyses.

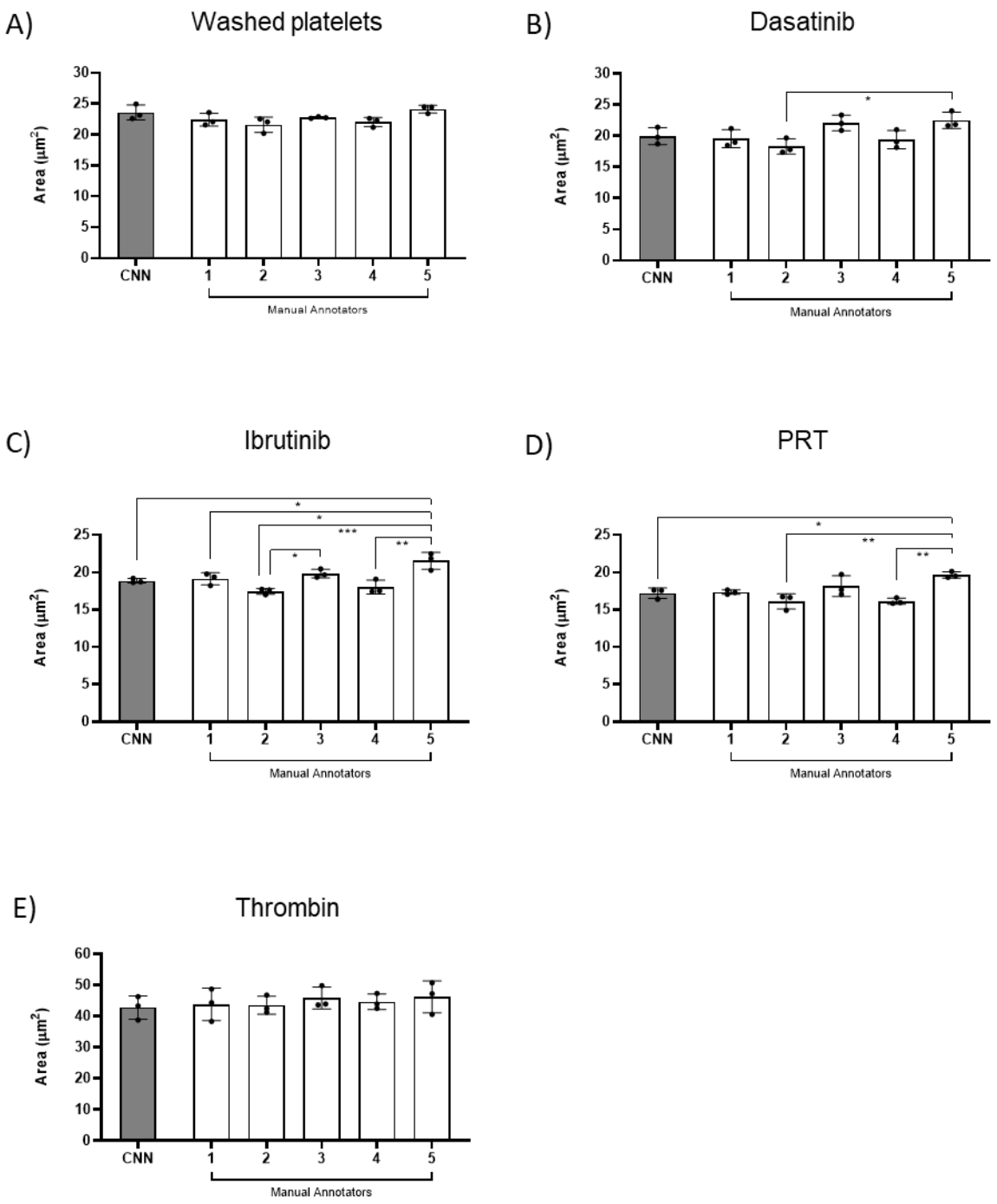

Figure 3.8 Spread area of platelets treated with inhibitors are estimated significantly differently between several manual annotators.

Manual annotations were compared to CNN quantification of platelet spread area. Washed platelets (1 x 10^7 /mL) (A), platelets treated with either Dasatinib [10 µM] (B), Ibrutinib [1 µM] (C), PRT-060318 [5 µM] (D), or Thrombin [0.1 U/mL] (E) were spread over a fibrinogen substrate [100 µg/mL]. The mean ± SD of three experimental replicates (n=3), where each experimental replicate was the mean of three fields of view, were analysed using one-way ANOVA with Bonferroni post-test. *p ≤ .05, **p ≤ .01, ***p ≤ .001, ****p ≤ .0001.

3.2.7 CNN eliminates differences in scientific conclusions between different manual annotators.

Next, the manually annotated images pre-treated with either inhibitor or agonist were directly compared to control washed platelets from the same manual annotator to identify if scientific conclusions were different between annotators.

Data for the washed platelet control (WPs) for both the CNN and the manual annotators were directly compared to either Dasatinib (Figure 3.9A), Ibrutinib (Figure 3.9B), PRT (Figure 3.9C) or thrombin (Figure 3.9D). There were no significant differences in surface area when directly comparing control washed platelets against Dasatinib treated platelets for both the CNN and all manual annotators (Figure 3.9A). Suggesting that firstly, there were little changes in surface area between control washed platelets and Dasatinib treated platelets, but secondly, that neither CNN nor manual annotators interpreted spread platelet area differently.

When comparing control washed platelets to Ibrutinib treated platelets (Figure 3.9B), there are no significant differences observed for the CNN, and manual annotators 1, 3 and 5. However, there were significant differences when directly comparing control washed platelets to Ibrutinib treated platelets for manual annotators 2 (WPs: 21.6 ± 2.1 μm^2, Ibrutinib: 17.5 ± 1.2 μm^2) and 4 (WPs: 22.0 ± 1.4 μm^2, Ibrutinib: 18.0 ± 1.5 μm^2), suggesting that these annotators identified the changes to platelet morphology differently than the CNN or other manual annotators.

Differences were also observed when comparing control washed platelets to PRT treated platelets (Figure 3.9C). There are no significant differences observed for the CNN, and manual annotators 1 and 2. However, there were significant differences when comparing control washed platelets to PRT treated platelets for manual annotators 3 (WPs: 22.8 ± 1.7 μm^2, PRT: 18.2 ± 2.3 μm^2), 4 (WPs: 22.0 ± 1.4 μm^2, PRT: 16.1 ± 1.3 μm^2) and 5 (WPs: 24.1 ± 0.2 μm^2, PRT: 19.7 ± 1.3 μm^2). Again, suggesting that these manual annotators interpreted the changes to platelet morphology differently than the CNN and other manual annotators.

Conversely, when comparing control washed platelets to thrombin treated platelets (Figure 3.9D), there were significant increases in the spread surface area of platelets pre-treated with thrombin for the CNN and all manual annotators. This suggests that the CNN and all manual annotators interpreted the spread area of platelets treated with thrombin similarly. This may be explained by the extreme change to platelet spreading in the presence of thrombin, where even annotated badly, would always result in a significant increase to platelet spread area.

Together this data identifies that there are significant differences in scientific conclusions when comparing the CNN with manual annotators for both Ibrutinib and PRT treated platelets. A CNN may, therefore, be beneficial in standardising analyses.

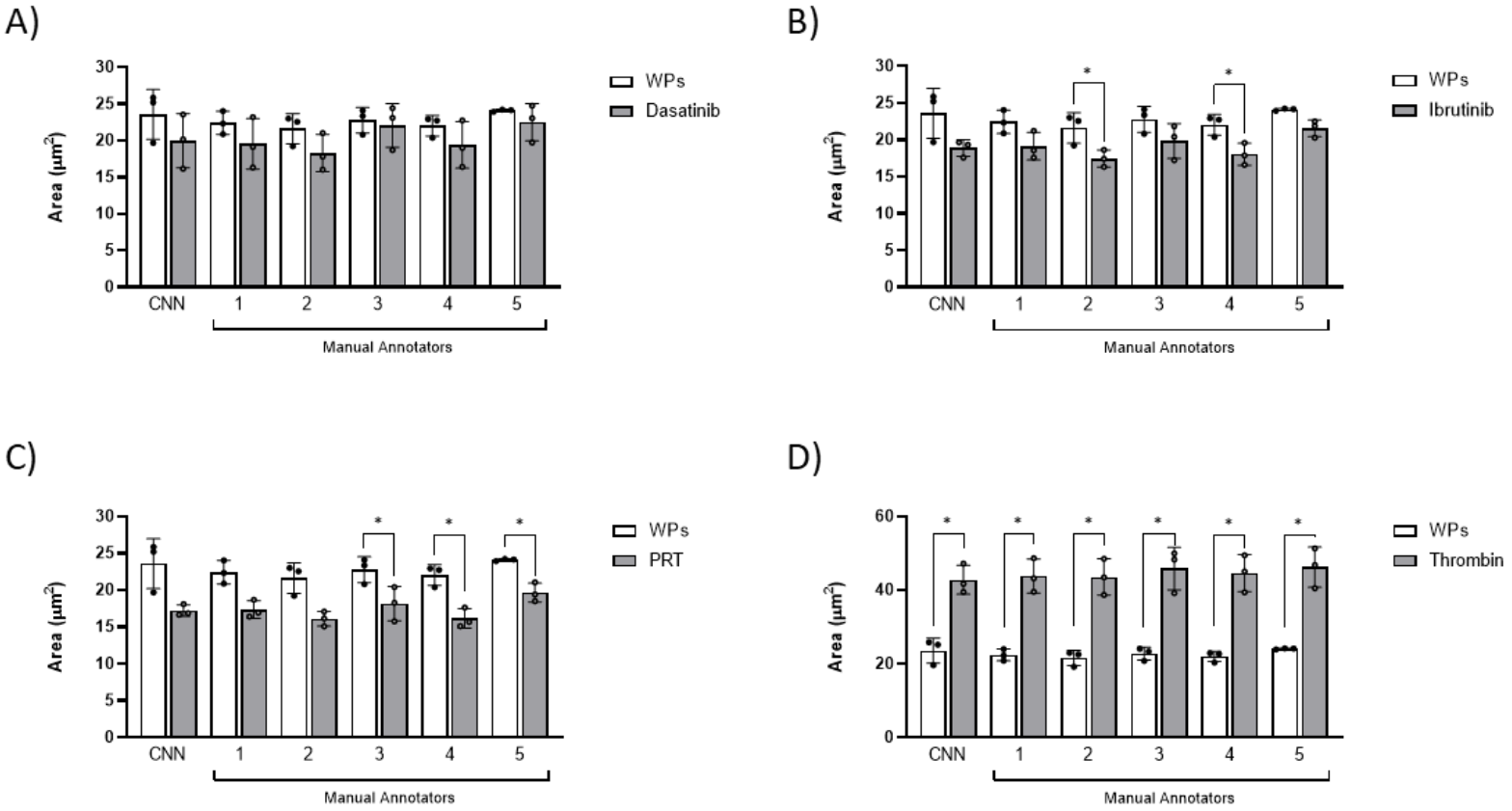

Figure 3.9 CNN identifies bias between different manual annotators when evaluating inhibitor and agonist-induced changes in platelet morphology.

Control washed platelets (WPs) quantified by the CNN and manual annotators were directly compared to platelets treated with Dasatinib (A), Ibrutinib (B), PRT-060318 (C) and Thrombin (D). The mean ± SD of three experimental replicates (n=3), where each experimental replicate was the mean of three fields of view, were analysed using a paired two-tailed T-test. *p ≤ .05, **p ≤ .01, ***p ≤ .001, ****p ≤ .0001.

3.2.8 Trained CNN can quantify the spreading of mouse platelets.

Mouse models are regularly used in the platelet field where genes of interest can be disrupted to generate platelets deficient in proteins of interest. It was therefore next evaluated if the CNN could quantify mouse platelet morphology imaged using DIC microscopy without any additional training.

Mouse platelets were spread over fibrinogen and, as with human platelets, the CNN was able to segment mouse platelets without further training (Figure 3.10). A representative image details a full-scale image of mouse platelet spreading, where the corresponding segmentation from the CNN could successfully depict individual mouse platelets (Figure 3.10A). The CNN could successfully quantify the surface area (Figure 3.10B), perimeter (Figure 3.10C) and circularity (Figure 3.10D) of mouse platelets spread over fibrinogen.

Furthermore, the spread surface area of mouse platelets determined using the CNN (14.6 ± 0.55 μm^2) was similar to the spread area of mouse platelets quantified in the literature by immunofluorescence [224], or the manual quantification of DIC images [225].

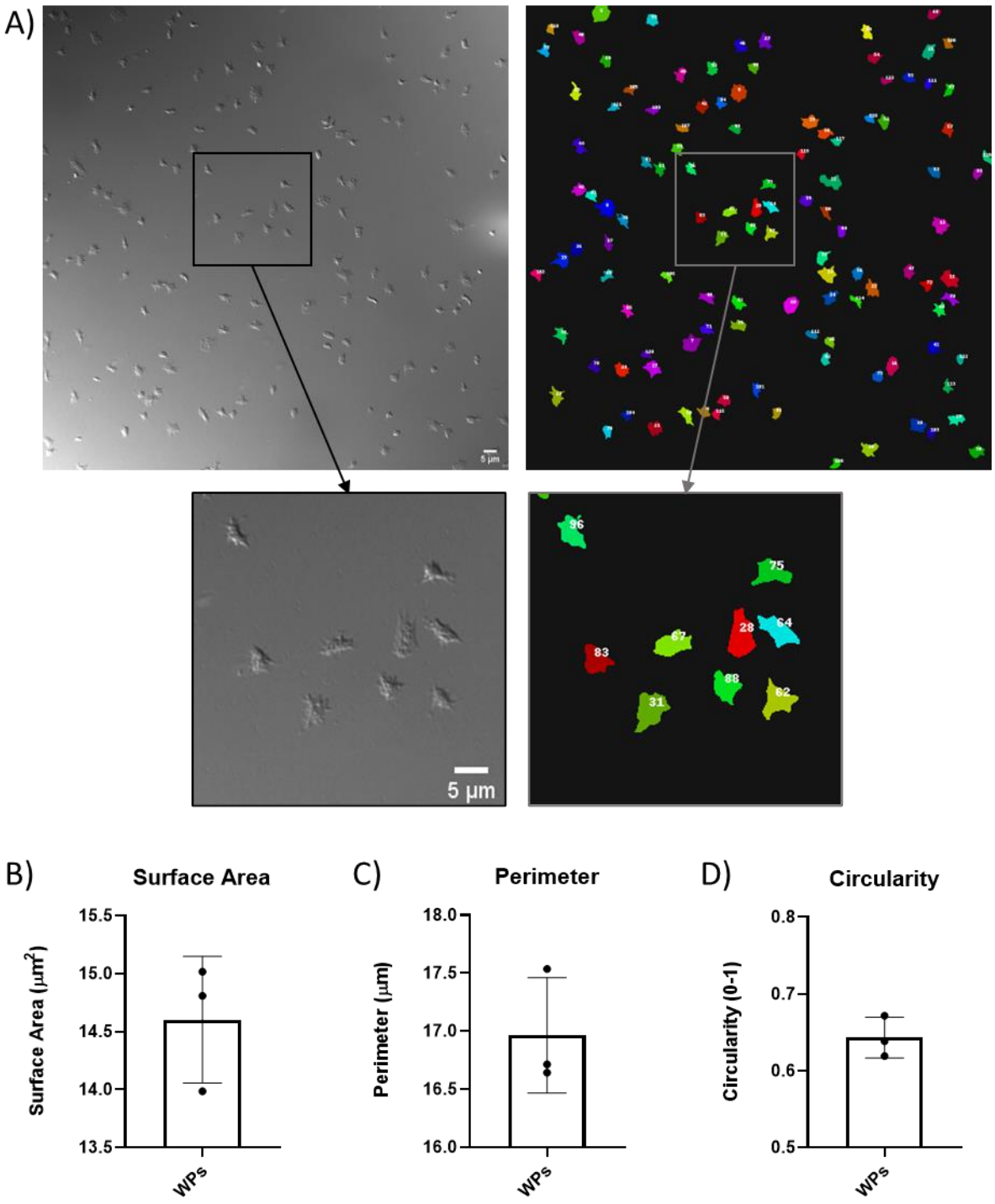

Figure 3.10 CNN can quantify the morphology of mouse platelets.

Washed mouse platelets (1 x 10^7 /mL) were spread over fibrinogen [100 µg/mL] to assess if the CNN could segment and quantify mouse platelets. A representative DIC image provides an example of mouse platelet spreading alongside a matched segmented prediction by the CNN (A). The CNN quantified surface area (B), perimeter (C) and circularity (D). Data represents the mean ± SD of three experimental replicates (n=3). Scale bar 5 µm.

3.2.9 Platelet parameters are not altered when fixing and permeabilising platelets.

As well as the imaging of unlabelled spread platelets, fluorescently labelled platelets are regularly used to quantify platelet morphology and cytoskeletal rearrangements in the field. Actin is the most abundant protein in platelets and is often investigated due to its essential role in platelet morphology and cytoskeletal rearrangements [50,52]. For example, probes targeting actin include fluorescently labelled Lifeact and fluorescently labelled phalloidin [48,49,226]. In order to label the actin cytoskeleton, spread platelets are typically fixed and permeabilised to allow fluorescently labelled antibodies and probes targeting actin to penetrate the cell membrane.

To compare the automated CNN output with fluorescently labelled platelets, it was first important to investigate if there was a difference between platelets which had been fixed and platelets which had been fixed, permeabilised and fluorescently labelled. The actin fibres of platelets which had been fixed and permeabilised were labelled using Alexa-Fluor 488 conjugated phalloidin.

Washed platelets which had been fixed were directly compared to fixed and permeabilised platelets (Figure 3.11). Dasatinib treated platelets and thrombin treated platelets were also compared (Figure 3.11). Platelet spread area (Figure 3.11A), perimeter (Figure 3.11B) and circularity (Figure 3.11C) were quantified using the CNN.

CNN quantification presented no differences in platelet spread area when comparing fixed platelets to fixed and permeabilised platelets for washed platelets, Dasatinib treated, and thrombin treated platelets (Figure 3.11A). Similarly, there were no differences when comparing fixed platelets to fixed and permeabilised platelets, when assessing platelet perimeter (Figure 3.11B) and platelet circularity (Figure 3.11C). Suggesting that permeabilisation of fixed platelets does not impact on platelet parameters when outputted by the CNN.

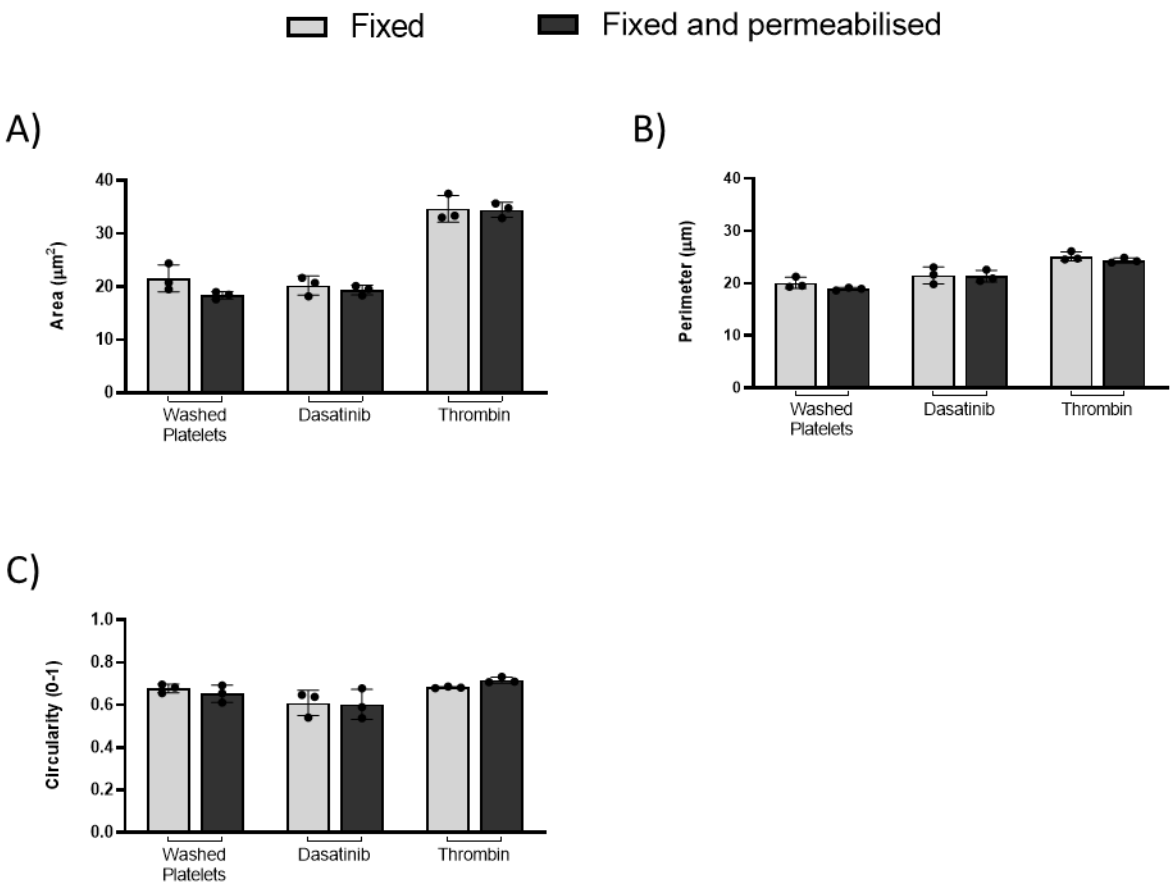

Figure 3.11 Quantification of fixed and permeabilised platelets are the same as fixed platelets.

Washed platelets (1 x 10^7 /mL) and platelets pre-treated with Dasatinib [10 µM] and thrombin [0.1 U/mL] were spread over fibrinogen [100 µg/mL] and either fixed or fixed and permeabilised. CNN quantification for surface area (A), perimeter (B) and circularity (C) assessed differences between the two methods. The mean ± SD of three experimental replicates (n=3), where each experimental replicate was the mean of three fields of view, were analysed using paired two-tailed T-tests. ns > .05.

3.2.10 Comparison of CNN outputs with fluorescently labelled platelets.

Since there were no differences identified between fixed and fixed and permeabilised platelets, it was next investigated if fluorescently labelled platelets identified similar platelet metrics to the CNN using commonly implemented thresholding analysis methods.

Representative images detail DIC images for washed platelets, Dasatinib treated platelets and thrombin treated platelets (Figure 3.12A). The segmentation of platelets as identified by the CNN are alongside the corresponding DIC image, while the final column details the extent of fluorescently labelled permeabilised platelets by phalloidin labelling (Figure 3.12A).

The CNN quantification was directly compared to fluorescent quantification for platelet spread area (Figure 3.12B), perimeter (Figure 3.12C) and circularity (Figure 3.12D) as before. A significant decrease in platelet spread area for washed platelets (14.7 ± 0.3 μm^2) and Dasatinib treated platelets (14.6 ± 0.7 μm^2) was observed in phalloidin labelled platelets when compared to the CNN segmentation for washed platelets (21.6 ± 2.5 μm^2) and Dasatinib treated platelets (20.2 ± 1.8 μm^2) (Figure 3.12B). This may, in part, be due to the nonuniform staining of the actin filaments in spreading platelets and the need to threshold the fluorescent images. There was no difference in the spread area of platelets as measured by the CNN or phalloidin labelling in the presence of thrombin.

No differences were observed when comparing platelet perimeter quantified by the CNN to phalloidin labelling of washed platelets in the presence or absence of Dasatinib or thrombin (Figure 3.12C). However, there was a significant decrease in platelet circularity when comparing the CNN output for washed platelets (0.68 ± 0.02) with phalloidin labelled washed platelets (0.57 ± 0.02) (Figure 3.12D). No significant differences were seen between the CNN and phalloidin labelling when calculating the circularity in platelets treated with Dasatinib or thrombin (Figure 3.12D).

To further investigate if the overall scientific conclusions between the CNN analysis and fluorescent analysis by phalloidin labelling were similar, the data was reanalysed so as to directly investigate the scientific outcomes for each analysis method (Figure 3.13). Both the CNN analysis and fluorescent analysis for spread platelet area identified significant differences when comparing both washed platelets (CNN: 21.6 ± 2.5 μm^2, phalloidin: 14.7 ± 0.3 μm^2) and Dasatinib treated platelets (CNN: 20.2 ± 1.8 μm^2, phalloidin: 14.6 ± 0.7 μm^2) directly to thrombin treated platelets (CNN: 34.7 ± 2.5 μm^2, phalloidin: 30.9 ± 5.3 μm^2) (Figure 3.13A). There were no differences when comparing the spread area of washed platelets to the spread area of Dasatinib treated platelets for either analysis method.

Similarly with platelet perimeter, both the CNN analysis and fluorescent analysis identified significant differences when comparing both washed platelets (CNN: 20.0 ± 1.1 μm, phalloidin: 18.0 ± 0.5 μm) and Dasatinib treated platelets (CNN: 21.5 ± 1.6 μm, phalloidin: 18.7 ± 0.7 μm) directly to thrombin treated platelets (CNN: 25.1 ± 0.9 μm, phalloidin: 27.1 ± 4.3 μm) (Figure 3.13B). There were no differences when comparing the perimeter of washed platelets to the perimeter of Dasatinib treated platelets for either analysis method. This contrasts with significant differences identified previously in Figure 3.7, and may, in part, be explained by a new subset of platelet donors and small sample sizes. There were also no significant differences for either analysis method when investigating platelet circularity which also contrasts with previous data in Figure 3.7 (Figure 3.13C).

Nevertheless, although this data demonstrates that while outputs from the CNN analysis cannot be directly compared to fluorescently labelled platelets by labelling with phalloidin (Figure 3.12), the overall scientific conclusion using each method is the same (Figure 3.13).

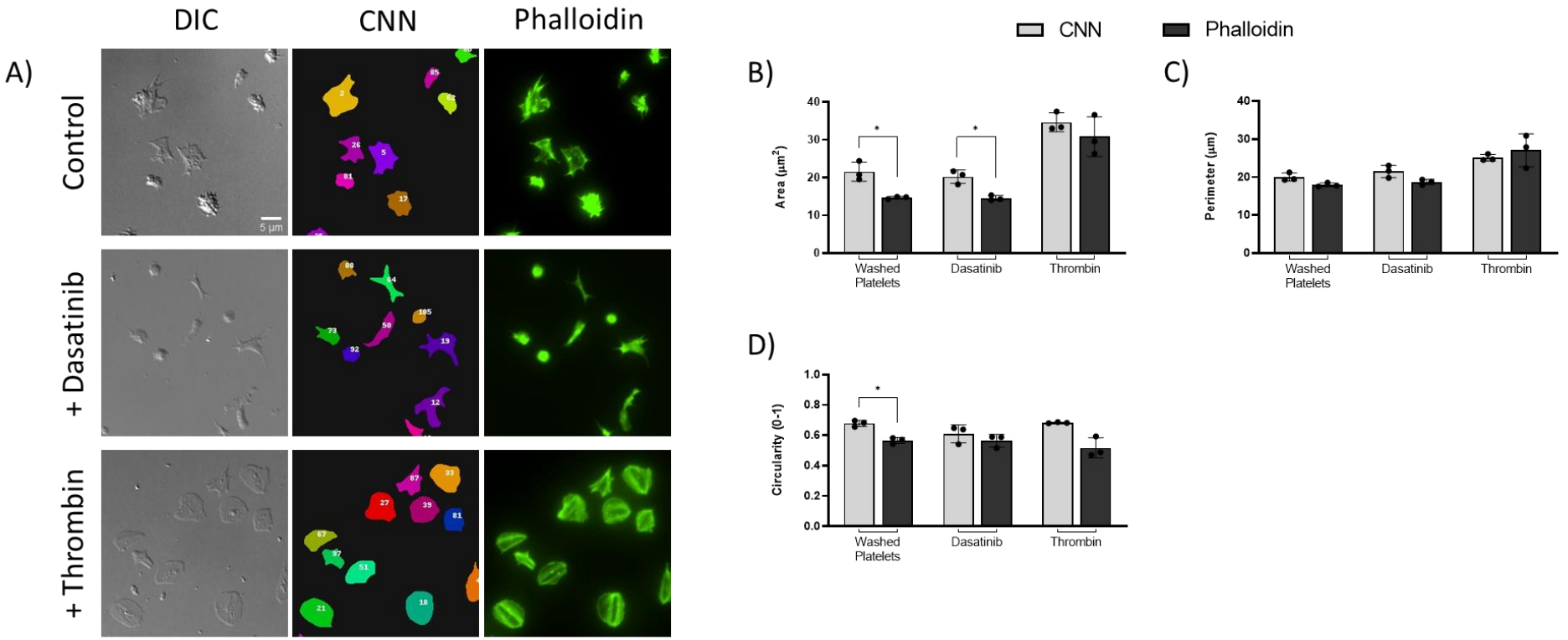

Figure 3.12 Comparison of platelet morphology by the CNN to fluorescently labelled platelets.

Washed platelets, treated with and without dasatinib [10 µM], and thrombin [0.1 U/mL] were spread over a fibrinogen substrate. Representative images (A) show a DIC image, matched CNN segmentation, and matched fluorescently labelled image of platelets stained with Alexa-Fluor 488 conjugated phalloidin [0.3 U/mL]. CNN data was compared to fluorescent analysis for spread platelet area (B), perimeter (C) and circularity (D). The mean ± SD of three experimental replicates (n=3), whereby each experimental replicate was the mean of three fields of view, were analysed using paired two-tailed T-tests. *p ≤ .05.

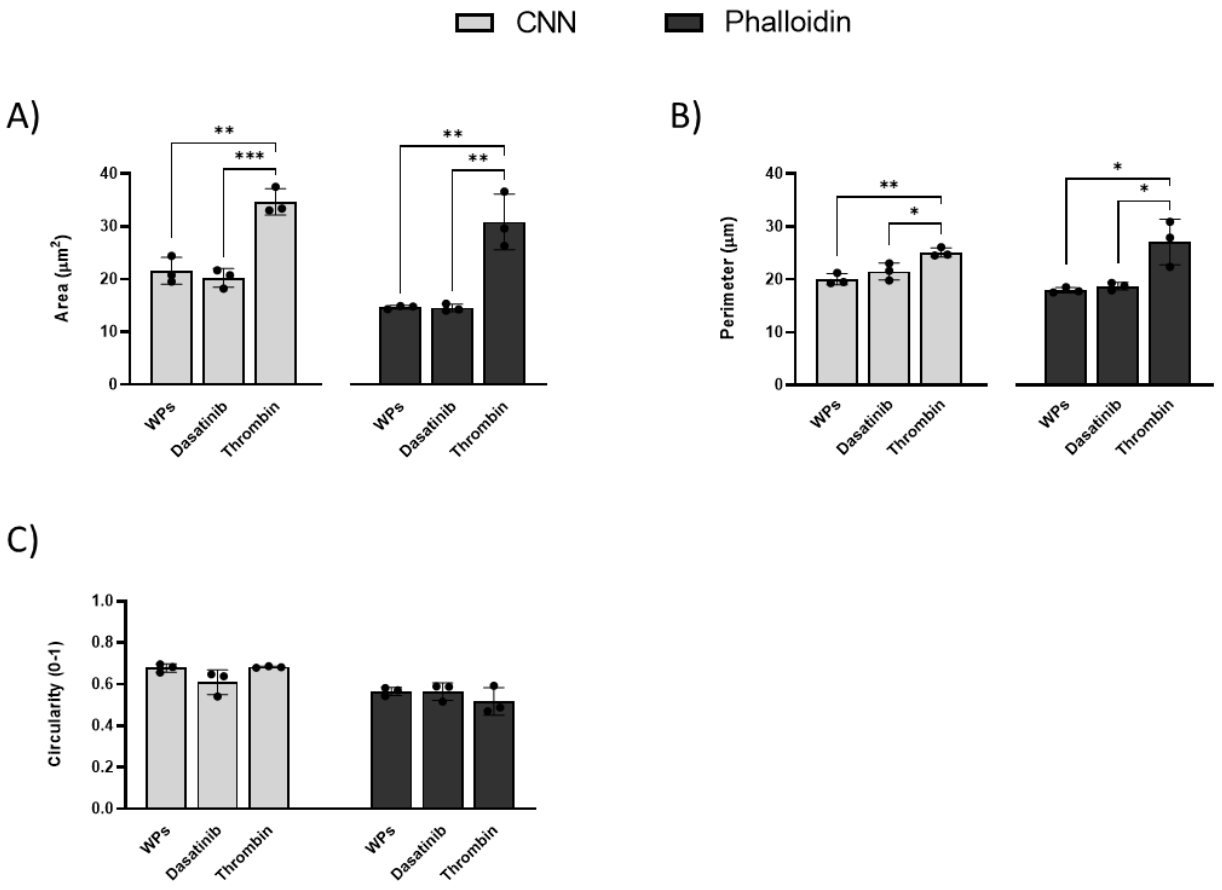

Figure 3.13 Comparison of CNN analysis method to fluorescent labelling analysis method.

Washed platelets (WPs) [1 x 10^7 /mL], treated with and without Dasatinib [10 μM], and thrombin [0.1 U/mL] were spread over a fibrinogen substrate. The CNN data and Phalloidin data were compared to identify differences between each analysis method for spread platelet area (A), perimeter (B) and circularity (C). The mean ± SD of three experimental replicates (n=3), where each experimental replicate was the mean of three fields of view, were analysed using one-way ANOVA with Bonferroni post-test. The mean of each group was compared to the mean of all groups which were analysed with the same analysis method; either CNN (light grey bars) or phalloidin analysis (dark grey bars). *p ≤ .05, **p ≤ .01, ***p ≤ .001.

3.3 Discussion

Here we demonstrate, for the first time, a method for fully automated platelet morphology analysis of DIC images by the implementation of a CNN. In this study we demonstrate that (i) a manageable increase in training material will improve CNN performance when assessing mAP; (ii) the CNN is consistent in quantifying the spread area of platelets when directly compared to manual annotators; (iii) the automated CNN has potential limitations in that its measurements of other commonly used platelet metrics, perimeter and circularity, are not always comparable to those of manual annotators; and (iv) the CNN is capable of segmenting and quantifying extremes in platelet morphologies when inducing inhibition or activation of biologically important pathways known to impact platelet spreading, and reveals bias associated with manual annotations.

This work presents a fully automated platelet spreading analysis approach facilitated by a supervised training set consisting of 120 DIC images. Although the curation of the initial training material can be time consuming, the substantial increase in the mapping function of the CNN when increasing the training material is evident. However, training material is typically generated by one or two expert annotators which can potentially incur bias of both the training material selected and manual interpretations. A community effort is recommended to minimise bias associated with training material [227]. This may include several expert annotators who each annotate independent training sets, and random sampling is then implemented to select a final training set. This avoids over-representation of a particular annotator for example. Nonetheless, this also raises the question of how many training images are required to reasonably train a CNN. While this question has not been answered in full during this project, it has been demonstrated that a realistic increase in training images returns a strong performance. Furthermore, successful identification of platelets in multiple independent experiments suggests that the trained CNN is generalised to different experimental set ups, including platelet spreading assays using mouse platelets.

In addition to being generalisable, this computational model removes user variability and bias associated with subjective decisions by manual annotators [227]. In particular, manual segmentation of DIC images, where the shadow artefact enhances contrast, may contribute to a difference in image interpretation between different manual annotators. It has been shown that the CNN successfully measures platelet spread area, a commonly used metric to assess platelet function and the impact of anti-platelet therapies. Spread area was consistent with manual annotators, and automated outputs were directly comparable with published data. Therefore, this CNN presents a robust, practical and fast method to automate large-scale platelet spreading analyses. With the ensemble approach applied in

this project, each image takes approximately 3 minutes to segment and requires a high-end graphics card (e.g., NVIDIA Quadro); hardware which would typically already exist in laboratories which routinely utilise microscopy and microscopy analysis facilities.

However, although platelet spread area was consistent with manual annotators and published literature, other commonly extracted measurements, such as platelet perimeter and circularity were not directly comparable to those obtained by manual segmentation. Quantitative outputs from the CNN identify a decreased perimeter, and consequently an increased circularity when compared to a trainer and 5 independent annotators. This may be a direct limitation of the pseudo shadow effect of the DIC imaging technique as discussed previously. This shadow artefact could be impacting on feature extraction by creating a smoothing effect which impacts segmentation, causing a difference between manual and automated measurements, and hence identifying limitations of a CNN. Other automated image analyses, namely thresholding analyses, performed using different cells do report perimeter and circularity, however, these are fluorescently labelled images [228,229]. To date, no reports are present in the literature comparing the automated analyses of unlabelled DIC images of platelets to manual platelet analyses, meaning it is difficult to conclude where the limitations lie.

Nonetheless, the CNN performs extremely well when quantifying extremes in platelet morphology when inducing inhibition to Syk and Src family kinase activation pathways, and by thrombin induced platelet spreading. The CNN successfully detected morphological extremes which may be typical of platelet defect phenotypes, which are abundantly researched in the platelet field. Additionally, automated analysis modalities such as this, may aid the clinical stratification of individuals at risk of bleeding or thrombosis. Clinical examples of spreading defects include macrothrombocytopenia caused by rare genetic variants of *TUBB1* [230], and dominant Glanzmann thrombasthenia (β3 integrin deficiency) [231]. Platelet spreading analyses are currently missing from standard haematology approaches due to the complexity of analysis and experience required of the researcher.

Overall, the application of deep learning models for biological image analysis has become increasingly prevalent in recent years and, as demonstrated in this study, abrogates time consuming manual analyses and removes individual subjectivity and bias. Yet, in an era where many science domains are producing unprecedented amounts of data, some challenges and limitations persist which should be considered prior to using automated outputs. Firstly, one of the challenges which remains in computational models is how to manage differences between data sets e.g., differing contrast and focus. Noise within images at acquisition can directly impact the learning accuracy and output accuracy of a

CNN [232,233]. Secondly, CNNs require a large amount of generalised training material which can be time consuming to curate yet, as demonstrated here, a realistic increase in training material substantially increases model performance [194]. Thirdly, all datasets will contain a level of bias. For any image, only a limited number of scenarios will occur. A CNN, therefore, may be biased towards a particular training set [234]. Although, data augmentation can assist training by artificially inflating the original training material, some studies demonstrate that performance is not improved when compared to those trained using real images [235]. These points highlight how fundamental generalised training material is to the performance of a CNN.

This CNN also has the potential to be adapted to alternative imaging modalities, such as phase contrast [236], if new training material is generated. Furthermore, the successful segmentation of adhered platelets by deep learning could open up the potential to exploit live cell tracking of dynamic platelet processes which are involved in platelet migration [237] and thrombus formation [238]. A limiting factor in live cell tracking by deep learning, and which adds additional computational complexity, is that most cell types will undergo cell division. However, platelets are non-dividing cells, and recent studies have shown successful live cell tracking in other non-dividing cell lines [239,240]. Interestingly, an active area of research has also involved using CNNs to investigate cell-cell interactions [241-243]. A quality control step has been maintained in the approach presented here to allow users to quickly assess and remove instances of platelet-platelet interactions since platelets may influence other touching platelets. However, the investigation of contact dependent pathways in response to vascular injury and extension of a platelet plug [179], as well as platelet interactions with immune cells [244], may be an area where automated analyses may be of interest in the future.

3.3.1 NC3Rs Impact

Since the CNN can detect mouse platelet spreading, this analysis method also offers the potential to reduce the number of mice per model used in the platelet field. The field is heavily reliant on mouse models to target genes of interest. So, in contrast to previous manual analyses, automated analysis of mouse platelet DIC spreading has the potential to offer robust, consistent, and reliable analyses which can be extended between platelet research groups. This presents an opportunity to standardise outputs which could ultimately lead to a reduction in the number of mice required within the platelet field.

3.3.2 Summary

In summary, the implementation of a CNN to enable automated analysis of platelet morphology removes subjective bias, which is associated with time consuming manual analysis methods, and offers the potential to deliver substantial increases in the quantity and consistency of large platelet data sets, where throughput has previously been limited.

Caution should be employed to fully understand the possible drawbacks of CNNs, and to carefully validate automated outputs. Nevertheless, an automated CNN is advantageous, and given the ease to implement CNN adaptations, there is potential for robust and collaboratively distributed platelet analyses between laboratories. Furthermore, this analysis approach has been implemented to analyse platelet spreading experiments following the fusion of fusogenic liposomes with platelets during results chapters 2 (Section 4) and 3 (Section 5).

Chapter 4: Fuse-It-Color

4.1 Introduction

As discussed previously, other methods of cargo delivery are either not compatible when used in combination with platelets or have not been attempted. Fusogenic liposomes, which are vesicles that can fuse with the membrane of a cell, have been used to successfully deliver cargo into nucleated mammalian cells [121], and this approach offers a promising alternative to interrogate molecular mechanisms in human platelets at the cellular level and in real-time. The overall aim of this project therefore seeks to utilise fusogenic liposomes as a vehicle to deliver cargo directly into the cytoplasm of human platelets *in vitro*.

Understanding the molecular mechanisms which govern platelet function is fundamental when understanding platelet responses during both health and disease. The unveiling of currently unknown molecular mechanisms may allow for the identification of novel drug targets to better treat cardiovascular related diseases. Furthermore, a consequence of research using human platelets directly will reduce the current need of sourcing platelets from genetically modified mouse models in platelet research. Genetically modified mice, where genes of interest have been disrupted in the mouse genome, are commonly used in the platelet field to allow platelets which are deficient in specific proteins to be researched. However, these findings do not always translate well to human platelets.

The first critical step of this project focussed on identifying if fusogenic liposomes can effectively fuse with human platelets without impacting normal platelet function. A commercial source of fusogenic liposomes containing a fluorescent lipophilic dye (Fuse-It-Color, Benaig) (Figure 4.1) were used to label the membrane of platelets by fusion. Fuse-It-Color fusogenic liposomes do not contain a specific cargo, are supplied as a solubilised solution in 20mM HEPES buffer (pH 7.4) and, following fusion, the lipophilic dye is incorporated into the platelet membrane. This chapter focusses on providing a robust method of using fusogenic liposomes in combination with human platelets which minimises unwanted platelet activation. Applications such as flow cytometry or fluorescent microscopy can be used to identify the extent of labelling when detecting the incorporation of the lipophilic dye in the platelet membrane.

Moreover, fusogenic liposome optimisation aims to characterise different aspects of platelet function and behaviour, such as granule release, phosphatidylserine translocation and morphological shape changes. Direct comparisons of platelet function, both in the presence and absence of Fuse-It-Color, will be applied to quantify any functional impact which fusion of liposomes has on normal platelet function.

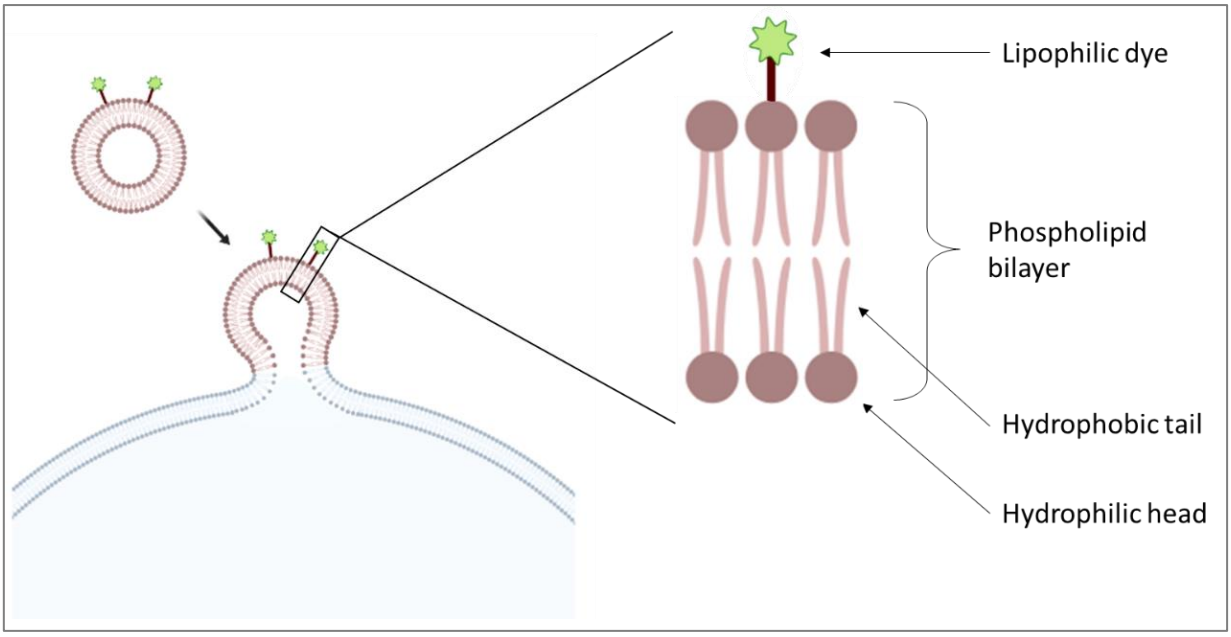

Figure 4.1 Fuse-It-Color

Fusogenic liposomes containing a green lipophilic dye were used to label the cell membrane of platelets. After Fuse-It-Color fusion, the fusogenic liposomes then become an extension of the cell membrane. The phospholipids of the fusogenic liposomes are compatible with the phospholipid bilayer of cell membranes. Schematic created with biorender.com.

4.2 Results

4.2.1 Washed platelets have variable levels of basal platelet activation.

Firstly, the level of background platelet activation of different platelet preparations was quantified to identify the extent of platelet activation prior to liposome fusion. It was anticipated that fusogenic liposomes may induce platelet activation since platelets are readily activated by factors such as inappropriate platelet preparation and changes in temperature [245-247]. It was therefore important to ensure platelet activation remains to a minimum during platelet isolation and the preparation of washed platelets in order to accurately identify any activation as a result of fusion.

P-selectin, a marker of α-granule release, was used as a measure of platelet activation by flow cytometry. Platelets were identified using forward scattered light (FSC) and side scattered light (SSC), a measure of size and granularity respectively (Figure 4.2A*i*). An isotype control was used to identify non-specific antibody binding, where a 2% gate was used to define a boundary to characterise platelet activation (Figure 4.2A*ii*). The extent of platelet activation was subsequently the level of P-selectin exposure by α-granule release above the 2% boundary for platelet rich plasma (PRP) preparations (Figure 4.2A*iii*) and washed platelet (WP) preparations (Figure 4.2A*iv*).

Unsurprisingly, likely due to the additional washing steps, WPs presented a significant increase in the percentage of P-selectin exposure (25.4 ± 12.3%) on the surface of platelets when compared to the PRP preparation (9.9 ± 2.4%) (Figure 4.2B). The median fluorescent intensity (MFI), a measure in the shift in fluorescence intensity of the whole platelet population, was also used to assess P-selectin exposure and compared to the percentage positive metric. When comparing the MFI, there was also a significant increase in P-selectin exposure of WPs (316.2 ± 152 AU) when compared to PRP (111.1 ± 17.9 AU) (Figure 4.2C).

As a result, the PRP preparation was taken forward as a preparation which induced lower platelet activation to identify if platelets can be fluorescently labelled by fusion using a commercial source of fusogenic liposomes (Fuse-it-Color, Benaig). Furthermore, comparisons between the two different data outputs, namely percentage positivity and MFI, identified the same scientific conclusions.

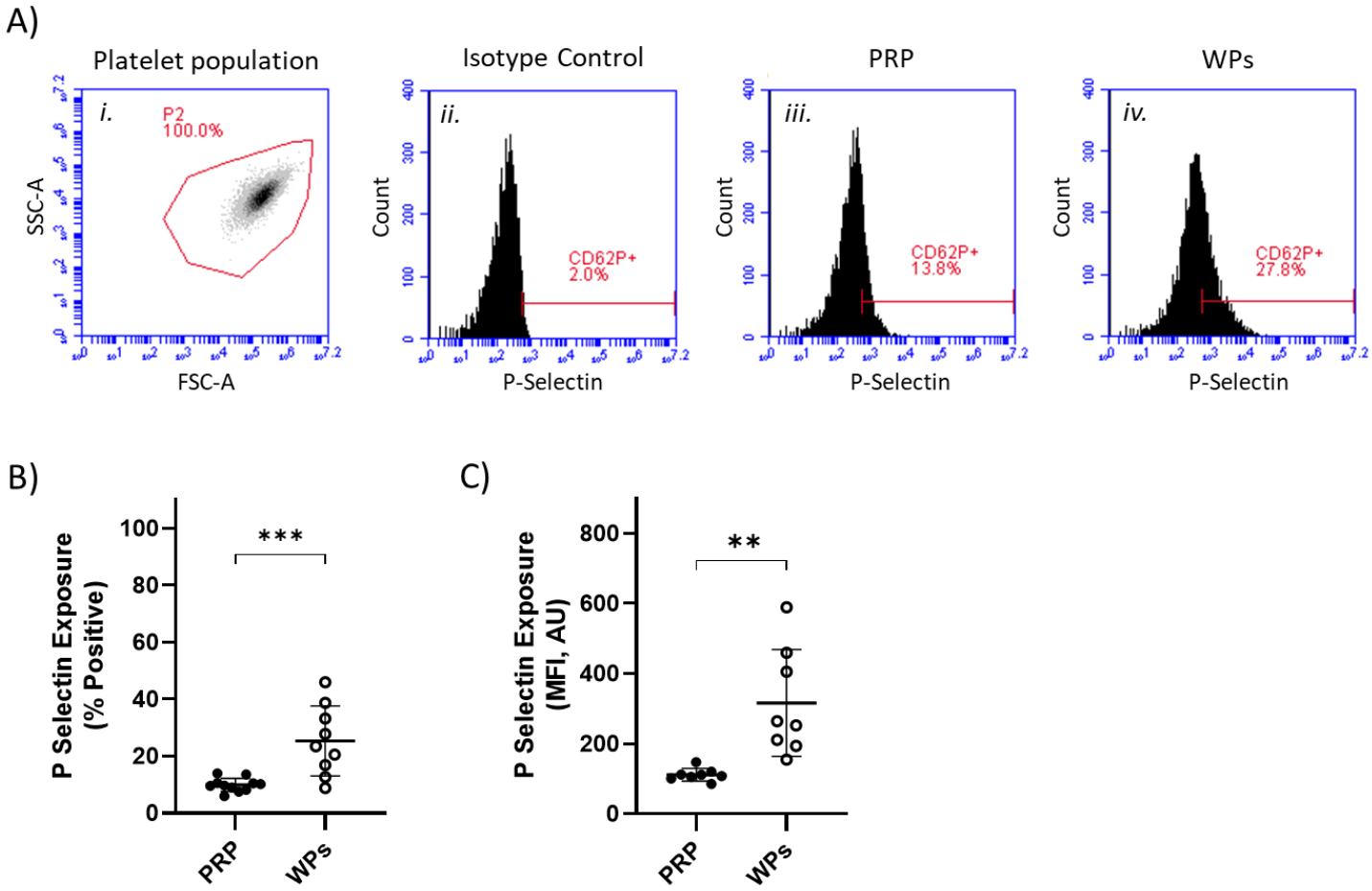

Figure 4.2 Different platelet preparations induce different levels of P-selectin exposure.

Platelets were prepared as platelet rich plasma (PRP) or washed platelets (WPs). The platelet population was first identified by forward (FSC) and side (SCC) scattered light representing size and granularity respectively (A*i*). An isotype control was used to set a 2% gate (A*ii*), where platelet activation beyond this boundary was recorded for PRP (A*iii*) and WPs (A*iv*). P-selectin exposure was used as a measure of platelet activation where PRP and WPs were directly compared for the percentage of positive platelets (B), and the median fluorescent intensity (MFI) (C). PRP represents eleven biological replicates (n=11) and WPs represent nine biological replicates (n=9). Data represents the mean ± standard deviation (SD) and statistical analysis was performed using an unpaired two-tailed t test (** $P \leq 0.01$, *** $P \leq 0.001$).

4.2.2 Fusogenic liposomes induce platelet activation.

PRP preparation was taken forward as a preparation which induced lower platelet activation when compared to washed platelets. The level of platelet activation of PRP, as assessed by P-selectin exposure, was used as a baseline to assess if commercial fusogenic liposomes resulted in further platelet activation.

In the first instance, platelets were incubated with fluorescently labelled fusogenic liposomes at a starting concentration of 30 µM which represented a concentration recommended by manufacturers. Representative flow cytometry traces provide an example of the gating strategy used to assess the extent of fusogenic liposome labelling (Figure 4.3A). Platelets were identified using forward scattered (FSC) light and side scattered (SSC) light, a measure of size and granularity respectively (Figure 4.3A*i*). The extent of platelets fluorescently labelled with fusogenic liposomes was assessed using an excitation wavelength of 488 nm. Similar to analyses performed with P-selectin, a 2% gate was set using the unlabelled control (PRP) (Figure 4.3A*ii*). The 2% gate provided a boundary where platelets which exceeded this 2% gate were identified as fluorescently labelled with fusogenic liposomes (Figure 4.3A*iii*).

As previously described, the percentage of platelets positive for P-selectin exposure, a measure of platelet activation, were plotted to assess platelet activation in the presence and absence of fusogenic liposomes (Figure 4.3B). A 2% gate set on the isotype control was used to define a boundary to characterise the extent of platelet activation. The flow cytometry data reveals that platelet activation, assessed by P-selectin, was significantly increased when directly comparing platelets fused with fusogenic liposomes (+FL; 33.3 ± 22.0%) to an unlabelled control from the same donor (PRP; 9.0 ± 1.6%) (Figure 4.3B). Platelet activation in the presence of fusogenic liposomes was variable between donors; with some donors presenting with low platelet activation as a result of fusogenic liposome fusion, and some donors with a high activation response to fusion. Furthermore, when observing descriptive statistics, such as the data range in percentage of platelet activation for PRP (range = 4.6%) and +FLs (range = 55.1%), the spread in data suggests that there is an impact on platelet activation due to fusion (Figure 4.3B).

Despite the difference in platelet activation, fluorescent labelling using Fuse-It-Color fusogenic liposomes resulted in highly efficient labelling (91.4 ± 8.8%) (Figure 4.3C). Where the labelling of platelets with Fuse-It-Color at a concentration of 30 µM resulted in >80% fluorescence in 12 out of 13 donors (Figure 4.3C).

As in previous analyses, the MFI of the platelet population for P-selectin exposure (Figure 4.3D) and the extent of platelet labelling by fusogenic liposomes was also observed (Figure 4.3E). Despite differences in platelet activation being non-significant for MFI, the data also presents a greater spread in platelet activation in the presence of fusogenic liposomes when comparing the data range for PRP (range = 62.5 AU) and +FLs (range = 2183 AU) (Figure 4.3D). While similar to percent positivity, the MFI of platelets labelled by fusogenic liposomes was highly efficient, presenting a considerable increase in fluorescence above the unlabelled PRP control (23.9 ± 5.0 AU) (Figure 4.3E; red dashed line).

Upon further investigation of the labelling data, there was a weak correlation when applying a linear regression model between the level of labelling and the level of platelet activation (Figure 4.4). When observing a correlation between the percentage of labelling and the percentage of P-selectin exposure the R-squared value was 0.011, indicating that the model explains 1% of variation within the data (Figure 4.4A). Suggesting that there is no relationship between the level of labelling and the level of platelet activation. This may, in part, be a result of the labelling efficiency being close to maximal labelling at 100%. MFI was therefore also correlated using a linear regression model (Figure 4.4B). The R-squared value when correlating the MFI of fluorescent labelling and the MFI of P-selectin exposure was 0.267, indicating that the model explains 27% of variation within the data. Despite this correlation being higher, there is a greater variation to the data points, suggesting there may be a weak correlation between the level of labelling and the level of platelet activation.

Overall, although the labelling of platelets with fluorescently labelled fusogenic liposomes was highly efficient, the data for P-selectin exposure suggests that concentrations of 30 μM fusogenic liposomes can induce platelet activation due to the fusion process. Although a linear regression model may suggest a weak relationship between the level of labelling and platelet activation, platelet activation is markedly elevated when directly compared to controlled platelets.

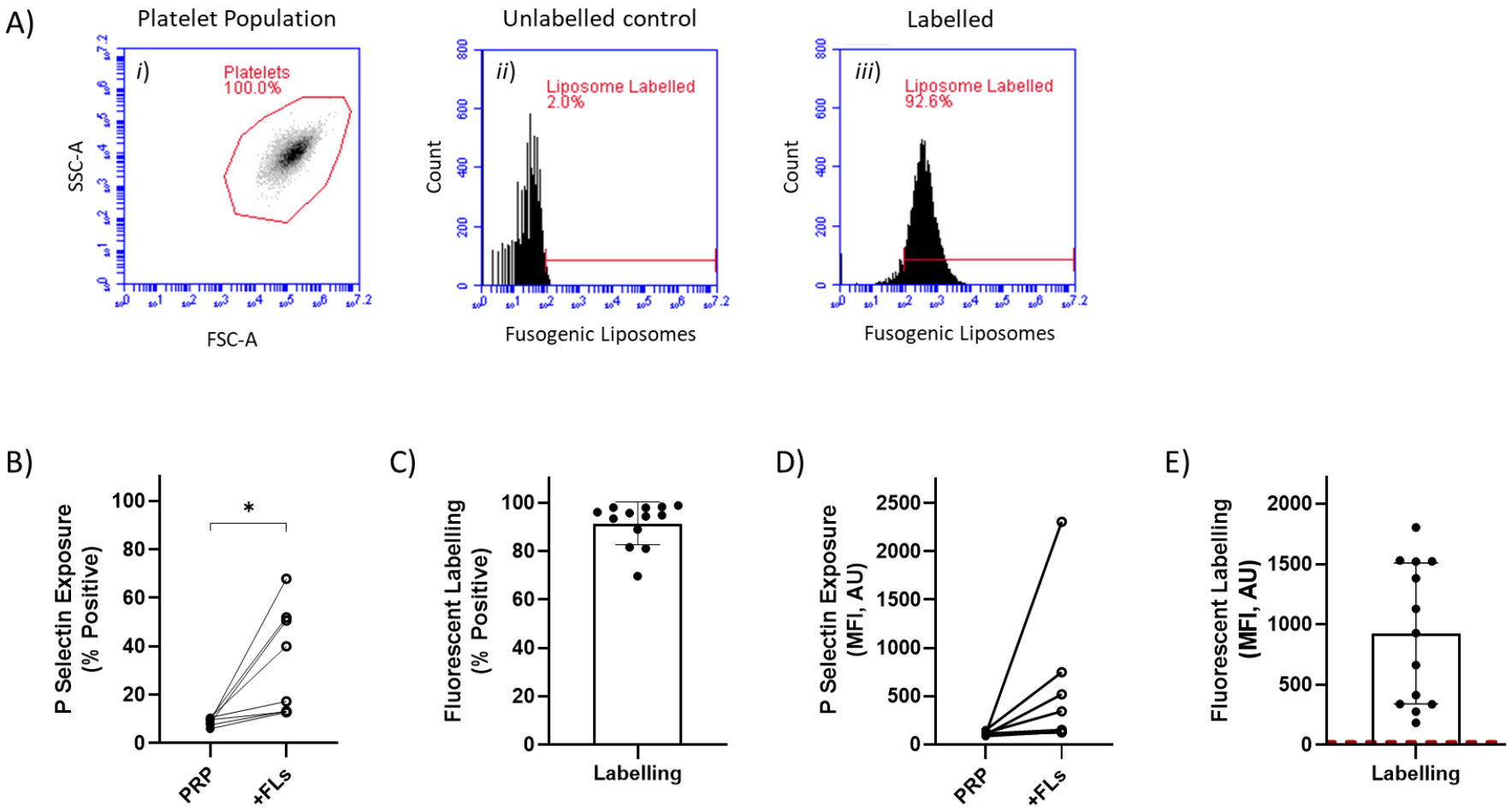

Figure 4.3 Fluorescently labelled fusogenic liposomes induce P-selectin exposure.

Representative flow cytometry traces detail the platelet population as identified by forward scattered (FSC) and side scattered (SSC) light, a measure of size and granularity respectively (A*i*). An unlabelled PRP control representative of a negative labelling control (A*ii*), and PRP positively labelled with fluorescent fusogenic liposomes [30µM] provide an example of labelling efficiency (A*iii*). P-selectin exposure was acquired as a measure of platelet activation where percentage of platelets positive in the PRP preparation was directly compared to PRP

pre-treated with fusogenic liposomes (+FLs) [30 μM] from the same donor (B). P-selectin data represents eight experimental replicates (n=8), which were plotted and analysed using a two-tailed paired t-test, * $P \leq 0.05$.

The percentage of fluorescently labelled platelets assessed labelling efficiency where data represents the mean ± SD of thirteen experimental replicates (n=13) (C).

Median fluorescent intensity (MFI) was also observed for both P-selectin exposure (D) (n=8) and fluorescent labelling where the red dashed line at the base of the plot indicates the MFI for the unlabelled control (E) (n=13).

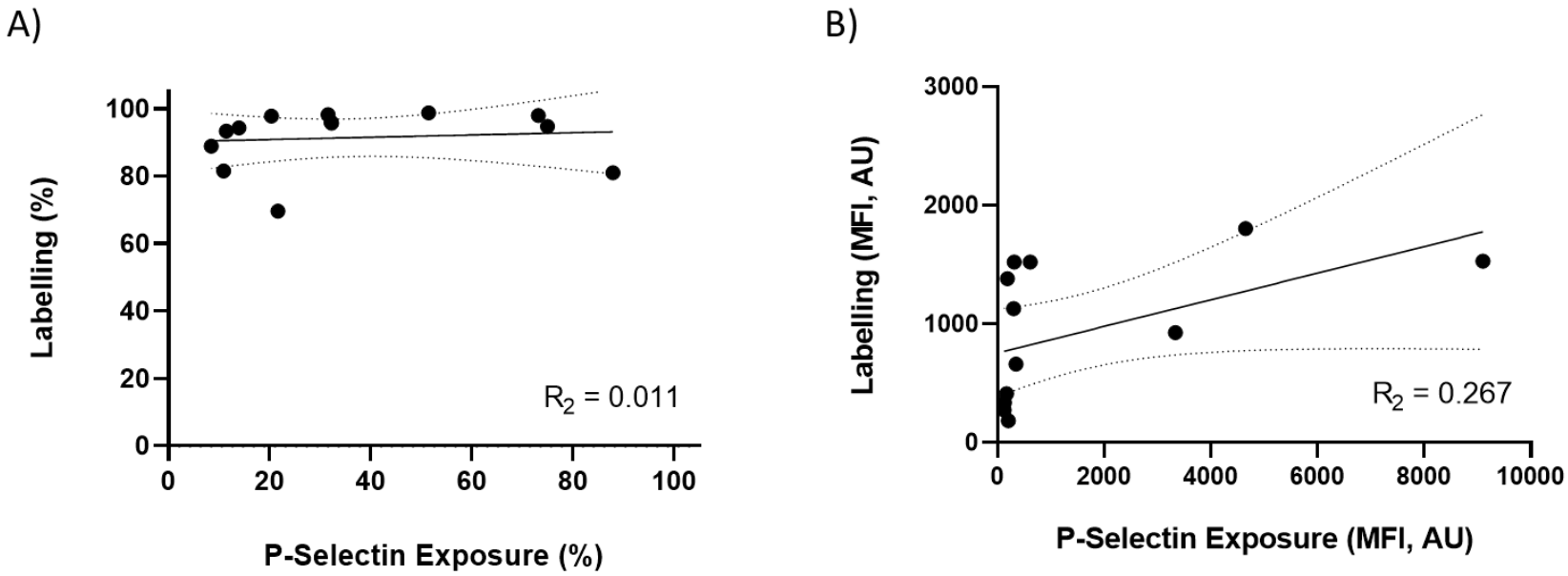

Figure 4.4 Linear regression model does not explain a relationship between fluorescent labelling and P-selectin exposure.

Labelling data from platelets fused with fusogenic liposomes [30 μM] was further investigated using a linear regression model. The percentage of fluorescent labelling was correlated with the percentage of P-selectin exposure (A). The median fluorescent intensity (MFI) of fluorescent labelling was correlated with the MFI of P-selectin exposure (B). Data represents thirteen biological replicates (n=13), where the R-squared (R_2) value was observed using a simple linear regression model (solid line) with 95% confidence Intervals (dashed lines).

4.2.3 Fusogenic liposomes can efficiently label platelets without impacting platelet activation.

The data so far shows that fusogenic liposome fusion with platelets can induce P-selectin exposure and consequently platelet activation. Fusogenic liposome concentration was therefore investigated to identify if a lower concentration of fusogenic liposomes can reduce the extent of platelet activation as measured by P-selectin exposure yet maintain the extent of fluorescent labelling to ≥ 80% labelled platelets. The latter will be an important factor during cargo delivery to maximise the amount of cargo delivered to the majority of platelets in any given sample.

A dose response curve was performed where platelets were incubated with reducing concentrations of fusogenic liposomes. P-selectin exposure was used as a measure of platelet activation to determine the percentage of α-granule release (Figure 4.5A). When observing the percentage of platelet activation by P-selectin exposure there were significant increases in platelet activation when platelets were labelled with Fuse-It-Color at 30 µM (50.5 ± 25.2 %) and 15 µM (47.0 ± 22.9 %), when compared to the unlabelled PRP control (15.5 ± 4.5 %) (Figure 4.5A). Yet, from 10 µM ranging down to 1.5 µM Fuse-It-Color, there were no significant increases in the percentage of platelet activation when compared to basal platelet activation (PRP; 15.5 ± 4.5%).

Unlabelled PRP provided a basal measure of platelet activation as well as a negative labelling control to determine the percentage of platelet labelling by liposome fusion (Figure 4.5B). When assessing the extent of fluorescently labelled platelets fused with Fuse-It-Color, there was a significant increase in the percentage of platelet labelling at concentrations of Fuse-It-Color at 30 µM (94.7 ± 6.8 %), 15 µM (89.9 ± 10.7 %), 10 µM (85.3 ± 9.5 %), 7.5 µM (71.5 ± 22.0 %), 6 µM (46.4 ± 21.3 %) and 3 µM (26.4 ± 16.6 %) when compared to the unlabelled PRP control (Figure 4.5B). There was no significant difference when using Fuse-It-Color at a concentration of 1.5 µM (15.7 ± 12.3 %). The concentrations of Fuse-It-Color which achieved a labelling efficiency of ≥80% ranged from 30 µM to 10 µM (Figure 4.5B).

As well as the percentage of P-selectin exposure and the percentage of fluorescent labelling by Fuse-It-Color, the MFI was also plotted to determine if similar conclusions could be drawn from different metrics. There was no significant increase in P-selectin exposure when observing MFI between the control group and the labelled groups (Figure 4.5C). However, there was an increased variability in P-selectin exposure for higher concentrations of Fuse-It-Color (Figure 4.5C). When assessing the extent of labelling, MFI was significantly increased when using Fuse-It-Color at 30 µM (1309 ± 375.3 AU), 15 µM (589.5 ± 323.8 AU) and 10 µM

(446.4 ± 174.3 AU) when directly compared to the unlabelled PRP control (24.4 ± 6.4 AU) (Figure 4.5D).

When taking into consideration the percent positivity and MFI for both P-selectin exposure and the labelling efficiency of Fuse-It-Color, 10 µM Fuse-It-Color indicated a concentration which did not induce significant platelet activation for percent positivity or MFI. This concentration also ensured either a significant increase or ≥ 80% of labelled platelets. The variability in platelet activation indicates that platelets from different donors respond differently to the fusion of Fuse-It-Color. This variability in P-selectin exposure between different donors was further investigated (Section 4.2.6) to reduce the amount of variation.

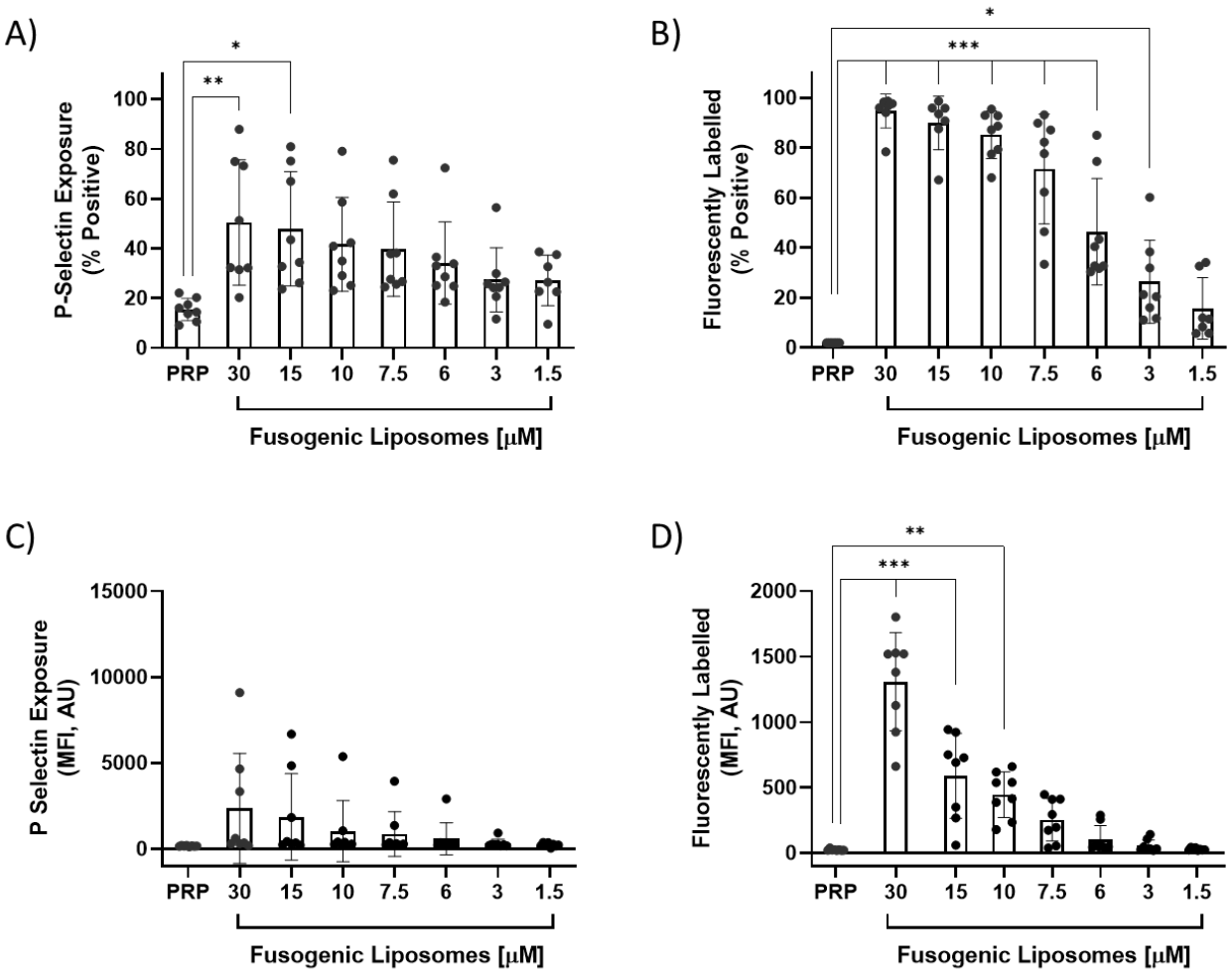

Figure 4.5 Fuse-It-Color efficiently labels platelets without significantly impacting P-selectin exposure

Platelets were labelled using fusogenic liposomes dose dependently. The percentage of P-selectin exposure (A) and the extent of fluorescently labelled platelets (B) were assessed using decreasing concentrations of Fuse-It-Color [30 μM to 1.5 μM] and directly compared to an unlabelled control (PRP). The median fluorescent intensity (MFI) of both P-selectin exposure (C) and fluorescent labelling (D) were also plotted to compare outcomes. Data represents 8 biological replicates (n=8), where the mean ± SD was analysed using one-way ANOVA with Bonferroni post-test with the control group (PRP) compared to platelets fused with different concentrations of Fuse-It-Color. *, $P \leq 0.05$. **, $P \leq 0.01$. ***, $P \leq 0.001$.

4.2.4 Fusogenic Liposomes do not alter normal platelet spreading and adhesion.

In addition to platelet activation and the extent of labelling, platelet spreading experiments were performed to assess platelet morphology and adhesion. During injury, platelets will spread over damaged endothelium to prevent bleeding. It was therefore important to determine if platelets fused with fusogenic liposomes had altered platelet morphology and adhesion when compared to control platelets.

Platelets were fused with Fuse-It-Color [10 µM] prior to spreading over a fibrinogen substrate [100 µg/mL] and compared to unlabelled control platelets. Representative DIC images show that there were no differences between the spreading and adhesion of control platelets (Figure 4.6A*i.*) when compared to platelets fused with fusogenic liposomes (+FLs) (Figure 4.6A*ii.*). Furthermore, the fluorescent images corroborated the flow cytometry data and showed a high efficiency of fluorescent labelling detected at 488 nm when platelets were fused with Fuse-It-Color (+FLs) (Figure 4.6A*ii.*).

Similar to previous analyses with flow cytometry, the same concentrations of fusogenic liposomes were added to platelets in a dose dependant manner starting with a concentration of 30 µM, ranging down to 1.5 µM. All images were acquired using a Ti2 epi-fluorescent microscope and quantification was automated by implementing the automated CNN to avoid biased manual analyses. There were no statistical differences in the spread area of platelets when comparing control unlabelled platelets (PRP) with platelets fused with Fuse-It-Color (Figure 4.6B). Furthermore, the spread area of platelets identified here (PRP: 23.4 ± 4.1 μm^2) were consistent with the findings of platelet spread area when spread over a fibrinogen substrate in the literature [138].

Likewise, there were no further differences in platelet perimeter (Figure 4.6C), circularity (Figure 4.6D), or the number of platelets able to adhere to fibrinogen (Figure 4.6E) when directly comparing unlabelled control platelets (PRP) to those platelets labelled with fluorescently labelled fusogenic liposomes. This data suggests that platelets fused with fusogenic liposomes can adhere to a fibrinogen substrate similar to that of controlled platelets and undergo rapid changes to morphology consistent with that of controlled platelets. Overall, Fuse-It-Color fusogenic liposomes do not impair normal platelet spreading.

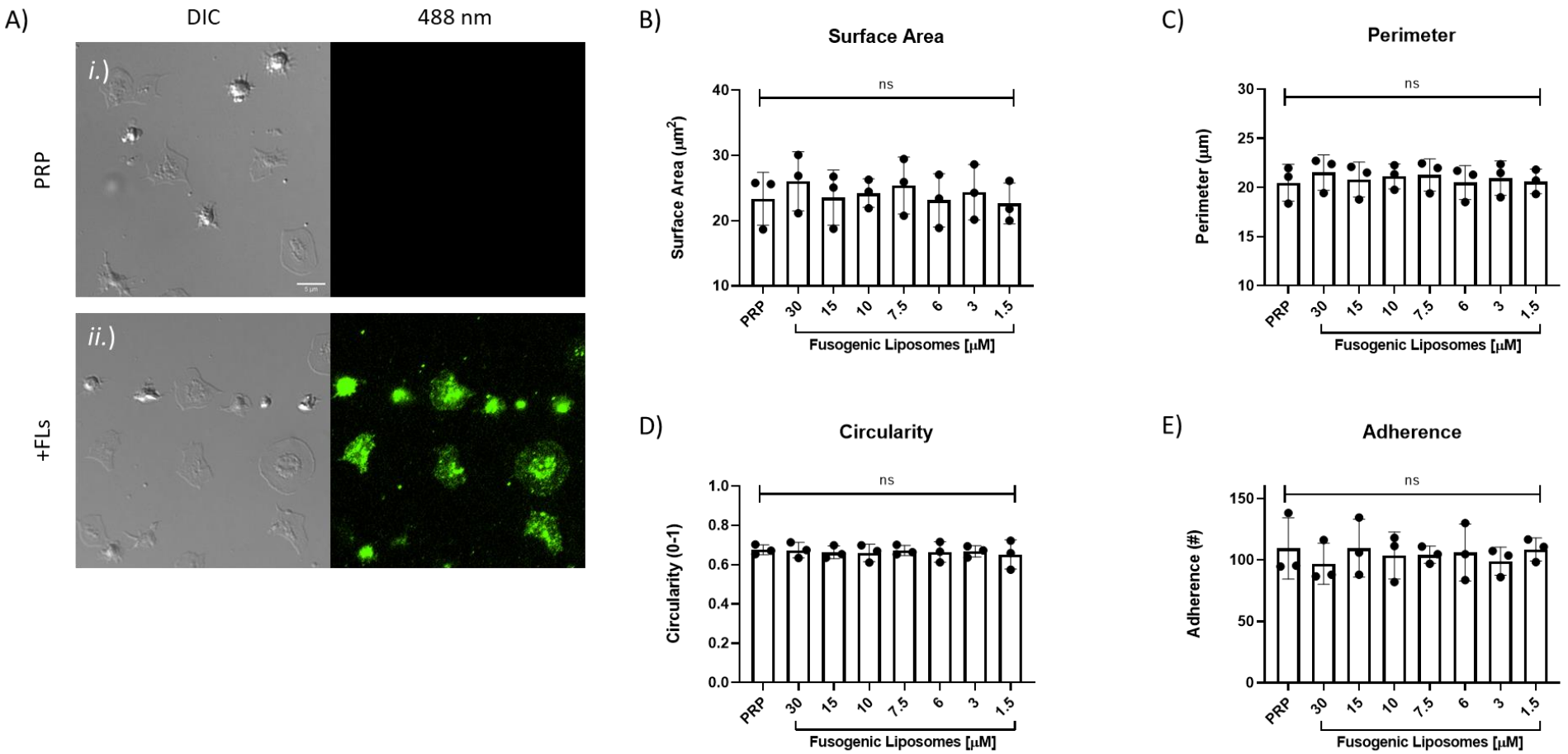

Figure 4.6 The addition of fluorescently labelled fusogenic liposomes does not alter platelet spreading.

Representative Differential Interference Contrast (DIC) images and corresponding fluorescent microscopy images of unlabelled control platelets (A*i*.) and platelets labelled with Fuse-It-Color [10 μM] (+FLs) (A*ii*.) were spread over a fibrinogen [100 μg/mL] substrate. Scale bar represents 5 μm. Each DIC image was analysed using an automated convolutional neural network (CNN). Platelet spread area (B),

perimeter (C), circularity (D) and the number of platelets per field of view (E) is representative of three biological replicates (n=3), where each biological replicate is the mean of three experimental images. Data represents the mean ± SD which was analysed using one-way ANOVA with Bonferroni post-test with the control (PRP) compared to platelets fused with Fuse-It-Color. Non-significant (ns), $P > 0.05$.

4.2.5 Fusogenic Liposomes do not induce phosphatidylserine translocation to the platelet surface.

Next, since some platelet activation is induced during fusion, the amount of phosphatidylserine (PS) on the surface of platelets treated with fusogenic liposomes was directly compared to untreated control platelets. For these experiments platelets were fused with 30 μM Fuse-It-Color, which represented the highest concentration in the dose response curve applied to previous experimentation and allowed possible correlations between platelet activation and PS exposure, as measured by Annexin V binding, to be observed.

Similar to previous flow cytometry analyses, the platelet population was first identified according to FSC and SSC light; a measure of size and granularity respectively (Figure 4.7A*i*). Ethylenediaminetetraacetic acid (EDTA) chelated calcium which impeded the binding of calcium dependent Annexin V to platelets and served as a negative control. This negative control was used to gate a 2% boundary (Figure 4.7A*ii*), where platelet events which were greater than this 2% boundary for rested (PRP or PRP.FLs) and stimulated (+STIM) samples, were categorised as Annexin V positive platelets (Figure 4.7A*iii* and *iv*). Stimulated platelets (+STIM) were stimulated using a dual agonist consisting of cross-linked collagen related peptide (CRP-XL, [3 μg/mL]) and thrombin receptor activator peptide 6 (TRAP-6, [15 μM]), a collagen mimetic and PAR1 agonist respectively. Literature had previously demonstrated agonist-induced exposure of PS using CRP-XL and thrombin in combination [248].

When compared to unlabelled control platelets (PRP; 2.3 ± 1.2%), fluorescently labelled platelets using Fuse-It-Color (PRP.FLs; 12.0 ± 7.9%) did not induce significant exposure of PS as measured by the percentage of Annexin V binding (Figure 4.7B). Furthermore, it was possible to induce a significant increase in apoptotic platelets for both unlabelled (+ STIM, black squares; 30.9 ± 8.7%) and labelled (+ STIM, green squares; 38.9 ± 11.8%) platelets using a dual agonist stimulation known to induce procoagulant platelets (Figure 4.7B).

In addition to Annexin V binding, P-selectin exposure was also acquired for the same samples. Unsurprisingly, there was a significant increase in the percentage of P-selectin exposure when controlled platelets (PRP; 10.4 ± 4.9%) were stimulated with a dual stimulation (+STIM; 95.7 ± 1.2%) (Figure 4.7C). Conversely, however, there were no significant differences in the percentage of P-selectin exposure when comparing platelets which had been labelled with Fuse-It-Color (PRP.FLs; 61.6 ± 31%) to labelled platelets stimulated with a dual stimulation (+STIM; 94 ± 1.7%) (Figure 4.7C). Furthermore, unlike previous analyses, there was no significant difference in the percentage of P-selectin exposure when comparing controlled platelets (PRP) to platelets which had been labelled

with Fuse-It-Color (PRP.FLs). This is likely a result of the broad spread of the data for PRP labelled with Fuse-It-Color (PRP.FLs).

Nevertheless, the data from previous experimentation has already identified that fusion of fusogenic liposomes induces significant levels of platelet activation. Literature suggests that there could be an intuitive relationship between P-selectin exposure and PS exposure [249,250]. When applying a linear regression model of P-selectin exposure against Annexin V binding, there is a moderate trend (R_2 = 0.53) between platelets with a higher level of P-selectin exposure also expressing elevated levels of PS exposure (Figure 4.7D). That is to say that the dependant variable, PS exposure, and the elevation of PS exposure on the surface of platelets fluorescently labelled with Fuse-It-Color, despite being non-significant, may be explained by elevated platelet activation.

The median fluorescent intensity (MFI) of data in this collection of experiments was not included in data interpretation due to the bimodal distribution of Annexin V binding, where the median value would have been skewed due to the distribution of data.

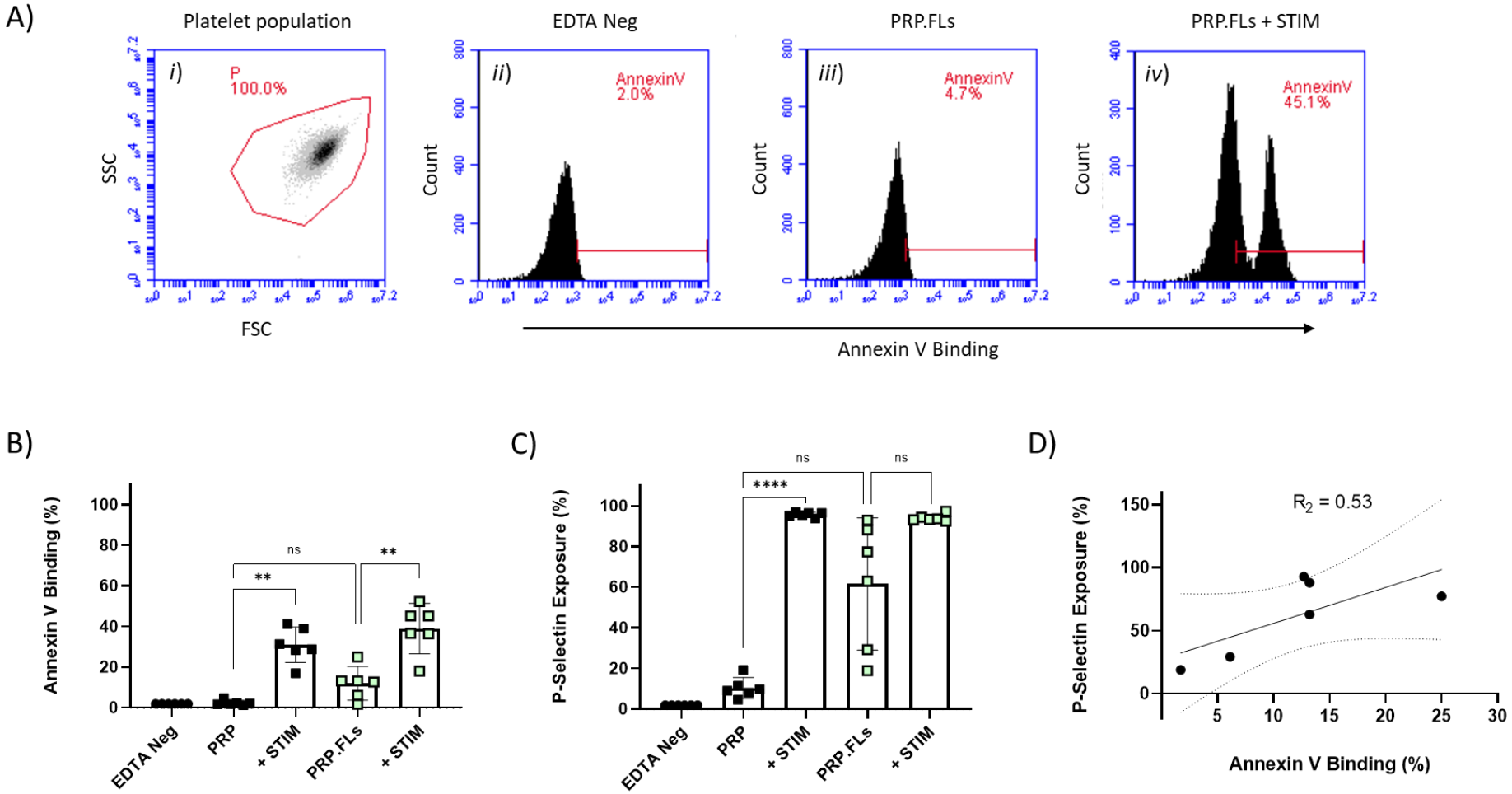

Figure 4.7 Fusogenic liposomes do not induce the translocation of phosphatidylserine to the outer cell membrane.

Representative flow cytometry traces of platelets labelled with Fuse-It-Color (PRP.FLs) detail the gating strategy implemented; the same gating strategy was also applied to control platelets (A). The platelet population was first identified by forward scattered (FSC), and side scattered (SSC) light, a measure of size and granularity respectively (A*i*). An EDTA control served as a negative control due to its calcium chelating properties and was consistently gated at 2% (A*ii*). Annexin V binding was used as a measure of phosphatidylserine (PS) residing

on the cell surface of control platelets (PRP) and platelets labelled with Fuse-It-Color [30 µM] (PRP.FLs) (A*iii*). Annexin V binding was further used as a measure of phosphatidylserine (PS) residing on the surface of agonist-induced apoptotic platelets in the presence of CRP-XL [3 µg/mL] and TRAP-6 [15 µM] (+STIM) (A*iv*).

The percentage of Annexin V binding was compared between all groups (B). P-selectin exposure was acquired as a marker of platelet activation (C). A linear regression model (R_2 = 0.53) compared the relationship between Annexin V binding and P-selectin exposure (D). Data represents the mean ± SD of five biological replicates (n = 5), analysed by one-way ANOVA with Bonferroni post-test where the mean of each group was compared to the mean of all other groups. The R-squared (R_2) value was observed using a simple linear regression model (solid line) with 95% confidence Intervals (dashed lines). ns, P > 0.05. **, P ≤ 0.01. ***, P ≤ 0.001. ****, P ≤ 0.0001.

4.2.6 An increase in platelet activation in the presence of fusogenic liposomes can be controlled by the addition of PGI_2.

The incubation of fusogenic liposomes with platelets can induce platelet activation which can impact on PS exposure and induce procoagulant activity. Prostaglandin I_2 (PGI_2) was therefore next investigated to identify if variability in platelet activation can be minimised during fusion. PGI_2 and Nitric Oxide (NO) released by intact endothelium readily regulate platelets by preventing unnecessary activation *in vivo* [251]. However, once platelets are removed from the bloodstream they are no longer subjected to the inhibitory effects of PGI_2 and NO. Platelets, therefore, can become easily activated, where, due to positive feedback mechanisms amplifying the release of bioactive molecules, leads to the recruitment of more platelets and triggers further activation [6,252]. Therefore, it was hypothesised that *in vitro* use of PGI_2 will dampen platelet response during fusion and diminish elevated platelet activation prior to further experimentation.

PGI_2 acts on the prostacyclin cell surface receptor (IP receptor) on platelets, and when activated leads to an intracellular increase of cyclic AMP [83] and protein kinase A (PKA), which leads to an inhibitory impact on platelet activation responses [84]. Interestingly, PGI_2 is known to have an extremely short half-life ($T_{1/2}$) of 10.7 +/- 2.3 minutes in citrated plasma [253], meaning that after a rest period of 30 minutes, platelets will no longer be influenced by the inhibitory effects of PGI_2. Washed platelets (WPs) are regularly prepared in the presence of PGI_2 [44 ng/mL] to avoid artifactual activation as a result of additional wash steps with no lasting impact on function [254].

Lyophilised PGI_2 (Caymen Chemicals) was reconstituted in dry ethanol (dETOH) to avoid water molecules entering the sample which would result in rapid hydrolysis. In the first instance, a 5% (v/v) volume of ethanol was added as a vehicle control directly to samples prior to the fusion of Fuse-It-Color in a dose dependent manner (Figure 4.8A). As before, flow cytometry was used to measure P-selectin exposure where platelets were identified according to FSC and SSC light, a measure of size and granularity, respectively. An isotype control was used to assess both antibody nonspecific binding and to set a boundary gate at 2%. As in previous experimentation, samples were positive for P-selectin exposure if they fell above this 2% threshold. All platelets were rested for 30 minutes prior to agonist-induced platelet activation or functional assays. This was to ensure complete PGI_2 hydrolysis.

A significant increase in the percentage of platelet activation was observed when comparing unlabelled control platelets (PRP; 10.5 ± 2.7 %) with platelets fused with fusogenic liposomes [10 µM] (PRP.FLs; 25.3 ± 16.3 %) during basal conditions (Figure 4.8A; filled circles). This is in contrast to the data for percent positivity in Figure 4.5A, and is likely a

result of a small number of biological replicates and different platelet donors, and provides further evidence to control the variation in platelet activation in the presence of fusogenic liposomes. When in the presence of CRP-XL [3 µg/mL], however, there was no difference to platelet activation when comparing PRP to PRP labelled with fusogenic liposomes (PRP.FLs) (Figure 4.8A; squares), suggesting that platelets labelled with fusogenic liposomes did not impair the GPVI pathway of activation. A dose response of PGI_2 concentrations ranging from 5950 ng/mL – 0.0235 ng/mL identified that there was a reduction in basal platelet activation when platelets had been pre-treated with PGI_2 prior to fusion (Figure 4.8A, filled circles). As a result of continued PGI_2 optimisation, all concentrations of the PGI_2 dose response consisted of two experimental replicates (n=2), therefore, statistical analyses were not performed.

As well as basal conditions for PGI_2 dose response, CRP-XL [3 µg/mL] was used to induce platelet activation to investigate platelet recovery after the addition of PGI_2 during fusion. This was to assess if, where platelet activation had been reduced during basal conditions, that platelets were also able to recover and activate as expected using a concentration of CRP-XL known to induce ~100% P-selectin exposure (Figure 4.8A, squares). However, it was found that the recovery of platelets pre-treated with PGI_2 prior to fusion was impacted, and agonist-induced platelet activation was not comparable to agonist-induced activation of the unlabelled control (PRP) in the presence of CRP-XL. An ethanol vehicle control (ETOH) was compared to platelets treated with both PGI_2 and Fuse-It-Color, and the unlabelled platelet control (PRP) in the presence of CRP-XL. It was found that ethanol inhibited platelet recovery by 19% after CRP-XL [3 µg/mL] induced platelet activation (Figure 4.8A).

MFI values were also observed and demonstrated an impact to platelet recovery in the presence of CRP-XL with ethanol inhibiting recovery by 47% (Figure 4.8B). However, although the ETOH vehicle impaired platelet recovery, the PGI_2 dose response did present promising results where platelet activation appeared diminished when platelets had been pre-treated with PGI_2 prior to fusion with fluorescently labelled Fuse-It-Color. By reducing the volume of ethanol vehicle to 1% (v/v), the inhibition of platelet recovery observed as a result of the ethanol vehicle at 5% (v/v) was resolved (Figure 4.9).

P-selectin exposure was quantified for platelets pre-treated with PGI_2 prior to fusion in the presence and absence of CRP-XL as before. As observed previously, there was a significant increase in the percentage of platelet activation when comparing the control PRP (8.8 ± 1.3 %) to platelets fused with fusogenic liposomes (PRP.FLs: 42.9 ± 22.9 %) (Figure 4.9A; filled circles). A dose response of decreasing PGI_2 concentrations from 46 ng/mL to 0.09 ng/mL was used to identify an optimal concentration which reduced platelet activation induced by

fusion. There was a statistically different decrease in platelet activation when comparing PRP in the presence of CRP-XL (94.6 ± 1.3 %) with fused platelets pre-treated with 6 ng/mL PGI_2 in the presence of CRP-XL (79.2 ± 10.1 %) (Figure 4.9A; squares). This data suggests that 6 ng/mL PGI_2 impacts platelet recovery when in the presence of an agonist known to induce ~100 % platelet activation. Concentrations >6 ng/mL were not included in the statistical evaluation since they represent only one biological replicate.

As before, the data for MFI was also observed and presented the same scientific conclusions as percent positivity (Figure 4.9B), where the fusion of fusogenic liposomes in the absence of PGI_2 (PRP.FLs: 823.4 ± 1002 AU) induced significant platelet activation when compared to the PRP control (108.4 ± 8.2 AU) (Figure 4.9B; filled circles). There was also a statistically different decrease in platelet activation when comparing PRP in the presence of CRP-XL (24,539 ± 3,123 AU) with fused platelets pre-treated with 6 ng/mL PGI_2 in the presence of CRP-XL (7,609 ± 6,353 AU) (Figure 4.9B; squares).

Overall, this data revealed the optimal concentration of PGI_2 required to reduce platelet activation at the point of fusion was 0.5 ng/mL in 1 µL ethanol per 100 µL PRP (blue vertical line). This concentration did not impair platelet recovery when assessed by agonist-induced platelet activation (Figure 4.9B, squares). Overall, this data confirms that PGI_2 can be used to minimise platelet activation prior to the fusion of fusogenic liposomes with the platelet membrane, and that platelet recovery is not impaired for downstream functional assays. Future experimentation will use 0.5 ng/mL PGI_2 prior to platelet fusion with Fuse-It-Color.

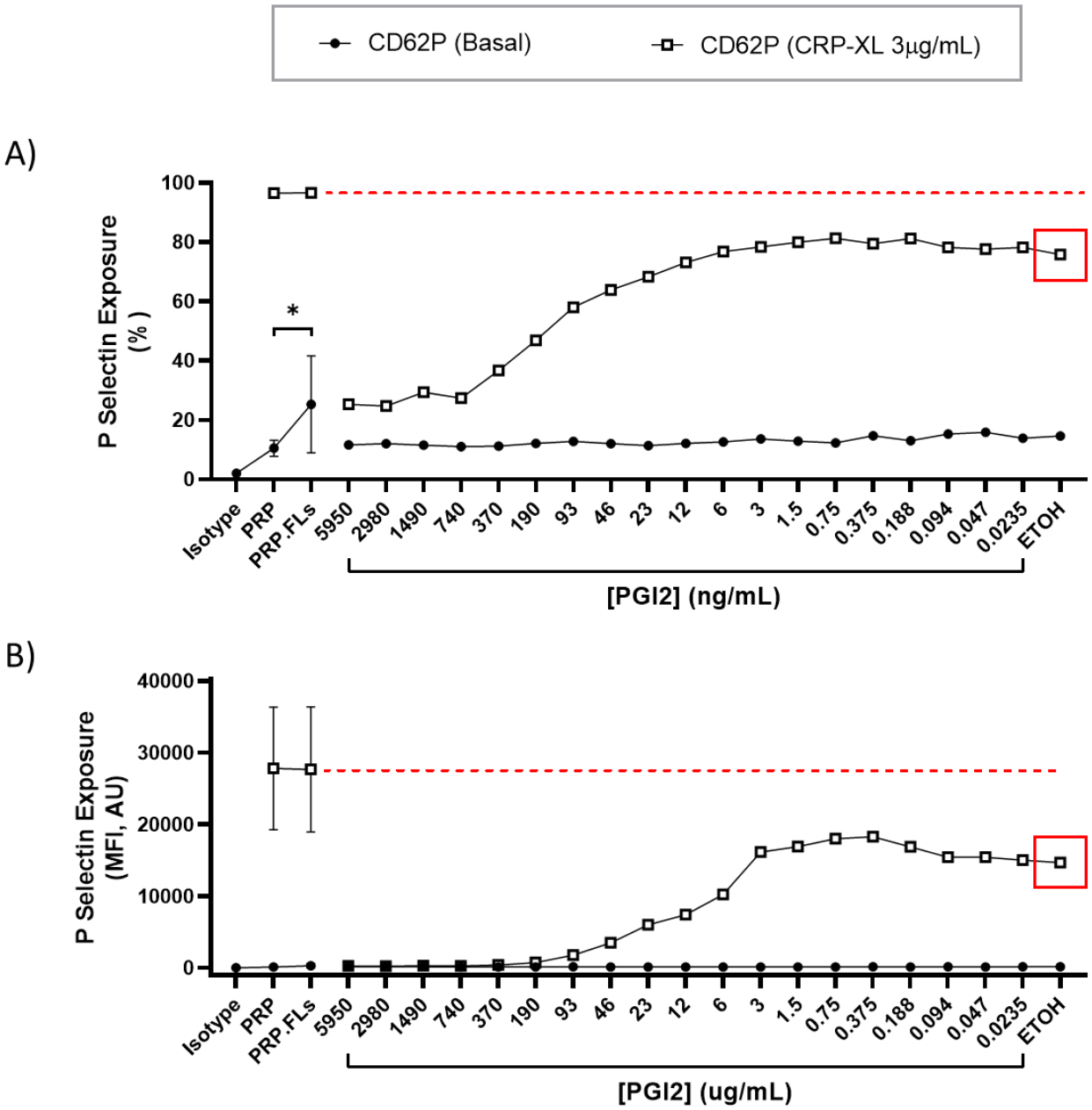

Figure 4.8 Prostacyclin (PGI_2) can reduce platelet activation induced by fusogenic liposome labelling.

The percentage of P-selectin exposure at basal conditions was quantified and compared to unlabelled control platelets (PRP), platelets which had been labelled with fusogenic liposomes [10 µM] (PRP.FLs), and platelets labelled with fusogenic liposomes [10 µM] which had been pre-treated with prostacyclin (PGI_2) diluted in 5 µL dry ethanol (ETOH) in a dose dependant manner [5950 ng/mL – 0.0235 ng/mL] prior to fusion (circles) (A). Agonist-induced platelet activation using CRP-XL [3 µg/mL] assessed if platelets fused and pre-treated with PGI_2 were able to recover when compared to control PRP (squares). Data for MFI was also plotted (B). The red dashed line indicates the level of agonist-induced platelet activation for PRP and PRP labelled with fusogenic liposomes (PRP.FLs) in the presence of CRP-XL (A & B).

A & B: Data represents the mean ± SD of seven biological replicates (n=7) for the isotype control, PRP and PRP.FLs, two biological (n=2) replicates for all PGI_2 concentrations, and one biological

replicate (n=1) for the ETOH control. Statistics were performed using one-way ANOVA with Bonferroni post-test when biological replicates were ≥3. Non-significant (ns), $P > 0.05$. **, $P \leq 0.01$. ***, $P \leq 0.001$. ****, $P \leq 0.0001$.

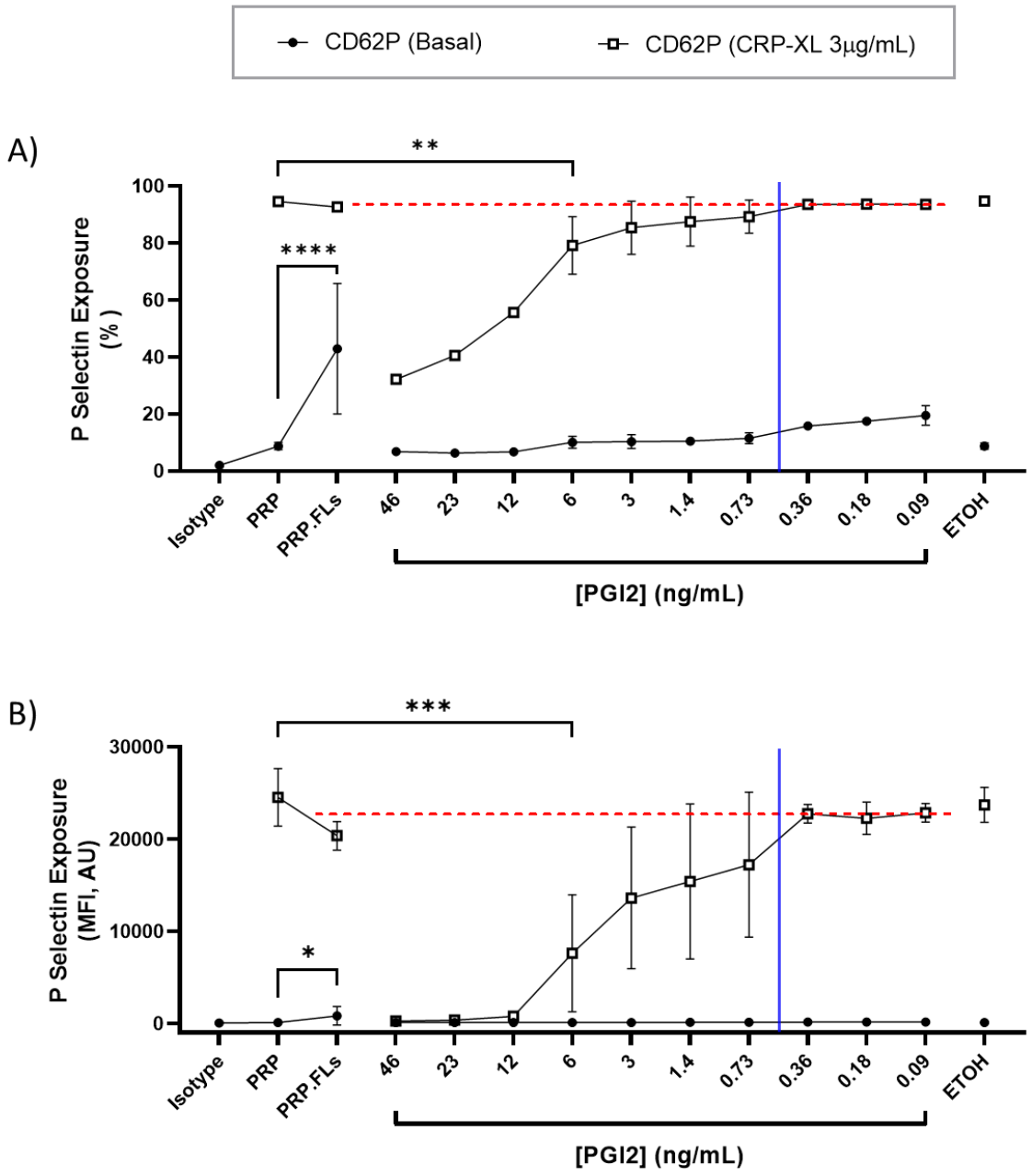

Figure 4.9 Prostacyclin (PGI_2) can reduce platelet activation induced by fusogenic liposome labelling without impairing recovery.

The percentage of P-selectin exposure at basal conditions was quantified and compared to unlabelled control platelets (PRP), platelets which had been labelled with fusogenic liposomes [10 µM] (PRP.FLs), and platelets labelled with fusogenic liposomes [10 µM] which had been pre-treated with prostacyclin (PGI_2) diluted in 1 µL dry ethanol (ETOH) in a dose dependant manner [46 ng/mL – 0.09 ng/mL] prior to fusion (circles) (A). Agonist-induced platelet activation using CRP-XL [3 µg/mL] assessed if platelets fused and pre-treated with PGI_2 were able to recover when compared to control PRP (squares). Data for MFI was also plotted (B). The red dashed line indicates the level of agonist-induced platelet activation for PRP and PRP labelled with fusogenic liposomes (PRP.FLs) in the presence of CRP-XL (A & B).

A & B: Data represents the mean ± SD of four biological replicates (n=4) for the Isotype control, PRP, PRP.FLs and the ETOH control, one biological replicate (n=1) for PGI_2 concentrations

ranging 46 – 12 ng/mL, four biological replicates (n=4) for PGI_2 concentrations 6 – 0.73 ng/mL, and three biological replicates for PGI_2 concentrations 0.36 - 0.09 ng/mL. The blue vertical line indicates the optimum concentration of PGI_2 selected. Statistics were performed using one-way ANOVA with Bonferroni post-test when biological replicates were ≥3. Non-significant (ns), $P > 0.05$. **, $P \leq 0.01$. ***, $P \leq 0.001$. ****, $P \leq 0.0001$.

4.3 Discussion

Overall, the data in this chapter identifies the successful labelling of platelets using a commercial source of fluorescently labelled fusogenic liposomes (Fuse-It-Color, Benaig). Using this experimental set-up, ≥80% of platelets can be fluorescently labelled, and with the addition of 0.5 ng/mL PGI_2, fusogenic liposomes do not impact on normal platelet function when assessing *i*) the level of P-selectin exposure as a measure of α-granule release, *ii*) the level of PS exposure as a measure of procoagulant platelets, and *iii*) platelet spreading as a measure of normal platelet morphology and adhesion to a fibrinogen substrate.

The overall aim of this chapter was to identify if Fuse-It-Color could be fused to platelets without impacting function, and the data contained within this results chapter can be used as a proof of principle. This chapter has focussed on single cell techniques aimed at understanding platelet activation in the presence of fusogenic liposomes and the interactions of fused platelets with immobilised ligands for example, yet this technique may also be appropriate for other applications which require the fluorescent labelling of platelets. For example, fluorescently labelled fusogenic liposomes offer a biocompatible and non-toxic method of labelling platelets *in vitro*, which could further be utilised in microfluidic systems in order to assess how platelets adhere together or interact with other cells when added into anticoagulated whole blood [255,256].

Platelets labelled with fusogenic liposomes could be applied *in vivo* too. Intravital microscopy is a technique used to investigate thrombosis models since cells can interact according to their native environment [257]. This technique often requires an injection of fluorescently labelled platelets [258], or genetically introduced models containing platelet-specific fluorescent protein expression [259]. Although this allows for multiple biological processes to be investigated at the same time, such as coagulation and interactions with the endothelium [260], several reports suggest that genetic based approaches may disrupt normal cellular approaches [261].

The labelling of platelets for use in these systems (microfluidic and intravital systems) typically requires an addition or injection of antibodies conjugated to a fluorescent fluorophore. However, labelling platelets with antibodies or probes may interfere with receptor function and processes associated with thrombus formation, meaning that this approach is not always suited to live imaging of platelets [260]. Labelling platelets with fusogenic liposomes may, therefore, offer an alternative to some of the current limitations associated with antibody labelling using these systems. With potential to further contribute to the understanding of platelet migration [262], interactions of platelets with other blood cells [263],

interactions with the endothelium [264], and when relating to different physiological conditions such as inflammation [265], infection [266] and cancer [267,268].

Since platelets can successfully be labelled using a commercial source of fusogenic liposomes, this work opens up the potential to optimise cargo delivery using fusogenic liposomes. Fuse-It-P (Benaig) is another commercial source of fusogenic liposomes and is supplied as a dry lipid film containing a proprietary blend of lipids. This dried lipid film can be reconstituted using a water-soluble cargo where, due to the nature of the phospholipids and their hydrophobic and hydrophilic interactions, should spontaneously form vesicles and encapsulate the cargo inside the vesicle lumen. However, although Fuse-It-P labelled the cell membrane of platelets with similar consistency to Fuse-It-Color, for reasons unknown, cargo delivery was not identified. Data for the optimisation of Fuse-It-P to fluorescently label the platelet membrane can be found in section '8. Appendix: Fuse-It-P'.

This time, a washed platelet preparation was optimised to use directly with Fuse-It-P to remove plasma proteins which may impair fusion with the cell membrane of platelets. The adsorption of plasma proteins directly onto Fuse-It-P fusogenic liposomes could alter fusogenic characteristics, not only impairing fusion, but also limiting cargo delivery directly into platelets [269,270]. Therefore, despite an increase to platelet activation as a result of additional wash steps, the optimisation in the appendix section aimed to maximise the amount of potential cargo delivery.

Similar to optimisation with Fuse-It-Color, the use of Fuse-It-P also comprised assays which focussed on the level of platelet activation, the level of fluorescent labelling, the ability of platelets to spread normally, and the level of surface phosphatidylserine (PS) in the presence of Fuse-It-P when compared to control washed platelets. It was found that in the presence of 10 ng/mL PGI_2 at the point of fusion, there was no increase to platelet activation above a washed platelet control when using 9.2 µM Fuse-it-P (Figure 8.2B), and there was a significant increase in the percentage of platelets which were fluorescently labelled by Fuse-It-P when compared to the washed platelet control (Figure 8.2C). Furthermore, when compared to a washed platelet control, Fuse-It-P does not impair the ability of platelets to spread over a fibrinogen substrate (Figure 8.4), or increase the level of PS residing on the surface of platelets fused with Fuse-It-P (Figure 8.5). As well as single cell analyses, aggregometry was also performed in the appendix section to investigate the way that platelets can adhere to each other in order to from a thrombus (Figure 8.6). Platelets which were fused with Fuse-It-P aggregated similarly to control washed platelets in the presence of collagen [3 µg/mL] and thrombin [0.5 U/mL] and did not display any increased tendency to spontaneously aggregate. However, Zetasizer data did unveil that the sonication method

recommended by manufacturers was not sufficient to reduce the size of Fuse-It-P after hydration in 20 mM HEPES (Figure 8.8), and although this could be a reflection of the capability of the sonicating water bath itself, it could also be indicative of lipid degradation.

Although Fuse-It-P optimisation has demonstrated a biocompatible and non-toxic method to fluorescently label platelets, unfortunately, and for reasons unknown, cargo delivery was not successful using this commercial source of lipids. Therefore, the next chapter of this project focussed on the use of fusogenic liposomes manufactured in-house to deliver cargo directly into platelets. The techniques and optimisation process detailed in this results chapter (Section 4), and the appendix (Section 8), were further employed in order to optimise the use of in-house fusogenic liposomes in the presence and absence of cargo with human platelets.

Chapter 5: In-house fusogenic liposomes

5.1 Introduction

Due to unsuccessful cargo delivery of Lifeact into CHO cells or platelets using a commercial source of fusogenic liposomes (appendix data, section 8), it was decided to investigate the possibility of making in-house fusogenic liposomes using published methods. This decision was due to the unknown proprietary composition of the lipids and fluorescent dyes used within the commercial source of fusogenic liposomes, as well as the storage conditions prior to purchase. In-house fusogenic liposomes would allow more control over the ratios and the type of lipids used.

In-house fusogenic liposomes were made from a mixture of lipids known to produce cationic fusogenic vesicles (Figure 5.1). Namely, 1,2-dioleoyl-sn-glycero-3-phosphoethanolamine (DOPE) which served as a neutral lipid (Figure 5.1A), 1,2-dioleoyl-3-trimethylammonium-propane (DOTAP) which served as a cationic lipid (Figure 5.1B), and a lipid analogue 1,1'-Dioctadecyl-3,3,3',3'-Tetramethylindotricarbocyanine Iodide (DiR) which was used as a fluorescent label (Figure 5.1C). DiR is well known as a near-infrared (IR) carbocyanine dye which is highly fluorescent and photostable once incorporated into the cell membrane. The fluorophore of DiR includes a planar heterocyclic structure which contains a heteroatom, in this instance nitrogen. It has been hypothesised that electrostatic interactions between the positively charged lipids, DOTAP, and the highly polarisable π-electron system of the fluorophore introduces membrane instabilities, allowing fusion to occur [271]. Once fusion with the membrane of a cell has occurred, the DiR dye moves laterally through the plasma cell membrane. Taken together, this approach opens up the opportunity to encapsulate cargo directly inside the lumen of fusogenic liposomes, which upon fusion with the cell membrane, can be delivered directly into the cytoplasm of platelets. Similar to the previous chapter, the first aim of this chapter is to establish if in-house fusogenic liposomes can be used in combination with platelets, and secondly, as a vehicle to deliver cargo intracellularly.

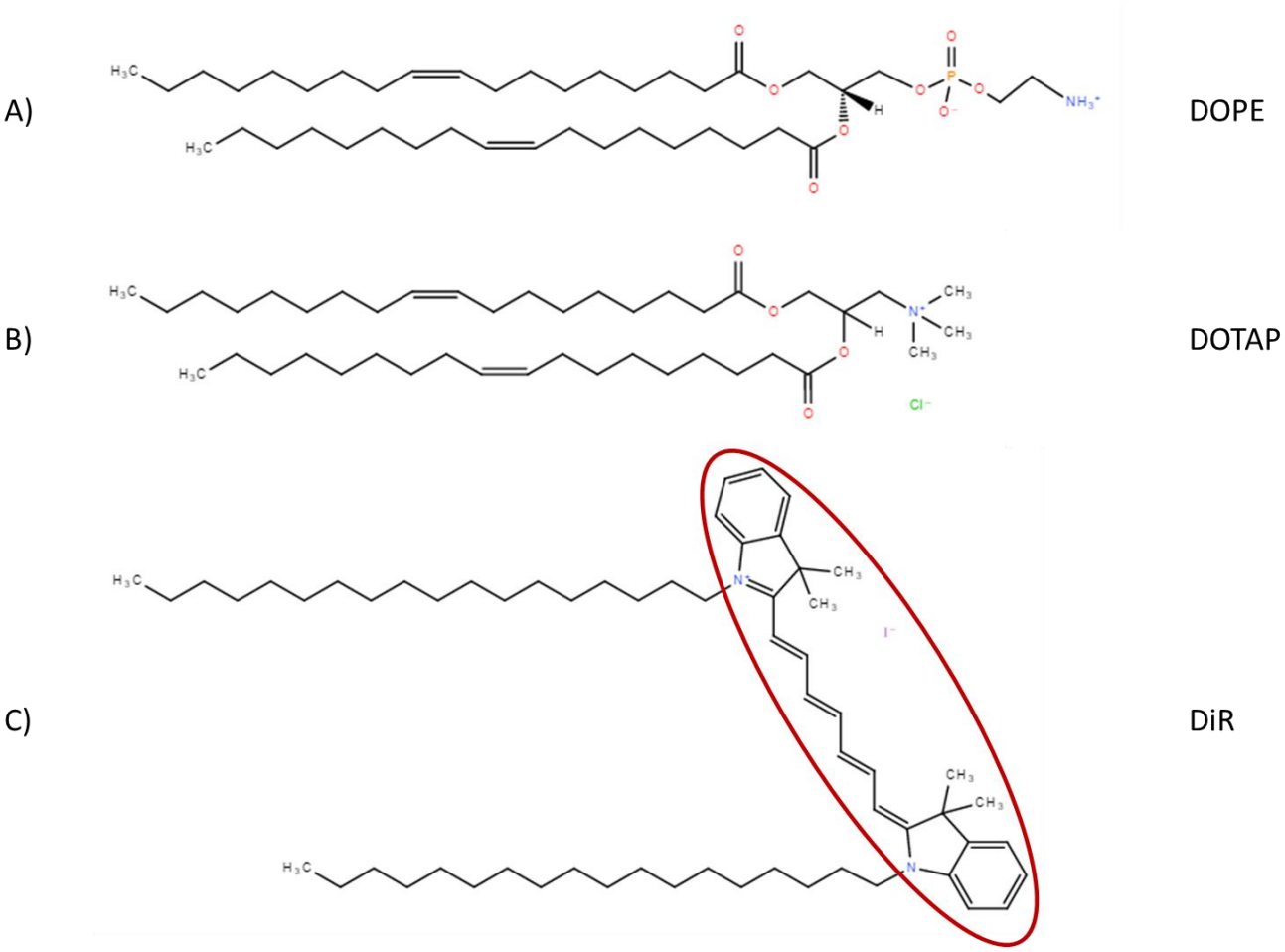

Figure 5.1 Chemical structures of lipids for preparation of in-house fusogenic liposomes

Chemical structure of the neutral lipid 1,2-dioleoyl-sn-glycero-3-phosphoethanolamine (DOPE) (A), 1,2-dioleoyl-3-trimethylammonium-propane (DOTAP) (B), and 1,1'-Dioctadecyl-3,3,3',3'-Tetramethylindotricarbocyanine Iodide (DiR) (C). The DiR carbocyanine fluorophore is indicated by the red circle (C). All structures drawn using LIPID MAPS® online software.

5.2 Results

5.2.1 Comparison of fusogenic liposome preparations: extrusion versus sonication.

The in-house fusogenic liposome preparation was further characterised to investigate the best method to generate uniform liposomes. Published literature mainly reports two methods to prepare unilamellar liposomes; either by sonication [121,145,151], or by extrusion [145,272,273]. Other approaches to generate unilamellar liposomes include freeze thawing methods using liquid nitrogen or dry ice, but this method is not appropriate for protein or enzyme-based cargo due to degradation and denaturation [274-276].

Here, sonication and extrusion methods were compared. Sonication included the use of a bench top ultrasonic bath to break up lipids which may have spontaneously formed into large or multilamellar vesicles due to the hydrophobic and hydrophilic interactions of lipids in an aqueous solution. Extrusion included the use of a mini extrusion apparatus (Avanti® Polar Lipids) where gas tight syringes were used to force dispersed lipids through a polycarbonate membrane consisting of a set pore size (100 nm). The back-and-forth motion caused by extrusion pushes larger vesicles through the small membrane pores, breaking up the larger lipid vesicles into smaller vesicles.

A Zetasizer (Malvern Panalytical) was used to measure both size and zeta potential of fusogenic liposomes which had either been sonicated or extruded (Figure 5.2). Firstly, size was measured using 90-degree dynamic light scattering (DLS) properties and the representative traces of the raw data were plotted for fusogenic liposomes which had been sonicated (Figure 5.2A.*i*) or extruded (Figure 5.2A.*ii*). The average size of the predominant peak was plotted for each fusogenic liposome replicate (Figure 5.2B). Although a greater variability in average fusogenic liposome size was observed using sonication (92.5 ± 34.1 nm), there was no significant size difference when compared to extruded fusogenic liposomes (134.5 ± 9.4 nm).

There was, however, a significant difference when comparing the polydispersity index (PDI) for sonicated and extruded fusogenic liposomes (Figure 5.2C). PDI is a measure of the heterogeneity of a given sample based on size. Where 0 represents a perfectly uniform sample when considering size and 1 represents a highly polydisperse sample containing numerous differently sized particle populations [277]. The PDI of sonicated fusogenic liposomes was significantly increased (0.26 ± 0.03) when compared to extruded fusogenic liposomes (0.09 ± 0.04) (Figure 5.2C). Indicating that fusogenic liposomes which had been sonicated were less uniform when compared to those which had been extruded. Despite this increase, the PDI for sonicated fusogenic liposomes in this experiment did not exceed 0.3. A

PDI of 0.3 or below is considered an acceptable PDI measure for lipid-based carriers such as fusogenic liposomes, indicating a homogenous population [278-280].

As well as size, zeta-potential was also acquired for the same fusogenic liposome samples. Any particle in suspension will exhibit a zeta potential [281], for example a fusogenic liposome or a polymer. There are different states of matter, including gases, liquids, and solids, and when one of these states is dispersed within another, for example fusogenic liposomes dispersed in a buffer, a colloidal system is created [282]. Zeta potential can be used to investigate the state of a particle surface, while the magnitude of zeta potential can predict the stability of the colloidal dispersion [283]. If particles have a large negative or positive zeta potential, they will repel each other and remain in a stable suspension [284]. If particles have a low negative or positive zeta potential, they will not repel strongly, generating an unstable suspension which will likely aggregate [284]. Particles with zeta potentials more positive than +30mV or more negative then -30mV are considered stable suspensions [284].

Raw zeta potential data was plotted for fusogenic liposomes which have been sonicated (Figure 5.2D.*i*) and extruded (Figure 5.2D.*ii*). The average zeta potential of sonicated fusogenic liposomes and extruded fusogenic liposomes were quantified (Figure 5.2E). Fusogenic liposomes which had been sonicated had a significantly increased zeta potential (68.2 ± 1.1 mV) when compared to extruded fusogenic liposomes (59.7 ± 3.8 mV). This suggests that sonicated fusogenic liposomes appear more stable in suspension when compared to extruded fusogenic liposomes, although, this may in part be due to an increased heterogeneous population increasing the zeta potential average.

Overall, the data indicates that fusogenic liposomes formed by sonication have a heterogeneous population when compared to fusogenic liposomes formed by extrusion which are highly uniform. Furthermore, extruded liposomes still present with a zeta potential greater than +30 mV suggesting that they are stable in a suspension. As a result, an extrusion method was taken forward during all further experimentation.

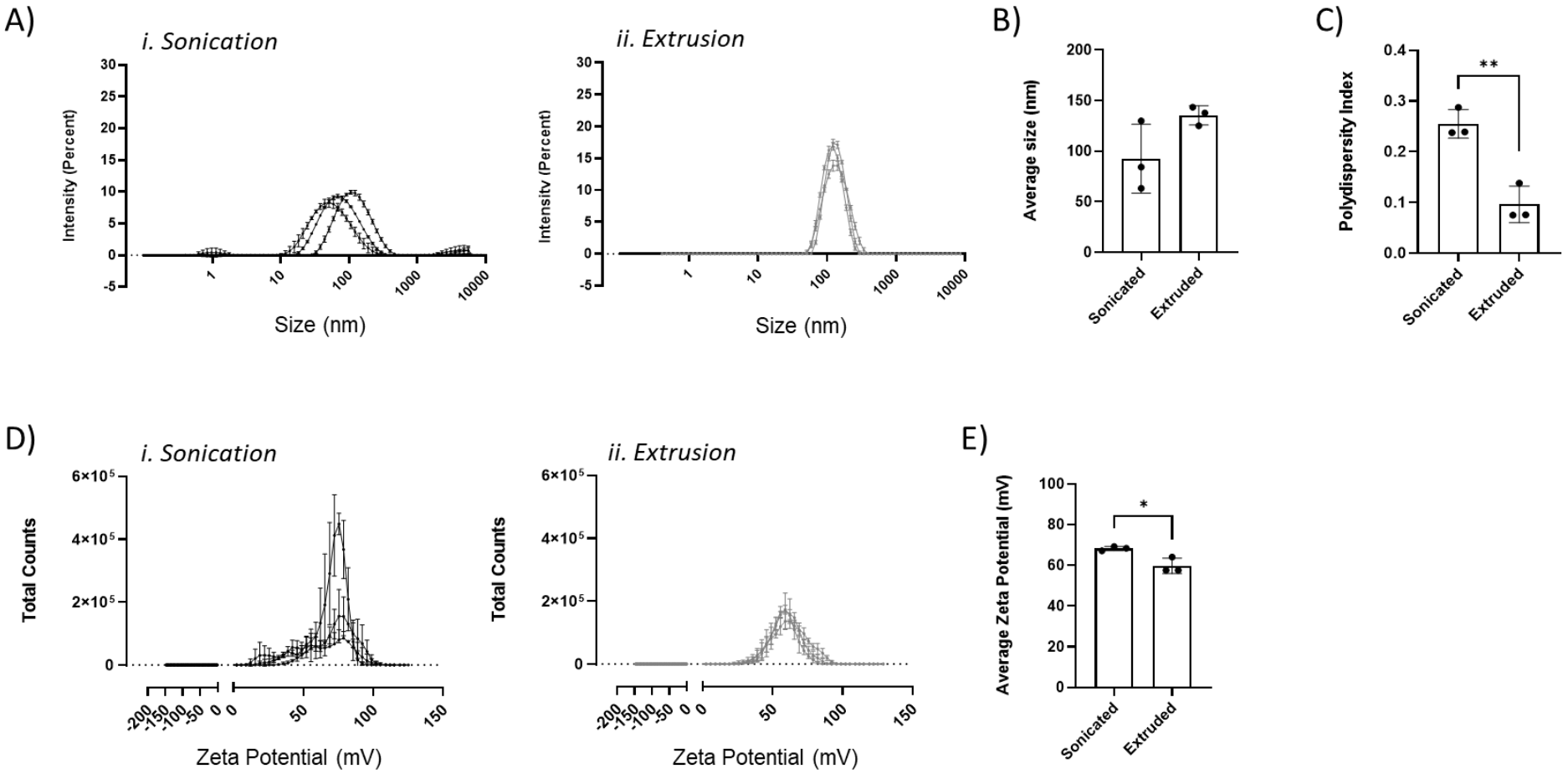

Figure 5.2 Sonication and extrusion result in differences to fusogenic liposome characteristics.

Lipid films were dispersed in 20mM HEPES buffer and either sonicated or extruded. Raw data indicates the percentage intensity of each peak at a given size for sonication (A.*i.*) and extrusion (A.*ii.*). The average size of each peak was quantified (B). Polydispersity index indicated how homogenously dispersed fusogenic liposomes were between sonication and extrusion methods (C). Raw data indicates the

total count of each peak at a given zeta potential for sonication (D.*i*.) and extrusion (D.*ii*.). The average zeta potential of each trace was quantified (E). Data represents the mean ± standard deviation (SD) of three fusogenic liposome replicates (n=3). Statistical analysis was performed using an unpaired two-tailed t test (* $P \leq 0.05$, ** $P \leq 0.01$).

5.2.2 In-house fusogenic liposomes can efficiently label platelets without impacting platelet activation.

Optimisation assays similar to those previously used for Fuse-It-Color were employed in order to identify the concentration of in-house fusogenic liposomes that efficiently labelled washed platelets without causing platelet activation. Therefore, washed platelets were incubated with fluorescently labelled in-house fusogenic liposomes in a dose dependent manner [20 µg/mL – 0.94 µg/mL]. An optimum concentration was deemed a concentration where platelets were not significantly activated yet were ≥ 80% fluorescently labelled by the DiR fluorescent tracer lipid.

This time washed platelets were pre-treated with PGI_2 prior to fusion at a final concentration of 1 ng/mL. Washed platelets permitted the removal of extracellular plasma proteins which can adsorb onto fusogenic liposomes and impair fusion by altering fusogenic characteristics [269,270]. Therefore, using washed platelets may increase not only the chance of fusion of in-house fusogenic liposomes directly with platelets, but increase the amount of cargo delivery also. Meanwhile, the concentration of PGI_2 was identified during the optimisation of a commercial source of cargo containing fusogenic liposomes (Fuse-It-P; data included in appendix, Section 8). This concentration of PGI_2 was a concentration which maintained platelet activation to similar levels as washed platelets after fusion and was therefore included during in-house fusogenic liposome optimisation.

As per previous analyses, P-selectin, a marker of α-granule release, was used as a measure of platelet activation by flow cytometry. Platelets were identified using forward scattered light (FSC) and side scattered light (SSC), a measure of size and granularity respectively. An isotype control was used to identify non-specific antibody binding, where a 2% gate was used to define a boundary to characterise platelet activation. The extent of washed platelet activation was subsequently the level of P-selectin exposure by α-granule release above this 2% boundary. A washed platelet control provided a basal level of platelet activation, and also served as a negative labelling control to investigate the percentage of platelet labelling by fusion.

The percentage of platelets positive for P-selectin exposure due to fusion was significantly increased when using in-house fusogenic liposome concentrations ≥ 10 µg/mL (60.1 ± 14.2 %) when directly compared to an unlabelled washed platelet control (WPs; 30.0 ± 12.7 %) (Figure 5.3A). In-house fusogenic liposome concentrations ranging from 7.5 µg/mL down to 0.94 µg/mL were not significantly different from the washed platelet control (Figure 5.3A).

The data for P-selectin exposure was also presented as MFI (Figure 5.3B). Platelet activation was significantly increased when fused with in-house fusogenic liposomes at concentrations of 20 µg/mL (1,959 ± 564.7 AU) and 15 µg/mL (1,465 ± 489.5 AU) when compared directly to the washed platelet control (WPs; 596.5 ± 57.8 AU). There were no significant differences for concentrations ranging from 10 µg/mL down to 0.94 µg/mL. This data presented similar scientific conclusions as percent positivity.

Despite differences to platelet activation in the presence of in-house fusogenic liposomes, fusion resulted in highly efficient labelling of platelets (Figure 5.3C). Labelling of platelets using in-house fusogenic liposomes presented significantly increased labelling at all concentrations tested when compared directly to the WP control where analyses were consistently gated at 2%. Labelling of platelets with in-house fusogenic liposomes resulted in ≥80 % fluorescent labelling when fusing with ≥ 2.5 µg/mL fusogenic liposomes (Figure 5.3C).

The data for MFI, however, did not indicate similar fluorescent labelling by in-house fusogenic liposomes when compared to percent positivity (Figure 5.3D). There were significant increases in fluorescent labelling when observing concentrations ≥ 10 µg/mL (14,891 ± 5,071 AU) when directly compared to the washed platelet control (233.8 ± 9.0 AU). There were no significant differences to fluorescent labelling for in-house fusogenic liposome concentrations ranging from 7.5 µg/mL to 0.9 µg/mL.

When taking into consideration the percent positivity and MFI for both P-selectin exposure and the labelling efficiency of in-house fusogenic liposomes, a concentration range was selected for further optimisation. In-house fusogenic liposomes ranging from 10 µg/mL down to 2.5 µg/mL were identified as a range which included platelets which had no significant increase in activation when measuring P-selectin exposure. Furthermore, although labelling efficiency for percent positive and MFI differed, platelets were efficiently labelled when compared to the washed platelet control within this concentration range. Further investigation involved the presence and absence of CRP-XL to identify if fused platelets stimulated with agonist can activate similarly to controlled platelets.

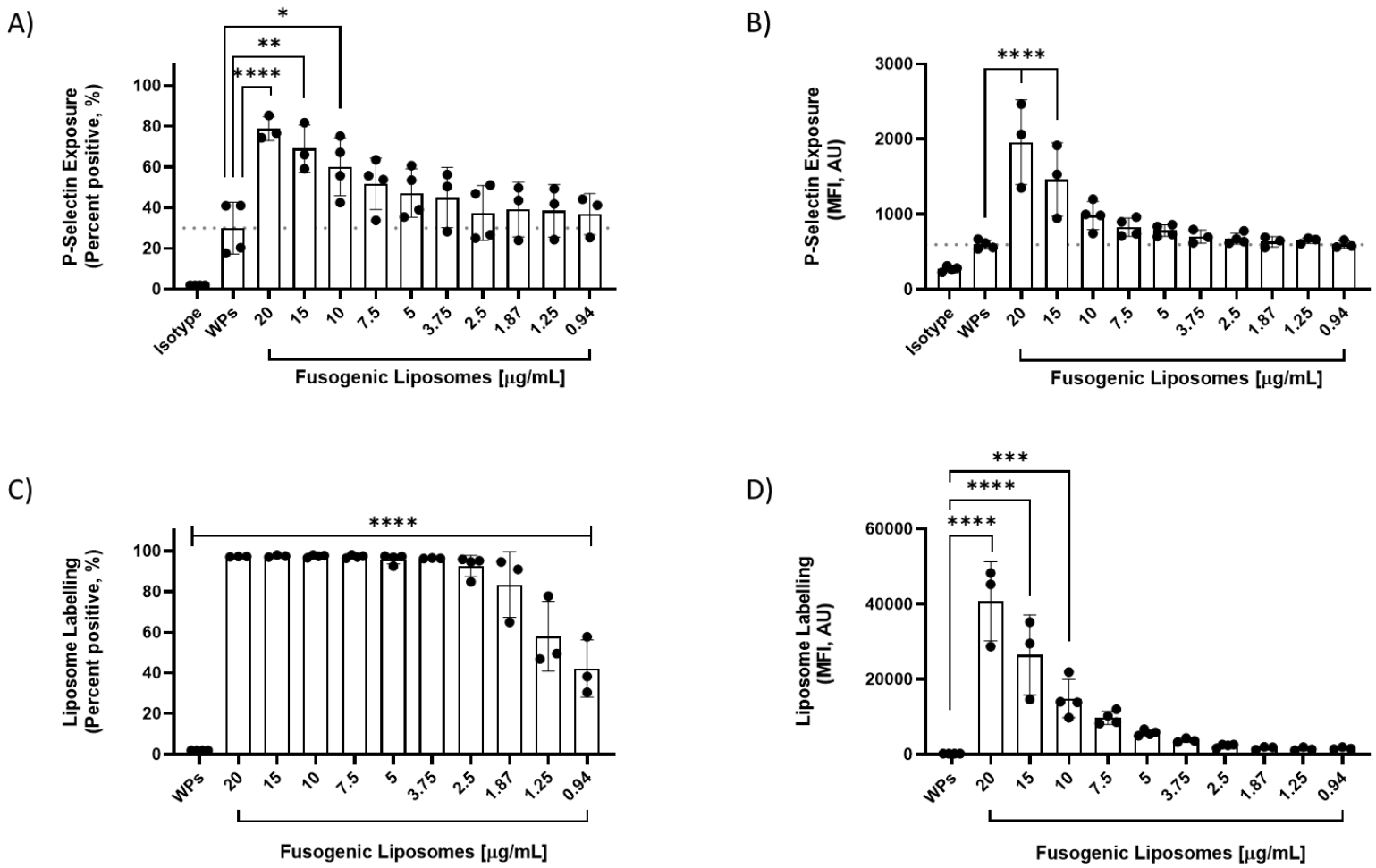

Figure 5.3 Fluorescently labelled fusogenic liposomes induce P-selectin exposure at high concentrations.

Platelets were labelled using fusogenic liposomes dose dependently. P-selectin exposure was directly compared between the isotype control, washed platelets (WPs) and WPs pre-treated with in-house fusogenic liposomes decreasing in concentration (20 µg/mL – 0.94 µg/mL) and data plotted as percent positivity (A) and MFI (B). The grey dashed line indicates the mean activation of washed platelets which

served as a vehicle control (A & B). Labelling efficiency was directly compared between WPs and WPs pre-treated with in-house fusogenic liposomes decreasing in concentration (20 µg/mL – 0.94 µg/mL) and data plotted as percent positivity (C) and MFI (D). The data represents 4 experimental replicates (n=4) for the isotype control, WPs and in-house fusogenic liposomes for 10 µg/mL – 0.94 µg/mL. Data represent 3 experimental replicates (n=3) for in-house fusogenic liposomes for 20 µg/mL and 15 µg/mL. The mean ± SD was analysed using one-way ANOVA with Bonferroni post-test. The mean of the control group (Isotype for P-selectin and WPs for labelling efficiency) was compared to the mean of platelets fused with in-house fusogenic liposomes. *, $P \leq 0.05$. **, $P \leq 0.01$. ***, $P \leq 0.001$. ****, $P \leq 0.0001$.

5.2.3 Platelets labelled with in-house fusogenic liposomes can respond as expected to the GPVI agonist CRP-XL.

Platelets which had been fused with in-house fusogenic liposomes ranging from 10 µg/mL down to 2.5 µg/mL were then subjected to agonist-induced activation using CRP-XL [3 µg/mL]. CRP-XL, upon interaction with the platelet cell surface receptor GPVI, induces a strong tyrosine phosphorylation of platelet proteins such as the tyrosine kinase Syk, phospholipase Cγ2 (PLCγ2) and a scaffolding protein, linker for activation of T-cells (LAT) [34]. CRP-XL is widely used in platelet function tests due to being a potent platelet activator.

Firstly, platelets fused with fusogenic liposomes in the absence of CRP-XL, were directly compared to a washed platelet control. Then, washed platelets and platelets fused with fusogenic liposomes, which were subsequently stimulated with CRP-XL, were directly compared to the unstimulated control. Data for these experiments consisted of a new subset of donors.

As per previous analyses, P-selectin, a marker of α-granule release, was used as a measure of platelet activation by flow cytometry. Platelets were identified using forward scattered light (FSC) and side scattered light (SSC), a measure of size and granularity respectively. An isotype control was used to identify non-specific antibody binding, where a 2% gate was used to define a boundary to characterise platelet activation. The extent of platelet activation was subsequently the level of P-selectin exposure by α-granule release above this 2% boundary for all samples. A washed platelet control provided a basal level of platelet activation and served as a negative labelling control to investigate the percentage of platelet labelling by fusion.

The percentage of platelets positive for P-selectin exposure due to fusion was significantly increased when using in-house fusogenic liposome concentrations of 10 µg/mL (63.7 ± 13.5 %) and 7.5 µg/mL (54.4 ± 12.6 %) when compared to an unlabelled washed platelet control (WPs; 32.1 ± 8.3 %) (Figure 5.4A). This contrasts with previous data which suggested that a concentration of 7.5 µg/mL did not induce significant changes (section 5.2.2). However, this is likely a result of small sample sizes and a different collection of biological data. In-house fusogenic liposome concentrations ranging from 5 µg/mL down to 2.5 µg/mL were not significantly different from the washed platelet control (Figure 5.4A).

There was a significant increase to platelet activation when comparing unstimulated washed platelets (32.1 ± 8.3 %) to washed platelets in the presence of CRP-XL (89.1 ± 2.0 %). Indicating that 3 µg/mL of CRP-XL can induce significant changes to platelet activation in untreated washed platelets. There were also significant increases to P-selectin for all

concentrations of fusogenic liposomes tested when comparing unstimulated fused platelets to those which had been stimulated with CRP-XL (Figure 5.4A), indicating that CRP-XL can induce significant changes to platelet activation in platelets fused with fusogenic liposomes.

The data for P-selectin exposure was also presented as MFI (Figure 5.4B). In contrast to percent positivity, there were no differences to P-selectin exposure when comparing the unstimulated washed platelet control to the unstimulated platelets which had been fused with fusogenic liposomes for all concentrations. This data is in agreement with the MFI data presented previously (section 5.2.2).

Like percent positivity, there were significant increases to MFI when comparing unstimulated washed platelets (571.0 ± 152.0 AU) to washed platelets in the presence of CRP-XL (3,164 ± 363.9 AU). There were also significant increases to P-selectin for all concentrations of fusogenic liposomes tested when comparing unstimulated fused platelets to those which had been stimulated with CRP-XL (Figure 5.4B).

There were further significant differences to MFI when comparing samples which had been stimulated with CRP-XL (Figure 5.4B). There were significant increases to P-selectin exposure when comparing washed platelets in the presence of CRP-XL (3,164 ± 363.9 AU), to platelets fused with fusogenic liposomes at 10 µg/mL in the presence of CRP-XL (4,458 ± 587.0 AU), and at 7.5 µg/mL in the presence of CRP-XL (4,835 ± 195.7 AU). This indicates that the combination of fusion with fusogenic liposomes at higher concentrations can potentiate further platelet activation in the presence of CRP-XL. This is likely a result of elevated platelet activation caused by fusion of the liposomes.

Collectively, this data indicates that platelets treated with fusogenic liposomes ranging from 10 µg/mL down to 2.5 µg/mL could be activated by CRP-XL. This indicates that the GPVI pathway of activation is unaffected by fusogenic liposome fusion, and that platelets fused with fusogenic liposomes can respond similarly to unfused control platelets.

Considering the elevation to P-selectin exposure when using 10 µg/mL and 7.5 µg/mL fusogenic liposomes for both percent positivity and MFI, and taking into consideration the potentiation of platelet activation in the presence of CRP-XL identified by MFI, the concentration for further experimentation was identified as 5 µg/mL fusogenic liposomes.

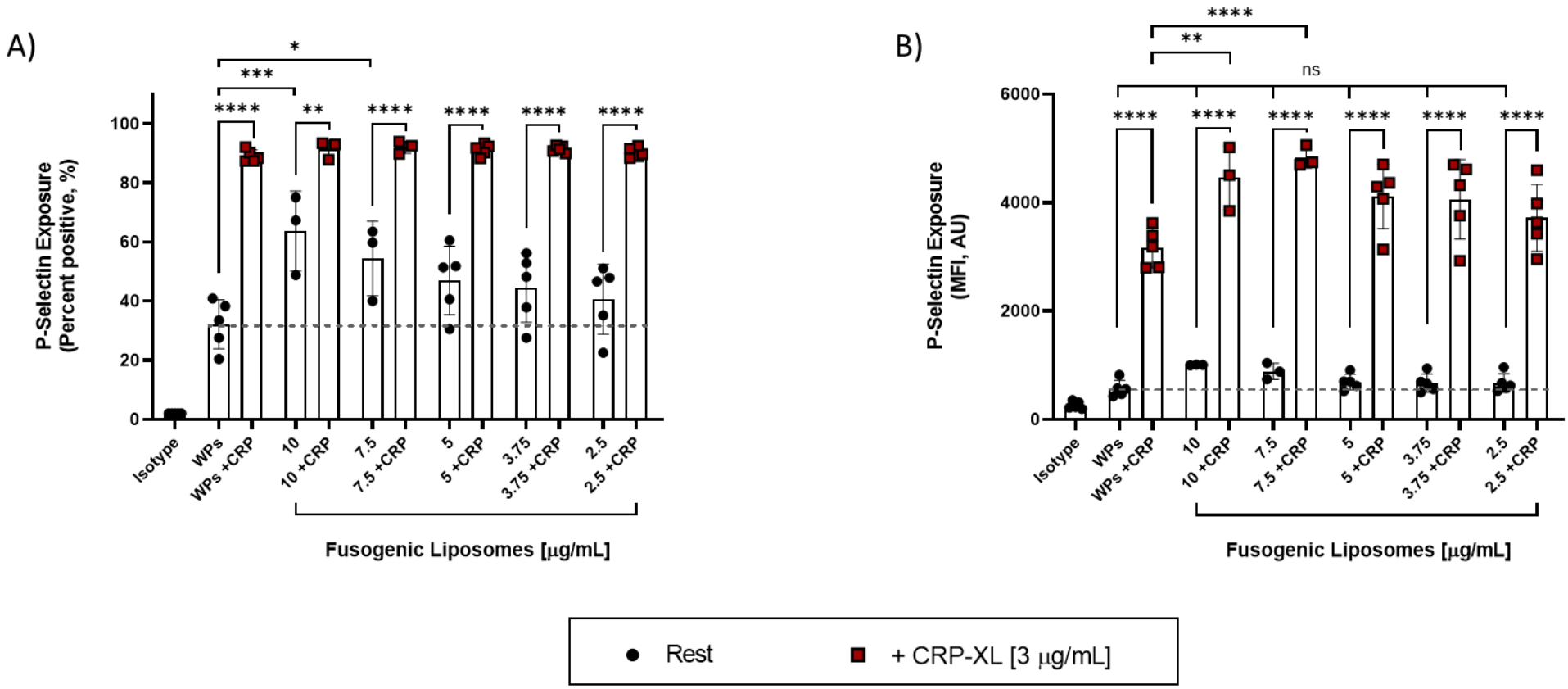

Figure 5.4 Platelets labelled with fusogenic liposomes can activate similarly to washed platelets in the presence of CRP-XL.

Platelets were labelled using fusogenic liposomes dose dependently in the presence and absence of CRP-XL [3 μg/mL]. The percentage of P-selectin exposure for platelets fused with fusogenic liposomes in the presence (red squares) and absence (black circles) of CRP-XL were assessed using decreasing concentrations of fusogenic liposomes [10 μg/mL – 2.5 μg/mL] and directly compared to an unlabelled washed platelet control (WPs). The median fluorescent intensity (MFI) for P-selectin exposure were also plotted to compare outcomes. Data represents 5 biological replicates (n=5) for WPs, and platelets labelled with fusogenic liposomes from 5 μg/mL down to 2.5 μg/mL. Data represents 3 biological replicates (n=3) for fusogenic liposomes concentrations of 10 μg/mL and 7.5 μg/mL. The grey dashed line is representative of the mean of the WPs for both percent positivity (A) and MFI (B). The mean ± SD was analysed using one-way ANOVA with Bonferroni post-test. The mean of each group was compared to the mean of all other groups. *, $P \leq 0.05$. **, $P \leq 0.01$. ***, $P \leq 0.001$. ****, $P \leq 0.0001$.

5.2.4 Fusogenic Liposomes do not impact on haematological parameters.

Additional evidence for choosing 5 µg/mL fusogenic liposomes in subsequent experimentation included haematological data for washed platelets (WPs) and platelets fused with fusogenic liposomes ranging from 20 µg/mL down to 0.94 µg/mL (Figure 5.5).

A 50 µL aliquot of each sample was assessed using a Sysmex XP-300 to measure haematological parameters. Firstly, the platelet count of platelets fused with fusogenic liposomes were directly compared to the platelet count of controlled washed platelets (Figure 5.5A). There was a significant decrease to platelet count when platelets were fused with fusogenic liposomes at 20 µg/mL (59.3 ± 5.8 x 10^3/µL), 15 µg/mL (63.0 ± 4.6 x 10^3/µL) and 10 µg/mL (68.3 ± 8.1 x 10^3/µL) when directly compared to the washed platelet control (80.3 ± 4.6 x 10^3/µL). This data suggests that either, there is a platelet loss due to too high a concentration of fusogenic liposomes, or platelets are becoming much larger due to fusion and are no longer recognised as platelets by the Sysmex algorithm.

Platelet distribution width (PDW) was also observed as an indicator of variability to platelet size (Figure 5.5B). An increased PDW is representative of a large variation in size and can be an indicator of platelet activation. Here, this parameter was used to identify if fusogenic liposomes were labelling platelets non-uniformly. There were no significant differences to PDW for all samples, suggesting that the uniformity of platelets which had been fused with fusogenic liposomes and were detected by the Sysmex were not impacted by the fusion process.

Mean platelet volume (MPV) assessed the average size of platelets in all samples (Figure 5.5C). There was a significant increase to the average platelet size when platelets were fused with 20 µg/mL fusogenic liposomes (10.2 ± 0.6 fL) when compared to the washed platelet control (8.9 ± 0.9 fL). This suggests that higher concentrations of fusogenic liposomes may increase the average size of platelets.

With that in mind, the forward scatter parameter acquired by flow cytometry, a measure of platelet size, was also plotted to determine if the same scientific conclusions could be made as MPV (Figure 5.5D). There was a significant increase in forward scattered light when platelets were fused with fusogenic liposomes at 20 µg/mL (224,050 ± 13,459 AU), 15 µg/mL (226,312 ± 3,871 AU) and 10 µg/mL (217,639 ± 7,327 AU) when compared to the washed platelet control (193,641 ± 9,188 AU). Suggesting that higher concentrations of fusogenic liposomes are increasing the average size of platelets. This may further conclude that automated counts using the Sysmex analyser may not accurately detect platelet count due

to an increased platelet size when platelets are fused with fusogenic liposome concentrations ranging from 20 µg/mL to 10 µg/mL.

When platelets were fused with a concentration of 5 µg/mL fusogenic liposomes, there were no significant differences in platelet count, PDW or MPV (Figure 5.5A, B & C respectively). There were also no significant increases to forward scattered analyses (Figure 5.5D). This data was interesting since an increase to platelet size, which was seen at high concentrations of liposomes, was expected after the fusion of fusogenic liposomes due to the nature of the fusion process where fusogenic liposomes become an extension of the platelet membrane. Despite this, it is possible to conclude that fusogenic liposomes do not significantly impact size and uniformity of platelets during fusion at a concentration of 5 µg/mL.

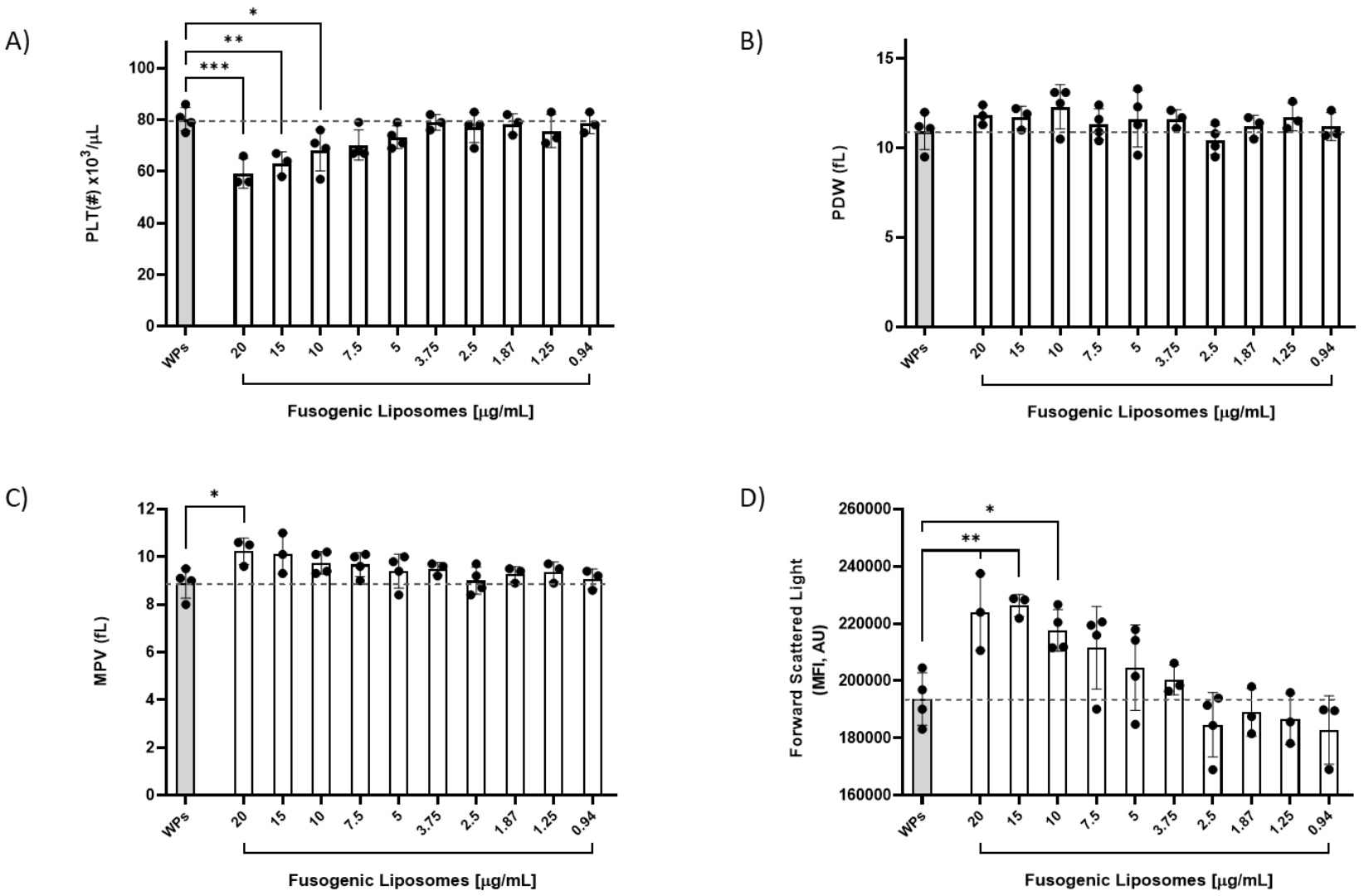

Figure 5.5 The addition of fluorescently labelled fusogenic liposomes does not alter haematological parameters.

Platelets were labelled using fusogenic liposomes dose dependently from 20 µg/mL down to 0.94 µg/mL. Haematological parameters were acquired for platelet count (x 10^3/µL) (A), platelet distribution width (PDW) (B) and mean platelet volume (MPV) (C). Forward scattered light,

representative of platelet size, was acquired by flow cytometry (D). Haematological and flow cytometry outputs for platelets fused with fusogenic liposomes were directly compared to an unlabelled washed platelet control (WPs). Data represents 4 biological replicates (n=4) for WPs, and platelets labelled with fusogenic liposomes from 10 µg/mL down to 5 µg/mL, and 1.87 µg/mL down to 0.94 µg/mL. Data represents 3 biological replicates (n=3) for fusogenic liposomes concentrations 20 µg/mL, 15 µg/mL and 3.75 µg/mL. The grey dashed line is representative of the mean of WPs. The mean ± SD was analysed using one-way ANOVA with Bonferroni post-test. The mean of each group was directly compared to the mean of the WP control. *, $P \leq 0.05$. **, $P \leq 0.01$. ***, $P \leq 0.001$.

5.2.5 Fusion of fusogenic liposomes to the platelet membrane can be visualised in spread platelets in real time.

The fusion of fluorescently labelled fusogenic liposomes can be detected by fluorescent microscopy. Once fusion occurs, the DiR lipid tracer will diffuse laterally through the phospholipid bilayer of the platelet membrane. It was therefore possible to identify real time fusion of the platelet membrane of spread platelets.

Fusogenic liposomes [5 µg/mL] were added directly to platelets which had already been spread over a fibrinogen substrate [100 µg/mL] (Figure 5.6). Representative DIC images were exported from a video focussed on a centrally located platelet over time (top panel). While representative fluorescent images exported from the same video identified the extent of labelling by fusogenic liposomes over the same time frames (bottom panel). The platelet identified in Figure 5.6 took approximately 58 seconds from initial attachment of a fusogenic liposome to full diffusion of the DiR tracer through the platelet membrane. This qualitative data suggests that the formulation of the in-house fusogenic liposomes can successfully fuse with the cell membrane of platelets.

Following confirmation that in-house fusogenic liposomes were able to fuse with platelets spread on a fibrinogen substrate, cargo delivery was attempted in spread platelets to identify if in-house fusogenic liposomes can firstly encapsulate cargo, and secondly, if delivery of the cargo directly into platelets is possible.

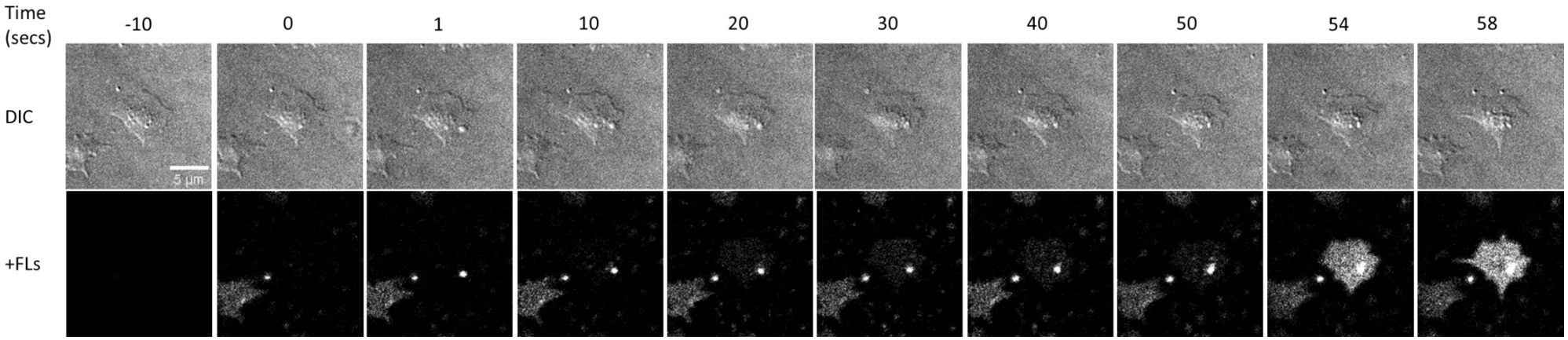

Figure 5.6 Fusogenic liposome fusion in spread platelets in real time.

Representative DIC image stills exported from a video identify a platelet (centrally located, top panels) before and after the addition of fusogenic liposomes from -10 seconds to +58 seconds. Corresponding fluorescent images detail the extend of fluorescent labelling by fusogenic liposome fusion (+FLs) over the same time frames (greyscale bottom panels).

5.2.6 Lifeact delivery into spread platelets using fusogenic liposomes as a delivery vehicle.

Lifeact, a 17-residue fluorescently labelled actin binding peptide derived from budding yeast [285], was chosen as a cargo to load into fusogenic liposomes for direct delivery into spread platelets. Lifeact is a small peptide and binds to actin filaments with high affinity, allowing the visualisation of actin structures and dynamics in live cells. Furthermore, the actin structures and dynamics in spread and spreading platelets have been extensively characterised in the literature. In particular, spread platelets presenting filopodia extensions and lamellipodia protrusions are well recognised and easily visualised using microscopy techniques. Therefore, it was attempted to deliver Lifeact conjugated to a 488 nm fluorescent label (Lifeact-488) directly into spread unfixed platelets to determine if Lifeact could be delivered and used to label actin structures in unfixed and permeabilised platelets.

Washed platelets were first spread over a fibrinogen substrate [100 µg/mL] prior to incubation with either an unloaded fusogenic liposome control, or fusogenic liposomes hydrated in either 10 µM, 50 µM or 100 µM Lifeact-488. The unloaded fusogenic liposomes were hydrated in 20 mM HEPES buffer only. Unencapsulated Lifeact-488 cargo was not separated from Lifeact-488 loaded fusogenic liposomes.

Representative images depict the DIC images of spread platelets (Figure 5.7A, column 1), those which have been fluorescently labelled by the fusion of fusogenic liposomes (Figure 5.7A, column 2), and those where Lifeact-488 is detected (Figure 5.7A, column 3). Fluorescently labelled Lifeact-488 can be observed at the location of spread platelets when fusogenic liposomes were loaded with 10 µM Lifeact-488. There was a qualitative increase in the amount of fluorescently labelled Lifeact-488 at the location of spread platelets when fusogenic liposomes were loaded with 50 µM and 100 µM Lifeact-488.

To ensure that unencapulated Lifeact-488 is not causing this labelling effect, unencapsulated concentrations of Lifeact-488 were added into unloaded preformed fusogenic liposomes prior to adding to spread platelets as before (Figure 5.7B). This control was used to determine if potential instabilities induced by fusogenic liposome fusion was allowing platelet membranes to be permeabilised or weakened. This could allow unencapsulated Lifeact-488 to enter the platelets and bind to actin filaments and could mistakenly be interpreted as delivery by fusogenic liposomes.

Surprisingly, some Lifeact-488 did appear to permeate the spread membrane of washed platelets in the absence of fusogenic liposomes when using a concentration of 50 µM Lifeact-488. Platelets which had been incubated with unloaded fusogenic liposomes also

containing unencapsulated concentrations of Lifeact-488 also showed evidence of Lifeact-488 permeabilisation. This contrasts with reports that suggest that Lifeact cannot permeate the membrane of platelets [51].

This may, in part, be attributed to platelets which could be more activated or fully spread, presenting weaknesses to membrane integrity. Further investigation, however, would be needed to conclude these suggestions. Furthermore, when observing the representative images, there were not always clear fluorescently labelled actin filaments which are typically observed after labelling with fluorescently labelled Lifeact, and may be a result of suboptimal levels of delivery.

This data represents three biological replicates and was subsequently quantified in order to identify absolute numbers and to make clear conclusions regarding Lifeact delivery in the presence and absence of liposomes and in the presence and absence of encapsulated Lifeact-488.

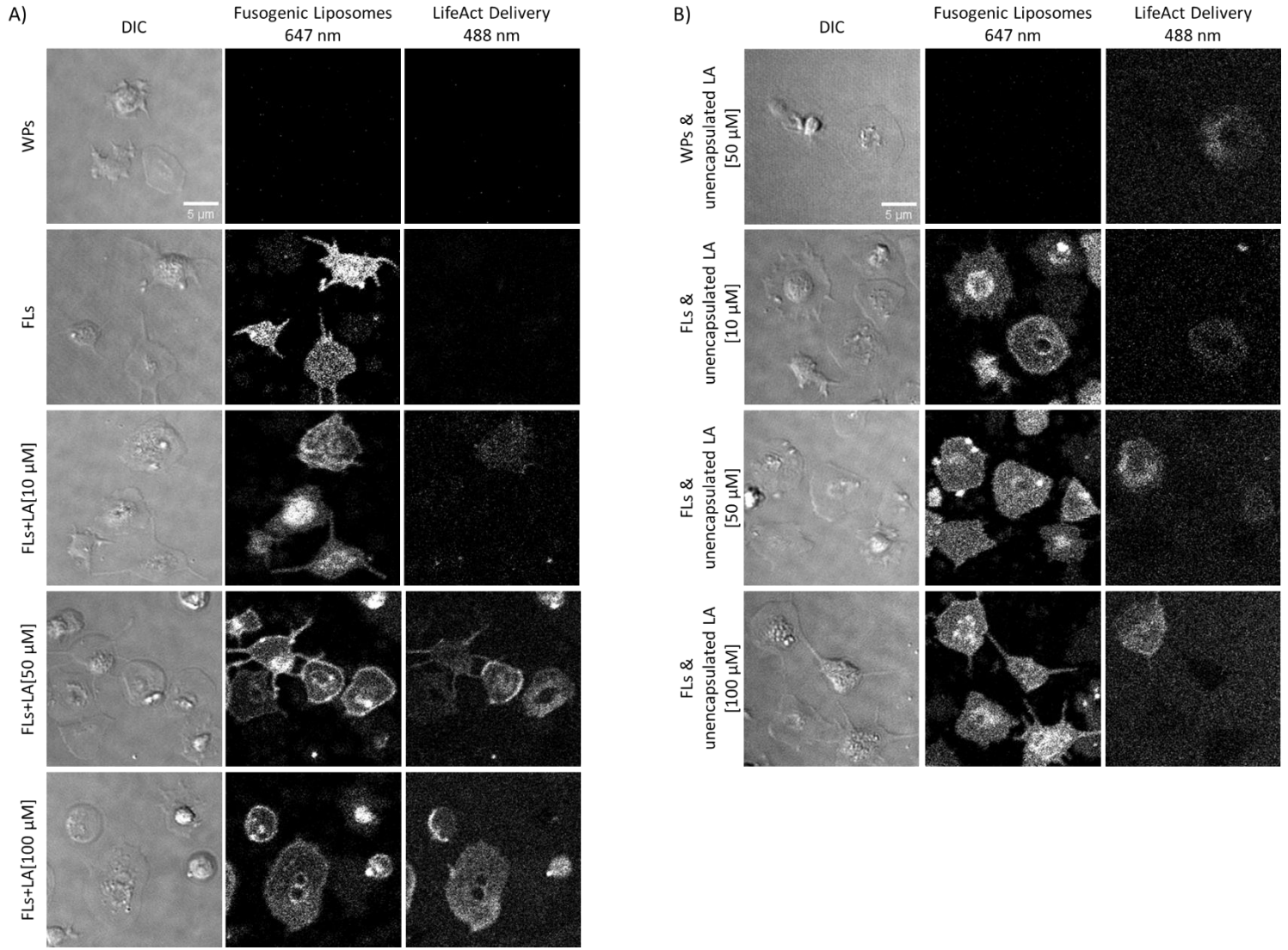

Figure 5.7 Delivery of Lifeact cargo into spread platelets using fusogenic liposomes.

Platelets were spread over a fibrinogen substrate [100 µg/mL] prior to labelling with fusogenic liposomes [5 µg/mL] for 15 minutes. Fusogenic labelling and extent of cargo delivery were compared to a washed platelet control (WPs). Unfixed spread platelets were treated with unloaded fusogenic liposomes (FLs), and fusogenic liposomes resuspended in increasing concentrations of Lifeact (LA) [10 µM, 50 µM

and 100 μM] diluted in 20 mM HEPES buffer (A). Unencapsulated Lifeact-488 was not removed from fusogenic liposome preparations, so unencapsulated concentrations of Lifeact-488 were subsequently spiked into unloaded fusogenic liposomes and added to unfixed spread platelets as before (B). All images were captured at the same laser intensity and exposure settings, contrast and brightness were enhanced for display purposes. Scale bars represents 5 μm.

5.2.7 Fluorescently labelled Lifeact can be delivered into spread platelets using fusogenic liposomes as a delivery vehicle.

To investigate the efficiency of fusogenic liposomes to deliver Lifeact-488 directly into the cytoplasm of platelets, images were used to quantify the total number of spread platelets and each platelet was assigned into a category depending on its fluorescent labelling (Figure 5.8). Platelets were assigned to one of four groups consisting of, 1) platelets which represented no fusogenic liposome labelling and no Lifeact-488 delivery (-FL, -LA), 2) platelets which represented fusogenic labelling and no Lifeact-488 delivery (+FL, -LA), 3) platelets which represented fusogenic labelling and Lifeact-488 delivery (+FL, +LA), and 4) platelets which represented no fusogenic labelling and Lifeact-488 delivery (-FL, +LA) (Figure 5.8, 1-4). The cell-counter plug-in for ImageJ was used for all counting analyses. Data consisted of three biological replicates, and counting analyses were based on the average of 5 fields of view per condition.

A series of experimental and control conditions were included to determine if Lifeact-488 was delivered directly into spread platelets as a result of fusogenic liposome fusion, or if delivery was a result of unencapsulated cargo being able to permeate the membrane of platelets independently of fusogenic liposome delivery. Washed platelets (WPs) were used as a negative labelling control. A second control included washed platelets with additional 50 μM unencapsulated Lifeact-488 (WPs+unencap.LA50). This condition represents unencapsulated free Lifeact-488 as during liposome formation unencapsulated Lifeact-488 was not removed.

The remaining conditions were all in the presence of the same concentration of fusogenic liposomes [5 μg/mL]. Firstly, fusogenic liposomes resuspended in 20 mM HEPES buffer (FLs) provided a baseline for fluorescent liposome labelling when in the absence of cargo and served as a control to determine if different concentrations of Lifeact-488 impaired fusion. Fusogenic liposomes were prepared using increasing concentrations of Lifeact-488: 10 μM Lifeact-488 (FLs+LA10), 50 μM Lifeact-488 (FLs+LA50), and 100 μM Lifeact-488 (FLs+LA100). The final three conditions represented fusogenic liposomes which had been first resuspended in 20 mM HEPES buffer before increasing concentrations of unencapsulated Lifeact-488 were added: 10μM (FLs+unencap.LA10), 50μM (FLs+unencap.LA50) or 100 μM (FLs+unencap.LA100) Lifeact-488. This would enable the amount of delivery, as a result of fusogenic liposome encapsulation (FLs+LA10, FLs+LA50, and FLs+LA100), to be compared to the platelet labelling observed in the presence of buffer containing fusogenic liposomes and unencapsulated Lifeact-488 cargo (FLs+unencap.LA10, FLs+unencap.LA50, and FLs+unencap.LA100).

Firstly, the total count of spread platelets was recorded (Figure 5.9A). There was no significant difference between the total number of platelets per condition, suggesting that the number of spread platelets between each condition was similar and that the addition of fusogenic liposomes or Lifeact-488 did not change the total number of platelets adhered. To account for variability in the total number of adhered platelets, all data was subsequently normalised between 0 and 1 by scaling counts according to the minimum and maximum values.

For all experimental and control conditions each platelet was categorised depending on its fluorescent status (Figure 5.9B). Unsurprisingly, the number of platelets which were labelled with fusogenic liposomes was significantly increased when directly comparing all labelling conditions to the washed platelets and washed platelets with unencapsulated Lifeact-488 controls (WPs and WPs+unencap.LA50) (Figure 5.9B*i*.). There was no difference to the number of platelets which had been fluorescently labelled with fusogenic liposomes between each of the experimental conditions (Figure 5.9B*i*.). This suggests that the number of platelets fluorescently labelled between each condition was similar, and that Lifeact-488 did not impact on the level of membrane fusion by fusogenic liposomes. This data was in agreement with the number of platelets which remained unlabelled after fusion between each condition which was also similar (Figure 5.9B*ii*).

When investigating the proportion of platelets labelled for both fusogenic liposomes and Lifeact-488 (Figure 5.9B*iii* (+FL+LA)) there was a significant increase in the proportion of double positive platelets when platelets were incubated with encapsulated and unencapsulated Lifeact-488 and compared to the controls (WPs and WPs+unencapLA50, (black lines)). This suggests that unencapsulated Lifeact-488 may enter the cytoplasm of platelets during fusion by fusogenic liposomes. This may, in part, be attributed to instabilities because of the fusion process itself or may be a result of high concentrations of unencapsulated Lifeact-488. Despite this, there was a significant increase in double positive platelets when Lifeact-488 was encapsulated in fusogenic liposomes and compared to the unencapsulated equivalent for 10 μM and 50 μM of Lifeact-488 (for example, between FLs+LA10 and FLs+unencapLA10, and between FLs+LA50 and FLs+unencapLA50 (blue lines)) but not for 100 μM Lifeact-488. This suggests that at lower concentrations of Lifeact-488, fusogenic liposomes may be delivering cargo into the cytoplasm of the platelets over and above indirect delivery.

Finally, the number of platelets labelled with Lifeact-488 in the absence of fusogenic liposomes was also investigated (Figure 5.9B*iv.*). There was a significant increase in the proportion of platelets that were labelled with Lifeact-488 in the presence of unencapsulated

concentrations of 50 µM Lifeact-488 (WPs+unencapLA50, 0.06 ± 0.02) when compared to all other conditions (Figure 5.9B*iv*). This suggests that free Lifeact-488 (at 50 µM) can, in the absence of fusogenic liposomes, permeate the membrane in approximately 6% of spread platelets. Furthermore, when comparing the proportion of platelets which were labelled with free Lifeact-488 (WPs+unencapLA50, panel Figure 5.9*iv*) to the condition of unencapsulated 50 µM Lifeact-488 in the presence of fusogenic liposomes (FLs+unencapLA50, panel Figure 5.9*iii*, (blue dashed line)), there was a significant increase in the amount of Lifeact-488 detected. This suggests that fusion of fusogenic liposomes with platelets results in an increase in Lifeact-488 labelling independently of delivery.

Taken together, while Lifeact-488 can enter the cytoplasm of platelets independently of direct cargo delivery by fusogenic liposomes, fusogenic liposomes may be delivering the Lifeact-488 cargo at lower concentrations since there is significant elevation in the number of platelets fluorescently labelled with Lifeact-488 during cargo encapsulation in the presence of 10 µM and 50 µM Lifeact-488 when compared to control conditions. However, the efficiency of Lifeact-488 delivery by fusogenic liposomes directly into the platelet cytoplasm remains low and may be a result of low encapsulation efficiencies,

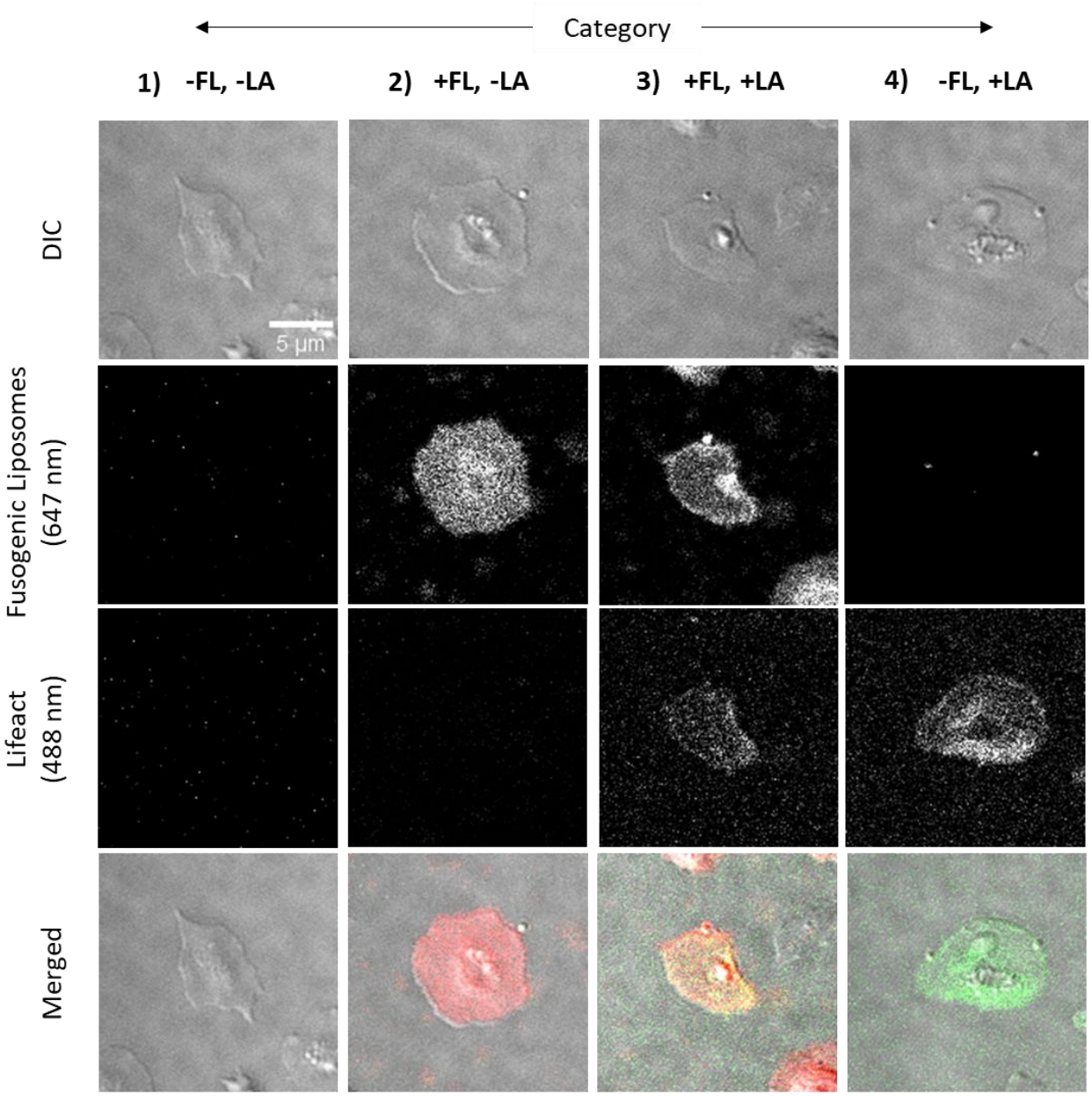

Figure 5.8 Quantification of Lifeact-488 cargo into spread platelets using fusogenic liposomes as a delivery vehicle.

Fusogenic liposomes [5 µg/mL] were prepared using different concentrations of Lifeact-488 [10 µM, 50 µM and 100 µM] and added to washed platelets (1 x 10^7 /mL) spread over a fibrinogen substrate [100 µg/mL]. Lifeact-488 delivery by fusogenic liposomes was quantified by counting the absolute number of spread platelets and assigning each platelet into a category depending on fluorescent labelling. The four categories included platelets which presented with no fusogenic liposome labelling and no Lifeact-488 delivery (-FL, -LA) (1), platelets which presented with fusogenic labelling and no Lifeact-488 delivery (+FL, -LA) (2), platelets which presented with fusogenic labelling and Lifeact-488 delivery (+FL, +LA) (3), and platelets which presented with no fusogenic labelling and Lifeact-488 delivery (-FL, +LA) (4). Red fluorescence (647 nm) indicates fusogenic liposome labelling, green fluorescence (488 nm) indicates Lifeact-488 labelling (Merged images). The 'cell-counter' plug-in for imageJ was used for all counting analyses, images are illustrative of labelling categories only. Scale bar represents 5 µm.

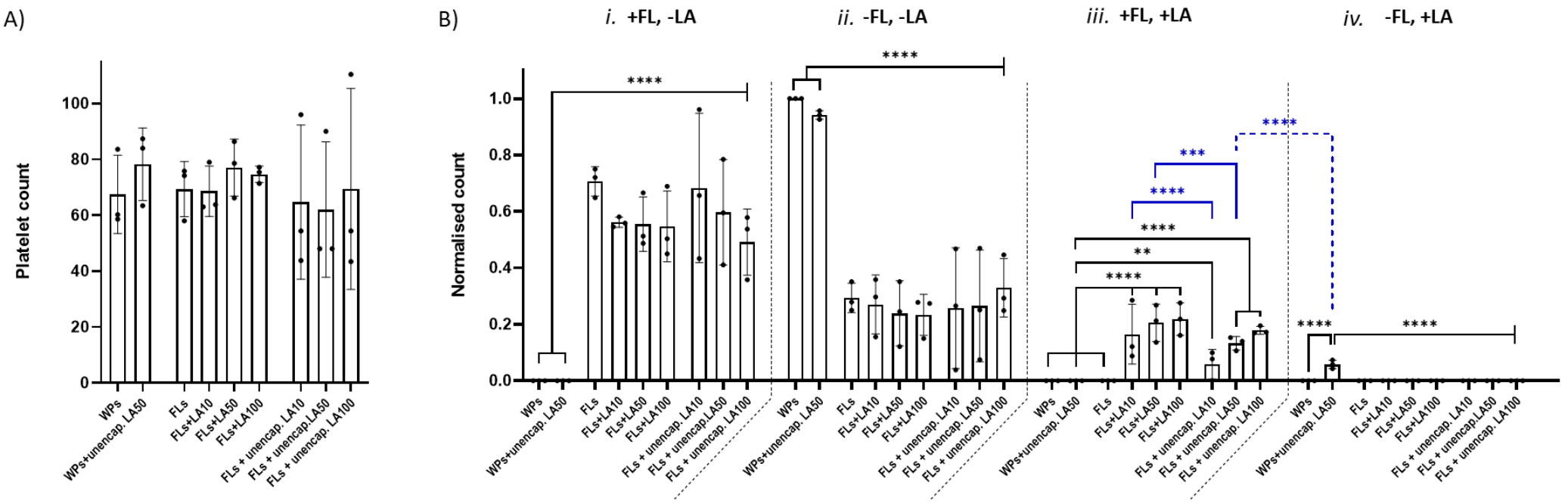

Figure 5.9 Delivery of Lifeact-488 cargo into spread platelets using fusogenic liposomes as a delivery vehicle.

Platelets were spread over a fibrinogen substrate [100 µg/mL] prior to fusion with fusogenic liposomes [5 µg/mL] for 15 minutes. Fusogenic liposomes were resuspended with increasing concentrations of Lifeact-488 [10 µM (FLs+LA10), 50 µM (FLs+LA50) and 100 µM (FLs+LA100)] and added to spread platelets, while fusogenic liposomes resuspended in 20 mM HEPES buffer containing the equivalent unencapsulated concentrations of Lifeact-488 [10 µM (FLs+unencap.LA10), 50 µM (FLs+unencap.LA50), 100 µM (FLs+unencap.LA100)] were also added to spread platelets. Unlabelled controls consisted of a washed platelet control (WPs) and washed platelets containing the unencapsulated 50 µM Lifeact-488 concentration (WPs+unencap.LA50). The total number of platelets in each field of view was quantified (A). Platelets were assigned a category based on fluorescent labelling. The total number of platelets which were fluorescent for fusogenic liposomes only (+FL,-LA) (B*i.*), the total number of platelets which remained unlabelled by either fusogenic liposomes or Lifeact-488 (-FL, -LA) (B*ii.*), the total number of platelets which were fluorescently labelled with both fusogenic liposomes and Lifeact-488 (+FL,+LA) (B*iii*.), and the total number of platelets which were labelled by Lifeact-488 only (-FL, +LA) (B*iv.*). Blue lines (solid & dashed) convey quantitative conclusions regarding Lifeact-488 delivery. Data represents the mean of five fields of view for three biological replicates (n=3) where the mean ± SD was analysed using two-way ANOVA with Bonferroni post-test. P ≤ 0.05. **, P ≤ 0.01. ***, P ≤ 0.001, ****, P ≤ 0.0001.

5.2.8 Antibody delivery into platelets in suspension by fusogenic liposomes is detected intracellularly.

For reasons unknown, Lifeact-488 delivery using fusogenic liposomes was only detected at low levels. Therefore, a different cargo consisting of fluorescently labelled whole antibodies was chosen to determine if antibody cargo delivery could be detected instead. Moreover, if whole antibodies can be delivered into platelets, this opens up the potential to directly investigate cytosolic targets in live platelets. There would also be the opportunity to investigate the Trim-Away method to degrade endogenous proteins at the cellular level in platelets [162]. An unspecific antibody, namely a Goat anti-Mouse IgG conjugated to an Alexa Fluor 488 nm fluorescent tag, was used as a cargo for encapsulation into fusogenic liposomes.

The antibody was firstly dialysed by equilibrium dialysis to buffer exchange the antibody storage solution to PBS. The antibody was then diluted [0.1 mg/mL, 0.25 mg/mL and 0.4 mg/mL] and used to rehydrate the dried lipid film of fusogenic liposomes.

Data was acquired using flow cytometry and representative traces identify the gating strategy used (Figure 5.10). Platelets were identified using forward scattered light (FSC) and side scattered light (SSC), a measure of size and granularity respectively (Figure 5.10*i.*). A washed platelet control served as a negative labelling control, where a 2% gate was used to define a boundary to characterise the percentage of platelet labelling by fusion (Figure 5.10*ii.*). The extent of platelet labelling in the presence of fusogenic liposomes (+FLs) was subsequently the percentage of fluorescence above this 2% boundary (Figure 5.10*iii.*). Platelets positively labelled by +FLs then served as an antibody delivery control, where a 2% gate was used to define a boundary to characterise the percentage of antibody delivery (Figure 5.10*iv.*). Platelets fused with fusogenic liposomes containing antibody cargo (FLs+Ab) were then assessed by fusogenic liposome labelling (Figure 5.10*v.*), and of those positively labelled with fusogenic liposomes were further assessed for antibody delivery (Figure 5.10*vi.*). An additional control consisted of washed platelets fused with fusogenic liposomes with the unencapsulated antibody concentration added in. This also assessed if antibodies were able to penetrate the cell membrane as a result of fusion. Gating was the same as previous, where fusogenic liposome labelling was identified (Figure 5.10*vii.*), and of those positively labelled, were further assessed for antibody delivery (Figure 5.10*viii.*).

Platelets in suspension were labelled efficiently when fused with fusogenic liposomes (+FLs) (92.3 ± 3.2 %) and compared to a washed platelets control consistently gated at 2% (Figure 5.11A*i.*). This also included antibody loaded fusogenic liposomes when antibody

concentrations were used at 0.1 mg/mL (FL+Ab 0.1; 89.9 ± 1.1 %) and 0.25 mg/mL (FL+Ab 0.25) (Figure 5.11A*i.*). However, antibody concentration at 0.4 mg/mL (FL+Ab 0.4) appeared to impact on fusogenic liposome labelling. No statistical analyses were performed for antibody concentrations of 0.25 mg/mL and 0.4 mg/mL due to a lack of biological replicates.

When observing the percentage of platelets positive for the Alexa Flour 488 conjugated antibody (Figure 5.11A*ii.*), platelets labelled with fusogenic liposomes loaded with 0.1 mg/mL antibody (FL+Ab 0.1; 60.5 ± 4.5 %) demonstrated a significant increase in 488 nm positive labelling when compared to platelets labelled with just fusogenic liposomes (FLs; 1.8 ± 0.7 %). Platelets labelled with fusogenic liposomes loaded with 0.1 mg/mL antibody appeared to deliver a greater percentage (60.5 ± 4.5 %) of antibody when compared to fusogenic liposomes containing 0.25 mg/mL antibody and 0.4 mg/mL antibody. However, scientific conclusions could not be made since data for these concentrations consisted of n=1 and n=2 respectively. Therefore, statistical analyses were not performed due to an inadequate number of biological replicates.

Since unencapsulated antibody was not separated from antibody encapsulated in fusogenic liposomes, the same concentration of unencapsulated antibody was added into a sample of both washed platelets and those containing unloaded fusogenic liposomes. This was to identify if the 488 labelled antibody was able to enter or bind to platelets in the absence or presence of fusion. When adding in the equivalent concentration of the unencapsulated antibody directly to washed platelets (WPs; 1.9 ± 0.7 %) and to platelets fused with unloaded fusogenic liposomes (FLs; 3.5 ± 4.0 %), there was no evidence of the secondary antibody being able to bind to platelets in either case (Figure 5.11A*iii.*)

An additional secondary antibody was further used to identify any fluorescent binding directly to the 488 nm labelled antibody. This was to identify if the antibody was absorbing onto the surface of platelets as a result of inefficient encapsulation into fusogenic liposomes. Therefore, a Donkey anti-Goat IgG conjugated to an Alexa Fluor 567 nm fluorescent tag was added to washed platelets (WPs) and platelets which had been labelled with fusogenic liposomes resuspended in the 488 nm labelled antibody (FLs+Ab 0.1). There was no evidence of the secondary antibody being able to bind to platelets in either case (Figure 5.11A*iv.*)

As an alternative approach to support the flow cytometry data, the remaining platelet samples were pelleted, washed and lysed directly into Reducing Sample Treatment Buffer (RSTB) for protein analysis by 12 % SDS-PAGE and western blotting (Figure 5.11B). This was to confirm the potential delivery of antibodies directly into platelets. There were no bands present for washed platelets (WPs), fusogenic liposomes (FLs), and fusogenic

liposomes containing the unencapsulated concentrations of antibody (FLs + unencap.Ab). However, there were visible bands at 50 kDa and 25kDa representing the antibody heavy and light chains respectively, when fusogenic liposomes were loaded with 0.1 mg/mL antibody (FLs+Ab 0.1). This suggests that antibody encapsulated in fusogenic liposomes is being delivered into the platelets. However, it is possible that the fusogenic liposomes are adsorbing to the surface of the platelets without releasing the antibody contents directly into the platelet cytoplasm.

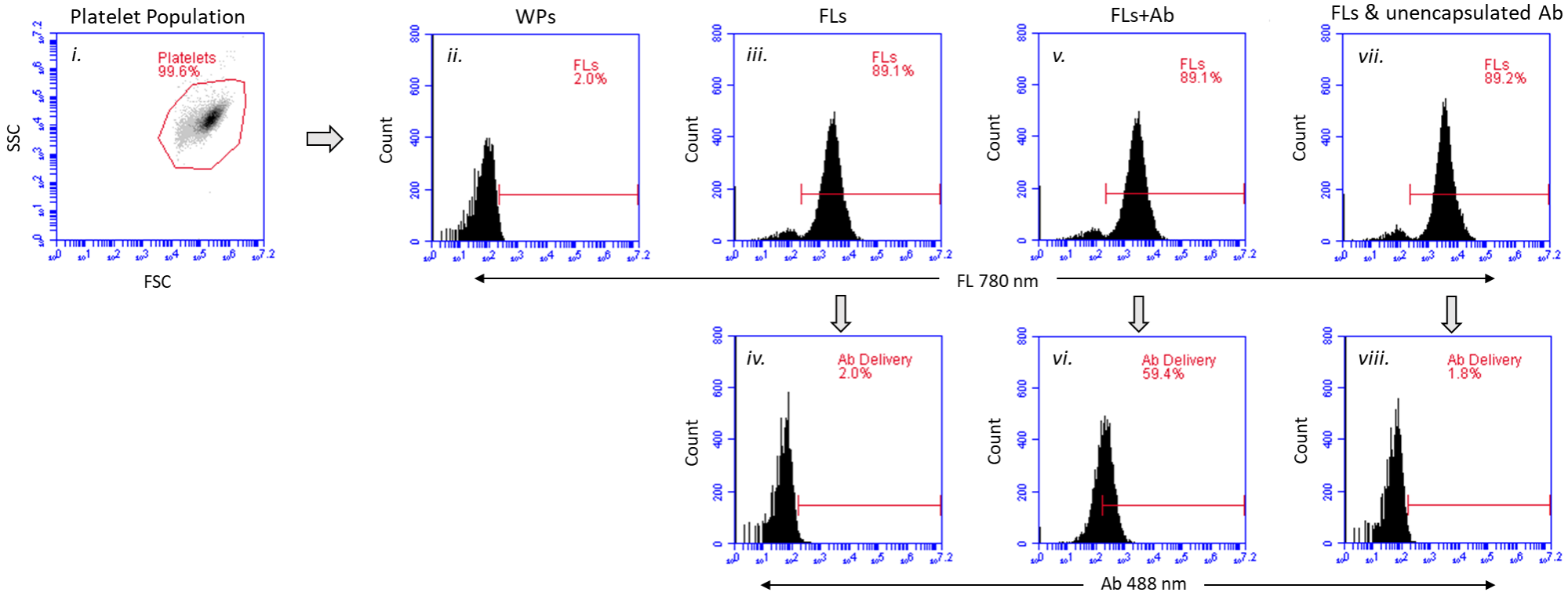

Figure 5.10 Gating strategy of the delivery of antibody cargo into platelets in suspension using fusogenic liposomes.

Fusogenic liposomes loaded with different concentrations of Alexa Fluor 488 conjugated IgG antibody [0.1 mg/mL, 0.25 mg/mL and 0.4 mg/mL] were added directly to platelets in suspension [400 x 10^6 /mL]. Representative flow cytometry traces detail the gating strategy used when assessing the percentage of platelets positive for liposomes and the percentage of platelets positive for the fluorescently labelled antibody.

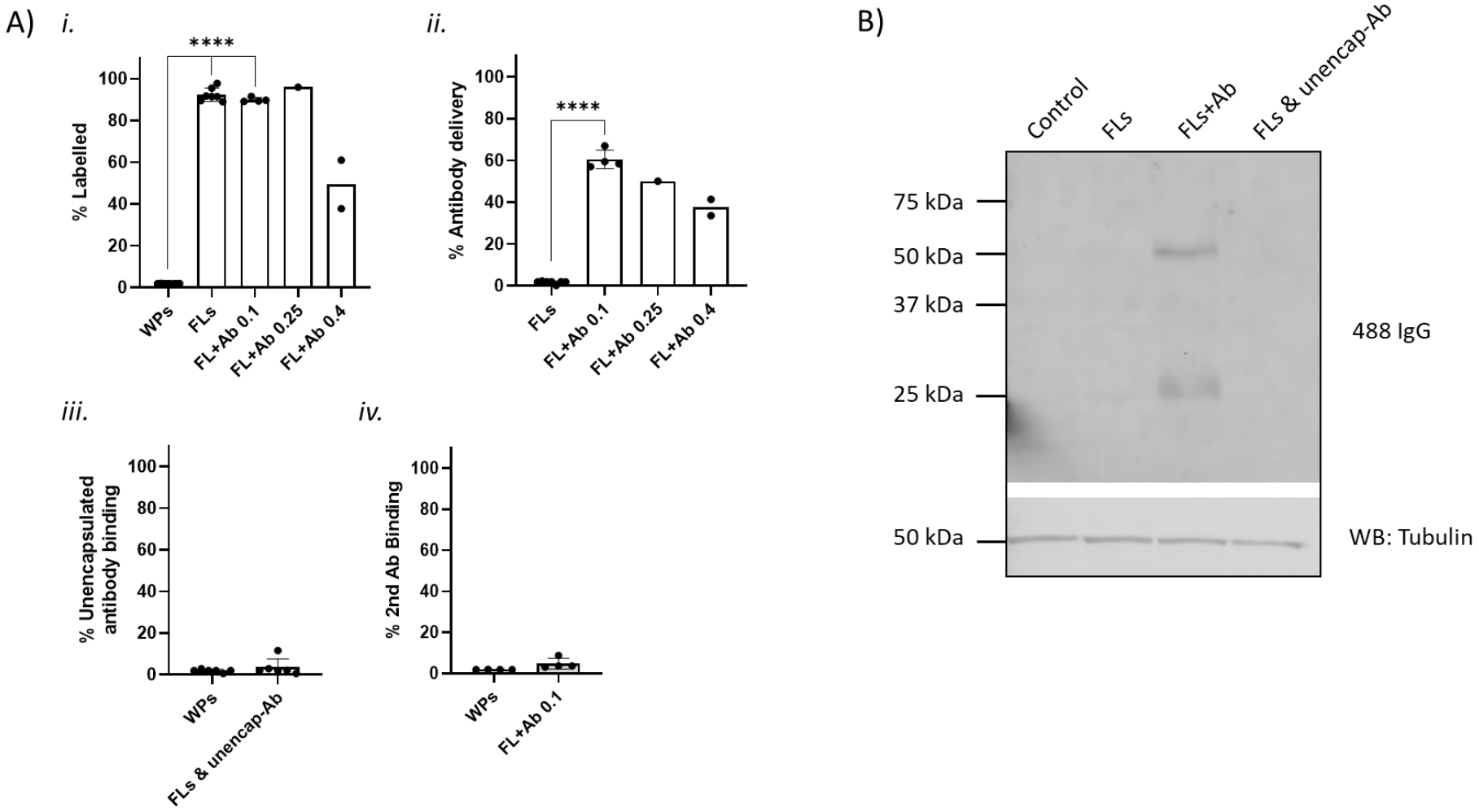

Figure 5.11 Delivery of antibody cargo into platelets in suspension using fusogenic liposomes.

Fusogenic liposomes loaded with different concentrations of 488 conjugated IgG antibody [0.1 mg/mL (FL+Ab 0.1), 0.25 mg/mL (FL+Ab 0.25) and 0.4 mg/mL (FL+Ab 0.4)] were added directly to platelets in suspension [400 x 10^6 /mL]. Flow cytometry data shows the percentage of fusogenic liposome labelling (A*i.*), the percentage of platelets positive for 488 conjugated antibody (A*ii.*), the percentage of unencapsulated 488 conjugated antibody able to bind to platelets in suspension (A*iii.*), and the percentage of unencapsulated 647

conjugated secondary antibody able to bind to platelets in suspension (A*iv.*). Data represents the mean ± SD of seven biological replicates for washed platelets (WPs) and platelets fused with fusogenic liposomes (FLs) (n=7), and four biological replicates for fusogenic liposomes resuspended with 0.1 mg/mL antibody (FL+Ab-0.1) (n=4), was analysed using two-tailed t-test. Data for samples comprising <3 biological replicates were not included in analyses. ****, $P \leq 0.0001$.

Protein samples for washed platelets (control), platelets fused with fusogenic liposomes (FLs), platelets fused with antibody resuspended fusogenic liposomes (FLs+Ab) [0.1 mg/mL], platelets fused with fusogenic liposomes and the concentration of unencapsulated antibody (FLs + unencap-Ab) were analysed under reducing conditions in 12% SDS-PAGE followed by western blot (B). Antibody detection was visualised at 488 nm, tubulin was used as a loading control, and data is representative of one biological replicate (n=1).

5.2.9 Fusogenic liposomes can deliver antibodies into the platelet cytoplasm.

To determine if the antibody resides in the platelet cytoplasm, platelets, incubated with antibody containing fusogenic liposomes, were spread over a fibrinogen surface and confocal microscopy was used to identify cytoplasmic delivery.

Firstly, platelets (400 x 10^6 /mL) were fused with fusogenic liposomes loaded with 0.1 mg/mL Alexa Fluor 488 conjugated Goat anti-Mouse secondary antibody (488 nm) as previously described prior to spreading over a fibrinogen substrate [100 µg/mL] (Figure 5.12). Washed platelets (WPs) represented a negative control to show that there was no background fluorescence detected by the bandpass filters set up to detect fusogenic liposome fluorescence (647 nm) or antibody fluorescence (488 nm) (Figure 5.12A*i.*). Platelets fused with fusogenic liposomes identify the successful labelling of platelets which had been fused prior to spreading (Figure 5.12A*ii.*). Platelets which had been fused with antibody loaded fusogenic liposomes reveal some successful fusion and antibody delivery, however, although the antibody can be detected in platelets, the antibody is not dispersed within the platelet cytoplasm and the fusogenic liposomes, for reasons unknown, did not appear to fuse efficiently with the platelet membrane of all platelets (Figure 5.12A*iii.*). This suggests that antibody cargo may hamper successful fusion preventing direct release of the antibody. However, from previous data, platelets are positively labelled by fusogenic liposomes resuspended in antibody when observing flow cytometry data, and western blot data reveals antibody presence in lysed platelets and may suggest that fusogenic liposomes are either adsorbing or undergoing hemifusion with the platelet membrane. For example, a fusogenic liposome may fuse with the outer lipid bilayer of the platelet, but a full fusion may be compromised, and therefore rendering the antibody cargo trapped within the lumen of the fusogenic liposomes. Techniques such as electron microscopy may reveal more information regarding what is impacting on antibody cargo delivery.

Similar to previous analyses when fluorescently labelled Lifeact-488 was delivered into spread platelets, fusogenic liposomes and fusogenic liposomes loaded with fluorescently labelled antibody were added directly to platelets (1 x 10^7 /mL) which had already been spread over a fibrinogen substrate (Figure 5.13). This was to identify if antibody delivery was successful when there was more platelet surface area available for fusion and subsequent cargo delivery.

Washed platelets (WPs) served as a negative control (Figure 5.13*i*.). In this instance, the unencapsulated concentration of antibody was also added into spread washed platelets prior

to imaging (Figure 5.13*ii*.). This provided evidence that unencapsulated antibody cannot permeate the membrane of spread platelets.

Fusogenic liposomes were fused with spread platelets and the diffusion of the DiR tracer (647 nm) is representative of successful fusion (Figure 5.13*iii.*). The concentration of the unencapsulated antibody was also added into the fusogenic liposomes prior to fusion with the platelets (Figure 5.13*iv.*). This was to identify if unencapsulated antibody could bind to the fusogenic liposomes or enter the platelets as an indirect result of fusion. Although some fluorescence (488 nm) was detected, this was markedly reduced when compared to fusogenic liposomes loaded with the fluorescently labelled antibody which showed delivery of antibody directly into the cytoplasm of spread platelets (Figure 5.13*v.*). Three out of the four platelets in the field of view successfully fused with fusogenic liposomes (647 nm) and also demonstrated intracellular fluorescence detected at 488 nm, revealing successful delivery of whole antibody by fusogenic liposomes.

Delivery of cargo directly into platelets which were already spread prior to fusion presents with the same caveat as before; where the fusogenic liposome concentration to platelet ratio is much higher, and there is greater surface area for fusogenic liposome fusion to occur. However, the successful delivery in spread platelets is proof of principle that cargo can be delivered into human platelets. While further investigation will be required to investigate the impact of adsorption or hemifusion on fusogenic liposome labelling and cargo delivery directly into platelets in suspension.

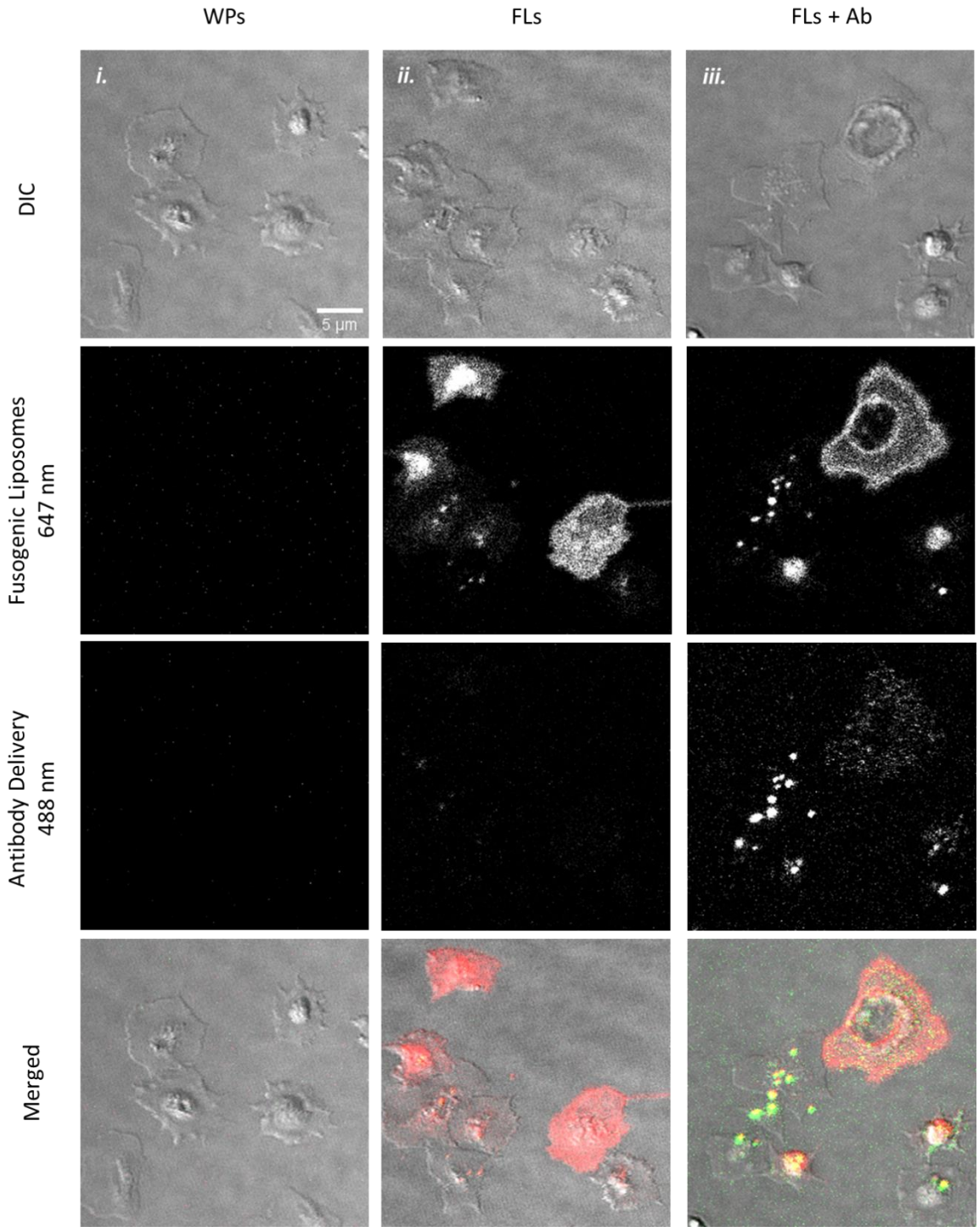

Figure 5.12 Delivery of antibody cargo by fusogenic liposomes into platelets in suspension.

Platelets in suspension (400 x 10^7 /mL) were fused with fusogenic liposomes (FLs) (*ii*) and fusogenic liposomes loaded with antibody (FLs+Ab) [0.1 mg/mL] (*iii*) and compared to a washed platelet control (WPs) (*i*) to observe antibody delivery at 488 nm. Images are representative of two biological replicates (n = 2). Red fluorescence (647 nm) indicates fusogenic liposome labelling, green fluorescence (488 nm) indicates Lifeact-488 labelling (Merged images). All images were captured at the same laser intensity and exposure settings, contrast and brightness were enhanced for display purposes. Scale bar represents 5 µm.

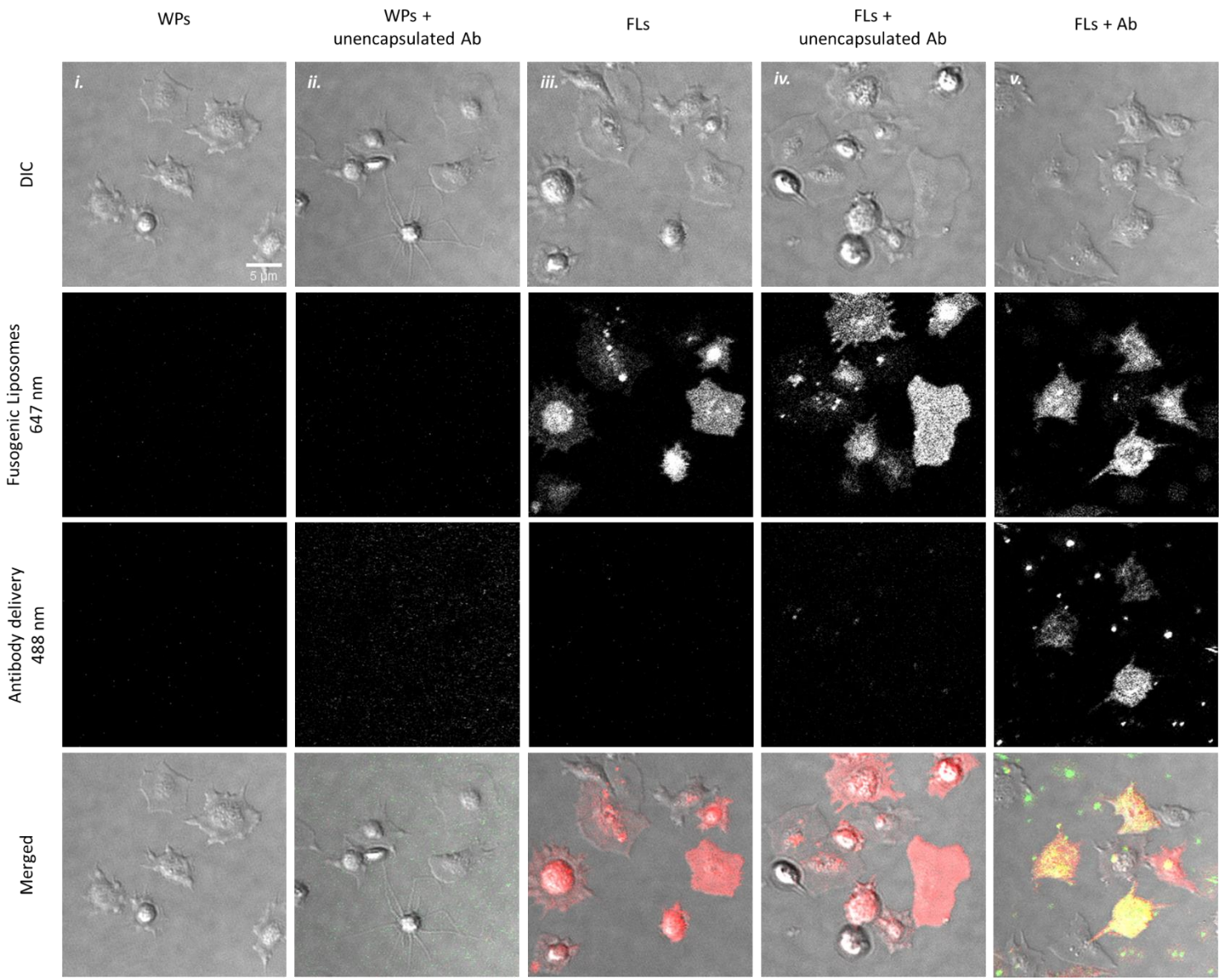

Figure 5.13 Delivery of antibody cargo by fusogenic liposomes into spread platelets.

Platelets (1 x 10^7 /mL) were spread over a fibrinogen substrate [100 µg/mL] and either remained untreated as a washed platelet control (WPs) (*i*), fused with fusogenic liposomes (FLs) (*iii*) or fused with fusogenic liposomes pre-loaded with antibody (FLs+Ab) (*v*). Since unencapsulated

antibody was not separated from fusogenic liposomes, the binding ability of the unencapsulated concentration of antibody was assessed in the presence of both washed platelets (WPs + unencapsulated Ab) (*ii*) and during the fusion of unloaded fusogenic liposomes (FLs + unencapsulated Ab) (*iv*). Images are representative of two biological replicates (n = 2). Red fluorescence (647 nm) indicates fusogenic liposome labelling, green fluorescence (488 nm) indicates Lifeact-488 labelling (Merged images). All images were captured at the same laser intensity and exposure settings, contrast and brightness were enhanced for display purposes. Scale bar represents 5 μm.

5.2.10 Characterisation of fusogenic liposomes by flow cytometry identifies successful cargo encapsulation.

Fusogenic liposomes resuspended using fluorescently labelled antibody were further quantified by flow cytometry to determine the percentage of fusogenic liposomes which were also positive for antibody. Firstly, the threshold of the flow cytometer was adjusted to 1000 to enable extruded fusogenic liposomes measuring approximately 100 nm to be acquired.

Representative flow cytometry traces detail a background control consisting of 20 mM HEPES buffer which was acquired in order to capture background noise as a result of the decreased threshold and subsequent increase in debris (Figure 5.14A*i.*). Fusogenic liposomes in the absence of cargo were also acquired which identified a clear positive population of fusogenic liposomes which were fluorescent at 670 nm due to the DiR tracer (Figure 5.14A*ii.*). Finally, fusogenic liposomes which had been loaded with Alexa Fluor conjugated antibody (Goat anti-mouse 488 nm, [0.1mg/mL]) demonstrated a double positive population where fluorescence is detected at 670 nm as a result of the DiR tracer, and also by 488 nm as a result of antibody fluorescence (Figure 5.14A*iii*.).

Data was quantified for three independent fusogenic liposome preparations (Figure 5.14B). When compared to the HEPES background control (3.5 ± 4.3 %), the percentage of fluorescence at 670 nm as a result of fusogenic liposome (FLs 670 nm; 87.5 ± 10.6 %) and cargo containing fusogenic liposome (FL+Ab 670nm; 87.5 ± 8.5 %) detection was significantly increased. Identifying minimal interference from background fluorescence, and confirming fluorescent detection is a result of fluorochromes being measured.

Furthermore, of the cargo containing fusogenic liposomes which were identified as positive for the DiR lipid tracer (FL+Ab 670 nm), 60.4 ± 12.1 % of these fusogenic liposomes also fluoresced green indicative for antibody cargo detection (Figure 5.14B, green bar). This encapsulation efficiency was high when compared to encapsulation efficiencies reported in the literature, which ranged from 1.2 - 50 % when using a dried lipid film to encapsulate a cargo [121,155,286,287]. Although this appears strong evidence for the encapsulation of antibody into the lumen of fusogenic liposomes, it is impossible to tell from this data alone if this is solely due to antibody encapsulation. It is typically considered that hydrophilic molecules are contained within the lumen, while hydrophobic molecules are contained in the lipid bilayer upon reconstitution [287,288]. It may, therefore, be possible that antibodies could also become contained within the lipid bilayer depending on the hydrophobic properties of the antibody.

Proteins, such as antibodies, are known to transition between their folded and partially-folded structures presenting different hydrophobic interactions between conformations, while a partially-folded conformation can also contribute to antibody aggregation [289]. Although

antibodies were centrifuged prior to dilution and resuspension with fusogenic liposomes, antibody aggregation may also impair encapsulation. Techniques such as cryo-electron microscopy (cryo-EM) may be utilised here to provide a more detailed investigation to determine if antibody cargo is being encapsulated in the lumen of fusogenic liposomes, the phospholipid bilayer, or not at all [290]. Unfortunately, other standard microscopy techniques do not have low enough resolution to provide detailed information regarding the structure of the bilayer, or the contents of the lumen, of fusogenic liposomes [291].

Overall, this data suggests that at least some cargo encapsulation into the lumen of fusogenic liposomes is possible. However, there is a possibility that encapsulated cargo may not be concentrated enough to detect a biological or fluorescent effect. How much antibody is encapsulated, and how much may be delivered, is unknown. Techniques such as High-Performance Liquid Chromatography (HPLC) may provide an insight into intracellular delivery concentrations since approximately 0.5-1 mg/mL is estimated for antibody mediated protein degradation (Trim-Away) [162]. However, for single molecule tracking approaches, less labelled Fab fragments (~50 kDa) would need to be delivered.

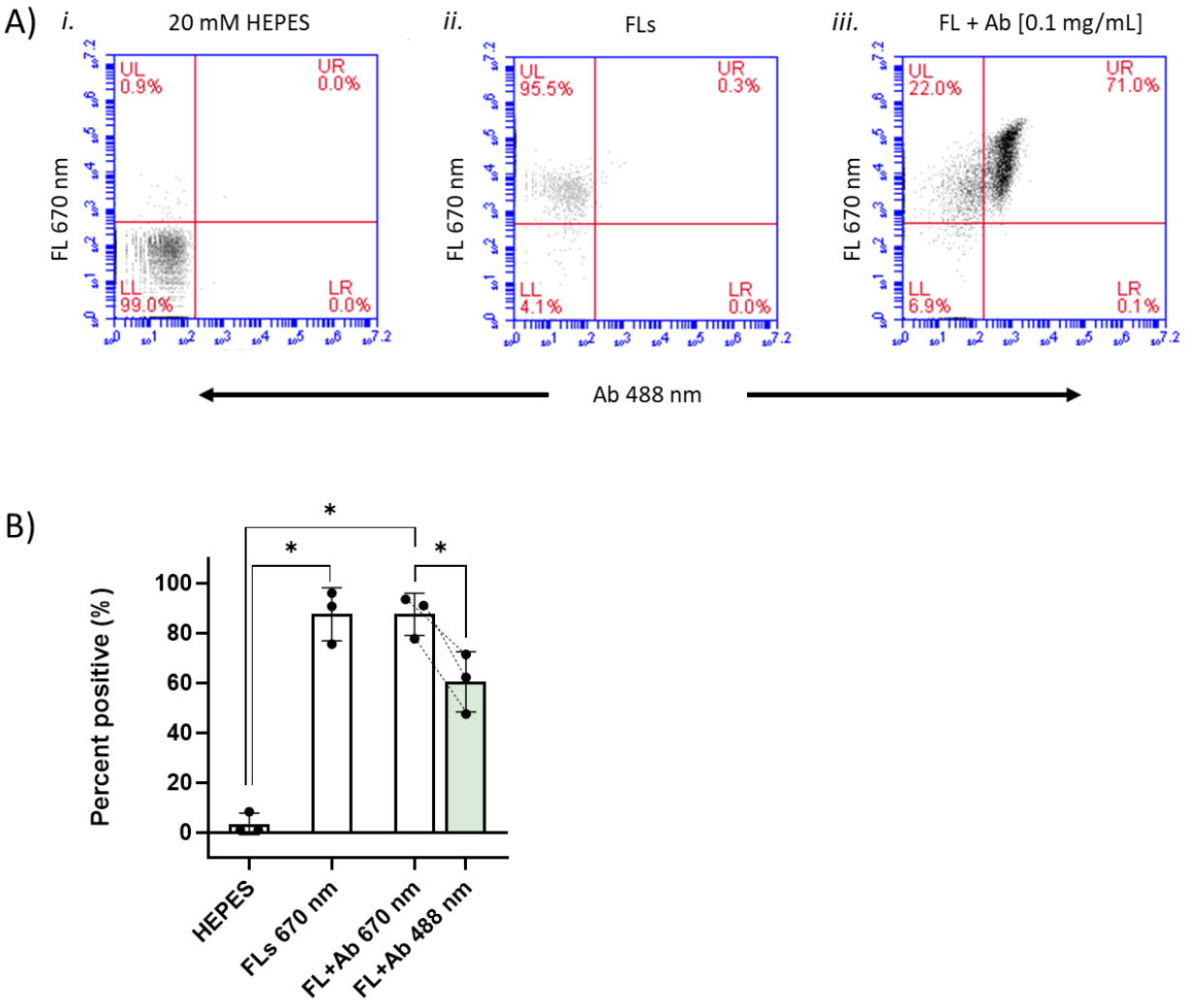

Figure 5.14 Quantification of liposomal encapsulation of whole antibody.

Fusogenic liposomes were acquired using flow cytometry by diluting 1:2 with 20mM HEPES buffer. The threshold of detection was reduced to 1000. Representative flow cytometry traces for 20 mM HEPES buffer (A *i.*), fusogenic liposomes (FLs) (A *ii.*), and fusogenic liposomes loaded with a secondary antibody (FL+Ab, [0.1 mg/mL]) (A *iii.*) identify the percentage of fusogenic liposomes which were either unlabelled (LL quadrants), positively labelled for fusogenic liposomes (UL quadrants), or double positively labelled for fusogenic liposomes and 488 conjugated antibody detection (UR quadrants). Data for percent positivity was quantified and represents the mean ± SD of three independent liposome preparations for both FLs and FL+Ab (n=3) (B). The dashed line indicates the percentage of antibody fluorescence detected according to the matched liposome preparation for FL+Ab (B). Statistics were performed using one-way ANOVA with Bonferroni post-test. *, $P < 0.05$. **, $P \leq 0.01$.

5.3 Discussion

This chapter has identified that in-house fusogenic liposomes are similar in size and zeta potential when comparing between sonication and extrusion methods of liposome preparation. The extrusion method provides more uniform fusogenic liposomes as well as a decrease in PDI score, suggestive of a more stable suspension when compared to liposomes prepared using the sonication method. It has been shown that in-house fusogenic liposomes prepared using extrusion can successfully fuse with the cell membrane of platelets both in suspension and when spread over a biologically relevant substrate within minutes, and is detectable by diffusion of the DiR tracer through the platelet membrane. This provides a method for fast and biocompatible labelling of platelets in suspension and has potential applications to aid platelet research.

For example, the fluorescent labelling of platelets is important for techniques such as microfluidic systems and intravital microscopy. *In vitro* microfluidic devices and flow-based systems are regularly used to assess how platelets adhere together or interact with other cells when added to anticoagulated whole blood [255,256], and intravital microscopy is a technique used to investigate models of thrombosis since cells can interact within their native environment [257]. Despite these systems allowing multiple biological processes to be investigated simultaneously, the labelling of platelets for direct use in these systems often require an addition of antibodies conjugated to a fluorescent fluorophore (microfluidic devices), an injection of antibodies conjugated to a fluorescent fluorophore (intravital microscopy) [258], or genetically altered models containing platelet-specific fluorescent protein expression (intravital microscopy) [259]. However, these approaches are not always suited to live imaging of platelets, for example the labelling of platelets with antibodies or probes may interfere with receptor function which could directly impact on thrombus formation [260], and some reports suggest that genetic based approaches may disrupt normal cellular processes [261].

The labelling of platelets with fluorescently labelled fusogenic liposomes may, therefore, offer an alternative and cost-effective method to some of the current limitations associated with antibody labelling using these systems. Although there would be a requirement for prior isolation and labelling of platelets with fusogenic liposomes before reintroducing those labelled platelets back into the system, there is potential to avoid interferences with receptor function since fusogenic liposomes would label the platelet membrane.

The delivery of cargo directly into the cytoplasm of platelets by fusion with fusogenic liposomes, either in suspension or when spread, however, remains to be explored further. Although there was delivery of both Lifeact and antibody into spread platelets, fluorescently labelled Lifeact did not resemble the actin stress filaments typically seen in spread and

spreading platelets. While antibody delivery was more uniform when antibody loaded fusogenic liposomes were fused with spread platelets as opposed to platelets in suspension. This can be explained in part by the increase in the ratio of fusogenic liposomes to spread platelets when compared to platelets in suspension. However, it remains unclear why cargo is not being delivered uniformly into platelets in suspension and may suggest that fusion is impaired by the structure of the resting platelet.

Structures such as the open canalicular system (OCS) and the glycocalyx of resting platelets may impact liposome fusion. The (OCS) is an internal and open membrane structure that is found in platelets, and occupies 3-4% of the total platelet volume [292]. The glycocalyx, found on all cells in the body, is a monosaccharide-rich layer which has been described as a thicker layer in platelets when compared to other cells [293]. It could be possible that cargo delivery by fusogenic liposomes may be impaired by the OCS or the glycocalyx. Electron microscopy may elucidate if either of the above may be impacting on the ability of fusogenic liposomes to deliver cargo, or indeed, to what extent fusion or hemifusion may be occurring since the DiR tracer is able to diffuse through the phospholipid bilayer of platelets in suspension.

In addition, alterations to the lipid composition may improve fusogenicity, stabilise lipid fluidity or improve cargo encapsulation. There may also be further opportunity to explore the encapsulation efficiency of different cargo, and if different encapsulation methods are more suited to cargo which have different physiochemical properties. A Zetasizer could be employed to provide physical characteristics regarding size, surface charge and PDI to determine if cargo encapsulation changes the chemical and physical properties of the fusogenic liposomes when compared to unloaded fusogenic liposomes.

Additionally, ligand-targeted approaches may offer more control over the binding site of fusogenic liposomes with platelets. For example, incorporating a peptide sequence into the lipid film of fusogenic liposomes to specifically interact with a platelet cell surface ligand maybe improve the consistency of fusion and increase cargo delivery by ligand interactions as well as membrane instabilities. Although, a caveat of this approach may trigger signalling cascades prior to cargo delivery which may disguise biological effects.

Nevertheless, the data concerning antibody delivery in this chapter has shown potential, and further investigation using electron microscopy may elucidate the nature of the current obstacles regarding direct delivery into platelets in suspension.

6. General discussion

6.1 Summary of results

This thesis firstly implements and validates an automated analysis method to quantify platelet metrics from unlabelled images captured by DIC microscopy using a CNN. This analysis method abrogates bias associated with manual analyses when compared to 5 manual annotators. The CNN successfully depicted extremes in platelet morphology when investigating inhibitors or agonist known to impact on platelet morphology, as well as successfully quantifying the spread area of mouse platelets. This method has the potential to standardise human and mouse platelet spreading analyses of unlabelled platelets across platelet laboratories where current analysis mainly consists of manually annotating the perimeter of each platelet in each field of view. The automated CNN therefore offers a superior and accessible way to quantify unlabelled platelets by DIC microscopy, requiring a minimal amount of new training material, and little prior computational knowledge.

Secondly, fusogenic liposomes containing a fluorescent probe can fuse with the platelet membrane without causing significant increases to platelet activation, without inducing PS exposure to the outer phospholipid bilayer of the platelet membrane, or impacting on the ability of platelets to spread normally. Therefore, providing a biocompatible, non-toxic and stable method of labelling ≥80% isolated platelets that have the potential to be introduced into microfluidic and intravital systems where fluorescently labelled antibodies may impact on receptor interactions or signalling pathways. This approach offers an alternative way to label platelets when investigating platelet migration, interactions with other cells, and interactions with the endothelium.

Finally, fusogenic liposomes can be manufactured in-house using commercially available lipids and fluorescently labelled lipid analogues which can successfully label the cell membrane of platelets and does not induce platelet activation, PS exposure or anomalies to platelet spreading. The delivery of fluorescently labelled Lifeact by fusion with spread platelets, however, was inconclusive such that actin filaments were not comparable to structures identified in the literature. Suggesting, for reasons unknown, that encapsulation efficiency was low. This may be a result of Lifeact residing in the lipid bilayer as opposed to the lumen of fusogenic liposomes, meaning that cargo release into the cytoplasm may be prevented. Furthermore, it was identified that unencapsulated Lifeact was able to permeate the platelet membrane after being added into preformed fusogenic liposomes resuspended in HEPES buffer. This may suggest that weaknesses are caused directly to the platelet membrane after fusion, or that small peptides may be able to pass through the unsaturated formulation of the fusogenic liposomes used during this project. Future experimentation when assessing the delivery of cargo directly into platelets should include a step to remove unencapsulated cargo from the fusogenic liposome preparation prior to fusion. Despite this,

non-specific antibody delivery directly into the cytoplasm of spread platelets using fusogenic liposomes as a delivery vehicle showed more potential, demonstrating successful delivery. For reasons unknown, qualitatively, this was not comparable to platelets in suspension, suggesting that full fusion may be impeded by the resting structure of platelets.

Therefore, the implementation of techniques such as electron microscopy should be employed to i) investigate if cargo resides in the lumen of fusogenic liposomes or the bilayer, and ii), investigate to what extent fusogenic liposomes may fuse with the cell membrane of platelets to identify if full fusion, hemifusion, or no fusion is occurring. Furthermore, techniques such as a spectrofluorometer, where emitted light is detected by photodiodes or photomultiplier tubes, may be able to provide insight on whether small peptides such as fluorescently labelled Lifeact can diffuse through the phospholipid bilayer of the fusogenic liposomes. Although this would first require the removal of unencapsulated cargo to provide a baseline fluorescence representative of 0% release, while maximum fluorescence could be achieved by lysis of fusogenic liposomes using a detergent [294].

6.2 Platelet features which may impact fusion of fusogenic liposomes.

6.2.1 Membrane systems present in platelets.

Platelets contain an open canalicular system (OCS) and a dense tubular system (DTS). Olav Behnke (1967) first described the existence of these two distinct membrane systems in rat platelets when using transmission electron microscopy [295]. These two membrane systems differ in the sense that the OCS is continuous with the plasma membrane, whereas the DTS is not [292].

The OCS system has been described as a network of interconnected channels where its membrane composition is identical to that of the platelet membrane [292]. The works of James White further identified a dual role of the OCS which includes the trafficking of molecules into platelets and the secretion of molecules out of platelets by α-granule release [296,297]. In particular, the uptake of gold labelled fibrinogen was localised to the OCS and swollen α-granules after thrombin stimulation, while endogenous fibrinogen was localised to α-granules during rested conditions and the OCS after thrombin stimulation [296,297]. Allowing researchers to conclude that the OCS is a common pathway for both the uptake and secretion of molecules simultaneously [296,297].

It was also demonstrated that the OCS acts as a membrane reserve during platelet spreading, where the eversion of membrane leads to a time dependent decrease in gold labelled fibrinogen located in the OCS [298]. Moreover, the lack of an OCS in bovine platelets,

where filopodia extensions are identified during spreading but not lamellipodia, has led researchers to hypothesise that this could be due to an absence of membrane reserve [299].

On the other hand, the DTS has been described as a derivative of the Golgi apparatus or residual endoplasmic reticulum from the megakaryocyte, whose membrane differs from that of the platelet membrane such that it's appearance has been described as a reticular membrane system [300,301]. The DTS functions to regulate platelet activation by actively sequestering calcium which, upon platelet activation, is rapidly discharged to raise cytoplasmic calcium levels [300,302].

It is therefore possible that fusogenic liposomes could be entering either the OCS or the DTS, with the OCS being more plausible since there is prior evidence of molecule transportation in this system. If this is the case, fusogenic liposomes may become entrapped by either adsorption or hemifusion with the internal membrane, or the fusogenic characteristics may become altered such that fusogenicity of the fusogenic liposomes is directly impacted. However, given that lateral diffusion of the DiR tracer is occurring in the platelet membrane, it is indicative that fusion to some capacity is occurring.

If single or multiple instances of hemifusion are occurring as opposed to full fusion, this could render the cargo trapped within the lumen of fusogenic liposomes and therefore, undeliverable to the platelet cytoplasm. However, hemifusion would still allow for the lateral diffusion of the DiR tracer from the external phospholipid bilayer of fusogenic liposomes through the external phospholipid bilayer of the platelet cell membrane. This may explain the reason for uniformly labelled platelets when investigating the level of labelling by fusion using fluorescence microscopy.

Conversely, fibrinogen is a molecule which has been identified as being transported via the OCS, and reported dimensions of one rod-shaped fibrinogen molecule is 46 nm in length [303]. It is therefore believed that fibrinogen can freely enter and pass through channels and branches of the OCS that serve to connect the entire platelet cell surface [292]. Moreover plasma membrane invaginations making up the OCS were identified as 20 – 30 nm wide when investigated using electron microscopy (EM) tomography [301]. The average size of the fusogenic liposomes (100 nm) is much larger when compared to the rod-like structure of fibrinogen and the openings to the OCS, and so it remains unlikely that fusogenic liposomes are entering and becoming entrapped, or resulting in hemifusion, within the OSC system. However, techniques such as electron microscopy may provide a better insight into the extent of fusion and labelling of platelets by fusogenic liposomes.

Despite the obstacles in cargo delivery when platelets are in suspension, antibody delivery appeared markedly improved when fusing antibody loaded fusogenic liposomes to platelets which had already been spread over a fibrinogen substrate. This is likely a result of the

increased surface area of the platelet when compared to platelets in suspension. Yet suggests that the fusion of fusogenic liposomes to the cell membrane of platelets is possible, and the mechanism by which fusion occurs can lead to successful fusion and cargo delivery when detected by fluorescent microscopy.

6.2.2 Platelet coating

Another potential influence where the fusion of fusogenic liposomes with platelets may be impacted is by a monosaccharide-rich layer, called a glycocalyx, which coats the membrane of platelets. In fact, all cells in the body are coated by a glycocalyx layer [304], however it has been suggested that the platelet glycocalyx is thicker than the glycocalyx which coats other cells in the body [293]. Monosaccharides such as glucose, mannose and galactose, are typically tethered to each other, to proteins or to lipids in the form of glycans, glycoproteins, proteoglycans, or glycolipids [304]. In recent years, the glycocalyx has been associated with both stabilising and protective functions. For example, the endothelial glycocalyx has been associated with a diverse range of functions including maintaining vascular integrity, supporting the production of NO, and the interaction of plasma proteins and cells [305].

Additionally, the endothelial glycocalyx has also been implemented in impairing nanoparticle uptake [306]. It was found that nanoparticle (50 nm) uptake was significantly increased in Human umbilical vein endothelial cells (HUVECs) after enzymatic degradation of the glycocalyx [306]. It could therefore be hypothesised that the glycocalyx may impact on fusion when platelets are in suspension and rested due to an intact glycocalyx. Yet, upon spreading of platelets over an immobilised ligand the glycocalyx may become dispersed, allowing successful fusion to occur. Enzymatic degradation of the platelet glycocalyx may, therefore, be important to explore. However, the use of enzyme degradation would first need to be investigated to ensure that this did not impact on platelet viability, platelet function or overall negative charge of the platelet.

In contrast, published literature describes the successful fusion and successful delivery of fluorescently labelled protein cargo directly into CHO cells using the same formulation of fusogenic liposomes used in this project [121]. However, animal cells also have a glycocalyx coating [307]. Yet, the glycocalyx has been identified to differ between species, including differences to the glycocalyx in different inter-vascular regions of the same species [308]. Therefore, the exploration of the platelet glycocalyx may be an area to investigate in the future using specialised microscopy techniques.

The depth of the glycocalyx can range from 10 – 100 nm, meaning conventional optical microscopy will not provide detailed insights into the fusion process. However, a method to investigate if the platelet glycocalyx impacts the fusion of fusogenic liposomes may include

super-resolution microscopy where nanoscale resolutions of 10 – 20 nm can be reached [309,310] and may show disruption, or gaps, to the glycocalyx in the event of successful fusion. Other methods would also include electron microscopy to identify if successful fusion is present.

6.3 Potential changes to the formulation of in-house fusogenic liposomes

There are several areas which could be investigated in regard to in-house fusogenic liposomes and the optimisation of fusogenicity and cargo delivery directly into the cytoplasm of platelets.

6.3.1 Different formulation of lipids

Positively charged liposomes, such as DOTAP, have regularly been applied to cell biology since the discovery of lipofection techniques where liposome/DNA complexes can successfully deliver plasmid DNA to kidney cells [311]. Negatively charged DNA and positively charged cationic lipids can form complexes such that they mimic natural viruses, acting as synthetic carriers to deliver extracellular DNA across cell and nuclear membranes [312]. Elucidation of the cellular uptake mechanisms, namely endocytosis, prompted researchers to improve transfection efficiencies by investigating the composition of liposomes [271].

It was found that the early stages of transfection are structure dependent, where the addition of a neutral helper lipid (DOPE) converted liposome complexes from a multilamellar structure (L_α) to a columnar inverted hexagonal (H_{II}) liquid-crystalline state, which improved transfection [312]. Other neutral lipids, such as dioleoyl phosphatidylcholine (DOPC), which form multilamellar (L_α) liposome complexes do not induce efficient transfection [312].

It was further demonstrated by Csiszer et al (2010) that the addition of an aromatic molecule to an equimolar mixture of DOPE and DOTAP converted the uptake of liposomes to direct fusion with the plasma membrane as opposed to an endocytic uptake method [151]. Furthermore, Kolašinac et al (2018) extensively investigated the relative importance of different lipid components for successful fusion [271]. In agreement with Csiszar et al (2010), Kolašinac et al (2018) also concluded that the addition of an aromatic molecule improves fusion. A correlation between the fusion ability of liposomes and a positive zeta potential suggested that liposome surface charge is also an important factor for fusion to occur [271]. A high zeta potential is also indicative of a highly stable colloidal system where particles remain suspended in equilibrium in a suspension.

Since lipid shape was also known to be an important factor to support fusion, cationic lipids consisting of a conical shape (where the tail group occupies more area than the head group, and vice versa) were found to fuse with the cell membrane with >90% efficiency when compared to lipids consisting a cylindrical shape (where the cross-sectional area is similar between the head group and tail group) which only supported fusion by ~30% [271]. Supporting earlier findings that lipid geometry producing a spontaneous curvature to bilayers are a necessary criterion to support fusion [271]. Although the presence of a neutral lipid (DOPE) was not found to be mandatory for membrane fusion to occur, the influence of neutral lipid containing a small head group was found to impact on fusion. Liposomes containing a neutral lipid which contained ceramide and demonstrated a small head group, N-oleoyl-D-erythro-sphingosine ceramide, fused extremely effectively such that liposomal concentrations were reduced to avoid toxicity [271]. This may, in part, also contribute to the spontaneous curvature required to induce successful fusion.

Kolašinac et al (2018) also investigated three different fluorophores where the chromophore resided at different locations, and all three lipids were able to induce fusion with the cell membrane when used at concentrations above 2.5 mol % (1/1/0.05 mol/mol) [271]. Although the exact mechanisms remain to be elucidated, it is thought that the inclusion of a lipid containing a fluorophore initiates membrane instabilities allowing fusion to occur [151,271].

Therefore, given the evidence in the literature that an aromatic molecule and a cationic lipid with a conical shape are essential for efficient fusion, and that a neutral lipid can be used to control efficiency, there is scope to investigate changes to the lipid formulation used in this project to identify if this impacts on fusion. Namely, an increase to the ratio of the aromatic lipid may impact fusogenicity since Kolašinac et al (2018) demonstrated that the signal intensity of successful fusion increased linearly with increasing aromatic lipid concentrations [271]. Additionally, it would be interesting to investigate if a neutral lipid containing a smaller headgroup, such as N-oleoyl-D-erythro-sphingosine ceramide, was able to improve fusion by adjusting lipid geometry such that cargo delivery could be delivered to the platelet cytoplasm.

6.3.2 Lipid fluidity

Another aspect of lipid formulation which may be beneficial to explore is that of lipid fluidity. Much like the arrangement of fusogenic liposome lipids used in this project, the lipids of the cell membrane arrange themselves where hydrophobic fatty acid tails are orientated inwards, while the polar headgroups are orientated outwards in contact with the aqueous environment. Complementary molecular shapes of the lipids which make up these membranes are essential to maintain the permeability barrier [313]. It could, therefore, be

hypothesised that this may be similar when considering the permeability of fusogenic liposomes since it is known that unsaturated phospholipids provide bilayer structures with increased permeability and low stability when compared to saturated phospholipids [314].

This is a result of double bonds present in the hydrocarbon chain of phospholipids which causes a bend. This disruption to the unsaturated lipid tails creates space between adjacent lipid tails and reduces phospholipid packing. However, although increasing the saturated lipid content may decrease lipid permeability by alternating the packing of the hydrocarbon chains, this would increase the phase transition temperature [315]. That is, the temperature required to cause a change from the ordered gel phase, where the hydrocarbon chains are closely packed, to a disordered liquid phase, where hydrocarbon chains are fluid [316]. Temperatures which fall above the transition temperature of the lipid allow multilamellar liposomes to be formed [287]. The phase transition temperatures for DOPE and DOTAP are approximately -16 ^{o}C and -11.9 ^{o}C respectively [315], and although DOPE and DOTAP are regularly used in fusogenic liposomes formulations, it may be hypothesised that temperatures in excess of their phase transition temperatures may therefore contribute to decreased permeability, especially for small peptides such as Lifeact. In contrast, the phase transition of their saturated equivalents, namely 1,2-distearoyl-sn-glycero-3-phosphoethanolamine (DSPE) and 1,2-stearoyl-3-trimethylammonium-propane (DSTAP), is 74 ^{o}C and 53 ^{o}C respectively [315]. Temperature transition, therefore, may be an avenue to explore when investigating encapsulation of cargo.

Likewise, cholesterol has been used in the formulation of liposomes to prevent liposome aggregation and improve the stability of the liposomal membranes [314]. Cholesterol is well known as a structural lipid of the cell membrane of mammalian cells [317]. It is a 27-carbon molecule containing a hydroxyl group, which can form hydrogen bonds with phospholipids, and a steroid ring [314]. Fusogenic liposomes containing cholesterol would remain biocompatible with platelets since the platelet membrane also contains cholesterol, as well as sphingomyelins, where both become enriched at specialised signalling areas termed lipid rafts [318].

The presence of cholesterol within the fusogenic liposome formulation may make the fusogenic liposomes less fluid and more stable when trying to encapsulate small peptides, such as the 17-residue peptide Lifeact. However, the optimum concentration of cholesterol to attain a suitable formulation has not yet been elucidated [314]. A phospholipid formulation suitable for fusogenic liposomes could be blended with varying molar ratios of cholesterol to determine if cholesterol could be beneficial to increasing retention of small water-soluble cargo. Potential permeation of encapsulated small peptides could be assessed over time using instruments such as a Nanosight (Malvern, Panalytical). This instrument can operate such that only fluorescently labelled particles are detected and measured. The extent of

fluorescent content inside fusogenic liposomes, where the lipids contain differing molar ratios of cholesterol, could be assessed over time. Although this is an area which may be useful to explore, it is important that optimisation does not disrupt fusogenicity of the fusogenic liposomes such that they can no longer fuse with the platelet membrane.

Furthermore, investigation into where Lifeact cargo resides during encapsulation using fusogenic liposomes (i.e. the lumen or within the bilayer) by electron microscopy would be advantageous to identify if liposome permeability or the Lifeact itself impacts on successful encapsulation. For example, although Lifeact is considered a hydrophilic peptide, it does contain a hydrophobic region formed by side chains which orientate to one side [319]. This hydrophobic region interacts with high affinity to a hydrophobic region located on F-actin [319]. It may be possible, therefore, that the peptide is becoming embedded with, or adsorbed onto, the hydrophobic bilayer of the fusogenic liposomes as they spontaneously form. This has been identified for other hydrophobic substances [320,321]. This may explain why Lifeact fluorescence can be detected upon fusion with fusogenic liposomes to the platelet membrane, yet why the F-actin fibers do not resemble the typical stress fibres expected by the binding of Lifeact to actin. As mentioned previously, electron microscopy may unveil if this is the case, or indeed whether permeability of the fusogenic liposome formulation used in this project is too fluid to retain the Lifeact cargo. Alternatively, it may suggest that the total amount of Lifeact delivered is not enough to demonstrate an effect.

6.3.3 Targeted ligand liposomal delivery

It may also be possible to investigate targeted ligand delivery by fusogenic liposomes. For example, a ligand could be incorporated into the fusogenic liposome formulation which could then interact directly with the receptor located on the platelet surface to investigate if receptor tethering could promote fusion and cargo delivery. This would be similar to the incorporation of a fibrinogen sequence to liposomes which binds to the platelet cell surface receptor GPIIb/IIIa (αIIbβ3) as described by Huang et al (2019) [148].

However, this binding would in turn trigger outside-in signalling events due to ligand mediated interactions. This may, therefore, directly impact on the biological question or investigation posed since there are several areas of cross talk between different pathways of platelet activation. Furthermore, the current issue regarding delivery is not a result of inability for the fusogenic liposomes to bind, more so the detection of cargo intracellularly. This project has demonstrated highly efficient labelling by fusogenic liposomes using both commercial and in-house sources of fusogenic liposomes.

Targeted delivery, therefore, is better suited to liposomal systems involved in the delivery of thrombolytic drugs to diseased areas such as at the site of a thrombus, where drug concentrations are designed to be cytotoxic [322-324].

6.4 Alternative approaches to assess cargo delivery.

6.4.1 Removal of unencapsulated cargo

As well as exploring changes to the formulation of fusogenic liposomes to investigate if this may improve encapsulation and subsequently cargo delivery, the removal of unencapsulated cargo should also be considered.

Published literature does not always describe the separation of unencapsulated cargo from encapsulated cargo contained within fusogenic liposomes. However, this project demonstrates, that at least for platelets, small peptides are able to penetrate the cell membrane of spread platelets after fusion with unloaded fusogenic liposomes (i.e. fusogenic liposomes resuspended in 20 mM HEPES buffer) when small peptides (Lifeact-488) are added to resemble unencapsulated concentrations. Suggesting that the fusion is either causing weaknesses to the cell membrane of platelets, the mechanism of fusion may be allowing peptide access at the point of fusion, or that small molecules can permeate the phospholipids which make up the fusogenic liposomes.

Therefore, removal of unencapsulated cargo would be best practise for any cargo to confirm successful delivery directly by fusogenic liposomes. Methods suitable for the removal of non-encapsulated cargo from fusogenic liposome preparations may be removed by gel-filtration chromatography [325], centrifugation [155] or dialysis [326].

6.4.2 Increasing the concentration of fusogenic liposomes

Most conclusions made regarding platelet activation and the level of labelling by fusogenic liposomes assessed both percent positivity and MFI. Where the percentage of platelets positive for the activation marker CD62P was always aimed to be kept non-significantly different to control platelets.

However, when assessing MFI, the concentrations of fusogenic liposomes which induced significantly elevated platelet activation were typically higher than that identified by percent positivity. Therefore, there may be scope to increase the concentrations of fusogenic liposomes added to washed platelets without causing significant increases to platelet activation when assessing MFI. Since there is already ≥80% fluorescent labelling using the concentrations selected in this thesis it is unlikely that improved labelling will be identified

since most platelets were already labelled. However, this could make a difference when considering cargo delivery, such that with an increased fusogenic liposome concentration there would likely be increased fusion and therefore the possibility of increased concentrations of cargo delivery, assuming that cargo is being encapsulated.

Increasing concentrations, for example from 5 µg/mL to 10 µg/mL for in-house fusogenic liposomes, still represents non-significant activation as measured by P-selectin exposure when observing MFI (Section 5, Figure 5.3). However, it is important that concentrations are not elevated so much that the concentration used directly impacts on platelet viability or function. This can be assessed by routine platelet function testing. The impact of fusogenic liposome fusion and potential platelet activation using elevated concentrations of liposomes could further be investigated by assessing ligand-binding to GPIbα and GPVI, and the surface expression levels of these glycoprotein receptors, since metalloproteolytic shedding is a consequence of receptor activation [327]. Fibrinogen binding to GPIIb/IIIa (αIIbβ3) could also be implemented as an additional measure of platelet activation where, upon activation, the conformation of the receptor has an increased affinity for soluble fibrinogen [328].

6.5 Future potential of fusogenic liposomes

Following the suggestions regarding further optimisation mentioned above, including the use of specialised techniques such as electron microscopy to confirm cargo encapsulation and direct fusion, the use of fusogenic liposomes to deliver cargo directly into human platelets offers huge potential. Novel molecular mechanisms and molecules could be directly investigated in human platelets which could expose new targets for therapeutics for cardiovascular related diseases.

6.5.1 Trim-Away

There is the potential to initiate antibody mediated protein depletion at the cellular level by utilising cellular TRIM21. The TRIM21 mechanism recognises and rapidly binds to incoming cytoplasmic antibody-bound pathogens. Binding with high affinity to the antibody Fc domain, the TRIM21 complex is ubiquitinated and directed to the proteosome for degradation. Clift et al (2017), therefore, repurposed this mechanism to degrade endogenous proteins at the cellular level named Trim-Away [162].

Trim-Away is a novel technique successfully used in mammalian cells to acutely degrade intracellular proteins at the protein level instead of prior genetic or transcriptional modifications [162]. Trim-Away has successfully targeted and degraded 9 different subcellular

proteins including membrane-anchored, chromatin bound and nuclear bound proteins, without degradation to non-targeted proteins or proteins in close spatial proximity [162]. Since the cellular machinery required to support the use of Trim-Away is present in platelets, namely TRIM21 and a functional proteasome [167], the successful delivery of whole antibodies directly into the cytoplasm of platelets would open up the potential to introduce this technique for use directly in human platelets.

The expression level of TRIM21 in human platelets has an estimated copy number of 2,200 copies per platelet [46]. While Syk for example, has an estimated copy number of 4,900 copies per human platelet [46]. The GPVI and CLEC-2 receptors, when activated by collagen, are known to activate the tyrosine kinase Syk upon tyrosine phosphorylation upstream of Syk [225,329]. Protein depletion of Syk by approximately half would likely impact on GPVI signalling when compared to platelets which are not depleted since phosphorylation of downstream targets, such as phospholipase Cγ2 (PLCγ2), may be impacted when compared to control platelets [225,329]. As in human platelets, mouse platelet GPVI signalling as a result of collagen also induces tyrosine phosphorylation of multiple platelet proteins including Syk and PLCγ2 [330]. Platelets from Syk-deficient mice have demonstrated reduced spreading [225], reduced tyrosine phosphorylation [225,330], and elevated cytosolic Ca^{2+} [331]. Therefore, the delivery of antibodies against Syk into human platelets, and the impact of subsequent protein degradation could be evaluated to identify if Trim-Away can be applied to platelets.

The expression level of TRIM21 in the platelet may be a limiting factor for abundantly expressed proteins of interest such as GPIb which has an estimated copy number of 49,000 copies per platelet [46], and a specific antibody against the intracellular tail would be required. However, this may also be overcome by co-administration of recombinant TRIM21 [170], using fusogenic liposomes as a delivery vehicle. It has recently been demonstrated that TRIM21 ubiquitination requires the clustering of at least three TRIM21 ring domains [332], which can be circumvented by the delivery of a TRIM21 construct containing these ring domains [332]. Mevissen et al (2022) has further shown that this TRIM21 construct can trigger fast and efficient antibody mediated protein degradation [333]. Trim-Away, therefore, may currently offer a superior method of protein depletion in platelets when compared to other protein depletion methods such as PROteolysis TArgeting Chimeras (PROTACs).

PROTACs work by selecting cellular proteins for degradation due to their heterobifunctional role covalently linking two head molecules [334,335]. While one head group consists of a ligand (such as a small molecule inhibitor) to selectively bind the target protein, the second head group consists of a ligand which recruits a cellular E3 ubiquitin ligase [334,336,337]. Due to the close proximity, the target protein is ubiquitinated and targeted for degradation by the proteasome system [334]. In contrast to antibody mediated protein depletion, PROTACs are not degraded meaning that one PROTAC can ubiquitinate and degrade multiple target

proteins [338]. Although this may be advantageous to the clinic where over expression caused by drug resistance or protein mutations may impact current treatments, the amount of cell permeable targets available currently remains limited [334].

That being said, PROTAC-mediated protein degradation has been applied directly to platelets, yet in one example the target protein was not degraded in the platelet when the same protein was successfully degraded in a MOLT-4 T lymphoblast cell line, suggesting the likelihood of different selectivity requirements between different cells [337,339]. On the other hand, PROTAC-mediated protein degradation was successful in platelets when using a PROTAC to target Bruton's tyrosine kinase (BTK), where GPVI-mediated platelet activation was directly impaired due to BTK playing an important role downstream of GPVI [340].

Although this most recent work demonstrates a proof of principle that PROTACs can successfully degrade proteins at the cellular level in platelets, the PROTAC applied also resulted in the degradation of TEC, another member of Tec family kinases also present in platelets [340,341]. Therefore, obtaining the insight and selectivity to design new PROTACs targeted to specific proteins of interest, where 80% of the human proteome was previously deemed undruggable, still requires a huge amount of research and development [334,336,342].

6.5.2 Vessel on a chip technology

Should the Trim-Away technique be successful in producing a rapid protein knock down directly in human platelets, these platelets can further be assessed as to how they interact with the endothelium and other cells in the blood. Providing direct insight into the function of proteins at the cellular level. This would be advantageous to the field given the compensatory mechanisms which can often develop as a result of genetically modified cell lines or animal models [156].

Over the past couple of years there have been substantial advances using *in vitro* technologies to directly model human aetiologies. These techniques have employed tissue engineering to design and generate 3D tissues which can mimic the human arterial or venous wall [343]. Delivering an investigative system containing native tissue to, for example, investigate thrombus formation directly using human tissue as an alternative to current *in vivo* models which do not always translate well to humans.

These arterial constructs, therefore, together with platelets labelled by fluorescently labelled fusogenic liposomes provide an opportunity for a complete humanised model to directly investigate platelet function and thrombus formation. Furthermore, the 3D printing of different constructs, and the protein knock down of proteins in human platelets, could provide insight into various human diseases with the added benefits of low costs and translatable data.

6.6 Summary

Firstly, a CNN abrogates time consuming and biased analyses associated with the manual interpretation of spread platelets by automating platelet spreading quantification for both human and mouse platelets. This provides a computational tool which can be used to standardise platelet spreading assays throughout the wider platelet field.

Fusogenic liposomes demonstrate a superior biocompatibility with the platelet membrane when compared to other delivery methods. During this project, platelets which have been labelled with fluorescently labelled fusogenic liposomes display no impact to platelet function, no anomalies to platelet spreading, and no impact on the ability of platelets to aggregate. Therefore, offering an alternative and biocompatible method to fluorescently label platelets for *in vitro* and *in vivo* applications when antibodies or probes may interfere with receptor function, such as in microfluidic or intravital microscopy techniques.

Specialised techniques such as electron microscopy would be advantageous to investigate the extent of fusion of fusogenic liposomes directly with the cell membrane of platelets, as well as investigating encapsulation efficiencies when loading fusogenic liposomes with the two different cargos focussed on during this project. Nevertheless, fusogenic liposomes delivered fluorescently labelled Lifeact peptides and whole antibody cargo into the platelet cytoplasm. This enables intracellular processes such as molecular mechanisms which govern platelet activation to be studied in live platelets, and opens up the potential to explore antibody mediated protein knockdown in human platelets *in vitro*. This would directly reduce the need to use platelets from genetically modified animal models where findings do not always translate well to humans.

7. References

1 Patel, S. R., Hartwig, J. H. & Italiano, J. E., Jr. The biogenesis of platelets from megakaryocyte proplatelets. *J Clin Invest* **115**, 3348-3354, doi:10.1172/jci26891 (2005).

2 Machlus, K. R. & Italiano, J. E., Jr. The incredible journey: From megakaryocyte development to platelet formation. *J Cell Biol* **201**, 785-796, doi:10.1083/jcb.201304054 (2013).

3 Seyoum, M., Enawgaw, B. & Melku, M. Human blood platelets and viruses: defense mechanism and role in the removal of viral pathogens. *Thrombosis Journal* **16**, 16, doi:10.1186/s12959-018-0170-8 (2018).

4 Giles, C. The Platelet Count and Mean Platelet Volume. *British Journal of Haematology* **48**, 31-37, doi:https://doi.org/10.1111/j.1365-2141.1981.00031.x (1981).

5 Smith, S. A., Travers, R. J. & Morrissey, J. H. How it all starts: Initiation of the clotting cascade. *Critical Reviews in Biochemistry and Molecular Biology* **50**, 326-336, doi:10.3109/10409238.2015.1050550 (2015).

6 Golebiewska, E. M. & Poole, A. W. Platelet secretion: From haemostasis to wound healing and beyond. *Blood Rev* **29**, 153-162, doi:https://doi.org/10.1016/j.blre.2014.10.003 (2015).

7 Rodvien, R. & Mielke, C. H., Jr. Role of platelets in hemostasis and thrombosis. *West J Med* **125**, 181-186 (1976).

8 Welsh, J. D., Kahn, M. L. & Sweet, D. T. Lymphovenous hemostasis and the role of platelets in regulating lymphatic flow and lymphatic vessel maturation. *Blood* **128**, 1169-1173, doi:10.1182/blood-2016-04-636415 (2016).

9 Josefsson, E. C., Vainchenker, W. & James, C. Regulation of Platelet Production and Life Span: Role of Bcl-xL and Potential Implications for Human Platelet Diseases. *Int J Mol Sci* **21**, doi:10.3390/ijms21207591 (2020).

10 Tyagi, T. *et al.* A guide to molecular and functional investigations of platelets to bridge basic and clinical sciences. *Nature Cardiovascular Research* **1**, 223-237, doi:10.1038/s44161-022-00021-z (2022).

11 Kaushansky, K. The molecular mechanisms that control thrombopoiesis. *The Journal of Clinical Investigation* **115**, 3339-3347, doi:10.1172/JCI26674 (2005).

12 Flamm, M. H. & Diamond, S. L. Multiscale systems biology and physics of thrombosis under flow. *Ann Biomed Eng* **40**, 2355-2364, doi:10.1007/s10439-012-0557-9 (2012).

13 Weisel, J. W. & Litvinov, R. I. Red blood cells: the forgotten player in hemostasis and thrombosis. *Journal of Thrombosis and Haemostasis* **17**, 271-282, doi:https://doi.org/10.1111/jth.14360 (2019).

14 Li, Z., Delaney, M. K., O'Brien, K. A. & Du, X. Signaling During Platelet Adhesion and Activation. *Arteriosclerosis, Thrombosis, and Vascular Biology* **30**, 2341-2349, doi:doi:10.1161/ATVBAHA.110.207522 (2010).

15 Denorme, F., Vanhoorelbeke, K. & De Meyer, S. F. von Willebrand Factor and Platelet Glycoprotein Ib: A Thromboinflammatory Axis in Stroke. *Front Immunol* **10**, doi:10.3389/fimmu.2019.02884 (2019).

16 Varga-Szabo, D., Pleines, I. & Nieswandt, B. Cell Adhesion Mechanisms in Platelets. *Arteriosclerosis, Thrombosis, and Vascular Biology* **28**, 403-412, doi:doi:10.1161/ATVBAHA.107.150474 (2008).

17 Aslan, J. E., Itakura, A., Gertz, J. M. & McCarty, O. J. T. in *Platelets and Megakaryocytes: Volume 3, Additional Protocols and Perspectives* (eds Jonathan M. Gibbins & Martyn P. Mahaut-Smith) 91-100 (Springer New York, 2012).

18 Shin, E.-K., Park, H., Noh, J.-Y., Lim, K.-M. & Chung, J.-H. Platelet Shape Changes and Cytoskeleton Dynamics as Novel Therapeutic Targets for Anti-Thrombotic Drugs. *Biomol Ther (Seoul)* **25**, 223-230, doi:10.4062/biomolther.2016.138 (2017).

19 Organisation, W. H. *Cardiovascular diseases*, <https://www.who.int/news-room/fact-sheets/detail/cardiovascular-diseases-(cvds)> (

20 Raskob, G. E. *et al.* Thrombosis: A major contributor to global disease burden. *Thrombosis Research* **134**, 931-938, doi:https://doi.org/10.1016/j.thromres.2014.08.014 (2014).

21 L.J. DOMINGUEZ *et al.* AGEING, LIFESTYLE MODIFICATIONS, AND CARDIOVASCULAR DISEASE IN DEVELOPING COUNTRIES. *The Journal of Nutrition, Health & Aging* **Volume 10** (2006).
22 Chen, Y., Yuan, Y. & Li, W. Sorting machineries: how platelet-dense granules differ from α-granules. *Biosci Rep* **38**, BSR20180458, doi:10.1042/BSR20180458 (2018).
23 Rendu, F. & Brohard-Bohn, B. The platelet release reaction: granules' constituents, secretion and functions. *Platelets* **12**, 261-273, doi:10.1080/09537100120068170 (2001).
24 Sharda, A. & Flaumenhaft, R. The life cycle of platelet granules. *F1000Res* **7**, 236, doi:10.12688/f1000research.13283.1 (2018).
25 Heijnen, H. & van der Sluijs, P. Platelet secretory behaviour: as diverse as the granules … or not? *Journal of Thrombosis and Haemostasis* **13**, 2141-2151, doi:https://doi.org/10.1111/jth.13147 (2015).
26 Flaumenhaft, R. & Sharda, A. in *Platelets (Fourth Edition)* (ed Alan D. Michelson) 349-370 (Academic Press, 2019).
27 Blair, P. & Flaumenhaft, R. Platelet alpha-granules: basic biology and clinical correlates. *Blood Rev* **23**, 177-189, doi:10.1016/j.blre.2009.04.001 (2009).
28 Fitch-Tewfik, J. & Flaumenhaft, R. Platelet Granule Exocytosis: A Comparison with Chromaffin Cells. *Frontiers in Endocrinology* **4**, doi:10.3389/fendo.2013.00077 (2013).
29 Guerrero, J. A. *et al.* Gray platelet syndrome: proinflammatory megakaryocytes and α-granule loss cause myelofibrosis and confer metastasis resistance in mice. *Blood* **124**, 3624-3635, doi:10.1182/blood-2014-04-566760 (2014).
30 Flaumenhaft, R. in *Platelets (Third Edition)* (ed Alan D. Michelson) 343-366 (Academic Press, 2013).
31 Ruggeri, Z. M. & Mendolicchio, G. L. Adhesion mechanisms in platelet function. *Circ Res* **100**, 1673-1685, doi:10.1161/01.RES.0000267878.97021.ab (2007).
32 Yau, J. W., Teoh, H. & Verma, S. Endothelial cell control of thrombosis. *BMC Cardiovasc Disord* **15**, 130, doi:10.1186/s12872-015-0124-z (2015).
33 Periayah, M. H., Halim, A. S. & Mat Saad, A. Z. Mechanism Action of Platelets and Crucial Blood Coagulation Pathways in Hemostasis. *Int J Hematol Oncol Stem Cell Res* **11**, 319-327 (2017).
34 Jung, S. M. & Moroi, M. in *Multichain Immune Recognition Receptor Signaling: From Spatiotemporal Organization to Human Disease* (ed Alexander B. Sigalov) 53-63 (Springer New York, 2008).
35 Rayes, J., Watson, S. P. & Nieswandt, B. Functional significance of the platelet immune receptors GPVI and CLEC-2. *J Clin Invest* **129**, 12-23, doi:10.1172/jci122955 (2019).
36 Phillips, D. R., Charo, I. F., Parise, L. V. & Fitzgerald, L. A. The platelet membrane glycoprotein IIb-IIIa complex. (1988).
37 Fullard, F. J. The Role of the Platelet Glycoprotein IIb / IIIa in Thrombosis and Haemostasis. *Current Pharmaceutical Design* **10**, 1567-1576, doi:http://dx.doi.org/10.2174/1381612043384682 (2004).
38 French, D. L. & Seligsohn, U. Platelet Glycoprotein IIb/IIIa Receptors and Glanzmann's Thrombasthenia. *Arteriosclerosis, Thrombosis, and Vascular Biology* **20**, 607-610, doi:doi:10.1161/01.ATV.20.3.607 (2000).
39 Matzdorff, A. & Voss, R. Upregulation of GP IIb/IIIa receptors during platelet activation: influence on efficacy of receptor blockade. *Thromb Res* **117**, 307-314, doi:10.1016/j.thromres.2005.03.007 (2006).
40 Alberio, L., Safa, O., Clemetson, K. J., Esmon, C. T. & Dale, G. L. Surface expression and functional characterization of α-granule factor V in human platelets: effects of ionophore A23187, thrombin, collagen, and convulxin. *Blood* **95**, 1694-1702, doi:https://doi.org/10.1182/blood.V95.5.1694.005k24_1694_1702 (2000).
41 Reddy, E. C. & Rand, M. L. Procoagulant Phosphatidylserine-Exposing Platelets in vitro and in vivo. *Frontiers in Cardiovascular Medicine* **7**, doi:10.3389/fcvm.2020.00015 (2020).
42 Agbani, E. O. & Poole, A. W. Procoagulant platelets: generation, function, and therapeutic targeting in thrombosis. *Blood* **130**, 2171-2179, doi:10.1182/blood-2017-05-787259 (2017).

43 Elmore, S. Apoptosis: a review of programmed cell death. *Toxicol Pathol* **35**, 495-516, doi:10.1080/01926230701320337 (2007).
44 Walker, E. & Tzima, J. H. Platelet annexin V: the ins and outs. *Platelets* **11**, 245-251, doi:10.1080/09537100050129251 (2000).
45 Zhernossekov, D. D., Roka-Moiia, Y. M. & Grinenko, T. V. Extracellular annexins in hemostasis system. *Biopolymers & Cell* **32**, 98-104, doi:http://dx.doi.org/10.7124/bc.000911 (2016).
46 Burkhart, J. M. *et al.* The first comprehensive and quantitative analysis of human platelet protein composition allows the comparative analysis of structural and functional pathways. *Blood* **120**, e73-e82, doi:https://doi.org/10.1182/blood-2012-04-416594 (2012).
47 Montague, S. J., Lim, Y. J., Lee, W. M. & Gardiner, E. E. Imaging Platelet Processes and Function-Current and Emerging Approaches for Imaging in vitro and in vivo. *Front Immunol* **11**, 78-78, doi:10.3389/fimmu.2020.00078 (2020).
48 Riedl, J. *et al.* Lifeact: a versatile marker to visualize F-actin. *Nat Methods* **5**, 605-607, doi:10.1038/nmeth.1220 (2008).
49 Cardo, L. *et al.* Accessible Synthetic Probes for Staining Actin inside Platelets and Megakaryocytes by Employing Lifeact Peptide. *Chembiochem* **16**, 1680-1688, doi:10.1002/cbic.201500120 (2015).
50 Paknikar, A. K., Eltzner, B. & Köster, S. Direct characterization of cytoskeletal reorganization during blood platelet spreading. *Progress in Biophysics and Molecular Biology* **144**, 166-176, doi:https://doi.org/10.1016/j.pbiomolbio.2018.05.001 (2019).
51 Cardo, L. *et al.* Accessible Synthetic Probes for Staining Actin inside Platelets and Megakaryocytes by Employing Lifeact Peptide. *Chembiochem* **16**, 1680-1688, doi:10.1002/cbic.201500120 (2015).
52 Poulter, N. S. *et al.* Platelet actin nodules are podosome-like structures dependent on Wiskott-Aldrich syndrome protein and ARP2/3 complex. *Nat Commun* **6**, 7254, doi:10.1038/ncomms8254 (2015).
53 CALAMINUS, S. D. J., THOMAS, S., McCARTY, O. J. T., MACHESKY, L. M. & WATSON, S. P. Identification of a novel, actin-rich structure, the actin nodule, in the early stages of platelet spreading. *Journal of Thrombosis and Haemostasis* **6**, 1944-1952, doi:https://doi.org/10.1111/j.1538-7836.2008.03141.x (2008).
54 Sandmann, R. & Köster, S. Topographic Cues Reveal Two Distinct Spreading Mechanisms in Blood Platelets. *Scientific Reports* **6**, 22357, doi:10.1038/srep22357 (2016).
55 Berrou, E. *et al.* Heterogeneity of platelet functional alterations in patients with filamin A mutations. *Arterioscler Thromb Vasc Biol* **33**, e11-18, doi:10.1161/atvbaha.112.300603 (2013).
56 Canobbio, I. *et al.* Altered cytoskeleton organization in platelets from patients with MYH9-related disease. *J Thromb Haemost* **3**, 1026-1035, doi:10.1111/j.1538-7836.2005.01244.x (2005).
57 Koupenova, M., Kehrel, B. E., Corkrey, H. A. & Freedman, J. E. Thrombosis and platelets: an update. *European Heart Journal* **38**, 785-791, doi:10.1093/eurheartj/ehw550 (2017).
58 Ruggeri, Z. M. & Mendolicchio, G. L. Adhesion Mechanisms in Platelet Function. *Circulation Research* **100**, 1673-1685, doi:doi:10.1161/01.RES.0000267878.97021.ab (2007).
59 Koupenova, M., Kehrel, B. E., Corkrey, H. A. & Freedman, J. E. Thrombosis and platelets: an update. *European Heart Journal* **38**, 785-791, doi:10.1093/eurheartj/ehw550 (2016).
60 Chernysh, I. N. *et al.* The distinctive structure and composition of arterial and venous thrombi and pulmonary emboli. *Scientific Reports* **10**, 5112, doi:10.1038/s41598-020-59526-x (2020).
61 Mackman, N. Triggers, targets and treatments for thrombosis. *Nature* **451**, 914-918, doi:10.1038/nature06797 (2008).
62 Foundation, B. H. *Heart & Circulatory Disease Statistics*, 2023).
63 Berger, P. B. *et al.* Bleeding Complications With Dual Antiplatelet Therapy Among Patients With Stable Vascular Disease or Risk Factors for Vascular Disease. *Circulation* **121**, 2575-2583, doi:doi:10.1161/CIRCULATIONAHA.109.895342 (2010).

64 Streiff, M. B. *et al.* Guidance for the treatment of deep vein thrombosis and pulmonary embolism. *J Thromb Thrombolysis* **41**, 32-67, doi:10.1007/s11239-015-1317-0 (2016).
65 Amin, A. P. *et al.* Nuisance Bleeding With Prolonged Dual Antiplatelet Therapy After Acute Myocardial Infarction and its Impact on Health Status. *Journal of the American College of Cardiology* **61**, 2130-2138, doi:doi:10.1016/j.jacc.2013.02.044 (2013).
66 Escofet Peris, M. *et al.* Long-Term Morbidity and Mortality after First and Recurrent Cardiovascular Events in the ARTPER Cohort. *J Clin Med* **9**, doi:10.3390/jcm9124064 (2020).
67 Rollini, F., Franchi, F., Muñiz-Lozano, A. & Angiolillo, D. J. Platelet function profiles in patients with diabetes mellitus. *J Cardiovasc Transl Res* **6**, 329-345, doi:10.1007/s12265-013-9449-0 (2013).
68 Ferroni, P., Basili, S., Falco, A. & Davì, G. Platelet activation in type 2 diabetes mellitus. *J Thromb Haemost* **2**, 1282-1291, doi:10.1111/j.1538-7836.2004.00836.x (2004).
69 Mansfield, M. W., Heywood, D. M. & Grant, P. J. Circulating Levels of Factor VII, Fibrinogen, and von Willebrand Factor and Features of Insulin Resistance in First-Degree Relatives of Patients With NIDDM. *Circulation* **94**, 2171-2176, doi:doi:10.1161/01.CIR.94.9.2171 (1996).
70 Catalano, I. *et al.* Fibrinogen and von Willebrand factor in type II diabetes mellitus. *Acta Diabetologica* **29**, 78-81, doi:10.1007/BF00572548 (1992).
71 Lambert, M. P. What To Do When You Suspect an Inherited Platelet Disorder. *Hematology* **2011**, 377-383, doi:10.1182/asheducation-2011.1.377 (2011).
72 Palma-Barqueros, V. *et al.* Inherited Platelet Disorders: An Updated Overview. *Int J Mol Sci* **22**, doi:10.3390/ijms22094521 (2021).
73 NURDEN, A. T., FRESON, K. & SELIGSOHN, U. Inherited platelet disorders. *Haemophilia* **18**, 154-160, doi:https://doi.org/10.1111/j.1365-2516.2012.02856.x (2012).
74 Perez Botero, J. & Di Paola, J. Diagnostic approach to the patient with a suspected inherited platelet disorder: Who and how to test. *Journal of Thrombosis and Haemostasis* **19**, 2127-2136, doi:https://doi.org/10.1111/jth.15484 (2021).
75 Weyrich, A. S. *et al.* Change in protein phenotype without a nucleus: translational control in platelets. *Semin Thromb Hemost* **30**, 491-498, doi:10.1055/s-2004-833484 (2004).
76 Hong, W. *et al.* Transfection of human platelets with short interfering RNA. *Clin Transl Sci* **4**, 180-182, doi:10.1111/j.1752-8062.2011.00279.x (2011).
77 Kondkar, A. A. *et al.* Transfection of Human Platelets Down-Regulates Endogenous mRNA. *Blood* **114**, 4026, doi:https://doi.org/10.1182/blood.V114.22.4026.4026 (2009).
78 Han, H. RNA Interference to Knock Down Gene Expression. *Methods Mol Biol* **1706**, 293-302, doi:10.1007/978-1-4939-7471-9_16 (2018).
79 Kieffer, N., Guichard, J., Farcet, J. P., Vainchenker, W. & Breton-Gorius, J. Biosynthesis of major platelet proteins in human blood platelets. *Eur J Biochem* **164**, 189-195, doi:10.1111/j.1432-1033.1987.tb11010.x (1987).
80 Thon, J. N. & Devine, D. V. Translation of glycoprotein IIIa in stored blood platelets. *Transfusion* **47**, 2260-2270, doi:10.1111/j.1537-2995.2007.01455.x (2007).
81 Mitchell, J. A., Ali, F., Bailey, L., Moreno, L. & Harrington, L. S. Role of nitric oxide and prostacyclin as vasoactive hormones released by the endothelium. *Experimental Physiology* **93**, 141-147, doi:https://doi.org/10.1113/expphysiol.2007.038588 (2008).
82 Hechler, B., Dupuis, A., Mangin, P. H. & Gachet, C. Platelet preparation for function testing in the laboratory and clinic: Historical and practical aspects. *Research and Practice in Thrombosis and Haemostasis* **3**, 615-625, doi:https://doi.org/10.1002/rth2.12240 (2019).
83 Smith, S. A. *et al.* Polyphosphate modulates blood coagulation and fibrinolysis. *Proceedings of the National Academy of Sciences of the United States of America* **103**, 903, doi:10.1073/pnas.0507195103 (2006).
84 Weiss, H. J. & Turitto, V. T. Prostacyclin (prostaglandin I2, PGI2) inhibits platelet adhesion and thrombus formation on subendothelium. *Blood* **53**, 244-250 (1979).
85 Kim, J. H., Lim, K. M. & Gwak, H. S. New Anticoagulants for the Prevention and Treatment of Venous Thromboembolism. *Biomol Ther (Seoul)* **25**, 461-470, doi:10.4062/biomolther.2016.271 (2017).

86 Crunkhorn, S. Engineered apyrase averts clot formation. *Nature Reviews Drug Discovery* **13**, 725-725, doi:10.1038/nrd4444 (2014).
87 Cattaneo, M. in *Platelets (Fourth Edition)* (ed Alan D. Michelson) 259-277 (Academic Press, 2019).
88 Strassel, C., Gachet, C. & Lanza, F. On the Way to in vitro Platelet Production. *Front Med (Lausanne)* **5**, 239, doi:10.3389/fmed.2018.00239 (2018).
89 Moreau, T. *et al.* Large-scale production of megakaryocytes from human pluripotent stem cells by chemically defined forward programming. *Nat Commun* **7**, 11208, doi:10.1038/ncomms11208 (2016).
90 Nakamura, S. *et al.* Expandable megakaryocyte cell lines enable clinically applicable generation of platelets from human induced pluripotent stem cells. *Cell Stem Cell* **14**, 535-548, doi:10.1016/j.stem.2014.01.011 (2014).
91 Takahashi, K. *et al.* Induction of Pluripotent Stem Cells from Adult Human Fibroblasts by Defined Factors. *Cell* **131**, 861-872, doi:10.1016/j.cell.2007.11.019 (2007).
92 Evans, A. L. *et al.* Transfer to the clinic: refining forward programming of hPSCs to megakaryocytes for platelet production in bioreactors. *Blood Adv* **5**, 1977-1990, doi:10.1182/bloodadvances.2020003236 (2021).
93 Sugimoto, N. & Eto, K. Platelet production from induced pluripotent stem cells. *Journal of Thrombosis and Haemostasis* **15**, 1717-1727, doi:https://doi.org/10.1111/jth.13736 (2017).
94 Blumberg, N., Heal, J. M. & Phillips, G. L. Platelet transfusions: trigger, dose, benefits, and risks. *F1000 Med Rep* **2**, 5, doi:10.3410/m2-5 (2010).
95 Junt, T. *et al.* Dynamic visualization of thrombopoiesis within bone marrow. *Science* **317**, 1767-1770, doi:10.1126/science.1146304 (2007).
96 Thon, J. N. *et al.* Platelet bioreactor-on-a-chip. *Blood* **124**, 1857-1867, doi:10.1182/blood-2014-05-574913 (2014).
97 De Masi, C., Spitalieri, P., Murdocca, M., Novelli, G. & Sangiuolo, F. Application of CRISPR/Cas9 to human-induced pluripotent stem cells: from gene editing to drug discovery. *Human Genomics* **14**, 25, doi:10.1186/s40246-020-00276-2 (2020).
98 DENIS, C. V. *et al.* Towards standardization of in vivo thrombosis studies in mice. *Journal of Thrombosis and Haemostasis* **9**, 1641-1644, doi:https://doi.org/10.1111/j.1538-7836.2011.04350.x (2011).
99 Sakamoto, K., Gurumurthy, C. B. & Wagner, K.-U. in *Mouse Genetics: Methods and Protocols* (eds Shree Ram Singh & Vincenzo Coppola) 21-35 (Springer New York, 2014).
100 Nagy, A. Cre recombinase: The universal reagent for genome tailoring. *genesis* **26**, 99-109, doi:https://doi.org/10.1002/(SICI)1526-968X(200002)26:2<99::AID-GENE1>3.0.CO;2-B (2000).
101 McCarthy, J. J., Srikuea, R., Kirby, T. J., Peterson, C. A. & Esser, K. A. Inducible Cre transgenic mouse strain for skeletal muscle-specific gene targeting. *Skeletal Muscle* **2**, 8, doi:10.1186/2044-5040-2-8 (2012).
102 Saunders, T. L. in *Transgenic Mouse Methods and Protocols* (eds Marten H. Hofker & Jan van Deursen) 103-115 (Humana Press, 2011).
103 Furie, B., Furie, B. C., Flaumenhaft, R. & Zwicker, J. I. Animal Models of Arterial and Venous Thrombosis. *Blood* **124**, SCI-2-SCI-2, doi:10.1182/blood.V124.21.SCI-2.SCI-2 (2014).
104 Schmitt, A., Guichard, J., Massé, J.-M., Debili, N. & Cramer, E. M. Of mice and men: Comparison of the ultrastructure of megakaryocytes and platelets. *Experimental Hematology* **29**, 1295-1302, doi:https://doi.org/10.1016/S0301-472X(01)00733-0 (2001).
105 Ware, J. Dysfunctional platelet membrane receptors: from humans to mice. *Thromb Haemost* **92**, 478-485, doi:10.1160/th04-05-0308 (2004).
106 Jirouskova, M., Shet, A. S. & Johnson, G. J. A guide to murine platelet structure, function, assays, and genetic alterations. *J Thromb Haemost* **5**, 661-669, doi:10.1111/j.1538-7836.2007.02407.x (2007).

107 Mangin, P. H. *et al.* A humanized glycoprotein VI (GPVI) mouse model to assess the antithrombotic efficacies of anti-GPVI agents. *J Pharmacol Exp Ther* **341**, 156-163, doi:10.1124/jpet.111.189050 (2012).
108 Arman, M. & Krauel, K. Human platelet IgG Fc receptor FcγRIIA in immunity and thrombosis. *Journal of Thrombosis and Haemostasis* **13**, 893-908, doi:https://doi.org/10.1111/jth.12905 (2015).
109 Smith, P., DiLillo, D. J., Bournazos, S., Li, F. & Ravetch, J. V. Mouse model recapitulating human Fcγ receptor structural and functional diversity. *Proc Natl Acad Sci U S A* **109**, 6181-6186, doi:10.1073/pnas.1203954109 (2012).
110 Seok, J. *et al.* Genomic responses in mouse models poorly mimic human inflammatory diseases. *Proc Natl Acad Sci U S A* **110**, 3507-3512, doi:10.1073/pnas.1222878110 (2013).
111 Takao, K. & Miyakawa, T. Genomic responses in mouse models greatly mimic human inflammatory diseases. *Proc Natl Acad Sci U S A* **112**, 1167-1172, doi:10.1073/pnas.1401965111 (2015).
112 Justice, M. J. & Dhillon, P. Using the mouse to model human disease: increasing validity and reproducibility. *Dis Model Mech* **9**, 101-103, doi:10.1242/dmm.024547 (2016).
113 Kappel, S., Hawkins, P. & Mendl, M. T. To Group or Not to Group? Good Practice for Housing Male Laboratory Mice. *Animals* **7**, 88 (2017).
114 Hankenson, F. C., Marx, J. O., Gordon, C. J. & David, J. M. Effects of Rodent Thermoregulation on Animal Models in the Research Environment. *Comparative Medicine* **68**, 425-438, doi:10.30802/AALAS-CM-18-000049 (2018).
115 Janssen, B. J. *et al.* Effects of anesthetics on systemic hemodynamics in mice. *Am J Physiol Heart Circ Physiol* **287**, H1618-1624, doi:10.1152/ajpheart.01192.2003 (2004).
116 Chang, Y. *et al.* Mechanisms Involved in the Antiplatelet Activity of Ketamine in Human Platelets. *Journal of Biomedical Science* **11**, 764-772, doi:10.1159/000081823 (2004).
117 Njoroge, W. *et al.* The Combination of Tissue-Engineered Blood Vessel Constructs and Parallel Flow Chamber Provides a Potential Alternative to In Vivo Drug Testing Models. *Pharmaceutics* **13**, 340 (2021).
118 O'Collins, V. E. *et al.* 1,026 Experimental treatments in acute stroke. *Annals of Neurology* **59**, 467-477, doi:https://doi.org/10.1002/ana.20741 (2006).
119 Tymianski, M. Can Molecular and Cellular Neuroprotection Be Translated Into Therapies for Patients? *Stroke* **41**, S87-S90, doi:doi:10.1161/STROKEAHA.110.595496 (2010).
120 Vyas, M. V., Gros, R. & Hackam, D. G. Translation of Cardiovascular Animal Models to Human Randomized Trials. *The American Journal of Cardiology* **137**, 141, doi:https://doi.org/10.1016/j.amjcard.2020.10.027 (2020).
121 Kube, S. *et al.* Fusogenic Liposomes as Nanocarriers for the Delivery of Intracellular Proteins. *Langmuir* **33**, 1051-1059, doi:10.1021/acs.langmuir.6b04304 (2017).
122 Guidotti, G., Brambilla, L. & Rossi, D. Cell-Penetrating Peptides: From Basic Research to Clinics. *Trends in Pharmacological Sciences* **38**, 406-424, doi:10.1016/j.tips.2017.01.003 (2017).
123 Frankel, A. D. & Pabo, C. O. Cellular uptake of the tat protein from human immunodeficiency virus. *Cell* **55**, 1189-1193, doi:https://doi.org/10.1016/0092-8674(88)90263-2 (1988).
124 Bechara, C. & Sagan, S. Cell-penetrating peptides: 20years later, where do we stand? *FEBS Letters* **587**, 1693-1702, doi:https://doi.org/10.1016/j.febslet.2013.04.031 (2013).
125 Kristensen, M., Birch, D. & Mørck Nielsen, H. Applications and Challenges for Use of Cell-Penetrating Peptides as Delivery Vectors for Peptide and Protein Cargos. *Int J Mol Sci* **17**, 185, doi:10.3390/ijms17020185 (2016).
126 DAVID, T. *et al.* Inhibition of adhesive and signaling functions of the platelet GPIb-V-IX complex by a cell penetrating GPIbα peptide. *Journal of Thrombosis and Haemostasis* **4**, 2645-2655, doi:https://doi.org/10.1111/j.1538-7836.2006.02198.x (2006).
127 Berndt, M. C., Shen, Y., Dopheide, S. M., Gardiner, E. E. & Andrews, R. K. The Vascular Biology of the Glycoprotein Ib-IX-V Complex. *Thromb Haemost* **86**, 178-188 (2001).

128 Dimitriou, A. A. *et al.* Inhibition of platelet activation by peptide analogs of the β3-intracellular domain of platelet integrin αIIbβ3 conjugated to the cell-penetrating peptide Tat(48–60). *Platelets* **20**, 539-547, doi:10.3109/09537100903324219 (2009).
129 Yakushkin, V. V. *et al.* Glycoprotein IIb-IIIa content and platelet aggregation in healthy volunteers and patients with acute coronary syndrome. *Platelets* **22**, 243-251, doi:10.3109/09537104.2010.547959 (2011).
130 Rana, A., Westein, E., Niego, B. e. & Hagemeyer, C. E. Shear-Dependent Platelet Aggregation: Mechanisms and Therapeutic Opportunities. *Frontiers in Cardiovascular Medicine* **6**, doi:10.3389/fcvm.2019.00141 (2019).
131 Shen, Y. *et al.* Functional analysis of the C-terminal flanking sequence of platelet glycoprotein Ibα using canine–human chimeras. *Blood* **99**, 145-150, doi:10.1182/blood.V99.1.145 (2002).
132 Shen, Y. *et al.* Leucine-rich Repeats 2-4 (Leu⁶⁰-Glu¹²⁸) of Platelet Glycoprotein Ibα Regulate Shear-dependent Cell Adhesion to von Willebrand Factor *. *Journal of Biological Chemistry* **281**, 26419-26423, doi:10.1074/jbc.M604296200 (2006).
133 Hunt, J. F. *et al.* A Biophysical Study of Integral Membrane Protein Folding. *Biochemistry* **36**, 15156-15176, doi:10.1021/bi970146j (1997).
134 Reshetnyak, Y. K., Andreev, O. A., Lehnert, U. & Engelman, D. M. Translocation of molecules into cells by pH-dependent insertion of a transmembrane helix. *Proc Natl Acad Sci U S A* **103**, 6460-6465, doi:10.1073/pnas.0601463103 (2006).
135 Thévenin, D., An, M. & Engelman, D. M. pHLIP-mediated translocation of membrane-impermeable molecules into cells. *Chem Biol* **16**, 754-762, doi:10.1016/j.chembiol.2009.06.006 (2009).
136 Davies, A., Lewis, D. J., Watson, S. P., Thomas, S. G. & Pikramenou, Z. pH-controlled delivery of luminescent europium coated nanoparticles into platelets. *Proceedings of the National Academy of Sciences* **109**, 1862-1867, doi:10.1073/pnas.1112132109 (2012).
137 Lukinavičius, G. *et al.* Fluorogenic probes for live-cell imaging of the cytoskeleton. *Nat Methods* **11**, 731-733, doi:10.1038/nmeth.2972 (2014).
138 Lickert, S. *et al.* Morphometric analysis of spread platelets identifies integrin α(IIb)β(3)-specific contractile phenotype. *Scientific reports* **8**, 5428-5428, doi:10.1038/s41598-018-23684-w (2018).
139 Scharbert, G., Franta, G., Wetzel, L. & Kozek-Langenecker, S. *Effect of pH levels on platelet aggregation and coagulation: a whole blood in vitro study*. (Crit Care. 2011;15(Suppl 1):P446. doi: 10.1186/cc9866. Epub 2011 Mar 11.).
140 Udenwobele, D. I. *et al.* Myristoylation: An Important Protein Modification in the Immune Response. *Front Immunol* **8**, 751, doi:10.3389/fimmu.2017.00751 (2017).
141 Nelson, A. R., Borland, L., Allbritton, N. L. & Sims, C. E. Myristoyl-Based Transport of Peptides into Living Cells. *Biochemistry* **46**, 14771-14781, doi:10.1021/bi701295k (2007).
142 Covic, L., Gresser, A. L., Talavera, J., Swift, S. & Kuliopulos, A. Activation and inhibition of G protein-coupled receptors by cell-penetrating membrane-tethered peptides. *Proceedings of the National Academy of Sciences* **99**, 643-648, doi:doi:10.1073/pnas.022460899 (2002).
143 Durgavati Yadav, K. S., Deepak Pandey and Ranu Kumari Dutta. Liposomes for Drug Delivery. *Journal of Biotechnology & Biomaterials* **7:4**, doi:10.4172/2155-952X.1000276 (2017).
144 Boggs, J. M. Lipid intermolecular hydrogen bonding: influence on structural organization and membrane function. *Biochimica et Biophysica Acta (BBA) - Reviews on Biomembranes* **906**, 353-404, doi:https://doi.org/10.1016/0304-4157(87)90017-7 (1987).
145 Akbarzadeh, A. *et al.* Liposome: classification, preparation, and applications. *Nanoscale Res Lett* **8**, 102-102, doi:10.1186/1556-276X-8-102 (2013).
146 Bozzuto, G. & Molinari, A. Liposomes as nanomedical devices. *Int J Nanomedicine* **10**, 975-999, doi:10.2147/IJN.S68861 (2015).
147 Paszko, E. & Senge, M. O. Immunoliposomes. *Curr Med Chem* **19**, 5239-5277, doi:10.2174/092986712803833362 (2012).

148 Huang, Y. *et al.* An activated-platelet-sensitive nanocarrier enables targeted delivery of tissue plasminogen activator for effective thrombolytic therapy. *Journal of Controlled Release* **300**, 1-12, doi:https://doi.org/10.1016/j.jconrel.2019.02.033 (2019).
149 Gravanis, I. & Tsirka, S. E. Tissue-type plasminogen activator as a therapeutic target in stroke. *Expert Opin Ther Targets* **12**, 159-170, doi:10.1517/14728222.12.2.159 (2008).
150 Takikawa, M., Fujisawa, M., Yoshino, K. & Takeoka, S. Intracellular Distribution of Lipids and Encapsulated Model Drugs from Cationic Liposomes with Different Uptake Pathways. *Int J Nanomedicine* **15**, 8401-8409, doi:10.2147/ijn.S267638 (2020).
151 Csiszár, A. *et al.* Novel Fusogenic Liposomes for Fluorescent Cell Labeling and Membrane Modification. *Bioconjugate Chemistry* **21**, 537-543, doi:10.1021/bc900470y (2010).
152 Cevc, G. & Richardsen, H. Lipid vesicles and membrane fusion. *Advanced Drug Delivery Reviews* **38**, 207-232, doi:https://doi.org/10.1016/S0169-409X(99)00030-7 (1999).
153 Chernomordik, L. V. & Kozlov, M. M. Membrane Hemifusion: Crossing a Chasm in Two Leaps. *Cell* **123**, 375-382, doi:https://doi.org/10.1016/j.cell.2005.10.015 (2005).
154 Matos, A. L. L., Pereira, G., Cabral Filho, P. E., Santos, B. S. & Fontes, A. Delivery of cationic quantum dots using fusogenic liposomes in living cells. *Journal of Photochemistry and Photobiology B: Biology* **171**, 43-49, doi:https://doi.org/10.1016/j.jphotobiol.2017.04.025 (2017).
155 Kolašinac, R. *et al.* Delivery of the Radionuclide 131I Using Cationic Fusogenic Liposomes as Nanocarriers. *Int J Mol Sci* **22**, 457 (2021).
156 Diss, G., Ascencio, D., DeLuna, A. & Landry, C. R. Molecular mechanisms of paralogous compensation and the robustness of cellular networks. *Journal of Experimental Zoology Part B: Molecular and Developmental Evolution* **322**, 488-499, doi:https://doi.org/10.1002/jez.b.22555 (2014).
157 Kusumi, A., Tsunoyama, T. A., Hirosawa, K. M., Kasai, R. S. & Fujiwara, T. K. Tracking single molecules at work in living cells. *Nature Chemical Biology* **10**, 524-532, doi:http://dx.doi.org/10.1038/nchembio.1558 (2014).
158 Li, N. *et al.* Single-molecule imaging and tracking of molecular dynamics in living cells. *National Science Review* **4**, 739-760, doi:10.1093/nsr/nww055 (2017).
159 Elf, J. & Barkefors, I. Single-Molecule Kinetics in Living Cells. *Annual Review of Biochemistry* **88**, 635-659, doi:10.1146/annurev-biochem-013118-110801 (2019).
160 Mallery, D. L. *et al.* Antibodies mediate intracellular immunity through tripartite motif-containing 21 (TRIM21). *Proc Natl Acad Sci U S A* **107**, 19985-19990, doi:10.1073/pnas.1014074107 (2010).
161 James, L. C., Keeble, A. H., Khan, Z., Rhodes, D. A. & Trowsdale, J. Structural basis for PRYSPRY-mediated tripartite motif (TRIM) protein function. *Proc Natl Acad Sci U S A* **104**, 6200-6205, doi:10.1073/pnas.0609174104 (2007).
162 Clift, D. *et al.* A Method for the Acute and Rapid Degradation of Endogenous Proteins. *Cell* **171**, 1692-1706.e1618, doi:10.1016/j.cell.2017.10.033 (2017).
163 Chen, X. *et al.* Degradation of endogenous proteins and generation of a null-like phenotype in zebrafish using Trim-Away technology. *Genome Biology* **20**, 19, doi:10.1186/s13059-019-1624-4 (2019).
164 Israel, S., Casser, E., Drexler, H. C. A., Fuellen, G. & Boiani, M. A framework for TRIM21-mediated protein depletion in early mouse embryos: recapitulation of Tead4 null phenotype over three days. *BMC Genomics* **20**, 755, doi:10.1186/s12864-019-6106-2 (2019).
165 Weir, E., McLinden, G., Alfandari, D. & Cousin, H. Trim-Away mediated knock down uncovers a new function for Lbh during gastrulation of Xenopus laevis. *Developmental Biology* **470**, 74-83, doi:https://doi.org/10.1016/j.ydbio.2020.10.014 (2021).
166 Junker, J. P. Detouring the roadblocks in gene expression. *Nature Reviews Molecular Cell Biology* **20**, 197-197, doi:10.1038/s41580-019-0107-5 (2019).
167 El-Kadiry, A. E. & Merhi, Y. The Role of the Proteasome in Platelet Function. *Int J Mol Sci* **22**, doi:10.3390/ijms22083999 (2021).

168 Grundler Groterhorst, K., Mannell, H., Pircher, J. & Kraemer, B. F. Platelet Proteasome Activity and Metabolism Is Upregulated during Bacterial Sepsis. *Int J Mol Sci* **20**, doi:10.3390/ijms20235961 (2019).
169 Colberg, L., Cammann, C., Greinacher, A. & Seifert, U. Structure and function of the ubiquitin-proteasome system in platelets. *Journal of Thrombosis and Haemostasis* **18**, 771-780, doi:https://doi.org/10.1111/jth.14730 (2020).
170 Foss, S. *et al.* TRIM21—From Intracellular Immunity to Therapy. *Front Immunol* **10**, doi:10.3389/fimmu.2019.02049 (2019).
171 Jones, C. I. *et al.* A functional genomics approach reveals novel quantitative trait loci associated with platelet signaling pathways. *Blood* **114**, 1405-1416, doi:10.1182/blood-2009-02-202614 (2009).
172 Schindelin, J. *et al.* Fiji: an open-source platform for biological-image analysis. *Nat Methods* **9**, 676-682, doi:10.1038/nmeth.2019 (2012).
173 Tsai, H.-F., Gajda, J., Sloan, T. F. W., Rares, A. & Shen, A. Q. Usiigaci: Instance-aware cell tracking in stain-free phase contrast microscopy enabled by machine learning. *SoftwareX* **9**, 230-237, doi:https://doi.org/10.1016/j.softx.2019.02.007 (2019).
174 Butler, G., Keeton, S. J., Johnson, L. J. & Dash, P. R. A phenotypic switch in the dispersal strategy of breast cancer cells selected for metastatic colonization. *Proceedings of the Royal Society B: Biological Sciences* **287**, 20202523, doi:doi:10.1098/rspb.2020.2523 (2020).
175 Millington-Burgess, S. L., Bonna, A. M., Rahman, T. & Harper, M. T. Ethaninidothioic acid (R5421) is not a selective inhibitor of platelet phospholipid scramblase activity. *British Journal of Pharmacology* **177**, 4007-4020, doi:https://doi.org/10.1111/bph.15152 (2020).
176 Kempster, C. *et al.* Fully automated platelet differential interference contrast image analysis via deep learning. *Scientific Reports* **12**, 4614, doi:10.1038/s41598-022-08613-2 (2022).
177 Kempster, C. & Butler, G. Images supporting 'Fully automated platelet differential interference contrast image analysis via deep learning'. doi:https://doi.org/10.17864/1947.000332 (2022).
178 Ruggeri, Z. M. Platelets in atherothrombosis. *Nature Medicine* **8**, 1227-1234, doi:10.1038/nm1102-1227 (2002).
179 Prevost, N., Woulfe, D., Tognolini, M. & Brass, L. F. Contact-dependent signaling during the late events of platelet activation. *Journal of Thrombosis and Haemostasis* **1**, 1613-1627, doi:https://doi.org/10.1046/j.1538-7836.2003.00327.x (2003).
180 Bearer, E. L., Prakash, J. M. & Li, Z. Actin dynamics in platelets. *Int Rev Cytol* **217**, 137-182, doi:10.1016/s0074-7696(02)17014-8 (2002).
181 Thomas, S., Calaminus, S., Auger, J., Watson, S. & Machesky, L. Studies on the actin-binding protein HS1 in platelets. *BMC cell biology* **8**, 46, doi:10.1186/1471-2121-8-46 (2007).
182 Furie, B. & Furie, B. C. Mechanisms of thrombus formation. *N Engl J Med* **359**, 938-949, doi:10.1056/NEJMra0801082 (2008).
183 Lee, D., Fong, K. P., King, M. R., Brass, L. F. & Hammer, D. A. Differential dynamics of platelet contact and spreading. *Biophys J* **102**, 472-482, doi:10.1016/j.bpj.2011.10.056 (2012).
184 Vicar, T. *et al.* Cell segmentation methods for label-free contrast microscopy: review and comprehensive comparison. *BMC Bioinformatics* **20**, 360, doi:10.1186/s12859-019-2880-8 (2019).
185 Morin, K. T., Carlson, P. D. & Tranquillo, R. T. Automated image analysis programs for the quantification of microvascular network characteristics. *Methods* **84**, 76-83, doi:10.1016/j.ymeth.2015.03.014 (2015).
186 LeCun, Y., Bengio, Y. & Hinton, G. Deep learning. *Nature* **521**, 436-444, doi:10.1038/nature14539 (2015).
187 Litjens, G. *et al.* A survey on deep learning in medical image analysis. *Medical Image Analysis* **42**, 60-88, doi:https://doi.org/10.1016/j.media.2017.07.005 (2017).
188 Berg, S. *et al.* ilastik: interactive machine learning for (bio)image analysis. *Nat Methods* **16**, 1226-1232, doi:10.1038/s41592-019-0582-9 (2019).

189 Yamashita, R., Nishio, M., Do, R. K. G. & Togashi, K. Convolutional neural networks: an overview and application in radiology. *Insights into Imaging* **9**, 611-629, doi:10.1007/s13244-018-0639-9 (2018).
190 Erickson, B. J., Korfiatis, P., Akkus, Z. & Kline, T. L. Machine Learning for Medical Imaging. *RadioGraphics* **37**, 505-515, doi:10.1148/rg.2017160130 (2017).
191 Schoepf, U. J. *et al.* Pulmonary Embolism: Computer-aided Detection at Multidetector Row Spiral Computed Tomography. *Journal of Thoracic Imaging* **22**, 319-323, doi:10.1097/RTI.0b013e31815842a9 (2007).
192 Di Cataldo, S., Ficarra, E., Acquaviva, A. & Macii, E. Automated segmentation of tissue images for computerized IHC analysis. *Computer Methods and Programs in Biomedicine* **100**, 1-15, doi:https://doi.org/10.1016/j.cmpb.2010.02.002 (2010).
193 Subašić, M., Lončarić, S. & Sorantin, E. Model-based quantitative AAA image analysis using a priori knowledge. *Computer Methods and Programs in Biomedicine* **80**, 103-114, doi:https://doi.org/10.1016/j.cmpb.2005.06.009 (2005).
194 Moen, E. *et al.* Deep learning for cellular image analysis. *Nat Methods* **16**, 1233-1246, doi:10.1038/s41592-019-0403-1 (2019).
195 Chen, E. H., Röthig, P., Zeisler, J. & Burschka, D. in *2019 IEEE Intelligent Transportation Systems Conference (ITSC).* 325-332.
196 Cho, J., Lee, K., Shin, E., Choy, G. & Do, S. How much data is needed to train a medical image deep learning system to achieve necessary high accuracy. *arXiv: Learning* (2015).
197 Ker, J., Wang, L., Rao, J. & Lim, T. Deep Learning Applications in Medical Image Analysis. *IEEE Access* **6**, 9375-9389, doi:10.1109/ACCESS.2017.2788044 (2018).
198 Chandra, A. & Yao, X. Evolving hybrid ensembles of learning machines for better generalisation. *Neurocomputing* **69**, 686-700, doi:https://doi.org/10.1016/j.neucom.2005.12.014 (2006).
199 Endenburg, S. C., Lindeboom-Blokzijl, L., Zwaginga, J. J., Sixma, J. J. & Groot, P. G. d. Plasma Fibrinogen Inhibits Platelet Adhesion in Flowing Blood to Immobilized Fibrinogen. *Arteriosclerosis, Thrombosis, and Vascular Biology* **16**, 633-638, doi:doi:10.1161/01.ATV.16.5.633 (1996).
200 Krizhevsky, A., Sutskever, I. & Hinton, G. ImageNet Classification with Deep Convolutional Neural Networks. *Neural Information Processing Systems* **25**, doi:10.1145/3065386 (2012).
201 Hansen, L. K. & Salamon, P. Neural network ensembles. *IEEE Transactions on Pattern Analysis and Machine Intelligence* **12**, 993-1001, doi:10.1109/34.58871 (1990).
202 Dietterich, T. G. in *Multiple Classifier Systems.* 1-15 (Springer Berlin Heidelberg).
203 Chandra, A. & Yao, X. Evolving hybrid ensembles of learning machines for better generalisation. *Neurocomputing* **69**, 686-700 (2006).
204 Everingham, M., Van Gool, L., Williams, C. K. I., Winn, J. & Zisserman, A. The Pascal Visual Object Classes (VOC) Challenge. *International Journal of Computer Vision* **88**, 303-338, doi:10.1007/s11263-009-0275-4 (2010).
205 Henderson, P. & Ferrari, V. in *ACCV.*
206 Hart, M. L. *et al.* Shaping the Cell and the Future: Recent Advancements in Biophysical Aspects Relevant to Regenerative Medicine. *Journal of Functional Morphology and Kinesiology* **3**, 2 (2018).
207 Mazharian, A., Ghevaert, C., Zhang, L., Massberg, S. & Watson, S. P. Dasatinib enhances megakaryocyte differentiation but inhibits platelet formation. *Blood* **117**, 5198-5206, doi:10.1182/blood-2010-12-326850 (2011).
208 Senis, Y. A., Mazharian, A. & Mori, J. Src family kinases: at the forefront of platelet activation. *Blood* **124**, 2013-2024, doi:10.1182/blood-2014-01-453134 (2014).
209 Bye, A. P. *et al.* Ibrutinib Inhibits Platelet Integrin αIIbβ3 Outside-In Signaling and Thrombus Stability But Not Adhesion to Collagen. *Arterioscler Thromb Vasc Biol* **35**, 2326-2335, doi:10.1161/atvbaha.115.306130 (2015).
210 Mangin, P. H. *et al.* Immobilized fibrinogen activates human platelets through glycoprotein VI. *Haematologica* **103**, 898-907, doi:10.3324/haematol.2017.182972 (2018).

211 Seifert, J., Rheinlaender, J., Lang, F., Gawaz, M. & Schäffer, T. E. Thrombin-induced cytoskeleton dynamics in spread human platelets observed with fast scanning ion conductance microscopy. *Scientific Reports* **7**, 4810, doi:10.1038/s41598-017-04999-6 (2017).
212 Andersen, H. *et al.* Protease-activated receptor 1 is the primary mediator of thrombin-stimulated platelet procoagulant activity. *Proceedings of the National Academy of Sciences* **96**, 11189-11193, doi:10.1073/pnas.96.20.11189 (1999).
213 Gratacap, M.-P. *et al.* The new tyrosine-kinase inhibitor and anticancer drug dasatinib reversibly affects platelet activation in vitro and in vivo. *Blood* **114**, 1884-1892, doi:10.1182/blood-2009-02-205328 (2009).
214 SÉVERIN, S. *et al.* Distinct and overlapping functional roles of Src family kinases in mouse platelets. *Journal of Thrombosis and Haemostasis* **10**, 1631-1645, doi:https://doi.org/10.1111/j.1538-7836.2012.04814.x (2012).
215 Zhang, Y. & Diamond, S. L. Src family kinases inhibition by dasatinib blocks initial and subsequent platelet deposition on collagen under flow, but lacks efficacy with thrombin generation. *Thromb Res* **192**, 141-151, doi:10.1016/j.thromres.2020.05.012 (2020).
216 Poulter, N. S. *et al.* Clustering of glycoprotein VI (GPVI) dimers upon adhesion to collagen as a mechanism to regulate GPVI signaling in platelets. *Journal of Thrombosis and Haemostasis* **15**, 549-564, doi:https://doi.org/10.1111/jth.13613 (2017).
217 Pallini, C. *et al. Immobilised collagen prevents shedding and induces sustained GPVI clustering and signalling in platelets*. (2020).
218 Nicolson, P. L. R. *et al.* Inhibition of Btk by Btk-specific concentrations of ibrutinib and acalabrutinib delays but does not block platelet aggregation mediated by glycoprotein VI. *Haematologica* **103**, 2097-2108, doi:10.3324/haematol.2018.193391 (2018).
219 Huang, J. *et al.* Platelet integrin αIIbβ3: signal transduction, regulation, and its therapeutic targeting. *Journal of Hematology & Oncology* **12**, 26, doi:10.1186/s13045-019-0709-6 (2019).
220 Hughan, S. C. & Watson, S. P. Differential regulation of adapter proteins Dok2 and Dok1 in platelets, leading to an association of Dok2 with integrin αIIbβ3. *Journal of Thrombosis and Haemostasis* **5**, 387-394, doi:https://doi.org/10.1111/j.1538-7836.2007.02307.x (2007).
221 Pike, J. A. *et al.* An adaptable analysis workflow for characterization of platelet spreading and morphology. *Platelets* **32**, 54-58, doi:10.1080/09537104.2020.1748588 (2021).
222 De Kock, L. & Freson, K. The (Patho)Biology of SRC Kinase in Platelets and Megakaryocytes. *Medicina (Kaunas)* **56**, doi:10.3390/medicina56120633 (2020).
223 Pollitt, A. Y. *et al.* Syk and Src family kinases regulate C-type lectin receptor 2 (CLEC-2)-mediated clustering of podoplanin and platelet adhesion to lymphatic endothelial cells. *J Biol Chem* **289**, 35695-35710, doi:10.1074/jbc.M114.584284 (2014).
224 Alshehri, O. M. *et al.* Fibrin activates GPVI in human and mouse platelets. *Blood* **126**, 1601-1608, doi:10.1182/blood-2015-04-641654 (2015).
225 Hughes, C. E., Finney, B. A., Koentgen, F., Lowe, K. L. & Watson, S. P. The N-terminal SH2 domain of Syk is required for (hem)ITAM, but not integrin, signaling in mouse platelets. *Blood* **125**, 144-154, doi:10.1182/blood-2014-05-579375 (2015).
226 Melak, M., Plessner, M. & Grosse, R. Actin visualization at a glance. *J Cell Sci* **130**, 525-530, doi:10.1242/jcs.189068 (2017).
227 Jost, A. P.-T. & Waters, J. C. Designing a rigorous microscopy experiment: Validating methods and avoiding bias. *Journal of Cell Biology* **218**, 1452-1466, doi:10.1083/jcb.201812109 (2019).
228 Cao, L., der Meer, A. D. v., Verbeek, F. J. & Passier, R. Automated image analysis system for studying cardiotoxicity in human pluripotent stem cell-Derived cardiomyocytes. *BMC Bioinformatics* **21**, 187, doi:10.1186/s12859-020-3466-1 (2020).
229 Garcia-Pardo, M. E., Simpson, J. C. & O'Sullivan, N. C. A novel automated image analysis pipeline for quantifying morphological changes to the endoplasmic reticulum in cultured human cells. *BMC Bioinformatics* **22**, 427, doi:10.1186/s12859-021-04334-x (2021).

230 Khan, A. O. *et al.* High-throughput platelet spreading analysis: a tool for the diagnosis of platelet-based bleeding disorders. *Haematologica* **105**, e124-e128, doi:10.3324/haematol.2019.225912 (2020).
231 Loredana, B. *et al.* Cytoskeletal perturbation leads to platelet dysfunction and thrombocytopenia in variant forms of Glanzmann thrombasthenia. *Haematologica* **101**, 46-56, doi:10.3324/haematol.2015.130849 (2016).
232 Caicedo, J. C. *et al.* Data-analysis strategies for image-based cell profiling. *Nat Methods* **14**, 849-863, doi:10.1038/nmeth.4397 (2017).
233 Yim, J. & Sohn, K.-a. Enhancing the Performance of Convolutional Neural Networks on Quality Degraded Datasets. *2017 International Conference on Digital Image Computing: Techniques and Applications (DICTA)*, 1-8 (2017).
234 Grys, B. T. *et al.* Machine learning and computer vision approaches for phenotypic profiling. *J Cell Biol* **216**, 65-71, doi:10.1083/jcb.201610026 (2017).
235 Wong, S. C., Gatt, A., Stamatescu, V. & McDonnell, M. D. in *2016 International Conference on Digital Image Computing: Techniques and Applications (DICTA).* 1-6.
236 Niioka, H. *et al.* Classification of C2C12 cells at differentiation by convolutional neural network of deep learning using phase contrast images. *Human Cell* **31**, 87-93, doi:10.1007/s13577-017-0191-9 (2018).
237 Gaertner, F. *et al.* Migrating Platelets Are Mechano-scavengers that Collect and Bundle Bacteria. *Cell* **171**, 1368-1382.e1323, doi:10.1016/j.cell.2017.11.001 (2017).
238 Sikora, J., Karczmarska-Wódzka, A., Bugieda, J. & Sobczak, P. The Use of Total Thrombus Formation Analysis System as a Tool to Assess Platelet Function in Bleeding and Thrombosis Risk—A Systematic Review. *Int J Mol Sci* **22**, 8605 (2021).
239 Lugagne, J.-B., Lin, H. & Dunlop, M. J. DeLTA: Automated cell segmentation, tracking, and lineage reconstruction using deep learning. *PLOS Computational Biology* **16**, e1007673, doi:10.1371/journal.pcbi.1007673 (2020).
240 Fujimoto, K. *et al.* in *Proceedings of the 12th ACM Conference on Bioinformatics, Computational Biology, and Health Informatics* Article 35 (Association for Computing Machinery, Gainesville, Florida, 2021).
241 Grützmacher, S., Kemkemer, R., Thies, C. & Curio, C. Detecting Lamellipodia in Epithelial Cell Clusters Using a Fully Convolutional Neural Network for Phase Contrast Microscopy Images. *Current Directions in Biomedical Engineering* **4**, 449-452, doi:doi:10.1515/cdbme-2018-0107 (2018).
242 Mochalova, E. N., Kotov, I. A., Rozenberg, J. M. & Nikitin, M. P. Precise Quantitative Analysis of Cell Targeting by Particle-Based Agents Using Imaging Flow Cytometry and Convolutional Neural Network. *Cytometry Part A* **97**, 279-287, doi:https://doi.org/10.1002/cyto.a.23939 (2020).
243 Anandakumaran, P. N., Ayers, A. G., Muranski, P., Creusot, R. J. & Sia, S. K. Rapid video-based deep learning of cognate versus non-cognate T cell-dendritic cell interactions. *Scientific Reports* **12**, 559, doi:10.1038/s41598-021-04286-5 (2022).
244 Kral, J. B., Schrottmaier, W. C., Salzmann, M. & Assinger, A. Platelet Interaction with Innate Immune Cells. *Transfus Med Hemother* **43**, 78-88, doi:10.1159/000444807 (2016).
245 Hechler, B., Dupuis, A., Mangin, P. H. & Gachet, C. Platelet preparation for function testing in the laboratory and clinic: Historical and practical aspects. *Res Pract Thromb Haemost* **3**, 615-625, doi:10.1002/rth2.12240 (2019).
246 Maurer-Spurej, E. *et al.* Room temperature activates human blood platelets. *Lab Invest* **81**, 581-592, doi:10.1038/labinvest.3780267 (2001).
247 Rao, G. H., Smith, C. M., 2nd, Escolar, G. & White, J. G. Influence of heat on platelet biochemistry, structure, and function. *J Lab Clin Med* **122**, 455-464 (1993).
248 Wei, H., Malcor, J.-D. M. & Harper, M. T. Lipid rafts are essential for release of phosphatidylserine-exposing extracellular vesicles from platelets. *Scientific Reports* **8**, 9987, doi:10.1038/s41598-018-28363-4 (2018).

249 Schoenwaelder, S. M. *et al.* Two distinct pathways regulate platelet phosphatidylserine exposure and procoagulant function. *Blood* **114**, 663-666, doi:10.1182/blood-2009-01-200345 (2009).
250 Reddy, E. C. & Rand, M. L. Procoagulant Phosphatidylserine-Exposing Platelets in vitro and in vivo. *Front Cardiovasc Med* **7**, 15, doi:10.3389/fcvm.2020.00015 (2020).
251 Yau, J. W., Teoh, H. & Verma, S. Endothelial cell control of thrombosis. *BMC Cardiovasc Disord* **15**, 130-130, doi:10.1186/s12872-015-0124-z (2015).
252 Hou, Y. *et al.* Platelets in hemostasis and thrombosis: Novel mechanisms of fibrinogen-independent platelet aggregation and fibronectin-mediated protein wave of hemostasis. *J Biomed Res* **29**, 437-444, doi:10.7555/JBR.29.20150121 (2015).
253 Lucas, F. V., Skrinska, V. A., Chisolm, G. M. & Hesse, B. L. Stability of prostacyclin in human and rabbit whole blood and plasma. *Thromb Res* **43**, 379-387, doi:10.1016/0049-3848(86)90082-4 (1986).
254 Kambayashi, J. *et al.* Mechanism of the cytoprotective effect of prostaglandin I2 and its analogue in human platelets. *Thromb Res* **44**, 439-444, doi:10.1016/0049-3848(86)90322-1 (1986).
255 Herbig, B. A., Yu, X. & Diamond, S. L. Using microfluidic devices to study thrombosis in pathological blood flows. *Biomicrofluidics* **12**, 042201, doi:10.1063/1.5021769 (2018).
256 Zhang, Y. *et al.* Emerging Microfluidic Approaches for Platelet Mechanobiology and Interplay With Circulatory Systems. *Frontiers in Cardiovascular Medicine* **8**, doi:10.3389/fcvm.2021.766513 (2021).
257 Kamocka, M. M. *et al.* Two-photon intravital imaging of thrombus development. *J Biomed Opt* **15**, 016020, doi:10.1117/1.3322676 (2010).
258 Baker, G. R., Sullam, P. M. & Levin, J. A simple, fluorescent method to internally label platelets suitable for physiological measurements. *Am J Hematol* **56**, 17-25, doi:10.1002/(sici)1096-8652(199709)56:1<17::aid-ajh4>3.0.co;2-5 (1997).
259 Abe, T. & Fujimori, T. Reporter Mouse Lines for Fluorescence Imaging. *Development, Growth & Differentiation* **55**, 390-405, doi:https://doi.org/10.1111/dgd.12062 (2013).
260 Montague, S. J., Lim, Y. J., Lee, W. M. & Gardiner, E. E. Imaging Platelet Processes and Function—Current and Emerging Approaches for Imaging in vitro and in vivo. *Front Immunol* **11**, doi:10.3389/fimmu.2020.00078 (2020).
261 Da, Q., Derry, P. J., Lam, F. W. & Rumbaut, R. E. Fluorescent labeling of endogenous platelets for intravital microscopy: Effects on platelet function. *Microcirculation* **25**, e12457, doi:https://doi.org/10.1111/micc.12457 (2018).
262 Gaertner, F. *et al.* Migrating Platelets Are Mechano-scavengers that Collect and Bundle Bacteria. *Cell* **171**, 1368-1382.e1323, doi:https://doi.org/10.1016/j.cell.2017.11.001 (2017).
263 Frydman, G. H. *et al.* Technical Advance: Changes in neutrophil migration patterns upon contact with platelets in a microfluidic assay. *Journal of Leukocyte Biology* **101**, 797-806, doi:https://doi.org/10.1189/jlb.1TA1115-517RR (2017).
264 Polak, D., Talar, M., Watala, C. & Przygodzki, T. Intravital Assessment of Blood Platelet Function. A Review of the Methodological Approaches with Examples of Studies of Selected Aspects of Blood Platelet Function. *Int J Mol Sci* **21**, doi:10.3390/ijms21218334 (2020).
265 Jenne, C. N., Wong, C. H. Y., Petri, B. & Kubes, P. The Use of Spinning-Disk Confocal Microscopy for the Intravital Analysis of Platelet Dynamics in Response to Systemic and Local Inflammation. *PLOS ONE* **6**, e25109, doi:10.1371/journal.pone.0025109 (2011).
266 McDonald, B. *et al.* Platelets and neutrophil extracellular traps collaborate to promote intravascular coagulation during sepsis in mice. *Blood* **129**, 1357-1367, doi:10.1182/blood-2016-09-741298 (2017).
267 Seynhaeve, A. L. & Ten Hagen, T. L. High-Resolution Intravital Microscopy of Tumor Angiogenesis. *Methods Mol Biol* **1464**, 115-127, doi:10.1007/978-1-4939-3999-2_11 (2016).
268 Turk, M., Naumenko, V., Mahoney, D. J. & Jenne, C. N. Tracking Cell Recruitment and Behavior within the Tumor Microenvironment Using Advanced Intravital Imaging Approaches. *Cells* **7**, doi:10.3390/cells7070069 (2018).

269 Wang, Y.-F. *et al.* Transportation of AIE-visualized nanoliposomes is dominated by the protein corona. *National Science Review* **8**, doi:10.1093/nsr/nwab068 (2021).
270 Caracciolo, G. Liposome–protein corona in a physiological environment: Challenges and opportunities for targeted delivery of nanomedicines. *Nanomedicine: Nanotechnology, Biology and Medicine* **11**, doi:10.1016/j.nano.2014.11.003 (2014).
271 Kolašinac, R., Kleusch, C., Braun, T., Merkel, R. & Csiszár, A. Deciphering the Functional Composition of Fusogenic Liposomes. *Int J Mol Sci* **19**, doi:10.3390/ijms19020346 (2018).
272 Cavalcanti, R. R. M., Lira, R. B. & Riske, K. A. Membrane Fusion Biophysical Analysis of Fusogenic Liposomes. *Langmuir* **38**, 10430-10441, doi:10.1021/acs.langmuir.2c01169 (2022).
273 Chen, F., Bian, M., Nahmou, M., Myung, D. & Goldberg, J. L. Fusogenic liposome-enhanced cytosolic delivery of magnetic nanoparticles. *RSC Advances* **11**, 35796-35805, doi:10.1039/D1RA03094A (2021).
274 Cao, E., Chen, Y., Cui, Z. & Foster, P. R. Effect of freezing and thawing rates on denaturation of proteins in aqueous solutions. *Biotechnol Bioeng* **82**, 684-690, doi:10.1002/bit.10612 (2003).
275 Park, B.-W., Yoon, D.-Y. & Kim, D.-S. Recent progress in bio-sensing techniques with encapsulated enzymes. *Biosensors and Bioelectronics* **26**, 1-10, doi:https://doi.org/10.1016/j.bios.2010.04.033 (2010).
276 Colletier, J. P., Chaize, B., Winterhalter, M. & Fournier, D. Protein encapsulation in liposomes: efficiency depends on interactions between protein and phospholipid bilayer. *BMC Biotechnol* **2**, 9, doi:10.1186/1472-6750-2-9 (2002).
277 Danaei, M. *et al.* Impact of Particle Size and Polydispersity Index on the Clinical Applications of Lipidic Nanocarrier Systems. *Pharmaceutics* **10**, doi:10.3390/pharmaceutics10020057 (2018).
278 Badran, M. FORMULATION AND IN VITRO EVALUATION OF FLUFENAMIC ACID LOADED DEFORMABLE LIPOSOMES FOR IMPROVED SKIN DELIVERY. *Digest Journal of Nanomaterials & Biostructures (DJNB)* **9** (2014).
279 Chen, M., Liu, X. & Fahr, A. Skin penetration and deposition of carboxyfluorescein and temoporfin from different lipid vesicular systems: In vitro study with finite and infinite dosage application. *International journal of pharmaceutics* **408**, 223-234 (2011).
280 Putri, D. C. A., Dwiastuti, R. & Marchaban, A. K. N. OPTIMIZATION OF MIXING TEMPERATURE AND SONICATION DURATION IN LIPOSOME PREPARATION OPTIMASI SUHU PENCAMPURAN DAN DURASI SONIKASI DALAM PEMBUATAN LIPOSOM. *Jurnal Farmasi Sains dan Komunitas* **14**, 79-85 (2017).
281 Marsalek, R., Kotyrba, M., Volna, E. & Jarusek, R. Neural Network Modelling for Prediction of Zeta Potential. *Mathematics* **9**, 3089 (2021).
282 Michel, R. & Gradzielski, M. Experimental aspects of colloidal interactions in mixed systems of liposome and inorganic nanoparticle and their applications. *Int J Mol Sci* **13**, 11610-11642, doi:10.3390/ijms130911610 (2012).
283 Midekessa, G. *et al.* Zeta Potential of Extracellular Vesicles: Toward Understanding the Attributes that Determine Colloidal Stability. *ACS Omega* **5**, 16701-16710, doi:10.1021/acsomega.0c01582 (2020).
284 Joseph, E. & Singhvi, G. in *Nanomaterials for Drug Delivery and Therapy* (ed Alexandru Mihai Grumezescu) 91-116 (William Andrew Publishing, 2019).
285 Asakura, T. *et al.* Isolation and characterization of a novel actin filament-binding protein from Saccharomyces cerevisiae. *Oncogene* **16**, 121-130, doi:10.1038/sj.onc.1201487 (1998).
286 Costa, C. A. M. d. & Moraes, Â. M. Encapsulation of 5-fluorouracil in liposomes for topical administration. *Acta Scientiarum-technology* **25**, 53-61 (2003).
287 Gonzalez Gomez, A., Syed, S., Marshall, K. & Hosseinidoust, Z. Liposomal Nanovesicles for Efficient Encapsulation of Staphylococcal Antibiotics. *ACS Omega* **4**, 10866-10876, doi:10.1021/acsomega.9b00825 (2019).

288 Csiszár, A. *et al.* Resveratrol Encapsulated in Novel Fusogenic Liposomes Activates Nrf2 and Attenuates Oxidative Stress in Cerebromicrovascular Endothelial Cells From Aged Rats. *The Journals of Gerontology: Series A* **70**, 303-313, doi:10.1093/gerona/glu029 (2014).
289 Li, W. *et al.* Antibody Aggregation: Insights from Sequence and Structure. *Antibodies* **5**, 19 (2016).
290 Baxa, U. in *Characterization of Nanoparticles Intended for Drug Delivery* (ed Scott E. McNeil) 73-88 (Springer New York, 2018).
291 Robson, A.-L. *et al.* Advantages and Limitations of Current Imaging Techniques for Characterizing Liposome Morphology. *Frontiers in Pharmacology* **9**, doi:10.3389/fphar.2018.00080 (2018).
292 Selvadurai, M. V. & Hamilton, J. R. Structure and function of the open canalicular system – the platelet's specialized internal membrane network. *Platelets* **29**, 319-325, doi:10.1080/09537104.2018.1431388 (2018).
293 Durán-Saenz, N. Z. *et al.* Platelet Membrane: An Outstanding Factor in Cancer Metastasis. *Membranes* **12**, 182 (2022).
294 Guo, X. & Szoka, F. C., Jr. Steric stabilization of fusogenic liposomes by a low-pH sensitive PEG--diortho ester--lipid conjugate. *Bioconjug Chem* **12**, 291-300, doi:10.1021/bc000110v (2001).
295 Behnke, O. Electron microscopic observations on the membrane systems of the rat blood platelet. *The Anatomical Record* **158**, 121-137, doi:https://doi.org/10.1002/ar.1091580203 (1967).
296 Escolar, G. & White, J. G. The platelet open canalicular system: a final common pathway. *Blood Cells* **17**, 467-485; discussion 486-495 (1991).
297 White, J. G. & Escolar, G. The blood platelet open canalicular system: a two-way street. *Eur J Cell Biol* **56**, 233-242 (1991).
298 Escolar, G., Leistikow, E. & White, J. G. The Fate of the Open Canalicular System in Surface and Suspension-Activated Platelets. *Blood* **74**, 1983-1988, doi:https://doi.org/10.1182/blood.V74.6.1983.1983 (1989).
299 Grouse, L. H., Rao, G. H., Weiss, D. J., Perman, V. & White, J. G. Surface-activated bovine platelets do not spread, they unfold. *Am J Pathol* **136**, 399-408 (1990).
300 Ebbeling, L., Robertson, C., McNicol, A. & Gerrard, J. M. Rapid ultrastructural changes in the dense tubular system following platelet activation. *Blood* **80**, 718-723 (1992).
301 van Nispen tot Pannerden, H. *et al.* The platelet interior revisited: electron tomography reveals tubular α-granule subtypes. *Blood* **116**, 1147-1156, doi:10.1182/blood-2010-02-268680 (2010).
302 White, J. G. Interaction of membrane systems in blood platelets. *Am J Pathol* **66**, 295-312 (1972).
303 Erickson, H. P. Size and Shape of Protein Molecules at the Nanometer Level Determined by Sedimentation, Gel Filtration, and Electron Microscopy. *Biological Procedures Online* **11**, 32, doi:10.1007/s12575-009-9008-x (2009).
304 Möckl, L. The Emerging Role of the Mammalian Glycocalyx in Functional Membrane Organization and Immune System Regulation. *Frontiers in Cell and Developmental Biology* **8**, doi:10.3389/fcell.2020.00253 (2020).
305 Milusev, A., Rieben, R. & Sorvillo, N. The Endothelial Glycocalyx: A Possible Therapeutic Target in Cardiovascular Disorders. *Front Cardiovasc Med* **9**, 897087, doi:10.3389/fcvm.2022.897087 (2022).
306 Möckl, L. *et al.* The glycocalyx regulates the uptake of nanoparticles by human endothelial cells in vitro. *Nanomedicine* **12**, 207-217, doi:10.2217/nnm-2016-0332 (2017).
307 Pavelka, M. & Roth, J. in *Functional Ultrastructure: Atlas of Tissue Biology and Pathology* (eds Margit Pavelka & Jürgen Roth) 160-161 (Springer Vienna, 2010).
308 Gromnicova, R. *et al.* Transport of Gold Nanoparticles by Vascular Endothelium from Different Human Tissues. *PLOS ONE* **11**, e0161610, doi:10.1371/journal.pone.0161610 (2016).

309 MOERNER, W. E. Microscopy beyond the diffraction limit using actively controlled single molecules. *Journal of Microscopy* **246**, 213-220, doi:https://doi.org/10.1111/j.1365-2818.2012.03600.x (2012).
310 Möckl, L. *et al.* Quantitative Super-Resolution Microscopy of the Mammalian Glycocalyx. *Developmental Cell* **50**, 57-72.e56, doi:https://doi.org/10.1016/j.devcel.2019.04.035 (2019).
311 Felgner, P. L. *et al.* Lipofection: a highly efficient, lipid-mediated DNA-transfection procedure. *Proc Natl Acad Sci U S A* **84**, 7413-7417, doi:10.1073/pnas.84.21.7413 (1987).
312 Koltover, I., Salditt, T., Rädler, J. O. & Safinya, C. R. An inverted hexagonal phase of cationic liposome-DNA complexes related to DNA release and delivery. *Science* **281**, 78-81, doi:10.1126/science.281.5373.78 (1998).
313 Kumar, V. V. Lipid molecular shapes and membrane architecture. *Indian J Biochem Biophys* **30**, 135-138 (1993).
314 Nakhaei, P. *et al.* Liposomes: Structure, Biomedical Applications, and Stability Parameters With Emphasis on Cholesterol. *Front Bioeng Biotechnol* **9**, 705886, doi:10.3389/fbioe.2021.705886 (2021).
315 Moghaddam, B., McNeil, S. E., Zheng, Q., Mohammed, A. R. & Perrie, Y. Exploring the correlation between lipid packaging in lipoplexes and their transfection efficacy. *Pharmaceutics* **3**, 848-864, doi:10.3390/pharmaceutics3040848 (2011).
316 Chen, W., Duša, F., Witos, J., Ruokonen, S.-K. & Wiedmer, S. K. Determination of the Main Phase Transition Temperature of Phospholipids by Nanoplasmonic Sensing. *Scientific Reports* **8**, 14815, doi:10.1038/s41598-018-33107-5 (2018).
317 Craig, M., Yarrarapu, S. N. S. & Dimri, M. in *StatPearls* (StatPearls Publishing

Copyright © 2022, StatPearls Publishing LLC., 2022).
318 O'Donnell, V. B., Murphy, R. C. & Watson, S. P. Platelet lipidomics: modern day perspective on lipid discovery and characterization in platelets. *Circ Res* **114**, 1185-1203, doi:10.1161/circresaha.114.301597 (2014).
319 Belyy, A., Merino, F., Sitsel, O. & Raunser, S. Structure of the Lifeact-F-actin complex. *PLoS Biol* **18**, e3000925, doi:10.1371/journal.pbio.3000925 (2020).
320 Xu, Q., Tanaka, Y. & Czernuszka, J. T. Encapsulation and release of a hydrophobic drug from hydroxyapatite coated liposomes. *Biomaterials* **28**, 2687-2694, doi:https://doi.org/10.1016/j.biomaterials.2007.02.007 (2007).
321 Chen, J. *et al.* Drug-in-cyclodextrin-in-liposomes: a promising delivery system for hydrophobic drugs. *Expert Opin Drug Deliv* **11**, 565-577, doi:10.1517/17425247.2014.884557 (2014).
322 Zhang, N. *et al.* Cyclic RGD functionalized liposomes encapsulating urokinase for thrombolysis. *Acta Biomater* **70**, 227-236, doi:10.1016/j.actbio.2018.01.038 (2018).
323 Absar, S., Nahar, K., Kwon, Y. M. & Ahsan, F. Thrombus-targeted nanocarrier attenuates bleeding complications associated with conventional thrombolytic therapy. *Pharm Res* **30**, 1663-1676, doi:10.1007/s11095-013-1011-x (2013).
324 Absar, S. G., N. Nahar, K. Ahsan, F. Engineering of plasminogen activators for targeting to thrombus and heightening thrombolytic efficacy. *Journal of Thrombosis and Haemostasis* **13**, 1545-1556, doi:10.1111/jth.13033 (2015).
325 Mustata, R. C., Grigorescu, A. & Petrescu, S. M. Encapsulated cargo internalized by fusogenic liposomes partially overlaps the endoplasmic reticulum. *J Cell Mol Med* **13**, 3110-3121, doi:10.1111/j.1582-4934.2009.00724.x (2009).
326 Adamala, K., Engelhart, A. E., Kamat, N. P., Jin, L. & Szostak, J. W. Construction of a liposome dialyzer for the preparation of high-value, small-volume liposome formulations. *Nat Protoc* **10**, 927-938, doi:10.1038/nprot.2015.054 (2015).
327 Gardiner, E. E. Proteolytic processing of platelet receptors. *Res Pract Thromb Haemost* **2**, 240-250, doi:10.1002/rth2.12096 (2018).
328 Addo, J. B., Bray, P. F., Grigoryev, D., Faraday, N. & Goldschmidt-Clermont, P. J. Surface Recruitment but Not Activation of Integrin α_{IIb}β₃

(GPIIb-IIIa) Requires a Functional Actin Cytoskeleton. *Arteriosclerosis, Thrombosis, and Vascular Biology* **15**, 1466-1473, doi:doi:10.1161/01.ATV.15.9.1466 (1995).
329 Manne, B. K. *et al.* Distinct pathways regulate Syk protein activation downstream of immune tyrosine activation motif (ITAM) and hemITAM receptors in platelets. *J Biol Chem* **290**, 11557-11568, doi:10.1074/jbc.M114.629527 (2015).
330 Poole, A. *et al.* The Fc receptor γ-chain and the tyrosine kinase Syk are essential for activation of mouse platelets by collagen. *The EMBO Journal* **16**, 2333-2341, doi:https://doi.org/10.1093/emboj/16.9.2333 (1997).
331 Jooss, N. J. *et al.* Role of Platelet Glycoprotein VI and Tyrosine Kinase Syk in Thrombus Formation on Collagen-Like Surfaces. *Int J Mol Sci* **20**, doi:10.3390/ijms20112788 (2019).
332 Kiss, L., Clift, D., Renner, N., Neuhaus, D. & James, L. C. RING domains act as both substrate and enzyme in a catalytic arrangement to drive self-anchored ubiquitination. *Nat Commun* **12**, 1220, doi:10.1038/s41467-021-21443-6 (2021).
333 Mevissen, T. E. T., Prasad, A. V. & Walter, J. C. Cell-free Trim-Away reveals the mechanism of antibody-mediated protein degradation by TRIM21. *bioRxiv*, 2022.2007.2023.501259, doi:10.1101/2022.07.23.501259 (2022).
334 Sun, X. *et al.* PROTACs: great opportunities for academia and industry. *Signal Transduction and Targeted Therapy* **4**, 64, doi:10.1038/s41392-019-0101-6 (2019).
335 Gao, H., Sun, X. & Rao, Y. PROTAC Technology: Opportunities and Challenges. *ACS Medicinal Chemistry Letters* **11**, 237-240, doi:10.1021/acsmedchemlett.9b00597 (2020).
336 Deshaies, R. J. Protein degradation: Prime time for PROTACs. *Nat Chem Biol* **11**, 634-635, doi:10.1038/nchembio.1887 (2015).
337 Li, X. & Song, Y. Proteolysis-targeting chimera (PROTAC) for targeted protein degradation and cancer therapy. *Journal of Hematology & Oncology* **13**, 50, doi:10.1186/s13045-020-00885-3 (2020).
338 Paiva, S. L. & Crews, C. M. Targeted protein degradation: elements of PROTAC design. *Curr Opin Chem Biol* **50**, 111-119, doi:10.1016/j.cbpa.2019.02.022 (2019).
339 Zhang, X. *et al.* Utilizing PROTAC technology to address the on-target platelet toxicity associated with inhibition of BCL-X(L). *Chem Commun (Camb)* **55**, 14765-14768, doi:10.1039/c9cc07217a (2019).
340 Trory, J. S. *et al.* Chemical degradation of BTK/TEC as a novel approach to inhibit platelet function. *Blood Advances* **7**, 1692-1696, doi:10.1182/bloodadvances.2022008466 (2023).
341 Atkinson, B. T., Ellmeier, W. & Watson, S. P. Tec regulates platelet activation by GPVI in the absence of Btk. *Blood* **102**, 3592-3599, doi:10.1182/blood-2003-04-1142 (2003).
342 Donovan, K. A. *et al.* Mapping the Degradable Kinome Provides a Resource for Expedited Degrader Development. *Cell* **183**, 1714-1731.e1710, doi:https://doi.org/10.1016/j.cell.2020.10.038 (2020).
343 Ranjbar, J., Yang, Y. & Harper, A. G. S. Developing human tissue engineered arterial constructs to simulate human in vivo thrombus formation. *Platelets* **34**, 2153823, doi:10.1080/09537104.2022.2153823 (2023).
344 Melis, Ç., Ali Demir, S. & Seyda, B. in *Application of Nanotechnology in Drug Delivery* (ed Sezer Ali Demir) Ch. 1 (IntechOpen, 2014).
345 Kee, M. F., Myers, D. R., Sakurai, Y., Lam, W. A. & Qiu, Y. Platelet mechanosensing of collagen matrices. *PLoS One* **10**, e0126624, doi:10.1371/journal.pone.0126624 (2015).
346 Inoue , O., Suzuki-Inoue , K., Dean , W. L., Frampton , J. & Watson , S. P. Integrin α2β1 mediates outside-in regulation of platelet spreading on collagen through activation of Src kinases and PLCγ2. *Journal of Cell Biology* **160**, 769-780, doi:10.1083/jcb.200208043 (2003).
347 Offermanns, S. Activation of Platelet Function Through G Protein–Coupled Receptors. *Circulation Research* **99**, 1293-1304, doi:doi:10.1161/01.RES.0000251742.71301.16 (2006).
348 Ulmer, C. Z. *et al.* A Review of Efforts to Improve Lipid Stability during Sample Preparation and Standardization Efforts to Ensure Accuracy in the Reporting of Lipid Measurements. *Lipids* **56**, 3-16, doi:10.1002/lipd.12263 (2021).

349 Musakhanian, J., Rodier, J.-D. & Dave, M. Oxidative Stability in Lipid Formulations: a Review of the Mechanisms, Drivers, and Inhibitors of Oxidation. *AAPS PharmSciTech* **23**, 151, doi:10.1208/s12249-022-02282-0 (2022).

350 Ickenstein, L. M., Sandström, M. C., Mayer, L. D. & Edwards, K. Effects of phospholipid hydrolysis on the aggregate structure in DPPC/DSPE-PEG2000 liposome preparations after gel to liquid crystalline phase transition. *Biochimica et Biophysica Acta (BBA) - Biomembranes* **1758**, 171-180, doi:https://doi.org/10.1016/j.bbamem.2006.02.016 (2006).

351 Chan, T.-H. *et al.* Autocatalytic Reaction in Hydrolysis of Difructose Anhydride III. *The Journal of Physical Chemistry A* **115**, 10309-10314, doi:10.1021/jp206494r (2011).

352 Elbaradei, A., Wang, Z. & Malmstadt, N. Oxidation of Membrane Lipids Alters the Activity of the Human Serotonin 1A Receptor. *Langmuir* **38**, 6798-6807, doi:10.1021/acs.langmuir.1c03238 (2022).

8. Appendix: Fuse-It-P

8.1 Introduction

Since it is possible to label the cell membrane of platelets with fluorescently labelled fusogenic liposomes using Fuse-It-Color, it opened up the potential to introduce cargo containing fusogenic liposomes. A commercial source of fusogenic liposomes containing a proprietary blend of lipids including a fluorescent lipophilic dye were used to label the membrane of platelets by fusion (Fuse-It-P), however, this time with the ability to deliver cargo directly into the cytoplasm of human platelets *in vitro*.

Conversely to Fuse-It-Color, Fuse-It-P fusogenic liposomes are supplied as a dried lipid film. This dried lipid film is resuspended in a water-soluble cargo of choice where, upon hydration of the lipid film, the lipids spontaneously form into vesicles due to the hydrophobic and hydrophilic interactions of phospholipids [344]. During spontaneous formation, the lipids encapsulate the cargo (e.g., labelled proteins or peptides) inside the lumen of the vesicles allowing, upon fusion, the direct delivery of cargo intracellularly (Figure 8.1).

Although the labelling of the cell membrane was possible using PRP platelet preparation using Fuse-It-Color, for Fuse-It-P a washed platelet preparation is essential in order to remove plasma proteins which could impair the fusion of Fuse-It-P with the cell membrane of platelets by adsorption with plasma proteins instead [270].

As a result, optimisation using washed platelets was introduced to ensure an efficient delivery of cargo as possible. Although platelet activation is significantly higher in washed platelet preparations (Chapter 4, Figure 4.2), platelet laboratories regularly use washed platelet preparations for further downstream functional assays. Washed platelets allow for the removal of the plasma environment which contains thrombin; an enzyme involved in the conversion of fibrinogen to stable fibrin during coagulation. The removal of such coagulation factors and other plasma components contributes to rested platelets. Optimisation, therefore, aimed to maintain similar levels platelet activation when platelets were fused with Fuse-It-P as rested washed platelets by using PGI_2 prior to fusion.

This chapter therefore aims to characterise different aspects of platelet function and behaviour both in the presence and absence of Fuse-It-P using washed platelet preparations. Any functional impacts as a result of the fusion of washed platelets with Fuse-It-P were quantified.

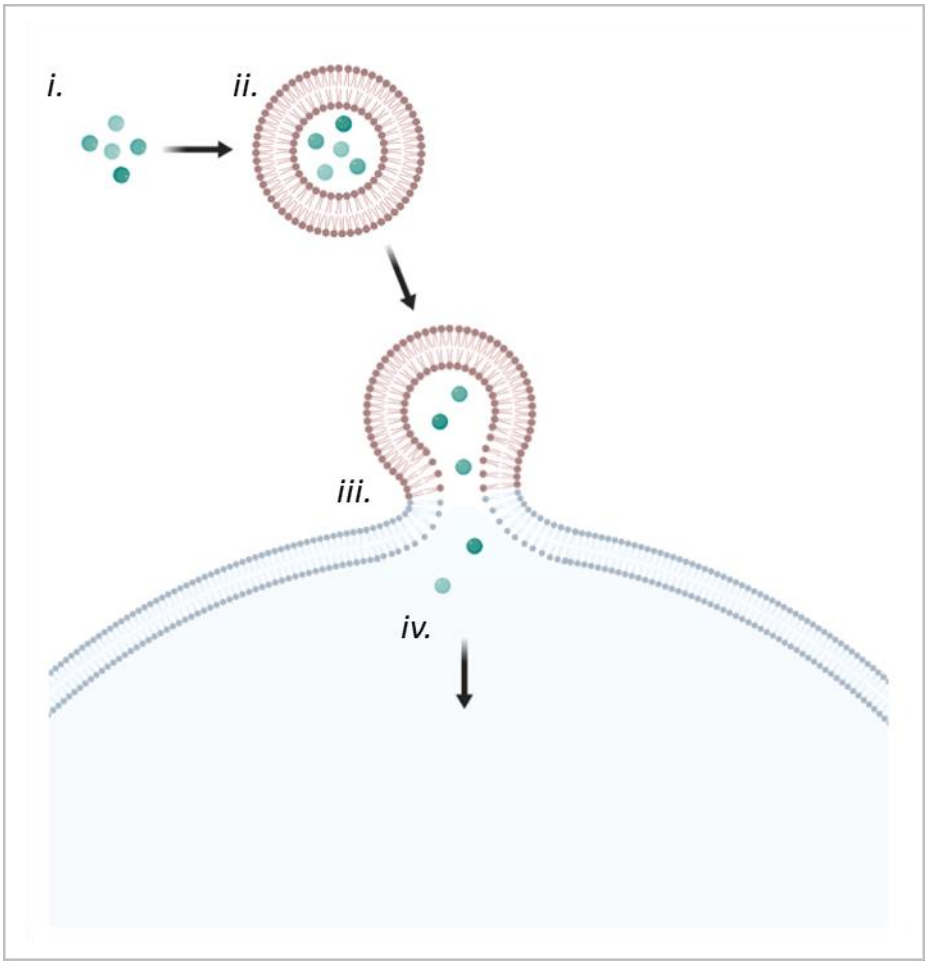

Figure 8.1 Fuse-It-P Schematic

Schematic illustrates the overall concept of cargo delivery using fusogenic liposomes. Water soluble cargo is used to reconstitute a dried lipid film (*i.*), cargo becomes encapsulated inside the lumen of spontaneously formed fusogenic liposomes (*ii.*). The overall positive charge of the fusogenic liposomes bring them into proximity of the overall negative charge of cell surface causing instabilities in both membranes allowing fusion to occur (*iii.*) and the release of cargo directly into the cytoplasm of platelets (*iv.*). Schematic created with biorender.com.

8.2 Results

8.2.1 Washed platelets can be labelled with Fuse-It-P without inducing significant platelet activation.

Platelets were incubated with fluorescently labelled Fuse-It-P in a dose dependent manner [30 μM - 2.7 μM] to establish an optimum concentration of fusogenic liposomes to use with washed platelets preparations. This enabled a concentration to be determines where platelets are not significantly activated, yet were ≥ 80% fluorescent labelled by the lipophilic dye present in Fuse-It-P.

As per previous analyses, P-selectin, a marker of α-granule release, was used as a measure of platelet activation by flow cytometry. Platelets were identified using FSC and SSC light properties, a measure of size and granularity respectively (Figure 8.2A*i*). An isotype control was used to identify non-specific antibody binding, where a 2% gate was used to define a boundary to characterise platelet activation (Figure 8.2A*ii*). The extent of washed platelet activation was subsequently the level of P-selectin exposure by α-granule release above this 2% boundary. Representative flow cytometry traces show this for a washed platelet control (WPs) (Figure 8.2A*iii*), and platelets labelled with Fuse-It-P (+FLs) (Figure 8.2A*iv*). The washed platelet control provided a basal level of platelet activation, and also served as a negative labelling control to investigate the percentage of platelet labelling by fusion.

Unsurprisingly given the level of platelet activation in the presence of Fuse-It-Color, cargo containing Fuse-It-P also induced platelet activation when labelling platelets in washed platelet preparations (Figure 8.2B).

The percentage of platelets which exposed P-selectin due to α-granule release as a result of fusion was significantly different for Fuse-It-P concentrations ≥ 10.9 μM when directly compared to unlabelled washed platelet control (WPs; 38.0 ± 15.4 %) (Figure 8.2B). Fuse-It-P concentrations ranging from 7.5 μM down to 2.7 μM were not significantly different from the washed platelet control.

Despite these differences to platelet activation in the presence of Fuse-It-P, the fluorescent labelling of platelets by fusion with Fuse-It-P resulted in highly efficient labelling (Figure 8.2C). All concentrations of Fuse-It-P used to label platelets were significantly different when compared directly to the WP control (2 ± 0 %) where analyses were consistently gated at 2%. However, a noticeable decrease in fluorescent labelling, and increase in labelling variation, could be observed when labelling platelets with ≤ 7.5 μM Fuse-It-P. Labelling of platelets with Fuse-It-P resulted in ≥80 % fluorescent labelling when taking into consideration the mean of the data when fusing with ≥ 10.9 μM Fuse-It-P (Figure 8.2C).

As in previous analyses, the median fluorescent intensity (MFI) of platelet activation as measured by P-selectin exposure (Figure 8.2D) and the extent of platelet labelling (Figure 8.2E) were also observed as clarification that similar data outcomes were observed.

When taking into account P-selectin exposure presented as MFI (Figure 8.2D), platelet activation was significantly increased when fusing with Fuse-It-P concentrations ≥ 12 µM when compared directly to the washed platelet control (WPs; 126.5 ± 75.3 AU). Representing similar scientific conclusions as percent positivity.

In contrast to percent positivity, where all concentrations of Fuse-It-P were significantly different to the control, the MFI of labelling efficiency by Fuse-It-P was only significantly different for concentrations ≥ 13.4 µM when directly compared to the washed platelet control (WPs; 51.8 ± 1.8 AU) (Figure 8.2E). Despite the labelling efficiency of platelets labelled with ≤ 12 µM Fuse-It-P being non-significant, observationally there was an increase to the level of labelling for concentrations 12 µM and 10.9 µM.

Overall, comparisons between percentage positivity and MFI identified similar scientific conclusions. When taking into consideration the percent positivity and MFI for both P-selectin exposure and the labelling efficiency of Fuse-It-P a concentration of 9.2 µM Fuse-It-P was chosen for further optimisation. This concentration represented a concentration that did not induce significant platelet activation for percent positivity or MFI when compared to the washed platelet control. Furthermore, this concentration achieved fluorescent labelling > 80% for percent positivity, and a shift in MFI was still increased when compared to the washed platelet control.

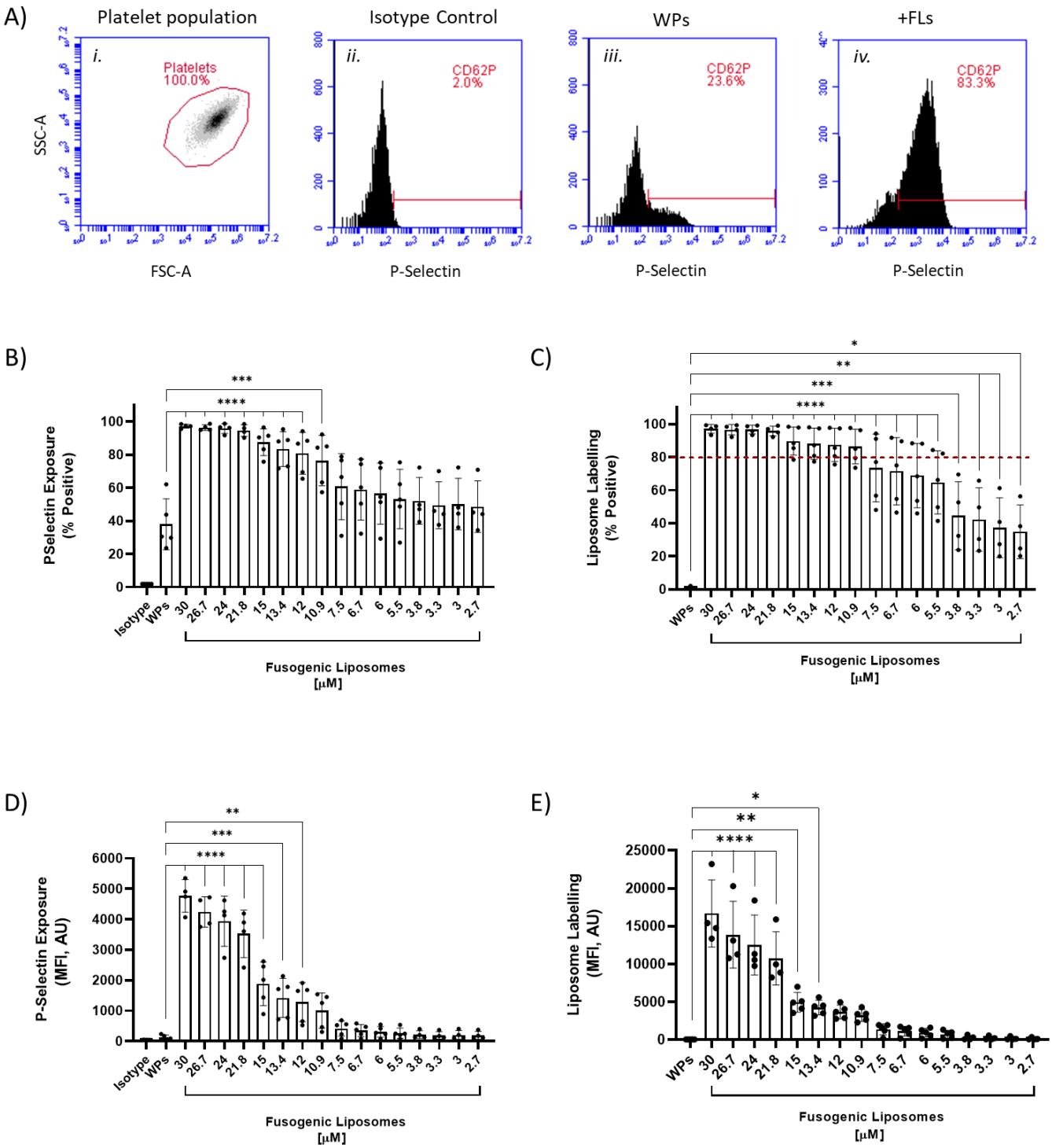

Figure 8.2 Washed platelets can be labelled with Fuse-It-P without inducing significant platelet activation.

Representative flow cytometry traces detail the platelet population as identified by forward scattered (FSC) and side scattered (SSC) light (A*i*), an isotype controlled for unspecific antibody binding and served as a negative control for P-selectin (A*ii*), unlabelled washed platelets (WPs) provided basal level of platelet activation and served as a labelling control (A*iii*), while the fusion of platelets with Fuse-It-P (+FLs) were assessed for P-selectin exposure and labelling efficiency (A*iii*). P-selectin exposure was directly compared between the isotype control, WPs and WPs pre-treated with Fuse-It-P using decreasing concentrations of Fuse-It-P (30 μM – 2.7 μM) and data plotted as

percent positivity (B) and MFI (C). Labelling efficiency was directly compared between WPs and WPs pre-treated with Fuse-It-P using decreasing concentrations of Fuse-It-P (30 µM – 2.7 µM) and data plotted as percent positivity (D) and MFI (E). The data represents 4 experimental replicates (n=4), whereby the mean ± SD was analysed using one-way ANOVA with Bonferroni post-test. The mean of the control group (Isotype for P-selectin and WPs for labelling efficiency) was compared to the mean of platelets fused with Fuse-It-P. *, $P \leq 0.05$. **, $P \leq 0.01$. ***, $P \leq 0.001$. ****, $P \leq 0.0001$.

8.2.2 An increase in platelet activation in the presence of Fuse-It-P can be controlled by the addition of PGI_2.

To reduce the variation in platelet activation as measured by P-selectin exposure when labelling platelets with Fuse-It-P [9.2 µM], dose dependent concentrations of PGI_2 from 46 µg/mL down to 0.3 µg/mL were added to washed platelets prior to fusion.

As per previous analyses, platelets were identified using FSC and SSC light properties, a measure of size and granularity respectively. P-selectin exposure was used as a measure of platelet activation above a 2% boundary set using the isotype control. Platelets which had been fluorescently labelled with Fuse-It-P (+FLs), as well as platelets pre-treated with different doses of PGI_2 prior to fluorescent labelling with Fuse-It-P (+PGI_2) were directly compared to unlabelled washed platelets from the same donor (WPs) and acquired by flow cytometry.

A significant increase in platelet activation could be observed when comparing unlabelled control platelets (WPs; 28.5 ± 5.1 %) with platelets fused with Fuse-It-P (+FLs; 74.0 ± 13.1 %) during rested conditions (Figure 8.3A). There were further significant differences when directly comparing unlabelled controlled platelets (WPs; 28 ± 5.1 %) with platelets labelled with Fuse-It-P which had been pre-treated with 0.7 ng/mL (52.2 ± 11.9 %) and 0.3 ng/mL (56.4 ± 13.0 %) PGI_2. This indicates that these concentrations of PGI_2 were not concentrated enough to reduce activation induced by Fuse-It-P fusion.

As well as basal conditions, CRP-XL [3 µg/mL] was also used to induce platelet activation. This was used to assess if platelets fused with Fuse-It-P in the presence of PGI_2 were able to recover and activate to similar levels as control platelets (Figure 8.3B). When in the presence of CRP-XL [3 µg/mL], there was no significant difference in platelet activation when comparing control washed platelets (WPs) to platelets either fused with Fuse-It-P (+FLs), or platelets pre-treated with PGI_2 prior to fusion (+PGI_2) (Figure 8.3B). This data indicated that agonist-induced activation for all conditions when measured by P-selectin exposure were similar. This result may, in part, be influenced by the percentage of positive platelets which are maximally activated in the presence of 3 µg/mL CRP-XL, or due to the greater spread in data.

To investigate this further, MFI was also observed to identify if the same scientific conclusions could be made. A significant increase in platelet activation could be observed when comparing unlabelled control platelets (WPs; 90.8 ± 21 AU) with platelets fused with Fuse-It-P (+FLs; 1235 ± 1108 AU) during resting conditions (Figure 8.3C). There were no further differences between platelets which had been pre-treated with PGI_2 and compared directly to controlled washed platelets. Furthermore, when in the presence of CRP-XL [3

µg/mL], there was no difference to platelet activation when comparing control washed platelets (WPs) to platelets either fused with Fuse-It-P (+FLs), or platelets pre-treated with PGI_2 prior to fusion (+PGI_2) (Figure 8.3D). This data indicates that platelets behave as expected when undergoing agonist-induced platelet activation after fusion with Fuse-It-P.

A dose response of PGI_2 concentrations ranging from 46 µg/mL – 0.3 µg/mL identified that there was a reduction in the variation in platelet activation when platelets had been pre-treated with higher PGI_2 concentrations prior to fusion. As a result, it was decided that a concentration of 10 ng/mL PGI_2 was sufficient to ensure platelet activation induced by the fusion with Fuse-It-P was similar to that of controlled platelets. Concentrations greater than 10 ng/mL PGI_2 plateaued and offered no additional reduction in platelet activation. Higher concentrations were therefore avoided in case of potential impact to further downstream analyses. The MFI of the same data identified similar conclusions.

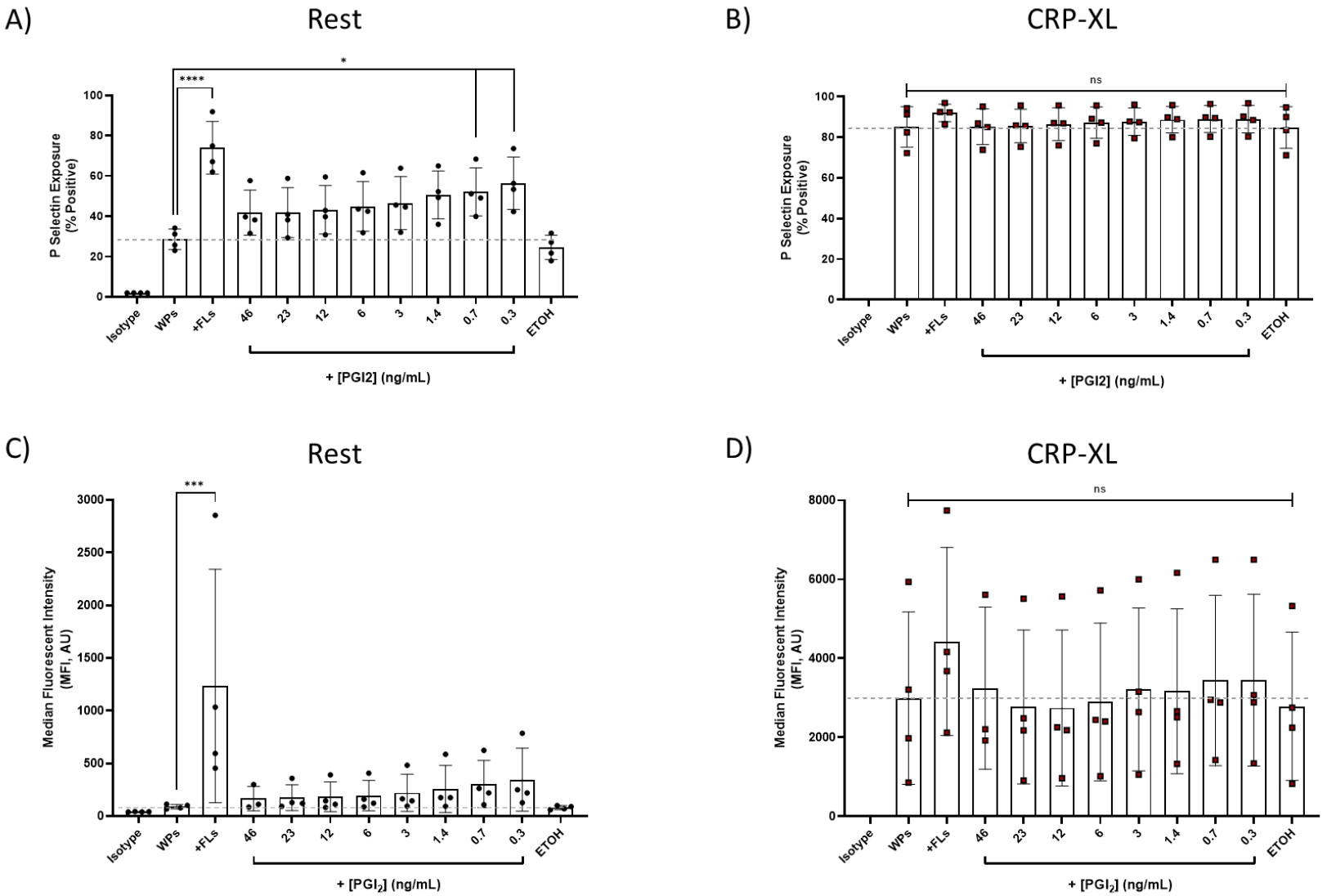

Figure 8.3 Prostacyclin (PGI_2) can reduce platelet activation induced by fusogenic liposomes without impairing recovery

Platelets labelled with Fuse-It-P [9.2 μM] were treated with prostacyclin (PGI_2) diluted in dry ethanol (ETOH) in a dose dependant manner whereby P-selectin exposure was quantified and compared to unlabelled control platelets (WPs) at rested conditions for percent positivity

(A) and MFI (C), and during agonist-induced platelet activation by CRP-XL [3 µg/mL] for percent positivity (B) and MFI (D). The grey dashed line represents the mean level of P-selectin exposure for controlled washed platelets (WPs). Data represents the mean ± SD of 4 biological replicates (n = 4). Statistics were performed using one way ANOVA with Bonferroni post-test where all groups were compared to the mean of controlled washed platelets (WPs). ns, P > 0.05. *, P ≤ 0.05. **, P ≤ 0.01. ***, P ≤ 0.001. ****, P ≤ 0.0001.

8.2.3 Fuse-It-P does not alter normal platelet spreading and adhesion.

In addition to platelet activation and the extent of labelling, platelet spreading experiments were performed to assess platelet morphology and adhesion. During injury, platelets will spread over damaged endothelium to prevent bleeding. It was therefore important to identify if platelets fused with Fuse-It-P presented any anomalies when compared to normal platelet morphology and adhesion.

Platelets were fused with Fuse-It-P prior to spreading over a fibrinogen substrate [100 µg/mL] and compared to unlabelled controlled platelets. Representative Differential Interference Contrast (DIC) images of controlled platelets (WPs) were compared to platelets fused with Fuse-It-P (+FLs) (Figure 8.4A). Representative images were acquired using a confocal microscope fitted with a 647 nm laser which was used to capture the extent of labelling by Fuse-It-P. Corresponding fluorescent images identify the extent of labelling by Fuse-It-P [9.2 µM] and identify a high efficiency of fluorescent labelling. This qualitative data supports the high degree of labelling observed when assessed by flow cytometry.

Analysis further included the same samples being acquired using a Ti2 epi-fluorescent microscope. This allowed for automated quantification using the convolutional neural network (CNN) which avoided biased manual analyses. There were no statistical differences in the spread area of platelets when comparing unlabelled control platelets (WPs) with platelets fused with Fuse-It-P (+FLs) (Figure 8.4B). Furthermore, the spread area of platelets identified here (WPs: 24 ± 3.6 μm^2 , FLs: 27.0 ± 2.1 μm^2) were consistent with the findings of platelet spread area when spread over a fibrinogen substrate in the literature [138].

Likewise, there were no further differences in platelet perimeter (Figure 8.4C), circularity (Figure 8.4D) and the number of platelets able to adhere to fibrinogen (Figure 8.4E) when directly comparing unlabelled control platelets (WPs) to those platelets fused with Fuse-It-P (+FLs). This data suggests that platelets fused with fusogenic liposomes can adhere to a fibrinogen substrate in a similar manner to that of control platelets and undergo rapid changes to morphology consistent with those seen in control platelets. Overall, this data concluded that Fuse-It-P fusogenic liposomes do not impair the ability of platelets to spread normally.

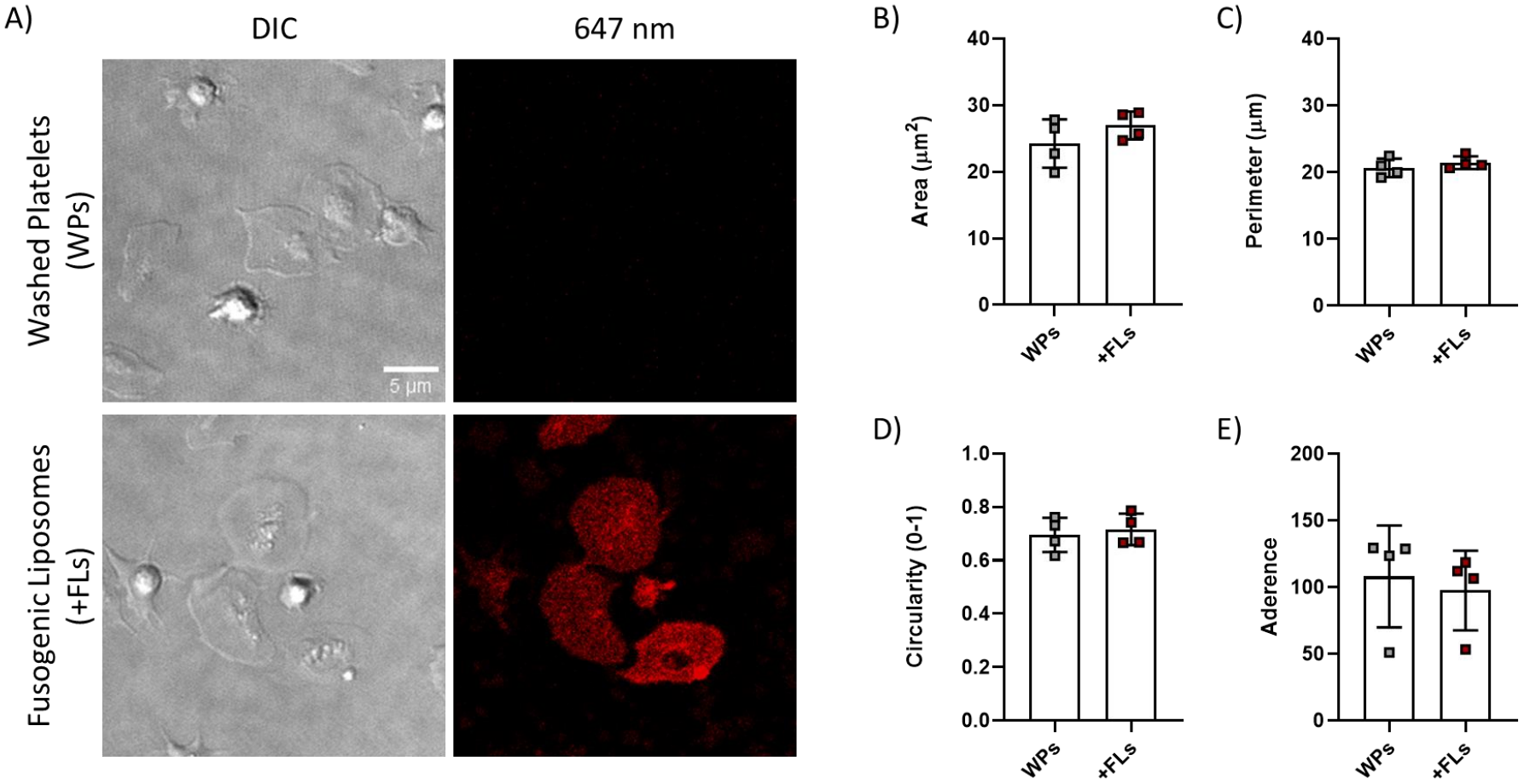

Figure 8.4 The addition of fluorescently labelled fusogenic liposomes does not alter platelet spreading.

Representative Differential Interference Contrast (DIC) images and corresponding fluorescent microscopy images of unlabelled control platelets (WPs) and platelets labelled with Fuse-It-P (+FLs) were spread over a fibrinogen [100 µg/mL] substrate (A). Platelet spread area (B), perimeter (C), circularity (D) and adherence (E) were quantified by a convolutional neural network. Data representative of four biological replicates (n=4) and represents the mean ± SD. Data statistically analysed using a paired t-test. ns, $P > 0.05$.

8.2.4 Fuse-It-P can efficiently label platelets without inducing significant phosphatidylserine translocation to the outer cell membrane.

Next, the amount of phosphatidylserine (PS) exposure, as measured by Annexin V binding, on the surface of platelets labelled with Fuse-It-P was directly compared to unlabelled control platelets. For these experiments platelets were fused with 9.2 μM Fuse-It-P to identify if cargo containing fusogenic liposomes induced apoptotic platelets.

Similar to previous flow cytometry analyses, the platelet population was first identified according to FSC and SSC light properties, a measure of size and granularity respectively. EDTA chelated calcium which impeded the binding of calcium dependent Annexin V served as a negative control. This negative control was used to gate a 2% boundary, whereby platelet events greater than this 2% boundary were categorised as Annexin V positive platelets.

When compared to unlabelled control platelets (WPs; 3.2 ± 0.7 %), fluorescently labelled platelets using Fuse-It-P (+FLs; 12.2 ± 0.5 %) did not induce significant exposure of PS as measured by Annexin V binding (Figure 8.5A). Furthermore, it was possible to induce a significant and similar increase in PS exposure on the surface of platelets for both control platelets (+ STIM, black squares; 32.9 ± 5.1 %) and platelets labelled by Fuse-It-P (+ STIM, grey squares; 36.7 ± 7.3 %) using a dual agonist stimulation (Figure 8.5A). The dual stimulation consisted of cross-linked collagen related peptide (CRP-XL, [3 μg/mL]) and thrombin [0.05 U/mL], a collagen mimetic and PAR receptor agonist respectively. Literature has previously demonstrated agonist-induced exposure of PS using a CRP-XL and thrombin combination [248].

The percentage of platelets positively labelled by Fuse-It-P was plotted to ensure a reasonable level of platelet labelling (Figure 8.5B) As expected there was a significant increase when assessing the extent of labelling by Fuse-It-P (+FLs; 85.4 ± 14.6 %) when compared to the unlabelled washed platelet control (WPs; 2 ± 0 %). However, P-selectin exposure was not acquired due to the spectral set up of the flow cytometer.

The median fluorescent intensity (MFI) of data in this collection of experiments was not included in data interpretation due to the bimodal distribution of Annexin V binding; whereby the median value would have been skewed due to the distribution of data. Overall, this data suggests that apoptotic platelets are not induced by the fusion of Fuse-It-P despite the small increase to PS exposure which may be due to membrane disruption at the point of fusion. Furthermore, when in the presence of a dual stimulation both unlabelled platelets and

platelets labelled with Fuse-It-P expose similar levels of PS exposure, further evidence that labelled platelets behave similarly to control platelets.

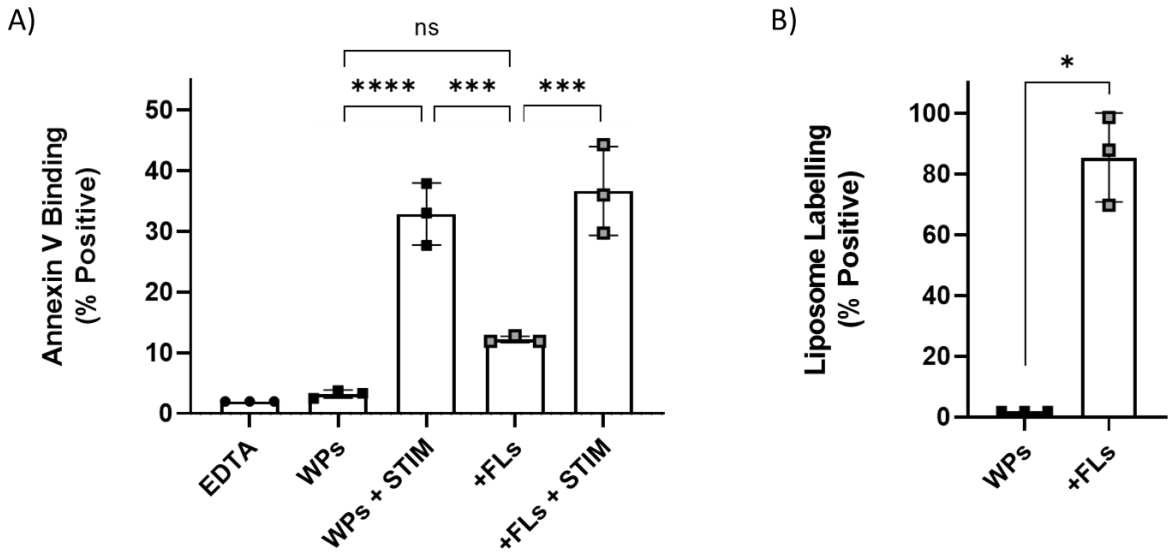

Figure 8.5 Fusogenic liposomes do not induce the translocation of phosphatidylserine to the outer cell membrane.

Annexin V binding was used as a measure of phosphatidylserine (PS) exposure on the platelet cell surface of control washed platelets (WPs) and platelets labelled with Fuse-It-P [9.2 μM] (+FLs) (A). Apoptotic platelets were induced using a dual agonist stimulation consisting of CRP-XL [3 μg/mL] and Thrombin [0.05 U/mL] for control washed platelets (WPs+STIM) and platelets which had been labelled with Fuse-It-P (+FLs+STIM). Data represents the mean ± SD of three biological replicates (n = 3). Annexin V data was analysed by one-way ANOVA with Bonferroni post-test which compared the mean of the control group (WPs) to the mean of all other groups. Liposome labelling data was analysed using a paired two-tailed t-test. ns, $P > 0.05$. **, $P \leq 0.01$. ***, $P \leq 0.001$. ****, $P \leq 0.0001$.

8.2.5 Fuse-It-P can efficiently label platelets without impacting on normal platelet aggregation.

Having looked at single cell analyses, experimentation then investigated if platelets which had been fused with Fuse-It-P could aggregate as expected. When platelets aggregate, they undergo rapid morphological shape changes, recruit other platelets to the site of injury and release contents of granules in order to sustain a growing thrombus.

Light transmission aggregometry (LTA) was used to assess any differences between unlabelled control platelets and platelets labelled with Fuse-It-P. LTA remains the main reference standard for identifying if patients have a platelet function disorder. In this instance, washed platelets (100 x 10^6 platelets/mL) were stirred in a glass cuvette incubated between a light source and a photocell. Upon the addition of a platelet agonist, platelets will become activated and aggregate together. As a result, the sample becomes clearer which allows more light to pass to the photocell. Data is recorded as time taken for aggregation to take place.

First, spontaneous aggregation was assessed to identify if platelets which had been fused with Fuse-It-P had a greater tendency to aggregate due to instabilities to the membrane as a result of fusion. Fused platelets were then directly compared to control washed platelets with no addition of agonist (Figure 8.6A). Aggregation was then assessed in the presence of two potent platelet agonists, collagen (Figure 8.6B) and thrombin (Figure 8.6C). Collagen was used to target the glycoprotein VI surface receptor which plays an important role during platelet adhesion and activation during injury [345]. Collagen will also interact with the cell surface integrin α2β1 which will mediate outside-in regulation of platelet spreading [346]. Thrombin, on the other hand, activates human platelets by cleaving and activating the PAR1 and PAR4 cell surface receptors at low and high concentrations, respectively [347].

There were no differences to maximal aggregation when comparing controlled washed platelets (WPs) to platelets which were labelled with Fuse-It-P when assessing spontaneous aggregation, collagen induced aggregation or thrombin induced aggregation (Figure 8.6D). This data indicates that platelets fused with Fuse-It-P can aggregate to similar levels of controlled platelets, providing further evidence that the addition of fusogenic liposomes do not impact on the normal behaviour of platelets.

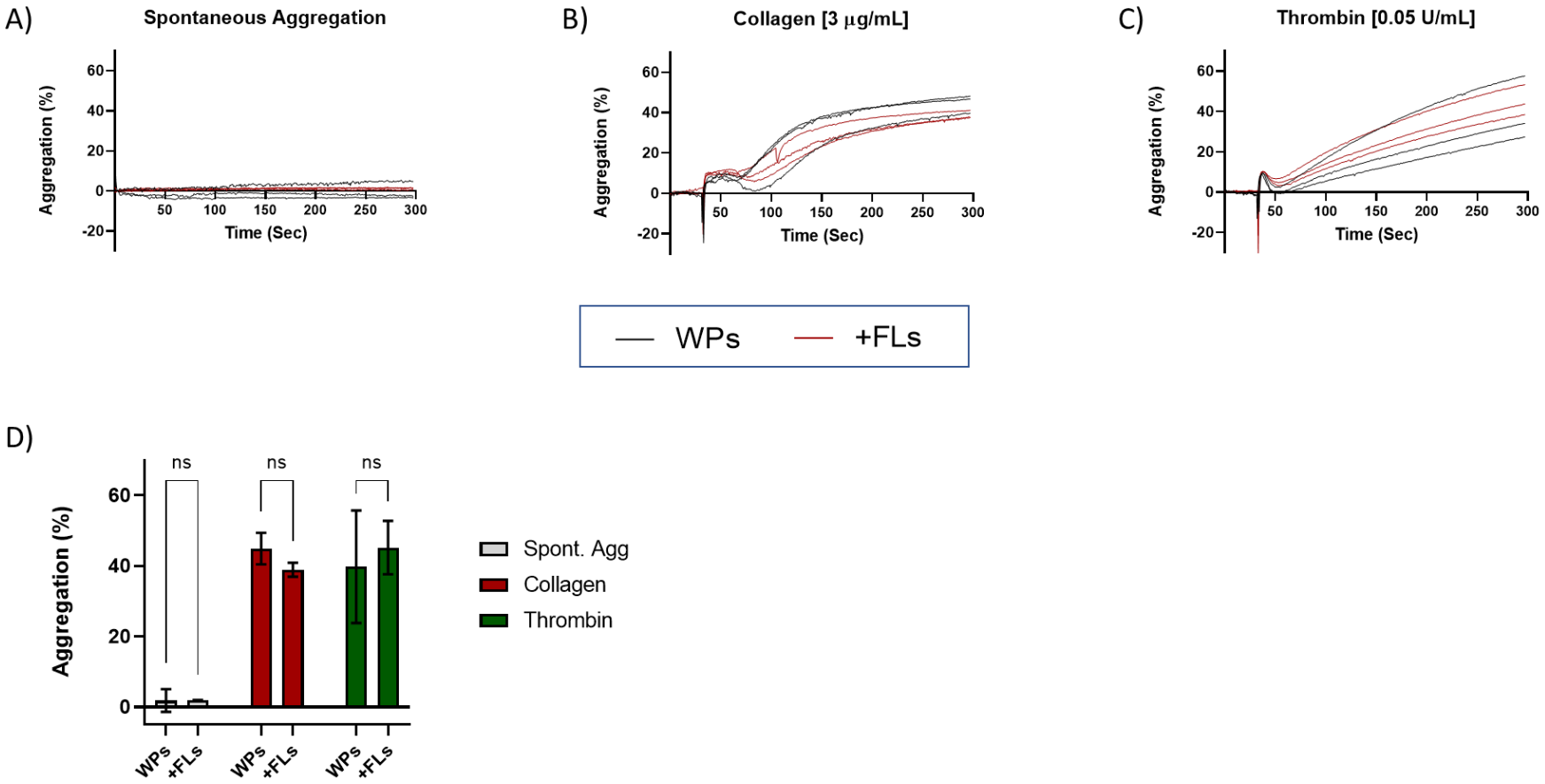

Figure 8.6 Fusogenic liposomes do not impact on normal platelet aggregation.

Light transmission aggregometry (LTA) was used to measure aggregatory responses for controlled washed platelets (WPs, black traces) and platelets labelled with Fuse-It-P (+FLs, red traces) for spontaneous aggregation (A), in the presence of collagen (B), and in the

presence of thrombin (C). Maximal aggregation responses were plotted (D). Data represents the mean ± SD of three biological replicates (n = 3) and analysed using a paired t-test. ns, $P > 0.05$.

8.2.6 Fuse-It-P can efficiently label CHO cells

There are several studies which have demonstrated the successful delivery of cargo using fusogenic liposomes as a delivery vehicle into other mammalian cells [121,154,155]. Therefore, Chinese hamster ovary (CHO) cells were maintained in culture to firstly provide a frequent supply of cells, and secondly to begin cargo delivery optimisation.

A dose response of Fuse-It-P (data not included) determined a suitable concentration [24 µM] to incubate with CHO cells when 3.5 μm^2 glass-bottomed culture dishes were 80% confluent. In the first instance, R-phycoerythrin (R-PE) was dialysed, diluted in 20mM HEPES and used to reconstitute Fuse-It-P (data not shown). Although labelling of CHO cells by fusogenic liposomes was highly efficient, no cargo was detected intracellularly. This may be due to a whole host of factors such as a large protein size, unsuccessful encapsulation and cargo charge which may all impact on fusogenic liposome physical characteristics.

Despite literature having demonstrated delivery of R-PE into CHO cells, a smaller molecule was next chosen for delivery into CHO cells to avoid such a large protein size [121]. Lifeact, a 17-residue peptide, which has also been delivered into rat myofibroblasts by fusogenic liposome delivery [121], was chosen due to its small size and its high binding affinity to actin structures (Figure 8.7A). An unlabelled culture dish served as a vehicle and labelling control (Figure 8.7A*i*). Similar to platelet labelling, Fuse-It-P could efficiently label the cell membrane of CHO cells in culture (Figure 8.7A*ii*). The fluorescent lipophilic dye incorporated into Fuse-It-P can be detected at 647 nm, and clearly demonstrates the cell membrane labelling of CHO cells. When Lifeact [10 µg/mL] was loaded into Fuse-It-P there seemed to be some green fluorescence indicating a low level of delivery (Figure 8.7A*ii*). However, Lifeact delivery was not comparable to a fixed and permeabilised control using the same loading concentration of Lifeact [10 µg/mL] (Figure 8.7A*iv*), or a phalloidin [0.27 U/mL] control (Figure 8.7A*v*). Once again, this may be due to a number of factors, including cargo concentration, cargo encapsulation or physical characteristics of the cargo or the lipids themselves.

Delivery of Lifeact was also attempted in washed platelets. Despite the efficient labelling of washed platelets Fuse-It-P, again for reasons unknown, there was no Lifeact delivery detected when assessing microscopy and flow cytometry data.

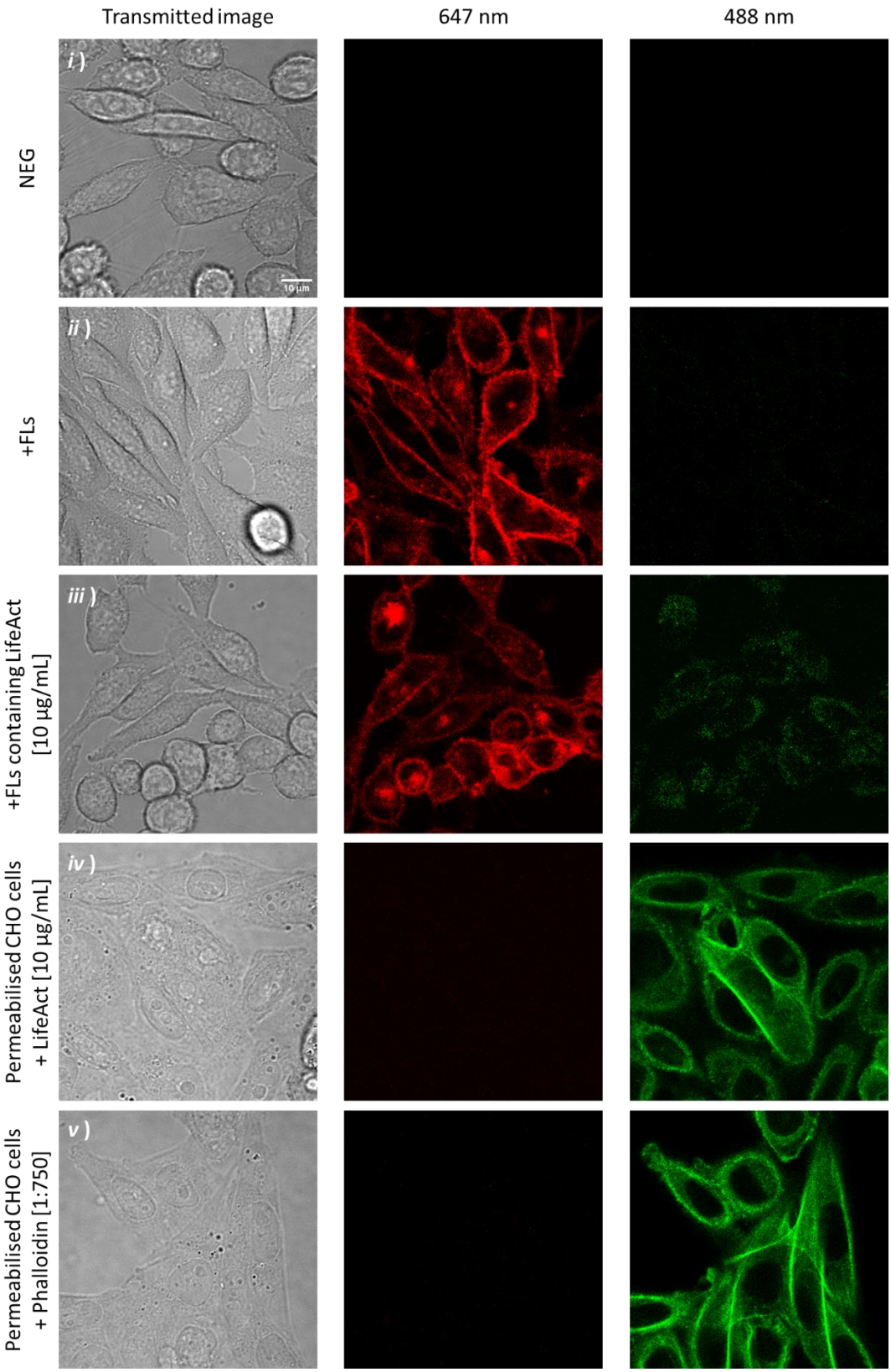

Figure 8.7 Fuse-It-P can efficiently label the cell membrane of CHO cells.

Liposome membrane labelling and Lifeact delivery into CHO cells using Fuse-It-P. CHO cells were incubated with a vehicle control (*i*), unloaded Fuse-It-P (*ii*), and Lifeact loaded Fuse-It-

P (+FLs+LA) (*iii*). Fixed and permeabilised CHO cells indicate actin structures in the presence of Lifeact [10 µg/mL] (*iv*) and Phalloidin [0.27 U/mL] (*v*). Appearance of CHO cells were observed by phase contrast (first column), fluorescent microscopy detected the fluorescent lipid tracer in Fuse-It-P (647 nm, second column), while fluorescently labelled Lifeact or Phalloidin could be detected at a different wavelength (488 nm, third column). The scale bar, 10 µm, applies to all images.

8.2.7 Zetasizer data suggests fundamental issues with experimental set-up when using Fuse-It-P

Since there was minimal to no cargo delivery observed when using Fuse-It-P, the size and charge characteristics of Fuse-It-P was next investigated to identify if sonication may impact on cargo encapsulation.

A Zetasizer (Malvern Panalytical) was used to measure both size and zeta potential of Fuse-It-P preparations which had either been sonicated or left resuspended (Figure 8.8). All measurements were performed at 20 °C and repeated three times at 1 min intervals. Firstly, size was measured using 90-degree dynamic light scattering (DLS) properties and the representative traces of the raw data were plotted for Fuse-It-P preparations which had been sonicated (Figure 8.8A.*i*) or extruded (Figure 8.8A.*ii*). The average size of the predominant peak was plotted for each Fuse-It-P preparation (Figure 8.8B). There were no significant size differences when comparing Fuse-It-P which had been sonicated to Fuse-It-P which had been left resuspended. Suggesting that sonication had no impact to liposome size after sonication for 15 minutes in a bench top ultrasonic bath.

There was no significant difference when comparing polydispersity index (PDI) for sonicated and resuspended Fuse-It-P (Figure 8.8C). PDI is a measure of the heterogeneity of a given sample based on size. Where 0.0 represents a perfectly uniform sample when considering size, whereas 1.0 represents a highly polydisperse sample containing numerous differently sized particle populations [277]. A PDI of 0.3 or below is considered an acceptable PDI measure for lipid-based carriers such as fusogenic liposomes, indicating a homogenous population [278-280]. The mean PDI for Fuse-It-P which had been sonicated (0.45 ± 0.14 PDI) or resuspended (0.39 ± 0.08 PDI) exceeded 0.3 meaning that both preparations were highly polydisperse and did not present a satisfactory PDI for lipid-based carriers.

As well as size, zeta-potential was also acquired for the Fuse-It-P samples which had been sonicated. Any particle in suspension will exhibit a zeta potential [281], for example a fusogenic liposome or a polymer. There are different states of matter, including gases, liquids, and solids, and when one of these states is dispersed within another, for example fusogenic liposomes dispersed in a buffer, a colloidal system is created [282]. Zeta potential can be used to investigate the state of a particle surface, while the magnitude of zeta potential can predict the stability of the colloidal dispersion [283]. If particles have a large negative or positive zeta potential, they will repel each other and remain in a stable suspension [284]. If particles have a low negative or positive zeta potential, they will not repel strongly, generating an unstable suspension which will likely aggregate [284]. Particles with zeta potentials more positive than +30mV or more negative then -30mV are considered stable suspensions [284].

Raw zeta potential data was plotted for Fuse-It-P preparations which had been sonicated (Figure 8.8D). The average zeta potential of sonicated Fuse-It-P were quantified where data indicates that the Fuse-It-P preparation 2 (61.7 ± 3.8 mV) was significantly different to preparations 1 (84.2 ± 2.0 mV) and 3 (78.1 ± 4.8 mV) (Figure 8.8E). However, this data is representative of only three biological replicates, and additional replicates should be considered to fully conclude the differences or similarities. Furthermore, despite the differences to average zeta potential between Fuse-It-P preparations, the repeats for each preparation were consistent and exceeded +30 mV suggestive of a stable liposome suspension (Figure 8.8E).

Overall, this data concludes that there is no difference between Fuse-It-P preparations which had been sonicated and resuspended. Suggesting that there could be fundamental issues with either the sonication equipment where the sonication step is not ensuring unilamellar vesicles, or an issue with the Fuse-It-P lipids themselves such as lipid oxidation. Furthermore, this may explain a lack of cargo delivery such that cargo is either entrapped within lumen of multilamellar vesicles, or that cargo is not sufficiently encapsulated at the point of resuspension.

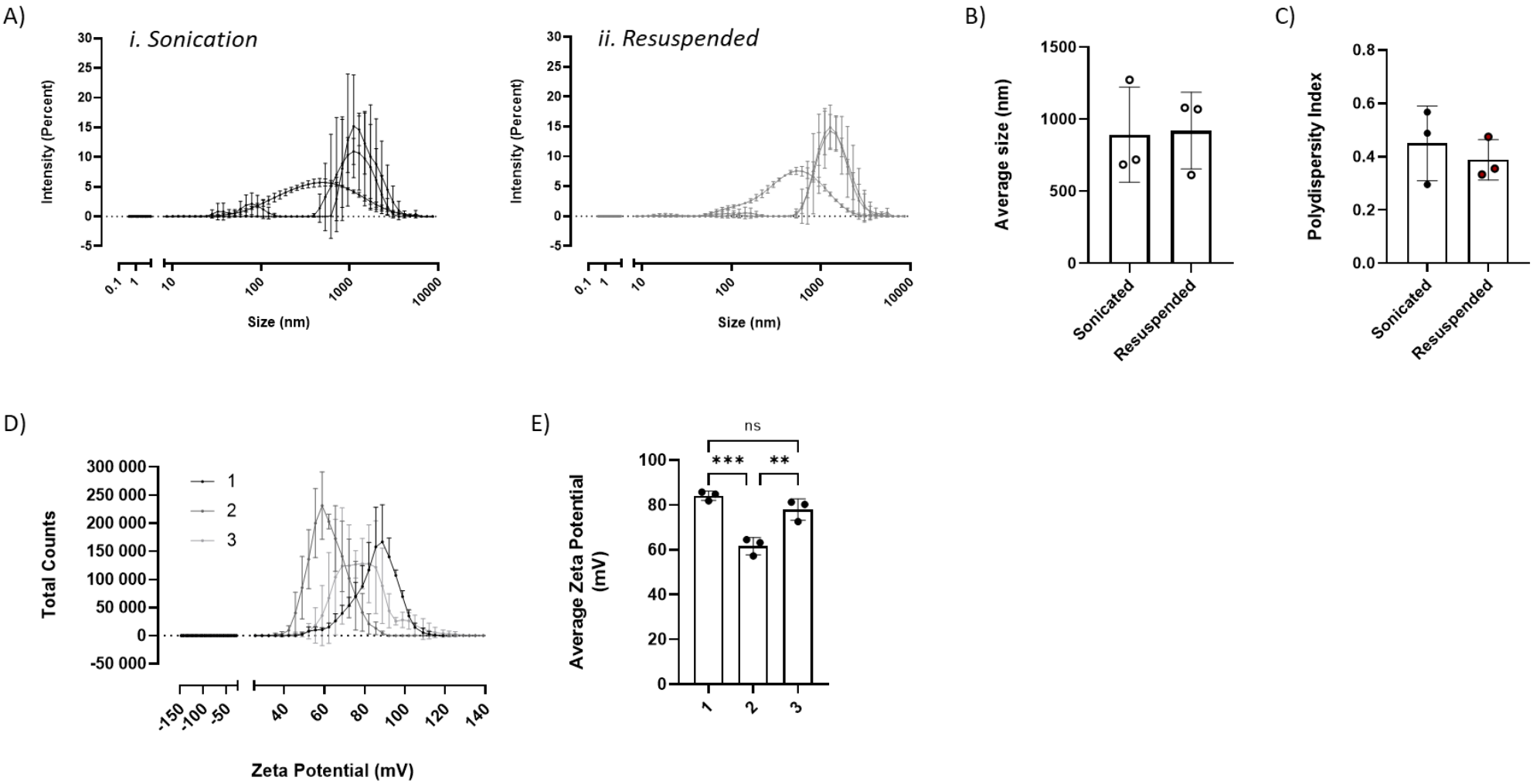

Figure 8.8 Zetasizer data unveils inconsistencies with Fuse-It-P.

The dried lipid films of three Fuse-It-P vials were dispersed in 20mM HEPES buffer where half the suspension was sonicated for 15 minutes, and half was left resuspended. Raw data indicates the percentage intensity of each peak at a given size when sonicated (A.*i*) and resuspended (A.*ii*). The average size of each peak was quantified (B). Polydispersity index indicated how homogenously dispersed Fuse-It-

P fusogenic liposomes were when sonicated and resuspended (C). Raw data indicates the total count of each peak at a given zeta potential for each Fuse-It-P preparation when sonicated (D). The average zeta potential of each peak was quantified (E). Data represents the mean ± standard deviation (SD) of three Fuse-It-P preparations (n=3). Statistical analysis was performed using an unpaired two-tailed t test (* $P \leq 0.05$, ** $P \leq 0.01$).

8.3 Discussion

Overall, the data in this chapter identifies the successful labelling of platelets using a commercial source of fluorescently labelled fusogenic liposomes (Fuse-It-P, Benaig). Using this experimental set-up, ≥80% of platelets can be fluorescently labelled by Fuse-It-P where P-selectin exposure is similar to controlled washed platelets in the presence of 10 ng/mL PGI_2 at the point of fusion. Furthermore, Fuse-It-P does not impact on normal platelet function when assessing *i*) platelet spreading as a measure of normal platelet morphology and adhesion to a fibrinogen substrate, *ii*) the level of PS exposure as a measure of procoagulant platelets, and *iii*) the ability of platelets to aggregate normally with no increased tendency to spontaneously aggregate.

Fuse-It-P optimisation has demonstrated a biocompatible and non-toxic method to fluorescently label platelets which may be applied both *in vitro* and *in vivo* for applications such as microfluidic systems and intravital microscopy, respectively. This would offer an alternative method to label platelets when investigating thrombus formation for example, where fluorescently labelled antibodies or probes may interfere with receptor function and processes associated with the formation of a thrombus [260].

Unfortunately, and for reasons unknown, cargo delivery was not successful using this commercial source of lipids. Additionally, Zetasizer data has demonstrated that the 10-minute sonication had no effect on liposome size. This suggests that either the specification of the sonicating water bath was not sufficient to break up the lipids, or there is a fundamental issue regarding the commercial lipids themselves such that degradation may have occurred prior to hydration. Oxidation and hydrolysis are the main degradation mechanisms which may impact lipids [348]. In terms of oxidation, unsaturated fatty acids are less stable than saturated fatty acids, such that the double bond in fatty acid chain of a phospholipid may become oxidised [349]. Phospholipid oxidation can be decreased when purged with nitrogen or argon. While over time, both saturated and unsaturated phospholipids will hydrolyse where for example, phospholipids can be broken down into several by-products [350]. The hydrolysis reaction also produces free protons (H+), meaning that the products of hydrolysis continue to amplify the rate of production by a chemical phenomenon known as an autocatalytic reaction [351]. However, while lipid degradation may not impact the overall extent to fluorescently label platelets, this will likely impact the ability of phospholipids to successfully encapsulate cargo as a result of destabilised bilayers [352].

The next step of this project included investigation of a preparation of in-house fusogenic liposomes using published methods (Chapter 5). In-house fusogenic liposomes were prepared using chloroform which was evaporated under vacuum to generate a dried lipid film

which could be resuspended in a buffer or cargo of choice. These in-house fusogenic liposomes, at first, were optimised similar to previous, to identify if they behaved similarly, or indeed if there are differences which may explain the absence in cargo delivery using Fuse-It-P as a commercial source of fusogenic liposomes. Furthermore, in-house fusogenic liposomes offer more control over the choice and quantity of lipids to use, the fluorescent markers to incorporate, and manufacturing processes can be carefully controlled.